Modelling of the Downstream Processing of a Recombinant Intracellular Enzyme

A thesis submitted to the University of London
for the degree of
DOCTOR OF PHILOSOPHY

by

Edward George Varga B.Eng (Hons)

September 1997

Advanced Centre for Biochemical Engineering
Department of Chemical and Biochemical Engineering
University College London
Torrington Place
London WC1E 7JE

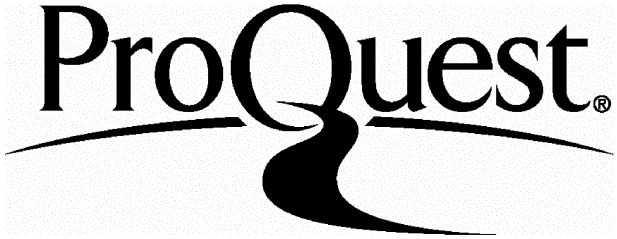

ABSTRACT

This thesis examines the generation and verification of robust and predictive models for key unit operations in the downstream processing of a recombinant intracellular enzyme. Computer models are becoming increasingly used in the biotechnology industry to assess process feasibility, ensure appropriate specification and achieve efficient operation of bioprocesses. With increasing pressure to bring bioproducts to market in the shortest possible time and at low cost, it is essential that these models can be generated early in the development cycle with a minimum of time and expense. Regulatory concerns over the use of recombinant systems also require a highly consistent product and a large degree of confidence in any final design. Models must therefore be verified against real process data in order to demonstrate and improve their validity.

The specific operations under study were cell disruption by high pressure homogenisation, enzyme fractionation and concentration by ammonium sulphate precipitation, and cell harvesting, debris removal and precipitate separation by disc stack centrifugation. Existing models based on the recovery of alcohol dehydrogenase (ADH) from natural bakers' yeast were applied to the processing of a protein engineered form of the enzyme (*pe*-ADH) and their validity assessed by comparison with experimental data obtained from small amounts of fermented recombinant material. Differences were observed in the processing of the natural and protein engineered enzyme and, although parameter re-evaluation was generally required to maintain model accuracy, the models were found to be generic in nature. Individual unit models were then arranged and linked in a modular fashion to produce a whole process model. Verification of the process model based on recombinant system parameters against pilot-scale data showed sufficient accuracy for use in feasibility studies (±30%). The inability to describe precipitant breakage in the disc stack centrifuge feed-zone was the major source of model inaccuracy.

The work highlighted the utility of scale-down systems as an aid to rapid and cost-effective model development. The importance of experimental verification in order to provide confidence in model accuracy and scalability was stressed, as was the need for modelling to be an integrated activity during bioprocess development.

ACKNOWLEDGEMENTS

I would like to thank my supervisor Professor Peter Dunnill and my advisor Dr. Nigel J. Titchener-Hooker for their guidance, encouragement and support throughout the preparation of this thesis.

I would also like to thank Kirsty Sinclair, Dr. Peter Piper, Dr. Sian Shore and Dr. John Ward for their work on recombinant strains that have subsequently been examined in this thesis and much helpful advice. The assistance of Somaiya Siddiqi, Dr. Mitra Deghani, Dr. Andrew Clarkson and Dr. Mark Bulmer with initial work was also appreciated.

I am also very grateful for financial support provided by the BBSRC sponsored Advanced Centre for Biochemical Engineering and the ORS Award scheme.

Special thanks must go to John Maybury and Dr. Emma Fischer for many useful discussions and help with experimental work. I would also like to express my gratitude to Billy Doyle, Chris Seaton and Alison Clayton for all their time and assistance in the UCL pilot plant, and to Nasreen Adibi for her help in completing analytical work. Thanks also go to the many others I have worked with at UCL, particularly on the 1st and 2nd floors of the Engineering building.

Finally, I would like to thank my parents and sister for their long distance support from Australia and my girlfriend Lynn for her help and encouragement.

TABLE OF CONTENTS

LIST OF FIGURES

LIST OF TABLES

ABBREVIATIONS

ADH	alcohol dehydrogenase
Al-DH	aldehyde dehydrogenase
ATP	adenosine tri-phosphate
CER	carbon dioxide evolution rate ($mmol.L^{-1}.h^{-1}$)
CDM	*Saccharomyces cerevisiae* strain MC1 defined media
CDH	*Saccharomyces cerevisiae* strain MC1 defined media with added histidine
CDTH	*Saccharomyces cerevisiae* strain MC1 defined media with added tryptophan and histidine
CSTR	continuous stirred tank reactor
DOT	dissolved oxygen tension (% saturation)
DNA	deoxyribonucleic acid
DM	defined media for ADH overexpressor strain
DUC	defined media for ADH overexpressor strain with added uracil and Casamino acids
DUCT	defined media for ADH overexpressor strain with added uracil, Casamino acids and tryptophan
G-6-P	glucose-6-phosphate
G-6-PDH	glucose-6-phosphate dehydrogenase
HIS	histidine
HK	hexokinase
HLADH	horse liver alcohol dehydrogenase
IPTG	isopropylthiogalactoside
OUR	oxygen uptake rate ($mmol.L^{-1}.h^{-1}$)
NAD	nicotinamide adenine dinucleotide
NADH	reduced form of nicotinamide adenine dinucleotide
PAGE	polyacrylamide gel electrophoresis
pe-ADH	protein engineered alcohol dehydrogenase
PPG	polypropylene glycol
PSD	particle size distribution
rec-HLADH	recombinant horse liver alcohol dehydrogenase

rpm	revolutions per minute
RQ	respiratory quotient
SDS	sodium dodecyl sulphate
SQP	successive quadratic programming
t-PA	tissue plasminogen activator
TRP	tryptophan
YADH	yeast alcohol dehydrogenase
YADH-I	yeast alcohol dehydrogenase isozyme I
YADH-II	yeast alcohol dehydrogenase isozyme II
YADH-III	yeast alcohol dehydrogenase isozyme III
YEPD	yeast extract peptone dextrose media
6-PG	6-phosphogluconate

1.0 INTRODUCTION

1.1 Background

Downstream processing is an important part of protein production and involves isolating a protein of a desired purity, quantity and biological activity. Traditionally, the design and operation of downstream processes has been carried out using empirical approaches such as scale-up methods (Clarkson, 1994). However, as pressures to bring a protein to market in the shortest possible time increase and the number of process alternatives grow there is rising recognition that the application of simulation and modelling can speed up bioprocess design and produce a more effective operating process (Cooney *et al.*, 1988; Gritsis and Titchener-Hooker, 1989; Petrides *et al.*, 1989; Narodoslawsky, 1991).

One of the main obstacles to a greater use of simulation in this area has been the lack of robust, predictive models (Gritsis and Titchener-Hooker, 1989). This has come about due to the complex nature of biochemical systems, which has led to a lack of available physical property data and poorly understood unit operations. Process interactions are also significant (Fish and Lilly, 1984) and must be incorporated into models to enable determination of overall process performance (Siddiqi *et al.*, 1991; Clarkson *et al.*, 1993; Middelberg *et al.*, 1992a; Middelberg 1995b; Zhou *et al.*, 1997). The increasing use of recombinant systems in the bioprocess industries to increase protein production and simplify downstream processing provides additional challenges to model development and the use of simulation. Although it has become possible to control the rate and location of protein production within an organism, or the structure of the protein itself, a highly consistent product and a large degree of confidence in any final process are required to satisfy safety and regulatory concerns.

At UCL, models have been developed for key unit operations in the downstream processing of proteins over many years by studying the recovery of the typical intracellular enzyme alcohol dehydrogenase (ADH) from natural strains of yeast. In this thesis, the modelling work is continued for the downstream processing of recombinant ADH.

In the next section the downstream processing of intracellular enzymes is outlined. In Section 1.3 the application of recombinant techniques during protein production and its effect on downstream processing is examined. In Section 1.4 process simulation is described and its application and implementation for biochemical processes and downstream processing in particular are explored. A description of the experimental systems utilised is given in Section 1.5 and aims of the research are then listed in Section 1.6.

1.2 Intracellular Enzyme Downstream Processing

1.2.1 Overview of Protein Production

Commercially, proteins are widely used as therapeutic agents, as pharmaceuticals and for medical diagnosis. They also have industrial applications in food processing and as catalytic enzymes. The steps required for the production of a protein are outlined in Figure 1.1 overleaf. The actual recovery of a protein product from the source is termed "downstream processing" and involves isolating the protein to a desired purity, quantity and biological activity, i.e. with the correct structure. The importance of downstream processing in the overall production of a protein is illustrated by the fact that the recovery costs for an enzyme product such as β-galactosidase are approximately twice that of the fermentation costs (Datar, 1986) and are even higher for pharmaceutical and diagnostic proteins such as monoclonal antibodies (Siletti, 1988).

The choice of specific recovery methods is limited by the physical, chemical and biochemical properties of the protein (e.g. molecular weight, solubility, sensitivity to heat/pH/shear) and largely determined by the eventual use and price of the protein product. In the case of an expensive small dosage human pharmaceutical for example, processes which provide a sufficiently high purity and eliminate dangerous contaminants will be required although costs are high and production levels low. While for a bulk industrial catalytic enzyme, low cost and large scale recovery methods will be required to produce a competitive product. Other factors which influence the recovery methods employed include the desired product yield, the location of the product i.e. intracellular or extracellular, how stable it is (for example it may be damaged by certain solvents) and

whether inclusion bodies are produced when a recombinant system is utilised (Section 1.3).

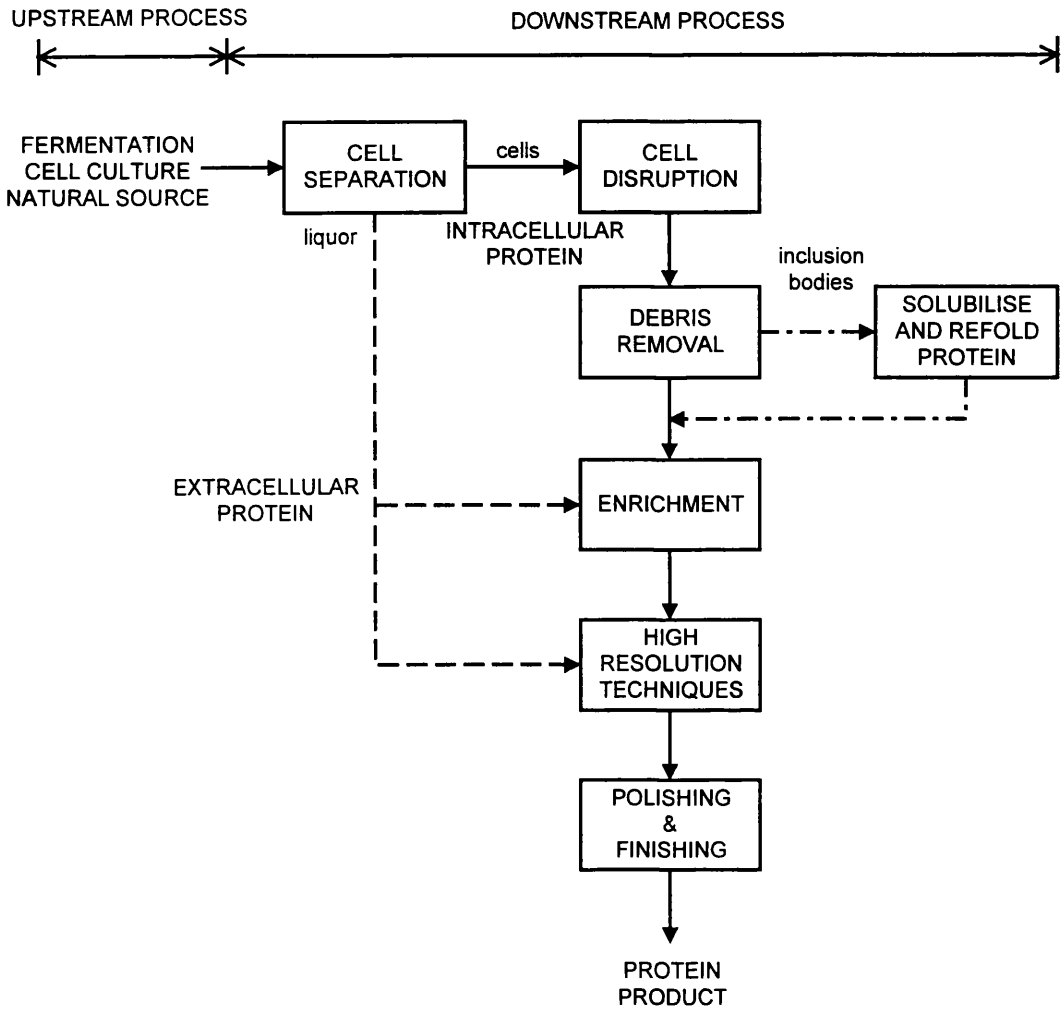

Figure 1.1: Outline of protein production.

A number of extensive reviews of the various downstream processing operations used during protein production are available in the literature (Scawen and Melling, 1985; Atkinson *et al.*, 1987; Belter *et al.*, 1988; Ogez *et al.*, 1989; Hamel and Hunter, 1990; Liddel, 1994). A brief outline of some of the main operations is therefore given below, with the specific intracellular enzyme recovery process and unit operations considered in this thesis described in more detail in Sections 1.2.2 and 1.2.3 respectively.

1.2.1.1 Cell Separation

The recovery of a protein usually starts with the separation of cells from the fermentation broth or cell culture medium and is often achieved using centrifugation or filtration.

Centrifugation involves the application of a centrifugal force to the cell suspension which causes the cells to sediment. A number of different centrifuge configurations are available. Fixed-volume and ultra centrifuges are operated as batch machines and are generally used on the laboratory scale (Hamel and Hunter, 1990). At larger scales, semi-batch machines such as the tubular bowl and multichamber centrifuge and continuous machines such as the disc stack and decanter centrifuge are more often employed. Filtration is a commonly used alternative to centrifugation and either conventional or membrane filtration can be used (Ogez *et al.*, 1989).

In the case of an extracellular product, the clarified liquid is then processed to obtain the desired protein. For an intracellular product, the separated cells must first be disrupted before enrichment and high resolution operations can be carried out. The reduction in volume produced by cell separation in the case of an intracellular product has the advantage of significantly reducing the scale of subsequent processing stages.

1.2.1.2 Cell Disruption

For proteins produced intracellularly cell disruption is required to break open the cell structure and release the protein, thereby facilitating recovery. In the simplest case the desired protein is soluble within the cell and fracture of the cell wall is sufficient to release it (Wheelwright, 1991). However if a recombinant expression system is used the protein is often overproduced and clumps together to form insoluble inclusion bodies (Section 1.3). The cells may therefore need to be thoroughly disrupted to allow complete release of the protein product. The various methods of cell disruption can be classified as either mechanical or non-mechanical (Wimpenny, 1967; Chisti and Moo-Young, 1986). Mechanical methods of disruption used on the laboratory scale are often chosen because they can very quickly process variable quantities of cells and include sonication, explosive decompression, agitation and freeze pressing. The mechanical methods of disruption most often utilised in the large scale production of proteins are high pressure homogenisation and high speed bead milling, the main reason being that large scale equipment is available at relatively low cost, having been adapted from other industries (Engler, 1985). Non-mechanical methods of cell disruption include enzyme lysis, osmotic shock, chemical lysis, freeze-thawing and heat treatment. The use of these methods is generally confined to the laboratory scale, however they show great potential for disruption on a larger scale

and for use in combination with mechanical methods to reduce power requirements (Middelberg, 1995a).

1.2.1.3 Debris Removal

A debris removal stage typically follows cell disruption. The aim of this stage is to remove cell fragments which have been produced during cell disruption in order to prevent fouling of subsequent process operations (Hearle *et al.*, 1993). The same unit operations can be used for separation of the debris as for cell separation i.e. centrifugation and filtration. However, in comparison to the recovery of cells from fermentation broth during cell harvesting, cell debris is more difficult to remove because:

- the viscosity and density of the liquid phase is increased due to the release of cellular components during cell disruption (Mosqueira *et al.*, 1981)

- the cellular debris has a reduced particle size compared to whole cells due to the rupture and possible micronisation of cells during disruption.

- the disrupted stream is often more concentrated since a reduction in volume is achieved during cell harvesting.

A balance must therefore be realised between the cell disruption conditions employed and the ease of subsequent debris removal (Siddiqi *et al.*, 1991; Middelberg, 1995a; Zhou *et al.*, 1997). When recombinant expression systems have been used and the protein product is in the form of inclusion bodies or virus-like particles (Section 1.3) the conditions used during debris removal operations must be carefully considered to ensure separation of the dense protein particles from other cell components and debris.

1.2.1.4 Solubilisation and Refolding

Production of biologically active protein from inclusion bodies produced by recombinant systems generally requires a refolding step. The protein within the inclusion bodies must first be solubilised under extreme conditions using denaturants such as guanidine hydrochloride, urea or sodium dodecyl sulphate (SDS) in the presence of reducing

compounds to disrupt disulphide bridges and convert polypeptides into a totally random structure (Ogez *et al.*, 1989; Heinrikson and Tomasselli, 1991). The perturbing influence is then removed and the polypeptides transferred to a buffer under oxidising conditions, often by using dialysis or diafiltration, to allow the protein to refold into the correct structure. Although the processing of inclusion bodies requires extra process stages, the protein within inclusion bodies is often relatively pure and therefore some simplification in subsequent purification operations can be achieved. The impact of recombinant techniques on protein production is examined in more detail in Section 1.3.

1.2.1.5 Enrichment Techniques

Protein enrichment is usually the first step in separating a specific protein from a mixture of other proteins and contaminants. The aim of protein enrichment is to concentrate the desired protein, either in a solid or liquid phase. The main advantage of using protein enrichment techniques is that the scale of subsequent high resolution operations is significantly reduced, thereby providing savings in both capital and operating costs. Commonly used enrichment operations include ultrafiltration, precipitation and extraction.

Both precipitation and extraction utilise differences in protein solubility behaviour as a basis for separation. In the case of precipitation, protein is transferred from a liquid to a solid phase. While in extraction, protein is transferred between two immiscible liquid phases (Wheelwright, 1991). A number of precipitation agents can be used, including neutral salts, polyelectrolytes, non-ionic polymers, metal ions, heat, pH adjustment and organic solvents. Extensive reviews of the various precipitation methods are given by Scopes (1988), Rothstein (1994) and Foster (1994). Extraction operations can involve transfer from the existing aqueous phase to either an aqueous or organic phase. Extraction with reversed micelles, aggregates of surfactant molecules in an aqueous or organic environment, and organic solvents can be used (Wheelwright, 1991). Liquid membranes, which consist of two immiscible phases dispersed in an external, continuous phase have also been developed (Hamel and Hunter, 1990). One of the two phases is encapsulated in the other immiscible phase which acts as a membrane, enabling proteins to be selectively partitioned from the external phase into the internal phase through the liquid membrane.

1.2.1.6 High Resolution Techniques

High resolution techniques are employed to increase the purity of the protein product to an acceptable level. The most widely used and versatile high resolution technique is chromatography, which involves the flow of a fluid through a column of material which selectively retards certain components of the fluid. It thereby becomes possible to separate a target protein from other proteins and contaminants with a high selectivity. Various types of chromatography are possible, including gel filtration, ion exchange, hydrophobic interaction (HIC), affinity and high performance liquid chromatography (HPLC). Electrophoresis can also be applied as a high resolution technique. The operation is based on the acceleration of charged proteins in an electric field and enables the separation of proteins with a different net charge. The use of electrophoresis has generally been limited to small scale protein purification due to scale-up difficulties that arise from product heating (Liddell, 1994).

1.2.1.7 Polishing and Finishing Operations

Finishing operations are carried out as the last stages of protein production. The actual operations used greatly depend on the intended use the final protein product and can be either simple or complex. The required scale of the operations will also depend on the type and volume of protein product. Where a solid product is required, crystallisation is often used. Crystallisation involves the formation of solid particles of protein with a defined shape and size in a supersaturated solution in order to give a high final product purity and an improved product appearance. The operation is usually followed by a filtration or centrifugation step to remove the solid protein crystals and a drying stage to stabilise the product and preserve activity. Several drying processes are possible, including spray drying, freeze drying, fluid bed drying and vacuum drying (Liddell, 1994). Where the final product is in liquid form, filtration operations can be used to concentrate the product in the liquid phase, desalt or change the buffer associated with the product and in theory achieve sterility.

1.2.1.8 Commonly Utilised Operations

A review of 100 papers on protein purification published in 1984 by Bonnerjea *et al.* (1986) revealed that, on average, four purification steps were required to purify proteins to homogeneity with an overall yield of 28% and a purification factor of 6,380. Just under 10% of the papers reported the use of recombinant systems. Ion exchange chromatography was the most commonly used operation, occurring in 75% of purification schemes. The most frequently employed first step in a purification process was homogenisation, with precipitation the most common second step. Three quarters of the precipitation methods used ammonium sulphate as the precipitant. It should be noted that a number of novel techniques are currently being developed, including magnetic separation, electrically assisted filtration and supercritical fluid extraction, which may become more widely used during protein production in the future (Liddell, 1994).

1.2.2 Typical Intracellular Enzyme Recovery Process

In this thesis, the typical intracellular enzyme recovery process shown in Figure 1.2 overleaf is considered. Cells are grown in a batch fermentation and separated from the fermentation broth using a disc stack centrifuge. If required, the recovered cells are also washed to reduce the carryover of contaminants from the fermentation stage by mixing with buffer and re-centrifuging. Cell disruption to release the target enzyme is achieved using a high pressure homogeniser operated in discreet pass mode, with subsequent debris removal carried out by disc stack centrifugation. Enrichment and purification is achieved using batch ammonium sulphate precipitation. A two stage fractional precipitation procedure is used, with batch ageing being carried out for each precipitation stage prior to precipitate separation using a disc stack centrifuge. The final product of the process is an enzyme rich precipitate. The unit operations of high pressure homogenisation, neutral salt protein precipitation and disc stack centrifugation used in this process are considered in more detail in Section 1.2.3.

The process shown in Figure 1.2 has been used by Clarkson (1994) and Alsaffar (1994) for the initial recovery of the intracellular enzyme alcohol dehydrogenase (ADH) from natural bakers' yeast at the pilot-scale of operation. Further purification of the enzyme rich precipitate can then be carried out using chromatography stages. A similar process, with a

heat treatment step after the debris removal stage for the precipitation of nucleic acids, was used by Higgins *et al.* (1978) for the initial pilot-scale recovery of β-galactosidase from *Escherichia coli.*

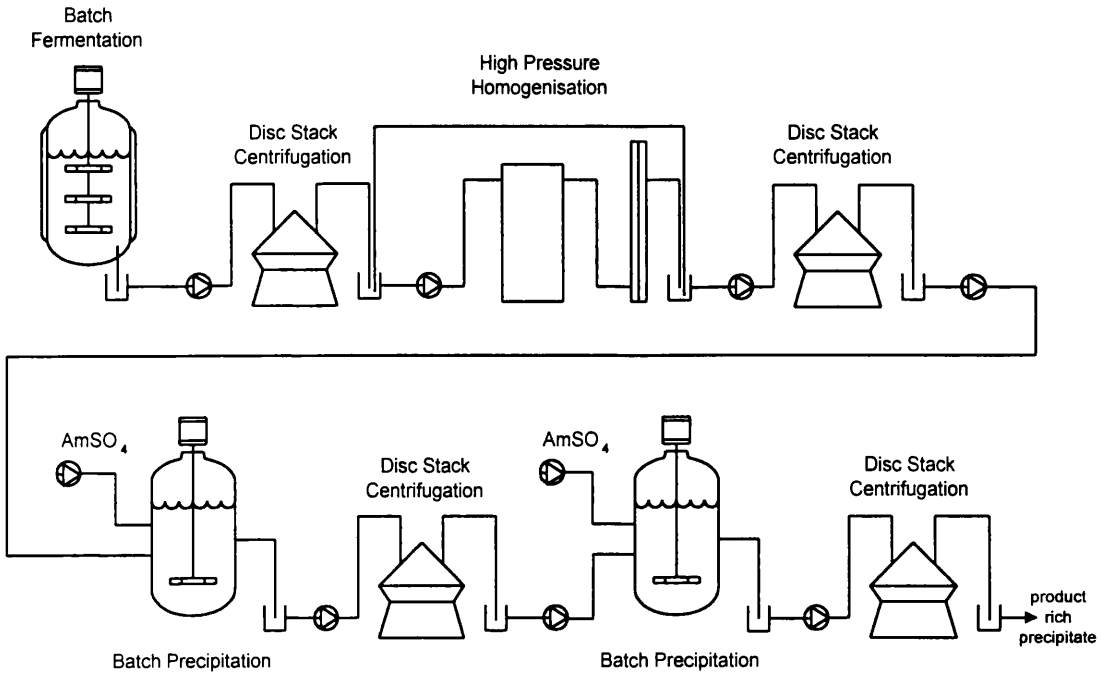

Figure 1.2: Typical intracellular enzyme recovery process.

1.2.3 Downstream Process Unit Operations

A general description of the unit operations considered in this thesis is given below. For an examination of the modelling of high pressure homogenisation, protein precipitation using neutral salts and disc stack centrifugation refer to Chapters 5.0, 6.0 and 7.0 respectively.

1.2.3.1 High Pressure Homogenisation

The high pressure homogeniser was originally used for emulsification in the diary industry (Atkinson *et al.*, 1987) and is now commonly used for the disruption of microorganisms during protein downstream processing (Middelberg, 1995a). In a high pressure homogeniser, cells are disrupted by forcing the cell suspension through an adjustable, restricted orifice valve under high pressure (Engler, 1985). The critical components of this device are the valve rod, valve seat and impact ring shown in Figure 1.3 overleaf. A

piston driven positive displacement pump is used to push the cell suspension between the valve seat and valve rod so that it impinges on the impact ring at high velocity of the order 200 to 300 $m.s^{-1}$ (Middelberg, 1995a). The valve rod is spring loaded or an automatic hydraulic system is employed to maintain a given clearance from the valve seat. The operating pressure of the equipment (as high as 2000 bar) can be adjusted by altering the distance between the valve rod and valve seat. Various designs for the valve seat can be used and typical designs for the disruption of micoorganisms are shown in Figure 1.4.

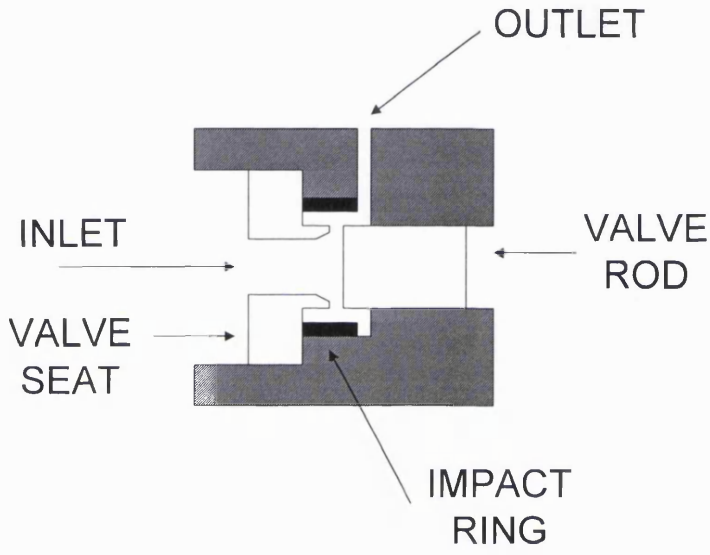

Figure 1.3: Cross section through a high pressure homogeniser valve, from Wheelwright (1991).

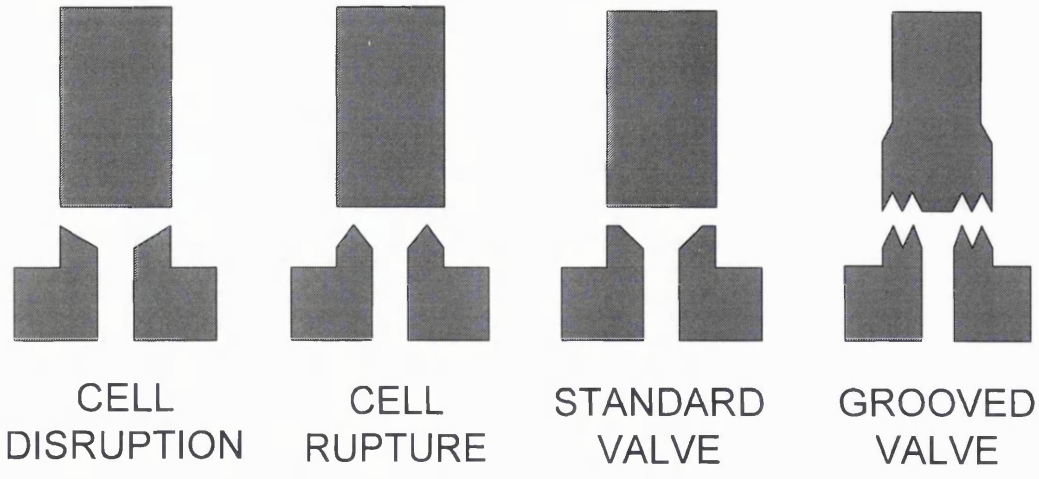

Figure 1.4: Diagram of various valve configurations used for disrupting microorganisms, from Wheelwright (1991).

Large-scale high pressure homogenisers with capacities as large as 5700 $L.h^{-1}$ (Wheelwright, 1991) and small-scale models that handle samples as small as 0.04 L are commercially available. High pressure homogenisers can either be operated with discrete passes (in which all of the processed cells are collected and passed through the homogeniser again) or with a recycle stream. The effectiveness of disruption can be assessed by monitoring the degree of cell breakage (Atkinson *et al.*, 1987) and/or the release of protein products. The actual level of disruption achieved will depend on the type of organism (Engler, 1985; Wheelwright, 1991), the conditions of cell growth (Engler and Robinson, 1981; Harrison, 1991), the operating pressure, the number of discrete passes or recycle rate and the operating temperature (Hetherington *et al.*, 1971; Keshavarz, 1990). To achieve cell breakage of 90% or more, multiple passes are usually required (Wheelwright, 1991). For natural bakers' yeast, the release of over 90% of soluble protein is achieved using 5 discreet passes at an operating pressure of 500 bar for cell concentrations between 30% and 60% (v/v) wet weight yeast (Hetherington *et al.*, 1971).

The mechanisms of disruption during high pressure homogenisation are difficult to determine because of the complex fluid dynamics involved. Wheelwright (1991) gives the three most likely mechanisms as cavitation, turbulence and shearing, while Harrison (1991) lists rapid pressure release, impingement and cavitation as the significant mechanisms causing initial cell rupture. In an early study of bakers' yeast disruption, Brookman (1974) gave the magnitude of the pressure release as the major factor in cell disruption. Kesharvarz-Moore *et al.* (1990) have shown a decrease in bakers' yeast cell disruption with increasing impact ring distances and attributed 80% of the disruption to impingement, indicating that this is the main mechanism for disruption. More recently, however, Shamlou *et al.* (1995) have concluded that the effects of elongational stresses prior to impingement best correlate the breakage of packed bakers' yeast. It is likely that a combination of stresses act to cause cell disruption and that the dominant stress depends on the organism and valve fluid dynamics (Middelberg, 1995a). Further research is clearly required in this area.

The resistance of different types of cells to breakage during disruption greatly varies and largely depends on the structure of the cell wall. Bacterial cell walls consist of a rigid matrix mostly composed of peptidoglycan, a network of glycan chains cross-linked by short peptides, although Gram-negative bacteria contain a much thinner layer of

peptidoglycan than Gram-positive bacteria (Engler, 1985). It is thought that the major resistance to disruption is this peptidoglycan matrix.

Yeast cell walls have a more complicated structure and are thicker than bacterial cell walls. In the case of bakers' yeast, the wall thickness is approximately 70 nm and increases with age (Engler, 1995). The precise structure of yeast cell walls has not been fully characterised, but the primary components are glucan, mannoprotein and chitin (Middelberg, 1995a). The resistance of the cell wall to disruption appears to be a function of how tightly cross-linked and how thick the structural portion of the cell wall is (Engler, 1985). The presence of budding scars, which cause local areas of weakness in the cell wall, may also influence the degree of breakage achieved (Engler and Robinson, 1981). The use of micromanipulation techniques has enabled the compressive force required to rupture yeast cells to be determined, with values of 40 μN and 90 μN obtained for brewers' yeast in the exponential and stationary phases of growth respectively (Roberts *et al.*, 1994). Mammalian cells, on the other hand, have a cell membrane but no cell wall and are therefore shear sensitive, only requiring a minimal energy input for disruption (Wheelwright, 1991).

Some of the main considerations when operating a high pressure homogenisers are:

- large amounts of heat are generated and cooling is therefore required to maintain enzyme activity.

- small debris are produced at high pressures and/or after repeated passes which may be hard to remove during subsequent processing stages. A trade-off between high pressure homogeniser operating conditions and the effectiveness of subsequent debris removal stages must therefore be realised (Zhou *et al.*, 1997).

- valve blockages may occur when filamentous organisms are disrupted at high cell concentrations.

- when recombinant cells are processed the containment of cellular material is required, however high pressure homogenisation systems originating from non-biotechnological industries may fail in this regard (Foster, 1995).

1.2.3.2 Neutral Salt Protein Precipitation

Precipitation has been used in the industrial scale production of proteins for over 130 years and is well established in the separation of proteins from blood plasma, microbial extracts and plant extracts (Foster, 1994). The method exploits differences in protein solubility behaviour in order to achieve separation, with proteins being precipitated as a non-crystalline solid. Effective recovery of the precipitate is therefore required and can be achieved using either centrifugation or filtration. Some of the characteristic features of protein precipitation given by Foster (1994) are that:

- a 10 to 50 fold reduction in process volumes can be achieved.

- protein precipitates are compact and stable, thereby allowing the recovery process to be held at an intermediate stage.

- a more stable environment is established for the protein product by the rapid separation from proteolytic enzymes and other biologically active substances.

- protein precipitation can be used as an aid to chromatography by achieving a degree of pre-purification.

The most widely used protein precipitation method is the addition of high concentrations of neutral salts, which is known as 'salting out'. At low salt concentrations, i.e. close to physiological conditions, proteins are very soluble as a result of polar interactions with the aqueous solvent, ionic interactions with the salt present and to some extent repulsive electrostatic forces between like charged molecules or aggregates (Scopes, 1988). This effect is often called 'salting in'. At higher salt concentrations solubility depends more on the hydrophobicity of the protein. Each protein has a distribution of hydrophilic and hydrophobic residues on its surface which determine solubility behaviour. When the hydrophobic residues are forced into contact in an aqueous environment, water molecules are 'locked' into place around these residues. If large amounts of salt are added, the salt molecules become solvated and as water molecules become scarce pull away the 'locked' molecules from the hydrophobic residues. The exposed residues can then interact to form a protein aggregate. As these protein aggregates attain a size and degree of solvation

which are no longer favourable to the solution phase, precipitation of a solid phase occurs (Foster, 1994). The initial formation of primary precipitate particles is known as nucleation. Subsequent growth of the primary particles then continues due to a diffusion-controlled mechanism, known as perikinetic growth. Above a limiting size, shear controlled aggregation (and breakage), known as orthokinetic growth, becomes the dominant mechanism.

The relative effectiveness of neutral salts in salting out, in particular the anions, is given by the lyotropic or Hofmeister series:

citrate > phosphate > sulphate > acetate >chloride > nitrate > thiocyanate

In practice, the most commonly used salt is ammonium sulphate due to its high solubility, cheapness and stabilising effect on some enzymes. However, ammonium sulphate is also corrosive when impure and evolves ammonia at high pH, making it difficult to handle at the large industrial scale (Richardson, 1987).

In order to selectively precipitate different proteins, fractional precipitation can be carried out, which involves a sequence of precipitation stages in which different precipitant concentrations (or 'cuts') are used. In a two cut fractional precipitation, the first cut involves addition of precipitant to a specific concentration such that contaminating proteins are precipitated while a more soluble target protein remains in solution. After the precipitate from the first cut has been removed, the second cut involves the addition of further precipitant to achieve a higher concentration in order to precipitate the target protein while leaving other less soluble contaminating proteins in solution. In this way, purification of the target protein can be achieved with respect to other contaminating proteins. A two-cut precipitation procedure has been used for the recovery of the enzyme alcohol dehydrogenase from bakers' yeast homogenate using ammonium sulphate concentrations of approximately 40% and 60% saturation for the first and second cut points respectively (Richardson, 1987; Alsaffar, 1994; Clarkson, 1994). The ammonium sulphate fractionation of β-galactosidase from recombinant *Saccharomyces cerevisiae* cell homogenate has also been examined by Zhang *et al.* (1995).

The main factors which are generally regarded as determining protein solubility and hence the extent of precipitation achieved are listed in Table 1.1. Mixing conditions and the rate and mode of salt addition may also have an effect (Foster, 1972; Foster *et al.*, 1976; Iyer and Przybycien, 1994). With the advent of recombinant techniques such as protein engineering it is now possible to alter protein characteristics (Section 1.3.2) and thereby influence solubility behaviour.

Protein Characteristics	**Solution Properties**
Size of molecule	Solvent availability e.g. water
Amino acid composition	pH
Amino acid sequence	Ionic strength
Number of ionisable residues	Dielectric constant
Ratio of polar/non-polar residues	Temperature
Distribution of polar/non-polar residues	Specific ion effects
Chemical nature of amino acid residues	
Dissociation constants	
Protein conformation	
Protein charge	
Ion binding properties	

Table 1.1: Parameters that determine the solubility of proteins, from Foster (1994).

The history of precipitate preparation will also influence the properties of the final precipitate formed and thereby determine the effectiveness of subsequent recovery operations. For efficient separation by centrifugation it is desirable that large, dense and strong precipitate particles are produced and this can be achieved using some form of conditioning. A common method is batch ageing, in which the precipitate is stirred in the precipitation vessel for a given time period. Both shear induced aggregate growth and breakage may occur, and careful consideration of ageing conditions is therefore required. The Camp number, given by Gt, is a typically used parameter to define the shear conditions, where G is the average shear rate, or mean velocity gradient, and t is the time of exposure to the shear. However, it should be noted that the Camp number does not account for the distribution of shear rates within the stirred tank. Values of Gt of 10^4 to 10^5

with values of G from 10 to 100 s^{-1} are recommended in the water treatment field for the formation of flocs in stirred tanks (Bell *et al.*, 1983).

Bell and Dunnill (1982a) found that Gt correlated the strength of isoelectric soya protein precipitate prepared in a batch reactor. The improved strength at Gt values of about 10^5 was thought to be due to rearrangement and infilling with smaller particles giving a closer, denser and more stable packing. Hoare (1982a) examined the batch ageing of ammonium sulphate precipitated casein and found that the maximum stable precipitate size was achieved at a Gt value of 10^5. While Clarkson *et al.* (1996a) found bakers' yeast protein precipitate at an ammonium sulphate saturation of 40% showed a reduction in fine aggregates of approximately 1.5 μm and an increase in the proportion of larger aggregates of 2 to 4 μm at a shear rate of 40 s^{-1} and Camp number of 10^5.

In order to achieve the continuous conditioning of precipitate, continuous reactors and acoustic treatments have been applied. Virkar *et al.* (1982) used a continuous tubular reactor and found increased growth rates of isoelectric soya protein precipitate at high shear rates and protein concentrations, although smaller particle sizes were also produced. Grid spacers were positioned at regular intervals along the reactor to induce high shear conditions. Bell and Dunnill (1982b) found that precipitate from the continuous reactor showed less resistance to breakage when comparing the strength of isoelectric soya protein precipitate prepared in a batch and continuous reactor using a capillary shear device. The use of a dual-source, low frequency acoustic treatment has been reported in the fractional precipitation of blood plasma (Foster and Watt, 1980). A study by Bell and Dunnill (1984) has shown that an increase in isoelectric soya protein precipitate size and density occurred after conditioning with dual-source, low frequency acoustic vibrations. The extent of ageing prior to acoustic conditioning was also found to be an important factor. Further work has been carried out by Titchener-Hooker *et al.* (1992), who investigated the effect of fluid-jet mixing on low frequency conditioning of isoelectric soya protein precipitate, and Titchener-Hooker and McIntosh (1993), who examined the effect of low-frequency conditioning on the centrifugation of ethanol-precipitated human albumin and found that the history of precipitate preparation was critical to the levels of improvement achieved.

1.2.3.3 Disc Stack Centrifugation

The disc stack centrifuge is one of the most commonly employed machines for the separation of biological materials in the biotechnology industry. Applications include the separation of cells from fermentation broth (Higgins *et al.*, 1978; Datar and Rosen, 1987), the removal of cell debris after cell disruption (Mosqueira *et al.*, 1981; Clarkson *et al.*, 1993), and the recovery of inclusion bodies (Jin *et al.*, 1994) and precipitates (Bell *et al.*, 1983; Clarkson *et al.*, 1996b).

The disc stack centrifuge consists of a bowl containing a series of discs around a central cone. During centrifuge operation the bowl is spun and liquid flowing through the discs is split into thin layers, with the sedimenting solids being thrown outwards, impinging on the underside of the coned discs and collected on the bowl wall (Figure 1.5 overleaf). This configuration provides a large settling area and a constant flow path which, unlike the tubular bowl or chamber centrifuges, is not reduced by the sedimenting solids (Atkinson *et al.*, 1987). The flow between the discs is also usually laminar which makes particle settling easier and drastically reduces the settling distance (Axelsson, 1985). However, high shear forces may exist in the centrifuge feed zone which can damage shear sensitive materials (Mannweiler *et al.*, 1989).

Solids retaining disc stack centrifuges are operated in a semi-batch manner, while intermittent-discharge disc stack centrifuges achieve continuous operation using a hydraulic bowl opening mechanism which allows for periodic discharging of the collecting solids. Nozzle disc stack centrifuges use nozzles fitted to the bottom of the bowl to continuously discharge the collecting solids. Disc stack centrifuges develop a relative centrifugal force (Section 7.2.1) in the range of 5,000-15,000 g (Brunner and Hemfort, 1988) and are operated on the industrial scale with bowl capacities of up to 60 L (Wheelwright, 1991). Flowrates through these centrifuges of up to 150,000 $L.h^{-1}$ are possible, compared to 15,000 $L.h^{-1}$ and 600 $L.h^{-1}$ for chamber centrifuges and tube centrifuges respectively (Wheelwright, 1991).

Important factors which effect the performance of a disc stack centrifuge are:

- the properties of the material being separated, which include the particle size, the density difference between solid and liquid phases, the suspension viscosity and the particle concentration.

- the centrifuge design and operating conditions, which include the number of discs and disc design, the bowl capacity, the discharge type and frequency, the bowl speed and the flowrate.

Centrifugation equipment currently used in the production of proteins and the biotechnology industry in general has mostly been adapted from existing centrifuge designs. Modifications which have been made include the use of contained systems to prevent the release of aerosols, bowl cooling to prevent thermal damage of heat sensitive materials, the introduction of "soft" feedzones to prevent air-liquid interfaces which cause shear damage, improved metallurgy to achieve higher acceleration forces and the capability of clean in place (CIP) and steam sterilisation (Erikson 1984).

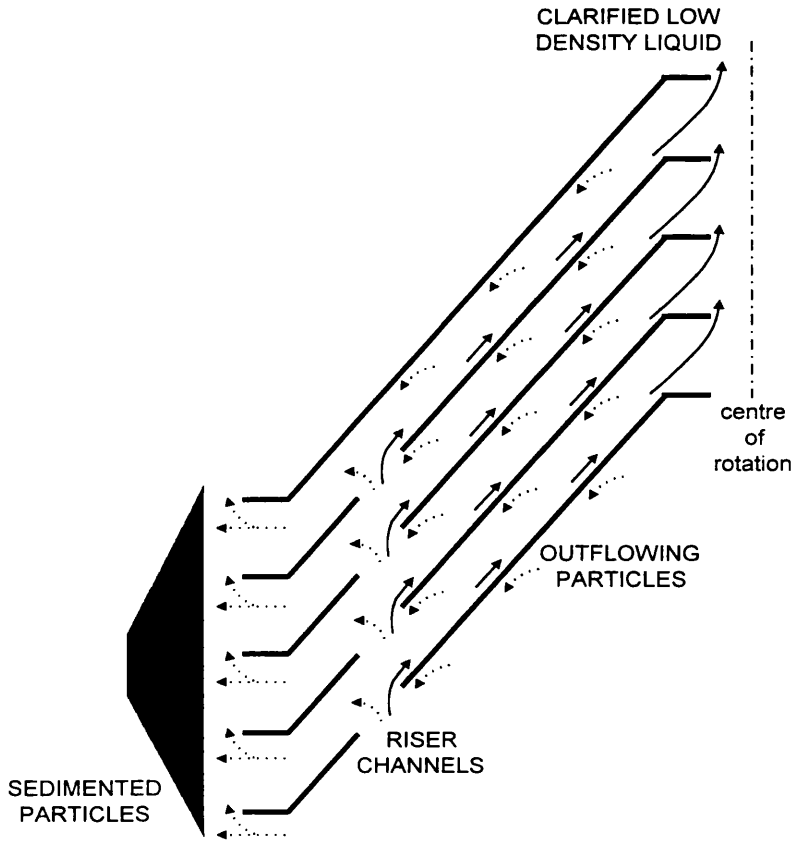

Figure 1.5: Flow of liquid and particles within the discs of a disc stack centrifuge.

1.3 Impact of Recombinant Techniques on Downstream Processing

1.3.1 Protein Production from Recombinant Cells

The ability to modify an organism through the manipulation of its genetic material, known as genetic engineering, has great potential to improve the production of proteins. It is now possible to develop "recombinant" cultures which are capable of producing valuable proteins such as human insulin, human growth hormone, interferon, antibody fragments, vaccines and industrial enzymes. Large scale microbial fermentations can then be used to produce these proteins, thereby increasing production volumes while lowering costs. The rate of protein production within cells, its location, control and the structure of the protein itself (Section 1.3.2) can also be modified to increase production, simplify downstream processing and reduce costs. Although the use of recombinant systems in the production of proteins can give many benefits, a number of safety and regulatory issues must also be considered.

The advances which have contributed to the development of genetic engineering given by Brock *et al.* (1988) include:

- the understanding of the composition and structure of deoxyribonucleic acid (DNA), the genetic material of cells.

- the understanding of the synthesis of proteins within cells and the role of DNA in this process.

- the development of procedures for the isolation, sequencing and synthesis of DNA.

- the discovery of restriction endonuclease enzymes, DNA ligases and DNA polymerases which can be used to manipulate DNA.

- the discovery of transformation methods, which allow free DNA to enter cells.

- the discovery of plasmids, DNA vectors which are capable of independent replication.

In terms of downstream processing, most of the advantages of a recombinant protein are due to its relative abundance with respect to contaminating proteins, especially when produced in bacterial or yeast systems (Heinrikson and Tomasselli, 1991). To ensure that this occurs it is essential that the protein is properly expressed or, if possible, overexpressed. The choice of a host organism is therefore important, since the correct replication of plasmids and their structural stability are influenced by the rate of mutation and the gene repair facilities of the host (Flaschel and Friehs, 1993). The type of plasmid used will also have an affect. By using so called multi-copy plasmids, for example, the number of plasmids per cell and hence the rate of gene expression can be increased. Incorporation of more than one copy of a gene into the plasmid may also increase the rate of expression.

To achieve efficient protein synthesis from a given gene, it is also essential to insert a promoter-operator system and termination sequence into the plasmid. The use of a strong promoter will give a high transcription rate. The control of transcription can be achieved by using an inducible promoter-operator system. In this case certain conditions, such as the introduction of a chemical or temperature change, are required for transcription to occur. Synthesis of a recombinant protein can then be induced only after the growth phase of the culture is complete, thereby avoiding possible breakdown of the desired product during cell growth. The best known inducible promoter-operator systems are those using operators derived from the lac system (which normally controls β-galactosidase and is induced using isopropylthiogalactoside), the trp system (which normally controls tryptophan synthetase and is induced using indolylacrylic acid) and the lamda system (which normally regulates lamda virus production and is temperature induced) (Flaschel and Friehs, 1993).

In order for sustained production of a recombinant protein during culture it is important that there is no plasmid loss from one generation of cells to the next, i.e. that plasmid stability remains high. Both the genetic design of recombinant systems and the culture conditions used effect plasmid stability (Kumar *et al.*, 1991). Use of a small plasmid reduces the metabolic burden on the host, while the inclusion of antibiotic resistance genes in the plasmid and addition of antibiotic to the culture medium will select for plasmid containing cells. Nutrient and oxygen limitation have been found to be detrimental to

plasmid stability, while the use of complex growth medium has been found to stabilise some plasmids during cultivation (Kumar *et al.*, 1991).

After the synthesis of a recombinant protein, the stability of the protein in the host cell will determine the level of obtainable protein product. This largely depends on the susceptibility of the protein to proteolytic decomposition (Flaschel and Friehs, 1993). Strategies for reducing or preventing proteolysis include the selection of mutation strains which are protease deficient or the deletion of genes for proteins which regulate proteolysis such as ubiquitin. Sinclair (1997) has shown an 8 fold overexpression of the enzyme alcohol dehydrogenase-II using a recombinant strain of *Saccharomyces cerevisiae* in which the gene for ubiquitin-4 production has been deleted.

Although it is difficult to predict what will happen when a mammalian protein is expressed in a bacteria, in many cases the protein aggregates together to form insoluble aggregates known as "inclusion bodies". In the case of yeast, proteins may also aggregate into small particles with antigenic properties known as virus like particles (VLPs). Expression of hepatitis B surface antigen in yeast results in the formation of VLPs which are processed to produce a vaccine preparation against hepatitis (Goodey *et al.*, 1987). Proteins contained in inclusion bodies are largely resistant to proteolysis (Brewer *et al.*, 1991). Inclusions also offer advantages for downstream processing, since they can easily be separated from other intracellular proteins. The reason why inclusion bodies form appears to be related to a high rate of expression and the inability of the protein to fold into the correct structure in the physiological conditions inside a bacterial cell (Brewer *et al.*, 1991). The main disadvantage of inclusions is that, because the protein is produced in a biologically inactive form, refolding is required to give the protein the correct structure. As part of the refolding procedure, the insoluble protein in the inclusion bodies must be denatured under extreme conditions in order to become solubilised (Flaschel and Friehs, 1993).

An alternate method of preventing proteolysis of a recombinant product is for the protein to be exported out of the host cell. This approach may also be required for proteins which are lethal for the host when overproduced. The production of an extracellular product instead of an intracellular product has the potential to reduce the number of downstream processing operations, unless it is very dilute or in a dirty medium. However, a secreted

protein may also be incorrectly folded, especially in the case of eukaryotic proteins synthesized by bacteria (Flaschel and Friehs, 1993). Transport of the protein into the periplasm of Gram negative bacteria is also possible. In the case of *Escherichia coli*, the periplasmic space represents 20 to 40% of the cellular volume and is large enough to accumulate high levels of protein. The application of gentle disruption techniques which only remove the cell capsule and outer membrane can then prevent contamination by proteolytic enzymes and other contents of the cytoplasm. For protein secretion to occur, the gene of the desired protein product must be coupled with an appropriate sequence of bases called a "signal leader" which, when translated to a polypeptide chain, initiates protein transport. The host organism must also have an appropriate transport system and the recombinant protein cannot have any properties which prevent secretion.

Many natural proteins, in particular eucaryotic proteins of pharmaceutical interest, require post-translational modifications to form the biologically active protein. Such modifications may consist of phosphorylation, glycosylation, the cleavage of sequences which enable protein secretion or the cleavage of the primary protein chain (Flaschel and Friehs, 1993). Although the transfer of genetic material from eucaryotic organisms to bacteria can readily be achieved and large amounts of protein obtained as a result, bacteria are not able to glycosylate the protein. If glycosylation is crucial for biological activity, another host system such as yeast may need to be used. However, although yeast cells have the ability to glycosylate proteins, they may use different glycosylic residues than those required. Because it is still not possible to use genetic engineering to incorporate post-translational modification into bacterial and yeast expression systems, cells of animal or human origin remain the system of choice for producing proteins requiring post-translational processing (Flaschel and Friehs, 1993).

Some important safety and regulatory issues must be considered when a recombinant system is to be used to produce a protein. These issues relate to:

- the ability of the recombinant system and subsequent recovery process to produce a consistent product.

- the effect of the recombinant organism and protein on the environment and operating personnel during production.

- the effect of the final protein product on the end user. This is particularly important in the case of proteins intended for human use.

Because the synthesis of a recombinant protein takes place intracellularly it cannot be controlled directly but only through environmental parameters such as temperature, oxygen supply, pH, metabolic products, phosphate regulation or feed back inhibition (Werner and Langlouis-Gau, 1989). Concerns may therefore arise over the stability of the system. This is illustrated by the production of tissue plasminogen activator (t-PA). Depending on the conditions a one chain t-PA or two chain t-PA can be synthesized, while preferentially glycosylated or sialic acid free t-PA may also be obtained (Werner and Langlouis-Gau, 1989). Because of this, characterisation of recombinant cell lines and validation of recombinant protein production process is required to maintain a consistent product. Process validation involves providing a written protocol for the validation procedure, including the number of runs that will demonstrate reproducibility, and documentary evidence of the suitability of materials, the monitoring of process variables and the performance and reliability of systems and equipment (Giorgio, 1988). Obtaining regulatory approval for the recombinant protein will depend on carrying out these steps. It is important to note, however, that regulatory approval will be given for the recombinant product and the specific process that produced it (Spalding, 1991). It is therefore essential that there is a high degree of confidence in the final design since any major change to the as-built process will require re-validation and re-approval.

The release of a genetically engineered organism into the environment has the potential to cause harm since unforeseen interactions can occur with natural organisms. Although there is currently no evidence of this actually occurring, it may be possible for a released bacteria which contains the plasmid for a recombinant protein to transfer this plasmid to a strain of bacteria naturally resident in humans, resulting in allergic reactions or disease. The likelihood of this scenario would be much greater if the released organism has the ability to survive outside the production environment. The host organism may itself also be toxic or pathogenic. Both fermentation and downstream processing operations may release bacterial or DNA fragments unless steps are taken to contain the material being processed. Recombinant organisms used in industrial processes generally have very low risk levels and/or a history of safe industrial use (Miller and Bergmann, 1993). For example, commercial *Escherichia coli* K-12 strains, used to produce human insulin and

human growth hormone, do not show any evidence of gene transfer and the high cell densities used during production give no advantage for surviving in the outside environment (Kane, 1993). However, a conservative approach to risk is taken in the biopharmaceutical industry and containment levels above those required are often used (Miller and Bergmann, 1993).

For recombinant proteins used as human pharmaceuticals and therapeutic agents it is often essential that the final product is identical to the natural protein to avoid allergic reactions in the user. However, this is often not the case for recombinant proteins produced by bacteria since the methionine at the N-terminus of the protein may be formylated to a variable extent (Brewer *et al.*, 1991). The authentic protein can be recovered by adding a particular sequence of bases at the start of the appropriate gene which, when translated, will give a chain of amino acids that are cleaved by a given enzyme. For example, Brewer *et al.* (1991) cite the case of recombinant human growth hormone produced with a N-terminal sequence cleaved by aminopeptidase I to give the authentic growth hormone. The absence of post-translational modifications in the products of bacterial and yeast systems may also make a recombinant protein unsuitable for use. The regulatory approval and licensing of a recombinant protein will depend on demonstrating the effectiveness of the product and a lack of adverse reactions.

1.3.2 Protein Engineering

The field of protein engineering has been described by Brewer *et al.* (1991) as the application of scientific knowledge to the practical design and construction of proteins. Some common aims of protein engineering are to:

- alter the action of a protein so that a more desirable action is obtained.
- allow a protein to function in a new environment in which protein action is desired.
- simplify the recovery of a protein to lower costs and/or reduce production time.
- allow the isolation of a protein in an active form thereby lowering costs and/or reducing production time.

These aims are typically achieved by modification of a natural protein through the alteration of its amino acid sequence or the attachment of an additional polypeptide chain.

Site-directed mutagenesis is a method of producing very specific changes in the amino acid sequence of a protein. It involves synthesizing a short DNA fragment containing the code for the desired change to the amino acid sequence and allowing this to pair with a single-stranded DNA containing the gene which expresses the protein of interest. The short single-stranded fragment of synthetic DNA is then extended using the enzyme DNA polymerase which copies the rest of the gene. The double stranded DNA molecule produced will be complete except for the short region of mismatch. This is then inserted into a host cell by transformation so that the modified DNA can be incorporated. Mutants producing the protein with the desired change are then selected. Brewer *et al.* (1991) describe the use of this technique to enable β-interferon to be isolated in an active form. The β-interferon was produced in an inclusion body and could not be refolded to the correct specific activity because it preferred to form the wrong disulphide pair. Site-directed mutagenesis was used to replace the miss pairing cysteine with a serine. This allowed the recombinant protein to be isolated with the correct activity.

Weijers and Van't Riet (1992) have described how the replacement of serine and threonine residues by cysteines in the enzyme substilisin increased thermostability, while the replacement of a methione residue by serine, alanine or leucine increased stability against oxidation although catalytic activity also decreased. Creaser *et al.* (1990) and Murali and Creaser (1986) have used site-directed mutagenesis to increase the activity of yeast alcohol dehydrogenase I towards alcohols larger than ethanol. This was achieved by replacing two amino acids in the substrate pocket with smaller amino acids, thereby increasing the size of the substrate pocket which enables the enzyme to oxidise larger alcohols. It should be noted that the structure of alcohol dehydrogenase has been widely studied in a number of organisms and that part of the full amino acid sequence is known for yeast (Williamson *et al.*, 1980). This highlights the point that a rational and consistently successful approach to protein engineering using site-directed mutagenesis requires a high level of understanding about the protein in question or alternatively a particularly simple strategy (Arnold, 1993).

When less is understood about the protein to be engineered, an alternate approach is to use random mutagenesis in conjunction with screening. This involves causing random

mutations in the gene expressing the protein by exposing it to radiation or chemical agents, thereby producing changes in the protein's amino acid sequence. Testing of the protein obtained from specific mutants is than carried out to see if it displays the desired behaviour. Screening is employed rather than selection (the survival of only those cells producing the protein with the property of interest) since the organisms producing the protein may be damaged or killed by the non-natural environments (Arnold, 1993). This method is well suited to producing proteins with features not required in vivo, thereby allowing these proteins to function in new and unusual environments. Examples listed by Arnold (1993) include α-amylase from *Bacillus licheniformis* produced with enhanced thermal stability and improvements in the activity of substilisin E in high concentrations of the organic solvent dimethyl formamide.

Recombinant DNA techniques can be used to insert the DNA coding sequence for a polypeptide chain into the gene expressing a given protein, thereby producing a "fusion protein", i.e. the natural protein with an attached polypeptide chain (Figure 1.6).

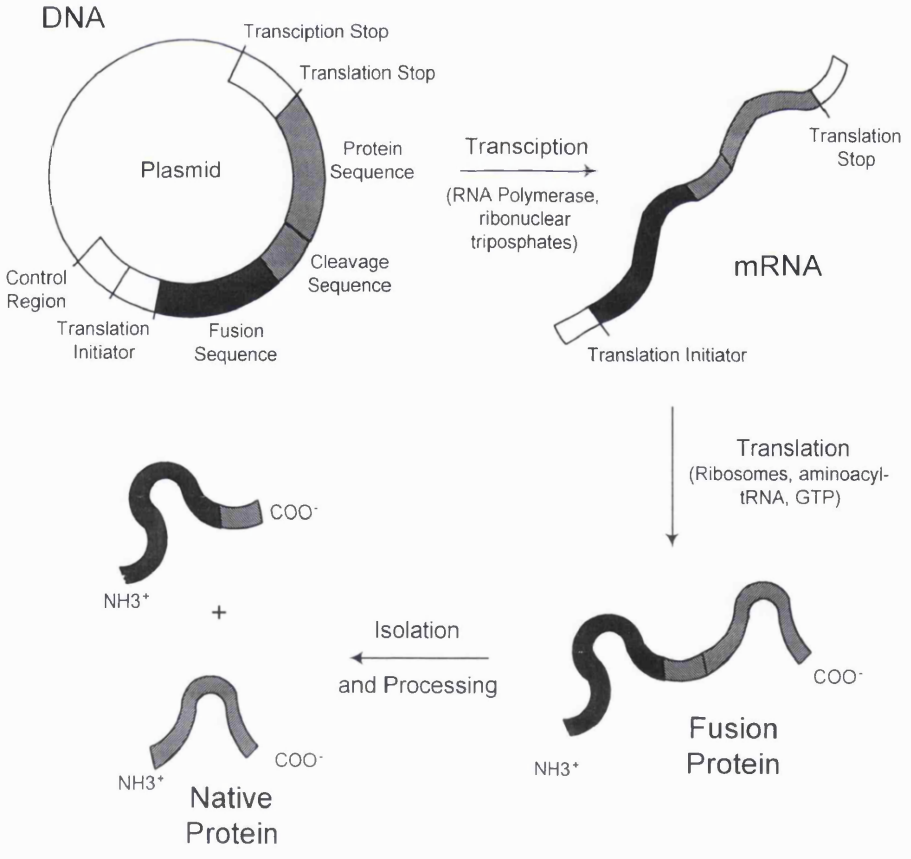

Figure 1.6: Synthesis and isolation of fusion proteins produced by bacteria, from Brewer et al. (1991).

Depending on the effect on protein behaviour and the eventual use of the protein, this modification may either be permanent or temporary. For example, if a protein is to be used as a diagnostic reagent or in a biochemical transformation and the modification does not reduce catalytic activity or specificity, respectively, it can be left in place. However, if the protein is to be used as a pharmaceutical and the modification will produce additional toxicity, the attached polypeptide chain must be removed before use. This can be achieved by including the DNA sequence for a cleavage site at the start of the DNA sequence of the additional polypeptide. Proteases which cleave peptide bonds within polypeptide chains (endopeptidases) or sequentially digest amino acids from the C or N terminus (exopeptidases) or chemical methods can then be used to remove the polypeptide extension and allow the native protein to be produced free from any extra amino acids (Brewer *et al.*, 1991).

The presence of an additional polypeptide chain can be exploited to allow the separation of the "fusion protein" to a high purity at large scale and/or with lower cost. For example, Brewer *et al.* (1991) describe an eight amino acid sequence which has been designed to combine a four residue antigenic site with an overlapping enterokinase cleavage site which enables the purification of a fusion protein with this peptide attached to the N terminus by immunoaffinity chromatography. Once the purification is complete, the enzyme enterokinase can be used to cleave the immunoaffinity sequence at the C terminus, thereby producing the natural protein free of any additional amino acids.

Brewer *et al.* (1991) also describe a fusion protein which contains a sequence of three charged amino acids at the C terminus which make the protein unusually acidic or basic and facilitate its purification by ion exchange chromatography. Because the additional amino acids are hydrophillic they extend away from the protein and therefore have a minimal effect on protein refolding and biological activity. For the case of C terminal arginine or lysine fusions the enzyme carboxypeptidase B can be used to specifically digest these amino acids while stopping when any other amino acid is reached. Provided the C terminal amino acid is not lysine or arginine the native protein can therefore be produced.

It should be noted that an increase in processing steps is required to remove a fusion utilised during purification. This means that the application of this type of protein

engineering may not be appropriate where a temporary fusion is required (such as for pharmaceuticals) and cost is a major concern. However in areas such as the production of bulk diagnostic enzymes and transformation proteins, permanent small hydrophilic fusions as described above which have little or no effect on protein structure or function should become widely used to improve and simplify production.

1.4 Bioprocess Simulation

Simulation has been used for many years in the chemical industries as a valuable tool for the design and operation of efficient, cost effective processes. In the bioprocess industry, the use of simulation is still a relatively new approach but it is becoming increasingly used as the demands on the performance of biochemical processes grow. For protein downstream processes, which often make up the significant proportion of total production costs, simulation is becoming recognised as an aid to achieving optimal process design and operation. By reducing the cost and time of process development, simulation can also play a crucial role in the success of a protein product.

1.4.1 Process Simulation

Process simulation or "flowsheeting" has found widespread use in the chemical industries for the evaluation and optimisation of process designs and the investigation of plant operation. A process simulation is carried out using computer models which mathematically describe the actions of major items of equipment or unit operations in a process thereby enabling mass and energy balances to be performed. The models may be performance based, i.e. feed stream information and equipment parameters are supplied and product stream information calculated, or design based, i.e. a combination of feed and product stream information relating to equipment function are supplied so that design calculations such as sizing and costing can be carried out (Jackson and De Silva, 1985).

The simulation problem itself is defined by:

- specifying the flowsheet topology i.e. the way the models are connected

- providing physical property data or calculation procedures

- supplying the required feed stream information

- specifying equipment parameters or product stream information depending on the type of models used.

A process simulator is a computer program which sets up the simulation problem with the input of the user and then carries out its solution.

There are three different methods of solving the model equations within a process simulator:

- the sequential modular approach

- the equation-orientated approach

- a combination of the sequential modular and equation-orientated approaches.

Sequential modular simulators were first developed in the late 1950's for use in the petrochemical industry (Biegler, 1989). In the sequential modular approach the output of each unit is calculated as a function of the input variables. The unit models are solved one after the other so that the calculation sequence parallels the flow of material in the actual process. Since each unit model is a self contained module, a large flowsheet can be constructed very quickly simply by specifying unit connections. The model equations within each unit module can also be altered, from simple to more rigorous, with minimum changes to the flowsheet topology. The main problem with this method is that awkward iteration loops are required when there are recycle streams and when design or optimisation calculations are performed (Biegler, 1989). The simplified structure of a sequential modular simulator is shown in Figure 1.7 overleaf.

In the academic community, most early research in process simulation was devoted to the equation-orientated approach (Biegler, 1989). In this approach, all of the unit equations are collected together and solved simultaneously. Flowsheets containing recycle streams

or design constraints can therefore be solved more easily with an equation-orientated approach than a sequential modular approach. The large amount of derivative and function information available in an equation-orientated simulator also allows more sophisticated optimisation strategies to be applied. However, this approach is limited by the capabilities of the equation solver, typically a Newton-Raphson method, and convergence failures may occur. The simplified structure of an equation-orientated simulator is shown in Figure 1.7.

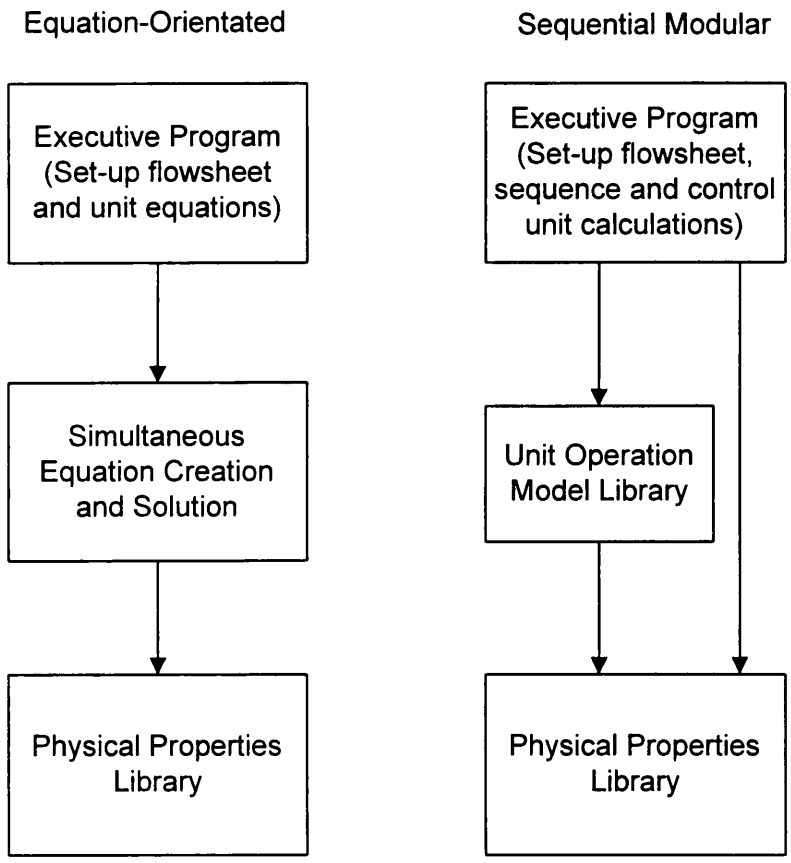

Figure 1.7: Structure of process simulators, from Biegler (1989).

By the late 1970's and early 1980's, combinations of the sequential modular and equation-orientated approaches were developed (Biegler, 1989). In simultaneous modular simulators, the sequential modular approach was modified to incorporate simultaneous solution of the streams connecting the unit modules, although the unit modules themselves remained intact. Equation-orientated approaches were also modified to include procedural sub-modules for the calculation of physical properties which linked in with the equation solver. The development of these new approaches was aided by the application of quasi-

Newton convergence methods, which require less derivative information than previously used Newton-Raphson methods but have a much faster convergence rate than sequential modular iteration loops (Biegler, 1989).

It is also possible to carry out two different types of process simulation, known as steady-state and dynamic. In steady-state simulations the equations which make up each unit model are algebraic and therefore can only describe continuous processes at steady-state conditions. On the other hand, in dynamic simulations the equations used are both ordinary differential equations and algebraic equations. This means processes which display transient behaviour, such as batch operations, can be described. Due to the complexity of dynamic systems, as much as ten times more computer power is required to solve the model equations then in steady-state simulations (Hunter *et al.*, 1989).

Most currently available process simulators perform steady-state simulations and utilise the sequential modular approach for solving the unit model equations, with options for simultaneous modular convergence. Examples include ASPEN-Plus, DESIGN-II and PROCESS (Biegler, 1989) which are available in PC versions.

Process simulators capable of dynamic simulation generally employ the equation-orientated approach. Examples of dynamic simulators are SPEEDUP, developed in the 1960's at Imperial College (Pantelides, 1988; Sargent and Westerberg, 1964), QUASILIN (Smith and Morton, 1988) and more recently gPROMS (Pantelides and Barton, 1993).

Many of the available simulators capable of steady-state simulation have been extended to allow dynamic simulations of some unit operations. New "hybrid" simulators are also being developed that combine steady-state and dynamic versions of a simulator in the one package (Fouhy, 1991). Major differences between the available process simulators also lie in their libraries of unit model equations and physical property data.

1.4.2 Simulation in Process Design and Operation

During the design of a new process, simulations provide the design engineer with predictions of stream compositions, required equipment sizes and operating conditions, and estimates of capital and operating costs for a potential flowsheet. As well as assessing

the feasibility of a given flowsheet, simulations can be used to optimise a process using case studies or numerical techniques such as successive quadratic programming (Gallier and Kisala, 1987) and to perform design calculations for individual unit operations.

In most design studies, steady-state simulation is used due to the lower requirement for computer power. The unit model equations are also simplified or ideal in most cases, and sizing and costing are usually noniterative calculations performed after convergence of the flowsheet (Biegler, 1989). With decreases in the cost of computer power and the growing complexity of process plants, dynamic simulation is also becoming increasingly used during the design stage to analyse the intrinsic controllability of a process and for the design of control systems (Pantelides and Barton, 1993). Dynamic simulation must be used for the design of batch processes, since time dependent behaviour is involved. The information generated by process simulation during the design stage reduces the time required to explore the effect of design changes and different operating conditions. More productive, efficient and safer processes can therefore be developed in a shorter time.

However, it should be highlighted that in existing process simulators the flowsheet topology must be specified before a simulation can be carried out. The task of deciding exactly which unit operations to use and how they should be connected to form the flowsheet is referred to as process synthesis (Stephanopoulous and Townsend, 1986). Expert systems (computer programs which apply the technique of logical inference to a knowledge base) can be employed to carry out the process synthesis task (Niida *et al.*, 1986; Siletti, 1988; Asenjo *et al.*, 1989; Turner *et al.*, 1994). Process simulation can also be used to choose between unit operation alternatives and examine the affect of changes in a flowsheet by using case studies to compare feasibility and perform sensitivity analysis. The development of graphical user interfaces that allow user interaction during simulations and the inclusion of database facilities within process simulators that can record and analyse simulation results will enable design engineers to carry out these case studies in less of an ad-hoc manner.

Shaw (1992) has suggested integrating process simulation and other process design tasks into a single environment called an "Engineering Toolkit" that allows full electronic transfer of data between the process simulator and other facilities using a process flow diagram representation as the interface. Stephanopoulous *et al.* (1987) have described an

object-orientated software support environment for process design called DESIGN-KIT which incorporates process simulation and process synthesis. However, Stephanopoulous (1990) has pointed out that computer-aided design environments containing database management systems "do not know" how the design is done and still require the guidance of a human designer. Application of the work of such as that of Pohjola *et al.* (1994) on a procedural model of the design process itself may one day lead to expert systems that can actually direct the design task.

For investigations of process operation, dynamic simulation is generally used since transient behaviour often occurs. Traditional applications include the study of the response of a continuous process to deviations from steady-state conditions and the tuning of controllers (Pantelides and Barton, 1993). There are increasing applications of dynamic simulation in performing hazard and operability studies, determining appropriate start up and shut down procedures, testing of control schemes and automatic emergency control procedures, for trouble shooting during production, and for operator training. Dynamic simulation is also used for on-line measurement and optimisation. Table 1.2 overleaf shows applications of dynamic simulation from conception to normal operation of a process plant (Naess *et al.*, 1993).

One of the main obstacles for efficient application of dynamic process simulation, especially in control and operator training when real time or faster simulation are needed, has been the lack of computing power (Moe and Hertzberg, 1994). This has also been a problem for both steady-state and dynamic simulations involving rigorous unit models (Haley and Sarma, 1989). The use of advanced computer architectures, such as supercomputers or parallel computers, has been one way to obtain the required computer power. Haley and Sarma (1989) found that the steady-state simulator PROCESS was an average 10.5 times faster on a Cray supercomputer than on a VAX mainframe and concluded that it was possible to transfer simulator software from a mainframe computer to a supercomputer. Moe and Hertzberg (1994), in a review of the application of advanced computer architectures in dynamic simulation, concluded that using parallel computers with equation-based simulators showed great potential for speeding up simulations. However, they pointed out that simulators should be programmed without attention to underlying computer architectures to increase their lifetime.

Project Phase	Examples of Activities
Feasibility	Screening Concepts Operability Analysis
Conceptual Design	Capacity Planning Check Safety Margins
Basic Engineering Detailed Design	Process Design Control System Equipment Design Integrated Design Scheduling
Commissioning and Take Over Startup	Operator Training Develop Test Procedures Initial Tuning Develop Operating Procedures Screening Alternatives
Normal Production	Trouble Shooting Revamp Studies Optimisation Increasing Operability

Table 1.2: Application of dynamic simulation in various project phases, from Naess et al. (1993).

Another development which will enable a more realistic description of the actual behaviour of process plants is stochastic simulation. This form of simulation includes a degree of randomness in the unit model input parameters and thereby accounts for uncertainty in the design and operation of a process. A new stochastic modelling block has been described for the ASPEN-Plus steady-state simulation package while a module providing random functions for gPROMS has been developed (Naf, 1994).

An alternate approach to describing plant behaviour which avoids the use of rigorous dynamic models is known as qualitative simulation. This form of simulation uses variables that can be in different states rather than having a numerical value. For example,

in the simplest one-dimensional case a variable has three possible states; -,0,+. To take into account dynamic behaviour this form of simulation uses qualitative derivatives that describe the evolution of a variable as increasing, decreasing or steady. The qualitative simulation then predicts trees of possible states of the process in time (Muratet and Bourseau, 1993). Qualitative simulation has been used by Oyeleye and Kramer (1988) to simulate the effects of equipment malfunctions on a process model.

1.4.3 Possible Improvements to Process Simulators

Some of the major areas of improvement among commercial simulators listed by Hunter *et al.* (1989) include increasing the user friendliness of the interfaces, extending the libraries of ready-made unit models, lowering the cost of hardware, improving the methods for solving the model equations and introducing diagnostic functions to troubleshoot plants.

Robertson (1989) has described the ideal process simulator as an easy to learn and interpret, user friendly, stand-alone software package that requires no manuals. The ideal process simulator should also be able to formulate reports and would include a database manager, stacked menus with user advice, and optimisation, uncertainty analysis and data reconciliation utilities. Robertson (1989) also makes the valid point that, even if the ideal process simulator is built, the ultimate design and operation of a process is still the ethical responsibility of the engineer and process operator - not the simulator.

1.4.4 Simulation of Biochemical Processes

Although process simulation has been used for many years in the chemical industry, it is still a relatively new approach in the bioprocess industries (Evans and Field, 1988). Reasons for this suggested by Narodoslawsky *et al.* (1993) are that bioprocesses were thought to be too complex for simulation programs and that bioprocess development is usually carried out in a more empirical fashion than chemical engineering design.

Some of the many advantages in carrying out simulations of biochemical processes are:

- it can reduce the time needed to take a biological product to market, which is vital for economic success (Petrides *et al.*, 1989). This is especially so for products with a limited patent life.

- it lessens the need for costly and time consuming pilot-plant trials during the design stage (Evans and Field, 1988).

- it increases the fundamental understanding of a bioprocess and can be used to improve the process knowledge of engineers and operators (Bhattacharya, 1993).

- it provides a consistent communication format between research, development and production which is a key to bringing new products to market and dealing with regulatory issues (Bhattacharya, 1993).

- it can provide confidence in the final design of a bioprocess and assess the benefit of process modifications. This is important for recombinant products since any major change to the as-built bioprocess will require re-validation and a new regulatory approval.

- it can provide higher economic and ecological efficiencies for bioprocesses (Narodoslawsky *et al.*, 1993).

Some of the problems that are encountered with the simulation of bioprocesses have been outlined by Cooney *et al.* (1988) as:

- there are many unit operations in the bioprocess industry that are not found in the chemical industry. These unit operations are poorly understood and, in many cases, no predictive models are available.

- there is a lack of physical property information for many biological materials.

- interactions exist between many unit operations in bioprocesses that are difficult to incorporate into simulations.

- there is a prevalence of batch and semi-batch unit operations in biochemical flowsheets.

Two approaches for the development of a bioprocess simulator have been considered by Gritsis and Titchener-Hooker (1989). The first approach is to adapt an existing simulation package developed for chemical process design by including unit models and physical property data specific to biochemical processes. The second is to use research information and data to develop models for biochemical unit operations and processes which can be solved using general purpose numerical techniques and simulation tools.

Evans and Field (1988) concluded that the first approach was the best since a large amount of effort would be required to duplicate the facilities already available in existing process simulators. Cooney *et al.* (1988) used this approach to develop a bioprocess simulator by adapting the sequential modular simulator ASPEN-Plus. This work lead to ASPEN Tech's BioProcess Simulator (BPS) the first commercially available simulation package specifically for the bioprocess industry (Grob, 1993; Bhattacharya, 1993). BioPro Designer, a new computer-aided bioprocess design tool available from Intellicorp (Petrides, 1994), contains a similarly developed simulator linked to an expert system for process synthesis via a user interface. The main disadvantage of this approach is that the structure of most existing process simulators developed for use in the chemical industry is unsuitable for the simulation of biochemical processes. The sequential modular architecture on which most existing simulators are based has limited ability to deal with batch processes and process interactions, the physical property calculation procedures in the simulators may not be applicable to bioprocesses, and the model building and predictive capabilities of the existing packages are restricted.

Researchers at UCL have adopted the second approach since it allows interactions between biochemical unit operations to be incorporated into the models and there is less restriction on model development. Gritsis and Titchener-Hooker (1989) demonstrated how this approach can be used to simulate the downstream processing of proteins. Examples of existing simulation packages suitable for use in this approach are SPEEDUP and gPROMS. Both of these simulators are equation-orientated, support model building and have a dynamic capability which enables them to deal with batch operations. Clarkson *et al.* (1992, 1996a, 1996b) have used SPEEDUP for the simulation of fractional precipitation and centrifugation, while Lu *et al.* (1994) have used gPROMS to simulate a

recovery sequence for intracellular proteins which included both batch and continuous operations. SPEEDUP has also been used by Ahtchi-Ali (1989) to study the performance of batch, fed-batch and continuous fermentations and by Barford *et al.* (1992) to simulate the continuous culture of *Saccharomyces cerevisiae.*

A third approach to the development of a bioprocess simulator is to produce a completely new software package with a structure more suited to the simulation of biochemical processes. Narodoslawsky *et al.* (1993) have used this approach to develop the SIMBIOS simulator for use in the design of bioprocesses. The main feature of this simulator is that both approximate linear models and rigorous models are used. Linear models for most of the common biochemical unit operations are included, however it is unclear which rigorous models are available. The predictive ability of the models within the simulator is also uncertain. Simon *et al.* (1994) have included physical property calculation procedures for pure compounds and their mixtures within the SIMBIOS simulator but it is as yet unable to estimate the properties of biomaterials.

A knowledge based software package with a novel structure called CAMBIO has also been developed by Farza and Cheruy (1993) for the simulation of biochemical processes. The package enables the user to build up models of biochemical reactions using a graphical interface. The information in the graphical model is then used to formulate dynamic material balance equations which are solved to provide a simulation of the biochemical process. The application of CAMBIO was demonstrated by Farza and Cheruy (1993) using an anaerobic digester process as an example. However, the use of this software package as a bioprocess simulator is limited since the descriptions of biochemical reactions obtained are relevant to the fermentation stage of a bioprocess and are not generally applicable to downstream processing operations.

1.4.5 Application of Simulation to Protein Downstream Processing

In recent years there has been increasing interest in the application of simulation, and computer techniques in general, to improve the design and operation of protein downstream processes. This has come about because the downstream process often forms the major cost in the production of a protein and its optimisation therefore represents a way for biotechnology companies to maintain a competitive advantage (Wheelwright,

1986). However, the bioprocess industry has traditionally used empirically based methods for the design of downstream processes, such as the scale-up of laboratory processes via a pilot-plant, and relied on labour-intensive techniques during protein manufacture which are often time consuming and/or expensive. The large number of alternatives currently available for each stage of a downstream process (Section 1.2), the increasing use of recombinant systems (Section 1.3) and commercial pressures which call for a bioprocess to be developed in a shorter time and at lower cost have also added to the difficulty of producing an optimal downstream process.

Attempts to rationalise the design of protein downstream processes have been made by Bonnerjea *et al.* (1986), Wheelwright (1986), Titchener-Hooker *et al.* (1991) and Leser and Asenjo (1992). This has led to a consolidation of the knowledge required for design and opened the way for an increasing use of computer tools in this area. Leser and Asenjo (1992) concluded that expert systems could be very useful for the synthesis of protein downstream processes and their application has been examined by Stephanopoulos and Stephanopoulos (1986), Siletti (1988), Asenjo *et al.* (1989) and Turner *et al.* (1994). At the synthesis stage of design, simulation can also be used to choose between alternative operations (Leser and Asenjo, 1992) and to examine the effect of changes in the sequence of operations using case studies.

Once synthesis is completed and a downstream processing sequence has been proposed, simulations can be used to assess the feasibility of the process by predicting product purity and yield, calculating required equipment sizes and estimating capital and operating costs. Optimisation of the process is also possible through the use of case studies or numeric techniques such as successive quadratic programming (SQP) and the effect of interactions within the process can be examined by simulating multiple operations.

Published work on the application of simulation to the design of protein downstream processes is reviewed below. The general purpose dynamic simulator SPEEDUP has been used to carry out simulations of downstream processes by:

- Gritsis and Titchener-Hooker (1989), who optimised a protein processing sequence consisting of ultrafiltration, precipitation and centrifugation using SQP to give the minimum processing time.

- Middelberg *et al.* (1989), who simulated the centrifugal recovery of porcine growth hormone inclusion bodies to find the best operating conditions for inclusion body separation. Middelberg *et al.* (1992a) also simulated interactions between the fermentation stage and subsequent homogenisation and debris removal stages used for inclusion body recovery. While Middelberg (1995b) used simulation to optimise protein refolding.

- Siddiqi *et al.* (1991), who simulated interactions between homogenisation and centrifugation and used a case study to demonstrate how conditions for efficient protein release and recovery can be optimised.

- Clarkson *et al.* (1992, 1996a, 1996b), who simulated fractional precipitation and centrifugation operations in the recovery of the intracellular enzyme alcohol dehydrogenase from bakers' yeast and carried out a case study to demonstrate how the recovery of precipitate particles could be improved. The importance of pilot-scale model verification was highlighted.

- Bogle *et al.* (1991, 1993), who simulated the production and recovery of porcine somatotropin inclusion bodies from *Escherichia coli* to optimise separation efficiency.

Lu *et al.* (1994) have also used the general purpose dynamic simulator gPROMS to simulate a typical downstream processing sequence for the production of intracellular enzymes. Wai *et al.* (1996) have used the dynamic simulator DYNSIM as part of an integrated approach to bioprocess design, with flowsheet simulations being used to test process feasibility and perform overall process optimisation. The model system under consideration was the recovery of bovine somatotropin, produced as an inclusion body by a recombinant *E. coli* strain. Samsatli and Shah (1996) have used a two stage approach to dynamically optimise the operation and then the scheduling of a typical intracellular enzyme recovery process. While Zhou *et al.* (1997) simulated a process consisting of a bakers' yeast fed-batch fermentation followed by cell harvesting, high pressure homogenisation and debris removal stages in order to examine process interactions using 'windows of operation', a graphical representation of the operational space determined by the system and engineering constraints (Woodley and Titchener-Hooker, 1996).

The chemical process simulator ASPEN-Plus has been used by Cooney *et al.* (1988) to simulate a downstream processing sequence consisting of vacuum filtration, ultrafiltration and spray drying for the recovery of a proteolytic enzyme. The effect of various operating conditions on the process economics was then examined, although no verification of user defined models was completed (Chapter 2.0).

While the application of Aspen Tech's BioProcess Simulator (BPS) to the design of downstream processes has been demonstrated by:

- Petrides *et al.* (1989), who simulated the production of porcine growth hormone (with the help of performance characteristics derived from laboratory and pilot-plant data) to perform simplified material balances and examine the economic feasibility of the process

- Healy *et al.* (1990), who used simulation as part of the development and design of a multi-product enzyme production plant

- Bhattacharya (1993), who simulated gel permeation chromatography for insulin separation and used case studies to examine the sensitivity of the process to elution flowrate.

BioProDesigner has been used by Petrides *et al.* (1995), who simulated a full production process for human insulin in order to enable equipment specification, calculate material balances, examine process scheduling and complete an economic and sensitivity analysis of the process. Most of the above work which has used the general purpose simulation packages SPEEDUP and gPROMS has focused on unit integration and/or optimisation and only part of the full downstream process has been simulated. On the other hand, the work with BPS and BioProDesigner has concentrated on analysing the economics and/or sensitivity of the full downstream process after steady-state material balances have been calculated.

The introduction of automation to protein manufacture, often incorporating modelling and simulation, is another way of producing a more optimal downstream process (Kossik and Miller, 1993). This involves utilising computer technology to add continuous process

monitoring, on-line measurement, automatic control and electronic batch scheduling to downstream processes, thereby making them semi-continuous (Ransohoff *et al.*, 1990). The benefits include increased productivity, lower operating costs, easier validation, better process control and improved safety. As in the chemical industry, the ability to perform real time dynamic simulation should also enable simulations to be used in the design and testing of control schemes, the development of operating procedures, operator training, trouble shooting during production and on-line optimisation (refer to Section 1.4.2). However, one obstacle which may need to be overcome before these applications are realised for protein downstream processes is the current lack of rigorous, predictive models (Chapter 2.0).

1.5 Experimental System

At UCL, bioprocess simulation and modelling studies have been carried out for the recovery of the enzyme alcohol dehydrogenase (ADH) from packed and fermented bakers' yeast using a typical downstream process sequence (Figure 1.2 on page 25). The reasons for utilising this experimental system are that, as a soluble intracellular protein product, ADH is typical of many industrially relevant proteins and biocatalysts and a large amount of data on the downstream processing of ADH from bakers' yeast already exists at UCL. Previous work using this experimental system includes:

- Hetherington *et al.* (1971) described an empirical model for the release of soluble protein from bakers' yeast during high pressure homogenisation. Follows *et al.* (1971) examined the release of intracellular enzymes from bakers' yeast during high pressure homogenisation. Siddiqi *et al.* (1995, 1996) developed a simulation describing the changes in debris particle size distribution of both packed and fermented bakers' yeast during high pressure homogenisation.

- Mannweiler (1989) developed a grade efficiency model to describe particle separation in a disc stack centrifuge. Clarkson *et al.* (1996b) developed and verified a simulation of disc stack centrifugation, based on the grade efficiency approach, for cell harvesting, debris removal and precipitate separation stages in a process for the recovery of ADH from bakers' yeast. The interaction between the high pressure homogenisation stage

and subsequent debris removal by disc stack centrifugation has been examined by Mosquiera *et al.* (1981) and Clarkson *et al.* (1993), and modelled by Zhou *et al.* (1997).

- Foster (1972) examined the ammonium sulphate precipitation of ADH and total protein from bakers' yeast homogenate. The fractional ammonium sulphate precipitation of bakers' yeast ADH has been examined and optimised by Richardson (1987). Niktari *et al.* (1989, 1990) described a semi-empirical model for the solubility of bakers' yeast ADH and total protein for use in control applications. Clarkson *et al.* (1996a) developed and verified a simulation for the fractional precipitation of ADH from bakers' yeast homogenate based on Niktari's model. Process interactions during fractional precipitation of ADH from bakers' yeast have been examined by Alsaffar *et al.* (1993).

- The scale-down of unit operations used in the downstream processing of ADH from bakers' yeast has been examined by Maybury (1997).

This experimental system has also been selected for further use in modelling studies of the downstream processing of a recombinant intracellular enzyme since a number of systems producing recombinant forms of ADH are available, namely:

- a yeast producing a protein engineered ADH which oxidises alcohols larger than ethanol at an increased rate compared to natural ADH (Creaser *et al.*, 1990; Murali and Creaser, 1986).

- a ubiquitin deficient yeast strain which overexpresses ADH (Sinclair, 1997).

- an *Escherichia coli* strain expressing a recombinant horse liver ADH (Van de Goor-Kucerova, 1992).

All of these recombinant systems are low risk, enabling existing facilities at UCL to be used for fermentations to produce recombinant material and for subsequent downstream processing studies. Characteristics of the recombinant strains and ADH's are described in Sections 1.5.1, 1.5.2 and 1.5.3.

1.5.1 *Saccharomyces cerevisiae* Strain MC1

The enzyme ADH catalyses the interconversion of various primary and secondary alcohols to the corresponding aldehydes and ketones. In yeast, the enzyme is a tetramer with a molecular weight of approximately 150,000. Wild type *Saccharomyces cerevisiae* is known to contain at least 3 isozymes of ADH (Ciriacy, 1975) which can be designated YADH-I, YADH-II and YADH-III. Of these isozymes, YADH-I is present under all growth conditions (Lutsorf and Megnet, 1968) and enables the conversion of glucose to ethanol, YADH-II is repressed in the presence of glucose and is involved in the utilisation of ethanol (Fowler *et al.,* 1971), while YADH-III is associated with the mitochondria (Ciriacy, 1975).

S. cerevisiae strain MC1 was formed by Creaser *et al.* (1990) by inserting plasmid pJC19R into a mutant yeast that lacked all YADH isozymes and was unable to produce tryptophan and histidine (originally formed by Williamson *et al.,* 1980). The inserted plasmid contains a modified YADH-I gene coding for a protein engineered form of the enzyme YADH-I and the gene for tryptophan production. The changes in the gene for YADH-I give a phenylalanine residue at amino acid position 93 instead of tryptophan (as in the wild type YADH-I) which has the effect of enlarging the isozyme's active site. The MC1 strain therefore only produces the protein engineered form of YADH-I (abbreviated as *pe*-ADH), which is able to oxidise secondary alcohols such as hexanol at a faster rate than the wild type YADH-I (refer to Table 1.3 overleaf for alcohol oxidation rates of wild type YADH-I and *pe*-ADH). It also cannot produce histidine, since the gene for histidine production is still missing, and this can be exploited in identifying the MC1 strain during culture (Figure 1.8 overleaf).

Alcohol	Rate of alcohol oxidation at a concentration of 10 mM (mol substrate oxidised. s^{-1}. mol active $site^{-1}$)	
	YADH-I*	***pe*-ADH***
Hexanol	0.66	1.21
Heptanol	1.61	2.89
Octanol	0.89	1.04

* from Creaser *et al.* (1990)

Table 1.3: Alcohol oxidation rates for natural and protein engineered yeast ADH.

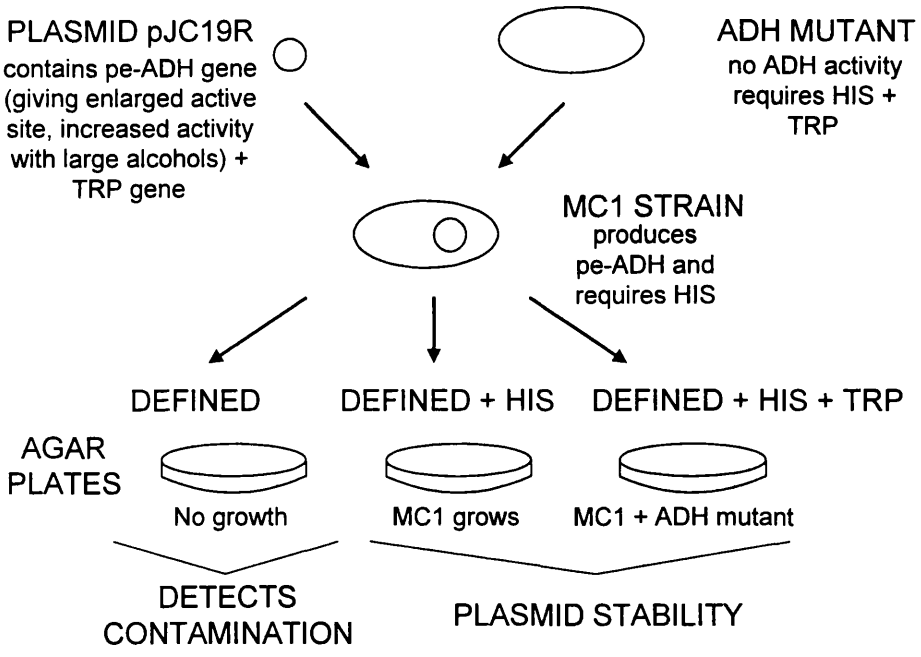

Figure 1.8: Formation of the MC1 strain.

(Note: histidine abbreviated to HIS, tryptophan to TRP)

1.5.2 ADH Overexpressing Strain

The ADH overexpressing strain was formed by Sinclair (1997) by transforming the YePlac 181 plasmid containing the gene for YADH-II (abbreviated to PMW5-ADH2) into *Saccharomyces cerevisiae* strain SUB63, in which ubiquitin production has been disrupted

by insertion of the gene for leucine. Due to the inability of the SUB63 strain to produce histidine, lysine, tryptophan and uracil, these compounds must be added to growth medium for the SUB63 strain. Since plasmid PMW5-ADH2 contains the gene for tryptophan production, the ADH overexpressor only requires the addition of histidine, lysine and uracil to the growth medium. The expression of the recombinant YADH-II only occurs in the absence of glucose, i.e. under respiratory conditions. An 8-fold overexpression of YADH-II has been reported with the highest levels obtained 72 to 96 h after inoculation.

1.5.3 Transformed *Escherichia coli* Strain WL2

There are at least three isozymes of horse liver ADH (designated E, SS and ES) which result from two 374 amino acid subunits known as E (for 'ethanol active') and S (for 'steroid active'). All three isozymes show activity towards ethanol, while only isozymes with the S subunit are active towards 3 β-hydroxysteroids (Van de Goor-Kucerova, 1992). Expression of a *rec*-HLADH in *Escherichia coli* was achieved by Van de Goor-Kucerova (1992) by inserting the HLADH expressing plasmid designated pKK45-1.9 into *E. coli* strain WL2. The plasmid pKK45-1.9 was in turn formed by inserting the 1125 base pair coding sequence for the E subunit of HLADH (HLADH-E) into the expression vector pKK223-3, which contains the strong trp-lac promotor and an operator. Cultures of the transformed *E. coli* strain WL2 cells were grown in liquid broth media containing the antibiotic ampicillin and expression of the *rec*-HLADH was induced by adding isopropylthiogalactoside (IPTG) to the culture medium.

1.6 Aims of Research

The primary aim of this thesis is to generate robust and predictive models for the unit operations of high pressure homogenisation, neutral salt protein precipitation and disc stack centrifugation found in a typical downstream process for the recovery of a recombinant intracellular enzyme.

Other aims of the work are to:

- compare the processing of recombinant and natural material in order to examine the impact of recombinant techniques on downstream operations and to increase the level of knowledge on the processing of recombinant material.

- generate the unit models with a minimum of time, cost and experimental data.

- examine the generic nature and scalability of the models.

- produce a full process model of the recovery sequence in order to examine process interactions and sensitivity.

- provide confidence in the results of unit and process models through the use of verification experiments at the small-scale and pilot-scale.

1.7 Summary

An overview of recombinant, intracellular protein production has been given, showing the range of downstream processing operations utilised. The typical recovery process and unit operations of high pressure homogenisation, neutral salt protein precipitation and disc stack centrifugation considered in this thesis have been described. The impact of recombinant techniques on the downstream processing of proteins has been examined and the application of simulation and modelling to bioprocesses in general and the downstream process in particular explored. The aims of the thesis have then been listed and the experimental system used described. With increasing use of recombinant systems in protein production, the need for generic, robust and predictive models for the evaluation of alternative processing schemes, to enable rational and confident design of the downstream process and to optimise recovery process performance has been highlighted.

2.0 BIOPROCESS MODEL DEVELOPMENT

2.1 Introduction

In this chapter, the development of bioprocess models is examined. In Section 2.2, a general description of process modelling is given and some approaches used for process model development are outlined. In Section 2.3, bioprocess modelling is specifically examined. Section 2.3.1 gives current approaches used to develop bioprocess models. Section 2.3.2 outlines the use of verification studies for model extension, which is the approach adopted in this thesis for the generation of models describing operations for the recovery of recombinant intracellular enzymes. Available modelling software packages are then evaluated and reviewed in Section 2.4, and overall conclusions are given in Section 2.5.

2.2 Process Modelling

A model is a representation or description of a given process. A basic division can be made into physical and mathematical models. Physical models are real systems which aim to mimic a process in some way, and include scaled-down systems which produce the same results or behaviour as a larger scale process. Mathematical models are composed of rules or equations that describe the process. In this chapter, the development of mathematical models is specifically considered. The reader is referred to the work of Maybury (1997) for further investigation into the development and use of scale-down systems for mimicking downstream processing operations.

It is the mathematical models within a simulator that provide the description of a process necessary to generate a simulation. These models incorporate a host of physical, chemical and biological phenomena (Evans and Field, 1988) as well as economic and environmental aspects of a process. Robertson (1989) has attributed the richness of a simulator to the variety of models included with respect to both their nature and the multiple levels of accuracy available.

The importance of process modelling has been highlighted by Benson (1997) who concluded that it will be one of the three core technologies, along with process control and catalysis, that sustain winning process companies in the world.

There are two basic types of model which can be used to describe the behaviour of a process:

- Theoretical Models: Accepted knowledge of the fundamental mechanisms occurring is used to develop a model of a given process. Theoretical models must be verified using experimental data to ensure they provide an accurate description of the process. This type of model can generally be extrapolated to cover the behaviour of the process under new conditions.

- Empirical Models: Experimental data is used to develop a model which describes the observed behaviour of a given process for a particular set of conditions. The use of an empirical model is only valid for the conditions under which the data was obtained. Generally these models take the form of mathematical equations or rules which match the patterns in the experimental data. Neural networks (which use artificial neurons to relate input and output parameters) can also be considered empirical models.

In practice, most models are the result of mixing empirical information with the knowledge of a few basic mechanisms. The stages in the development of a model are shown in Figure 2.1 overleaf. The traditional approach to the development of a model starts by producing a visual or verbal representation of the process which identifies parameters that have an effect on the process (inputs) and parameters that are affected by the process (outputs). The form and complexity of this representation will depend on the intended use of the model and available knowledge of the process. In the case of an empirical model the representation may simply be a "black box", while for theoretical models it may take into account interactions of different mechanisms or sub-processes.

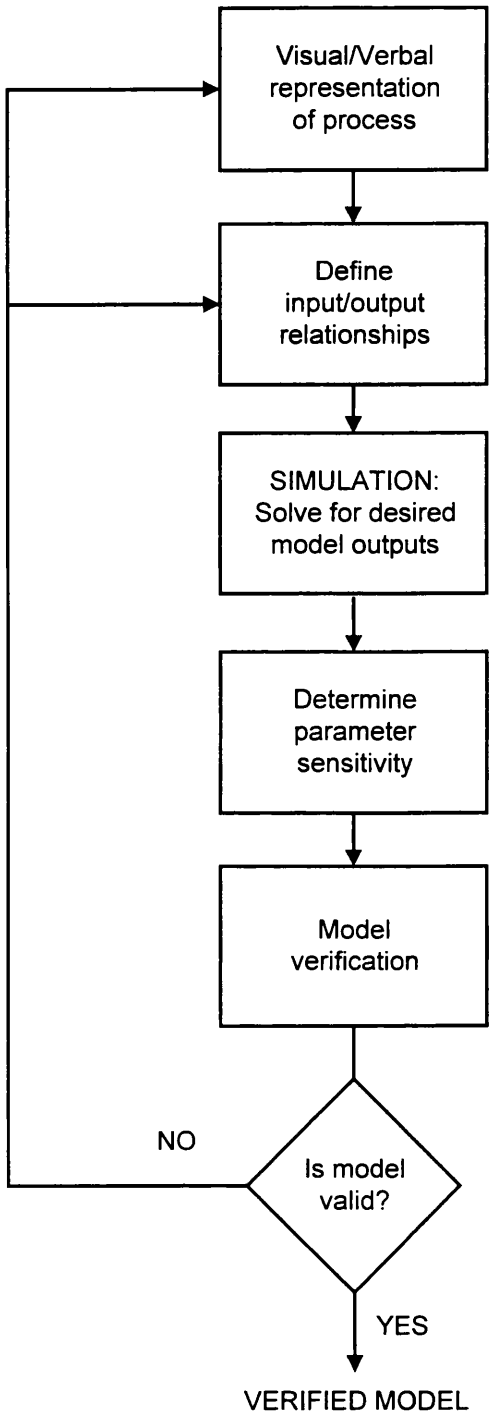

Figure 2.1: Traditional approach to model development.

The next step in model development is to relate the model inputs and outputs using rules or mathematical equations. For theoretical models this may require simplifying assumptions, while for empirical models the application of numerical techniques may be required. Once the model's rules or mathematical equations are defined they can be solved to give the values of desired outputs for a given set of inputs. Although the model can now provide a description of the process, model development does not stop here.

Since the particular parameters included in the model may influence the simulation results, the sensitivity of the model to parameter variations must be examined. Small changes in a parameter may completely alter the results. The model must also be verified to ensure it provides a realistic description of process behaviour. This can be achieved by solving the model for a range of conditions and comparing the simulation results to the actual behaviour of the process using standard statistical analysis techniques. If the results do not match the real process behaviour or are too sensitive to parameter variations then the model must be modified, re-formulated and re-verified. Model development is therefore a cyclical process in which a model is improved over time.

Although models developed using the traditional approach form the backbone of currently available chemical process simulators (Robertson, 1989), their use has resulted in many limitations. The operations performed by these models are predetermined and tend to be specific for solving one type of problem. The inputs on which these operations are carried out to give the values of desired outputs are also fixed and the form of the model equations is often linked to the solution procedures employed by the simulator. Other problems listed by Stephanopoulos (1990) are:

- the time and cost of model development are high.
- the resulting models are difficult to document and maintain.
- the re-use of models is minimal.
- the models cannot be synthesized automatically by the simulator.
- for interactive model building in existing simulators the user is required to be highly skilled in programming.

The result of the weaknesses in the traditional approach to model development has been an enormous duplication of modelling efforts. Accumulated modelling knowledge is almost impossible to use since the underlying model purpose, assumptions and simplifications have never been documented and rationalised (Stephanopoulos, 1990).

The trend in process simulators developed for the chemical industry has been to include libraries of steady-state unit operation models. This has lead to many chemical companies reducing the amount of expensive in-house model development (Hunter *et al.*, 1989). The inclusion of a library of models within a simulator adds some flexibility since a range of different models can be made available for each unit operation depending on the application. This allows simple or more rigorous models and performance based or design based models (Section 1.4.1) to be used when necessary. The library can also be updated with the new version of a model when it becomes available. Although this overcomes some of the limitations of models developed using the traditional approach, Pantelides and Barton (1993) have pointed out that for dynamic simulation many different applications require significantly different models for similar unit operations and a "comprehensive" library of dynamic unit operation models is probably an unattainable goal. Pantelides and Barton concluded that powerful model development facilities were therefore essential for dynamic simulators.

One development which may overcome some of these problems is a shift towards general-purpose simulation packages in which a common model is used in different forms for varying applications. A step in this direction is MODEL.LA, a formal modelling language designed by Stephanopoulos *et al.* (1990). MODEL.LA has the ability to capture and utilise both quantitative and qualitative information, represent a process at any level of detail, automatically generate a set of basic relations that describe a given system, and offer documentation, assumptions and simplifications that give rise to a particular model. It has been incorporated into DESIGN-KIT, a software environment for process design (Stephanopoulos,1990). Preisig (1996) has also developed a generic object-orientated modelling approach based on the two basic components of systems and connections from which a physical topology for use in control applications can be built.

A related approach, which comes from work in the field of artificial intelligence, is to transfer the model building task to the computer. This is known as automatic model building and involves selecting and combining appropriate elementary relationships at a proper level of detail to form a model which can be used to solve a given problem (Muratet and Bourseau,1993). Software packages for limited applications have been produced by Nemeth *et al.*(1992) and Farza and Cheruy (1993) which formulate model equations from user supplied information. Nemeth *et al.* (1992) developed a modelling

tool that uses a graphical user interface to capture information on thermodynamic interactions and produce qualitative dynamic models for control applications. Farza and Cheruy have produced CAMBIO, which uses a similar graphical approach to form dynamic material balance equations for biochemical processes (Section 1.4.4). The main drawback of both of these approaches is that knowledge of the elementary mechanisms occurring in a process is required. Verification of common models is also still required and must be carefully considered, since different forms of a model generated for particular problems will vary in accuracy.

The fusion of equation-based mathematical models with rule based models, such as expert systems, and databases can also lead to the development of hybrid models. Lubbert and Simutis (1994) have concluded that, in the future, the nature of process modelling is likely to shift towards making use of information in whatever form it is available.

2.3 Bioprocess Models

2.3.1 Current Approaches to Bioprocess Model Development

A large number of papers have been published on the development of models for single unit operations and many of the common unit operations in biochemical processes have been covered (Cooney *et al.*, 1988). However, most of this work has focused on the initial fermentation stage of a bioprocess while many downstream operations have been neglected since they are less well understood (Gritsis and Titchener-Hooker, 1989). Many of the models which have been produced to describe biochemical unit operations are also difficult to use in simulations since they contain parameters which cannot be determined. This has resulted from a scarcity of physical property data for biomaterials and a lack of any prediction methods. In these cases, experimental studies are required during model development to determine the unknown parameters (Cooney *et al.*, 1988) or alternatively empirical models must be developed using the parameters which are known.

The importance of interactions in biochemical processes, highlighted by Fish and Lilly (1984), requires an integrated approach to the development of bioprocess models and bioprocess design in general (Titchener-Hooker *et al.*, 1991). This involves examining

more than one unit operation at a time, along with a consideration of the whole bioprocess. However there has been little work in the past on the modelling of multiple unit operations for biochemical processes (Cooney *et al.*, 1988). Recent modelling studies have started to address this issue. Interactions between fermentation, high pressure homogenisation and debris removal stages have been modelled by Middelberg (1995b) and Zhou *et al.* (1997). Clarkson *et al.* (1992, 1994) have modelled interactions between fractional precipitation and centrifugation. While integrated modelling and optimisation has been carried out for a typical intracellular enzyme recovery process by Samsatli and Shah (1996), and for inclusion body recovery processes by Bogle *et al.* (1991, 1993) and Wai *et al.* (1996).

As highlighted in Section 2.2, the verification of model results against experimental data is an essential part of model development. Clarkson *et al.* (1992, 1994, 1996a, 1996b) have demonstrated the importance of verification in the development of bioprocess models by using experimental data to significantly improve the capabilities of models for fractional precipitation and centrifugation. Model verification can also be used to assess the limits of a given simulation and give confidence in the simulation results. For example, Narodoslawsky (1991) has compared experimental and simulation results for the production of bakers' yeast to conclude that existing bioprocess models are sufficiently precise for use in bioprocess design work, although they are not accurate enough for control applications. A lack of credible comparisons between the actual performance of industrial scale bioprocesses and model results has been given by Narodoslawsky (1991) as one of the obstacles to a broader application of simulation in bioprocess engineering.

A new holistic approach for the development of bioprocess models which strongly links modelling and experimental work and is known as the "formal macroapproach" has been described by Moser (1993). Accepting the constraints of shortages in money and time, Moser (1993) concluded that a process model should be formed in three steps:

- a first working hypothesis is created from intuition and some knowledge from literature.

- an initial process model is then produced without deep scientific consideration, i.e. no mechanistic work, and is solved to give an understanding of the global process behaviour.

- experimental work is carried out to check the validity of the model and to estimate model parameters.

The desired outcome is a process model which is suitable for a given application, even though the accuracy may not be high. The significant and decisive factor of the formal macroapproach is that the description of interactions between individual parts of the whole process is captured in a model, rather than the types of models used to describe subprocesses or subunits of the process. The approach was illustrated by Moser (1993) using the examples of bakers' yeast, antibiotic and amino acid production. Other possibilities from this approach given in the same paper are the simulation of interactions between kinetics and physics (for example using structured mixing models), the simulation of the entire process pattern of a whole bioplant, the modelling of integrated bioprocesses and the supplementation of conventional economic criteria in design work with ecological criteria. However, the disadvantage of the formal macroapproach is that a model developed for a given process with a particular application in mind may not be suitable for a different application, and hence additional model development is required to produce a new process model for new applications.

An appropriate approach for the development of models describing the recovery of recombinant proteins which attempts to deal with many of the problems listed above and involves the use of verification studies to extend existing bioprocess models is presented in the next section.

2.3.2 Use of Verification Studies for Model Extension

In the case of the downstream processing of recombinant material, the challenge in developing bioprocess models is to produce accurate models with available knowledge and a minimum of research data. The existing difficulties in modelling bioprocesses still hold (Section 2.3.1), with added complications arising due to the use of the recombinant material:

- because recombinant techniques can produce significant changes in the target organism or protein (Section 1.3), physical properties and processing characteristics cannot be

assumed to be the same as those of the natural organism or protein. Predicting the changes in these properties may be difficult.

- during process development, only small amounts of recombinant material may be available for the generation of experimental data. Premature scaling up of recombinant cultures will be costly if the material is subsequently found to be unsuited to large scale production.

- there is a need for accurate simulations and confidence in any final design since demonstrating that a consistent product can be produced is crucial in obtaining regulatory approval. Any major changes to the as-built process utilising recombinant material will also require revalidation and new regulatory approval.

- the need to bring a protein product to market in the shortest possible time to ensure economic success (Petrides *et al.*, 1989) and to gain the most from products with a limited patent life adds pressure for fast process (and therefore model) development.

An appropriate approach for the development of bioprocess models describing the recovery of recombinant proteins which meets the above challenges is the extension of existing models through the use of verification studies. An outline of the approach is shown in Figure 2.2 overleaf. Basic knowledge of the recombinant system is used to identify differences between the recombinant and natural material. By examining the parameter sensitivity of existing models for the natural process, the models can be re-formulated to give an initial simulation of the recombinant process. This information can then be used to target verification experiments to test the validity of the models and enable further model re-evaluation using a minimum of experimental trails and hence a minimum of time and data. The outcome of this process will be models which have been extended to give an accurate simulation of the processing of the recombinant protein.

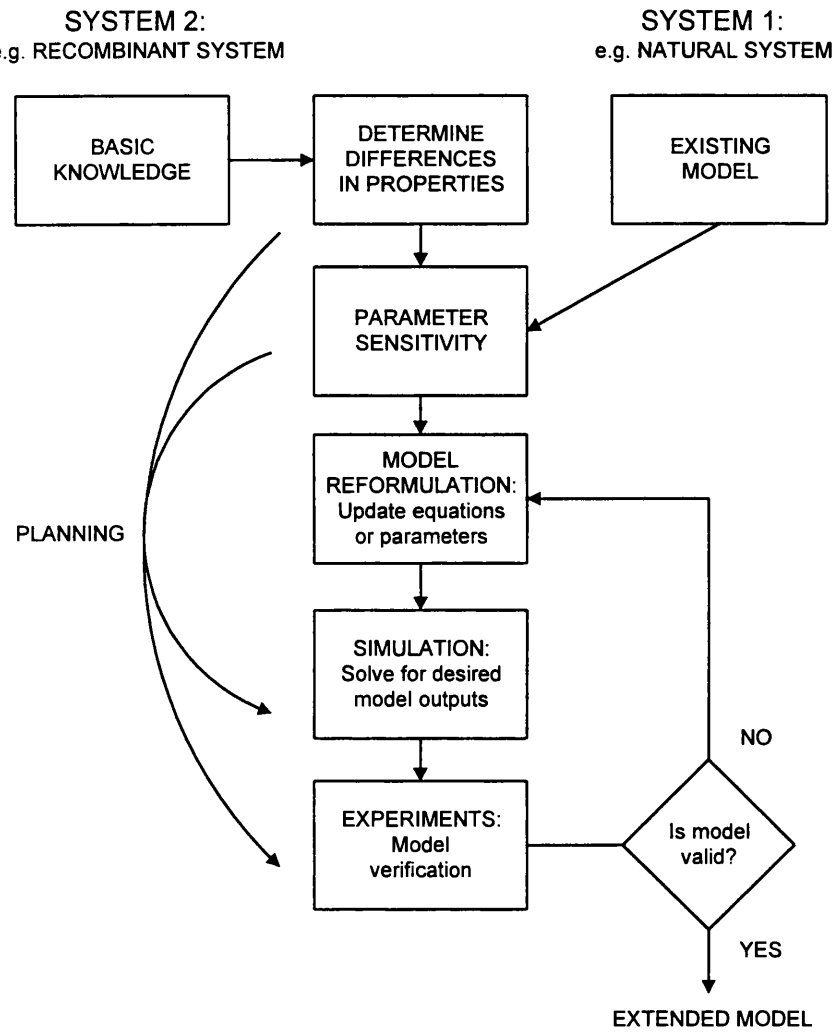

Figure 2.2: Model extension approach.

Some advantages of this approach are:

- duplication of modelling effort is reduced since existing models are used, while knowledge of the recombinant system and bioprocessing unit operations is increased.

- the scope of verification studies can be tailored to match the intended use of the models. Only a small number of verification experiments will be required to develop models to test initial process feasibility at fixed conditions, while more comprehensive experiments will be needed to develop models for detailed design.

- the scale of the verification studies can match the stage of process development. By utilising scale-down equipment, verification studies and therefore model extension can be carried out on small amounts of recombinant material early in process development.

2.4 Available Modelling Software Packages

A number of software packages were available for the implementation of bioprocess models in this study. The strengths and weaknesses of each type of software were evaluated and are reviewed below:

2.4.1 Spreadsheets

Spreadsheets, such as EXCEL (Microsoft, Redmont, USA), contain cells of data which can be manipulated. They enable large amounts of process data to be stored, analysed and correlated. They can be operated by people with only a reasonable level of computer skills. Steady state models can easily be implemented and goal seek routines allow a small degree of optimisation to be performed. However, dynamic models are difficult to program.

2.4.2 Computer Languages

Simulations can be carried out using programs written in various computer languages, such as FORTRAN, BASIC or C. Both steady state and dynamic models can be coded and solved, along with optimisation procedures. A large degree of numerical analysis and programming skills are required to produce a simulation and the level of graphical output may be low. Long simulation development times are to be expected.

2.4.3 Special Application Packages

A number of computer packages are available for special applications that can be utilised to generate simulations. For example MATLAB (The Mathworks, Massachusetts, USA) is designed for solving mathematical functions, while LABVIEW (National Instruments, Austin, USA) is used for monitoring and control applications and contains an object orientated programming language that allows a process simulation to be implemented (Zhou *et al.*, 1997). In both cases specific programming skills for the particular package are required. Steady state models are easily programmed and subroutines for solving dynamic models, optimisation and production of graphical output are generally available which can reduce programming time.

2.4.4 General Purpose Simulators

A number of general purpose simulators are available in which models can be solved and a process simulation produced. Optimisation routines and graphical output are generally available. An example is SPEEDUP (AspenTech, Massachusetts, USA), which is an equation based package specifically designed to perform steady state or dynamic simulations (Pantelides, 1988). Difficulty may be experienced with simulations in which both steady state and dynamic models are present, which is often the case for bioprocesses (Clarkson, 1994). Another example is gPROMS, which is currently being developed at Imperial College, London, UK. gPROMS can describe processes including both dynamic and steady state models and enables scheduling of process operations to be examined (Lu *et al.*, 1994). Again, specific programming skills for each package are required.

2.4.5 Process Simulators specifically for Bioprocesses

Simulation packages specifically for bioprocesses are now commercially available, namely BioProDesigner (Intelligen, New Jersey, USA) and ASPEN-plus BPS (ASPEN Tech, Massachusetts, USA). Libraries of models for typical bioprocess operations are included and the package helps the user set up and solve the simulation. Sensitivity analysis, optimisation and costing functions are also available. In the case of BioProDesigner, the scheduling of operations can be examined and Gantt charts produced (Petrides, 1994). ASPEN-plus is a chemical process simulator and now has the BioProcess Simulator (BPS) available as an add-on (Bhattacharya, 1993). Steady-state mass and energy balances are calculated and user models can be programmed. However, the implementation of dynamic models and the incorporation of distributed properties, such as particle size distributions, is difficult. In both cases only a reasonable level of computing skills are required to operate the simulators.

2.4.6 Selected Software Packages

As the EXCEL spreadsheet package (Microsoft, Redmont, USA) was already being utilised for the analysis of experimental data during the preparation of this thesis (Section 3.5) it was also used for the implementation of steady state unit models. The

MATLAB software package (The MathWorks, Massachusetts, USA) was chosen for the implementation of dynamic unit models and process sequences involving both steady state and dynamic modelling. MATLAB can be described as a numerical computation and visualisation software package. Numerical analysis, matrix computation and graphics are integrated through the use of a simple, command based programming structure. High flexibility was the main advantage of this package over the other available software, including the ability to easily incorporate distributed parameters through the use of matrix functions, the presence of an in-built 4th order Runge Kutta method for solving dynamic equations, a programming structure suited to making rapid model alterations and the capability of modelling both steady state and dynamic operations through the use of a sequential modular approach.

2.5 Conclusions

Models provide the description of a process necessary to generate a simulation. Both theoretical and empirical models are possible, but in practice most models are the result of a mixture of empirical data and basic knowledge. For the modelling of bioprocesses it is important that process interactions are also incorporated. Various approaches for the development of process models can be used, but the verification of models is always essential to assess the limits of a model and give confidence in simulation results.

For the simulation of the recovery of recombinant proteins, an appropriate approach for model development is the extension of existing models through the use of verification studies. The advantages of this approach are that it minimises duplication of modelling effort, shortens model development time and increases understanding, while the scope and scale of the verification studies can be tailored to match the intended use of the models and stage of process development.

A number of software packages are currently available for the implementation of bioprocess models. Based on an evaluation of this software, the EXCEL spreadsheet package and MATLAB numerical computation package were selected for use in this thesis due to ease of use and high flexibility respectively.

3.0 MATERIALS AND METHODS

3.1 Introduction

This section details the various materials, analytical techniques and experimental methods that have been used in the preparation of this thesis. Section 3.2 describes the general analytical techniques employed, Section 3.3 describes cell culture and fermentation procedures, Section 3.4 describes the procedures and equipment used in downstream processing studies and Section 3.5 describes the software packages used for data analysis and modelling studies. All chemicals used were from BDH, Leicestershire, U.K. unless otherwise stated.

3.2 Analytical Techniques

3.2.1 Assays

3.2.1.1 Alcohol Dehydrogenase

Alcohol dehydrogenase (ADH) activity was assayed according to the method of Bergmeyer (1983) by measuring the rate of change in absorbance at 340 nm due to the following reaction which is catalysed by ADH:

$$Ethanol + NAD^{+} \xleftrightarrow{ADH} Acetaldehyde + NADH + H^{+}$$

The reaction mixture consisted of 600 mM ethanol, 1.8 mM NAD (Sigma Chemical Co. Ltd., Dorset, U.K.), 1.0 mM glutathione (Sigma Chemical Co. Ltd., Dorset, U.K.), 0.62 mM semicarbazide HCl in 50 mM Tris-HCl buffer pH 8.8. The semicarbazide was included to prevent the back reaction, while the glutathione acts as a stabilising agent during dilution.

The reaction was started by adding 25 μL of sample to 1.5 mL of reaction mixture in a cuvette and mixing by inversion. The rate of change of absorbance was monitored for 60 s at 5 s intervals using a Beckman DU-650 spectrophotometer (Beckman Instruments,

Buckinghamshire, U.K.). A linear fit on the absorbance data was automatically carried out by the instrument to determine the rate of change, with the result being deemed acceptable if the linear regression coefficient, r_c, was above 0.97. The enzyme activity, E, in the sample was calculated as units of activity, U, per mL using the following equation:

$$E = \frac{1}{\varepsilon_{340}} \frac{\Delta A_{340}}{\Delta t} \frac{V_f}{V_s} D_N$$

(equation 3.1)

where $\Delta A_{340}/\Delta t$ is the rate of change of absorbance at 340 nm, V_f is the final volume of reaction mixture and added sample, V_s is the sample volume, D_N is the dilution factor and ε_{340} is the absorptivity of NAD at 340 nm and equals 6.22 cm^2 μmol^{-1}. 100mM potassium dihydrogen phosphate buffer pH 6.5 was used to dilute the samples to give changes in absorbance less than 0.5 per minute.

Measurement variability of the assay, expressed as standard deviation from a mean value, had previously been determined by Deghani (1996) as ±5.4% of measured ADH activity. Repeat measurements carried out over a range of activities confirmed that the standard deviation was within this value. In practice samples were assayed in triplicate to give the mean ADH activity.

3.2.1.2 Total Protein

The concentration of protein was determined using Coomassie Blue G-250 reagent (Bio-Rad Laboratories Ltd., Hertfordshire, U.K.). The method is based on the work of Bradford (1976) and involves binding of protein to the reagent which suppresses protonation and results in a colour change from pale orange-red to blue.

Samples to be assayed were diluted to within the range of 200-1000 $\mu g.mL^{-1}$ protein using 100 mM potassium dihydrogen phosphate buffer pH 6.5. Care was taken to ensure ammonium sulphate levels were below 1.0 M in all cases to prevent interference with the assay. 100 µL of sample and 2.9 mL of assay reagent were mixed in a cuvette and the change in absorbance at 595 nm was recorded after 300 s using a Beckman DU-650 spectrophotometer (Beckman Instruments, Buckinghamshire, U.K.). A standard curve

produced using bovine serum albumin (Sigma Chemical Co. Ltd., Dorset, U.K.) enabled the protein concentration to be calculated.

Measurement variability of the assay, expressed as standard deviation from a mean value, had previously been determined by Deghani (1996) as ±3.6% of measured protein concentration. Repeat measurements over a range of concentrations confirmed that the standard deviation was within this value. In practice samples were assayed in triplicate to give the mean protein concentration.

3.2.1.3 Glucose

The concentration of glucose was determined using Sigma Glucose HK reagent (Sigma Chemical Co. Ltd, Dorset, U.K.). The assay gives quantitative, enzymatic determination of glucose concentration at 340 nm and is based on the following reactions:

$$Glucose + ATP \xrightarrow{HK} G-6-P + ADP$$
$$G-6-P + NAD^{+} \xrightarrow{G\text{-}6\text{-}PDH} 6-PG + NADH$$

Glucose is first phosphorylated by adenosine triphosphate (ATP) in a reaction catalysed by hexokinase (HK). The glucose-6-phosphate (G-6-P) formed is then oxidised to 6-phosphogluconate (6-PG) in the presence of NAD. This reaction is catalysed by glucose-6-phosphate dehydrogenase (G-6-PDH).

10 µL of sample and 1.5 mL of assay reagent were mixed in a cuvette and the increase in absorbance at 340 nm due to the reduction of NAD to NADH was measured after 5 minutes using a Beckman DU-650 spectrophotometer (Beckman Instruments, Buckinghamshire, U.K.). The glucose concentration, C_{glu}, was then calculated in $mg.L^{-1}$ from the following equation:

$$C_{glu} = \frac{1}{\varepsilon_{340}} \frac{\Delta A_{340}\, V_f\, MW_{glu}}{l\, V_s\, 1000}$$

(equation 3.2)

where ΔA_{340} is the change in absorbance at 340 nm, MW_{glu} is the molecular weight of glucose and equals 180.16 $g.mol^{-1}$, and l is the lightpath and equals 1 cm.

Measurement variability of the assay, expressed as standard deviation from a mean value, has previously been determined by Deghani (1996) as ±0.3% of measured glucose concentration up to a maximum of ±0.053 g/L. Repeat measurements over a range of concentrations confirmed that the standard deviation was within this value. In practice samples were assayed in triplicate to give the mean glucose concentration.

3.2.1.4 Ethanol

The concentration of ethanol was determined using Boehringer Mannheim UV method kits (Boehringer Mannheim Ltd, East Sussex, U.K.). The method is based on the following reactions:

$$Ethanol + NAD^+ \xleftrightarrow{ADH} Acetaldehyde + NADH + H^+$$

$$Acetaldehyde + NAD^+ + H_2O \xrightarrow{Al\text{-}DH} Acetic\ acid + NADH + H^+$$

Ethanol is first oxidised to acetaldehyde in the presence of the enzyme ADH. The equilibrium of this reaction lies on the side of ethanol and NAD. However, it can be completely displaced to the right at alkaline conditions and by trapping of the acetaldehyde formed. To achieve this the acetaldehyde is oxidised to acetic acid in the presence of aldehyde dehydrogenase (Al-DH). The change in absorbance at 340 nm due to the reduction of NAD to NADH in this reaction alone, A_1, was measured first and then the change in absorbance at 340 nm due to the reduction of NAD to NADH from both reactions acting at the same time, A_2, was measured. The absorbance difference was calculated as A_2 minus A_1. The absorbance difference for a blank was then subtracted from that of the sample, giving the final absorbance difference ΔA.

100 µL of sample or deionised water was mixed with 3 mL of assay reagent containing Al-DH in a cuvette and the change in absorbance at 340 nm after 180 s was measured using a Beckman DU-650 spectrophotometer (Beckman Instruments, Buckinghamshire, U.K.) to give A_1. 50 µL of assay reagent containing ADH was then added, the cuvette contents mixed by inversion and the change in absorbance at 340 nm measured after 300 s using a Beckman DU-650 spectrophotometer (Beckman Instruments, Buckinghamshire,

U.K.) to give A_2. ΔA was then determined and the concentration of ethanol, C_{eth}, in $g.L^{-1}$ calculated using the following equation:

$$C_{eth} = \frac{1}{\varepsilon_{340}} \frac{\Delta A \, V_t \, MW_{eth}}{l \, V_s \, 2 \times 1000}$$

(equation 3.3)

where MW_{eth} is the molecular weight of ethanol and equals 46.07 $g.mol^{-1}$.

Measurement variability of the assay, expressed as standard deviation from a mean value, has previously been determined by Deghani (1996) as ±0.6% of measured glucose concentration up to a maximum of ±0.025 g/L. Repeat measurements over a range of concentrations confirmed that the standard deviation was within this value. In practice samples were assayed in triplicate to give the mean glucose concentration.

3.2.2 Dry Weight Determination

The following methods were used to determine dry weights:

3.2.2.1 Filtered Dry Weight

Cellulose nitrate 47 mm diameter filters of 0.2 μm pore size (Whatman, Maidstone, U.K.) were dried at 100°C to constant weight before use. Care was taken not to touch the filters and also to prevent the build up of static as this could reduce the accuracy of weighing. The pre-weighed filters were placed in a vacuum filter rig (Millipore, Whatford, U.K.). A known volume of sample was placed onto the filter and a vacuum applied. The filtrate produced was collected and stored at -20°C for later analysis. The solids were then washed with deionised water and, once drained, the filter was dried at 100°C to constant weight (approximately 24 h) and re-weighed. Samples were analysed in duplicate giving a reproducibility of within ±10%.

3.2.2.2 Microtube Dry Weight

Microtubes (BDH, Leicestershire, U.K.) were dried at 100°C to constant weight before use. Dry weights were then determined by placing a known volume of the sample into a

pre-weighed tube, drying to constant weight at 100°C (approximately 24 h) and re-weighing. Samples were analysed in duplicate giving a reproducibility of within ±10%.

3.2.3 Optical Density Determination

Sample optical densities were determined at either 600 nm or 670 nm using a Beckman DU-650 spectrophotometer (Beckman Instruments, Buckinghamshire, U.K.). Samples were diluted with 100 mM potassium dihydrogen phosphate buffer at pH 6.5 to give a spectrophotometer absorbance reading below 1.0. Samples were analysed in duplicate giving a reproducibility of within ±5%.

3.2.4 Microscopic Counts

Microscopic examination of cell and homogenate samples was carried out using an Olympus optical microscope (Olympus Optical Co. Ltd., London, U.K.) under magnifications of 400x (phase contrast) and 1000x (phase contrast/ oil immersion). The fraction of viable and budded cells was determined by staining with 1% methylene blue and counting the number of viable unbudded and budded cells, i.e. those cells that had retained the stain, with a haemocytometer (Hawksley & Sons Ltd., Lancing, U.K.) under 400x magnification.

3.2.5 Aqueous Fraction Determination

3.2.5.1 Centrifuge Method

Aqueous fractions were determined by pipetting 400 μL of sample into a 500 μL microcentrifuge tube (Fisher, Leicestershire, U.K.) and centrifuging at 14,000 rpm (40,000 g) for 0.5 h in a MSE Micro Centaur lab centrifuge (MSE Ltd., Leicestershire, U.K.). The volume of the sample occupied by the aqueous and solid phases was measured to an accuracy of 5 μL by comparison to a pre-graduated 500 μL microcentrifuge tube. Aqueous and solid fractions were then calculated by dividing by the total volume. Samples were analysed in duplicate giving a reproducibility of within ±10%.

3.2.5.2 Dilution Method

Aqueous fractions of homogenate samples were determined by carrying out a series of dilution experiments using the same procedure as Hetherington *et al.* (1971). Known volumes of homogenate suspension were diluted with 100 mM potassium dihygrogen phosphate buffer at pH 6.5 and both diluted and undiluted samples were centrifuged at 14,000 rpm for 0.25 h in a MSE Micro Centaur lab centrifuge (MSE Ltd., Leicestershire, U.K.). The resultant supernatant for both diluted and undiluted samples was assayed for total protein (Section 3.2.1.2) and the aqueous fraction, F, calculated using the following equation:

$$F = \frac{V_d}{V_{hs}} \frac{C_{pd}}{C_{pu} - C_{pd}}$$

(equation 3.4)

where V_d is the volume of diluent, V_{hs} is the volume of homogenate suspension, C_{pd} is the protein concentration of a diluted sample, and C_{pu} is the protein concentration of an undiluted sample. All samples were analysed in duplicate giving an error in aqueous fraction of within ±5%.

3.2.6 Gel Elecrophoresis

3.2.6.1 Protein Gels

Proteins were fractionated by size under denaturing conditions using SDS polyacrylamide gel electrophoresis (SDS-PAGE) and by size and charge under non-denaturing conditions using native polyacrylamide gel electrophoresis (native-PAGE). The gel electrophoresis was performed with Tris-HCl Mini-PROTEAN II ready gels containing 15% acrylamide (Bio-Rad Laboratories Ltd., Hertfordshire, U.K.) in conjunction with the Mini-PROTEAN II dual slab cell (Bio-Rad Laboratories Ltd., Hertfordshire, U.K.).

Samples to be run under denaturing conditions using SDS-PAGE were prepared using the following cleanup procedure in order to remove contaminants:

i) 1 mL of the sample, pre-diluted with 100 mM potassium dihydrogen phosphate buffer pH 6.5 to contain 1 μg of protein, and 333 μL of 100% trichloroacetic acid were mixed in

a microcentrifuge tube and stored at 0°C for 1 h in order to precipitate proteins present in the sample.

ii) The mixture was spun at 14,000 rpm in a MSE Micro Centaur lab centrifuge (MSE Ltd., Leicestershire, U.K.) for 0.25 h and the supernatant decanted.

iii) The remaining solid pellet was resuspended in 1 mL of 5 mM hydrochloric acid in acetone and the mixture was spun at under vacuum at a low drying rate in a SC110 Speed Vac (Savant Instruments Inc., New York, U.S.A) until the volatile components had been driven off and a dry solid pellet remained.

iv) The resulting pellet was resuspended in 1 mL of acetone and respun under vacuum at a low drying rate in a SC110 Speed Vac (Savant Instruments Inc., New York, U.S.A) until the volatile components had been driven off.

v) step (iv) was repeated

vi) The dry solid pellet was dissolved in sample buffer containing 10% (v/v) glycerol, 20% (v/v) of 10% (w/v) SDS (Gibco, Life Technologies Inc., Paisley, Scotland, U.K.), 12.5% (v/v) 0.5 M Tris-HCl pH 6.8, 5% (v/v) β-mercaptoethanol (Sigma Chemical Co. Ltd., Dorset, U.K.), 5% (v/v) of 0.5% bromophenol blue and 47.5% (v/v) deionised water. The mixture was boiled for 240 s to fully denature any proteins present.

Two Mini-PROTEAN II ready gels were assembled in the Mini-PROTEAN II dual slab cell and 10 μL of the denatured sample was loaded onto wells in the ready gels. High and low molecular weight standards (Bio-Rad Laboratories Ltd., Hertfordshire, U.K.) were also loaded on each gel. The running buffer contained 3 $g.L^{-1}$ Tris base, 14.4 $g.L^{-1}$ glycine (Gibco, Life Technologies Inc., Paisley, Scotland, U.K.) and 1 $g.L^{-1}$ SDS (Gibco, Life Technologies Inc., Paisley, Scotland, U.K.) in deionised water. Electrophoresis was carried out at a constant voltage of 200 V with a typical run taking approximately 45 minutes. The gels were stained by shaking at room temperature for 2 h in 45% (v/v) methanol, 10% (v/v) acetic acid and 0.1% (w/v) coomassie blue G-250 (Bio-Rad Laboratories Ltd., Hertfordshire, U.K.) in deionised water. Destaining of the gels was

carried out by shaking in 45% (v/v) methanol, 10% (v/v) acetic acid in deionised water until protein bands were visible.

Samples to be run under non-denaturing conditions using native-PAGE were prepared by adding 200 μL of sample to 800 μL of sample buffer containing 10% (v/v) glycerol, 12.5% (v/v) 0.5 M Tris-HCl pH 6.8, 5% (v/v) of 0.5% bromophenol blue and 72.5% (v/v) deionised water. Two Mini-PROTEAN II ready gels were assembled in the Mini-PROTEAN II dual slab cell and 10 μL of the mixture was loaded onto wells in the ready gels. The running buffer contained 3 $g.L^{-1}$ Tris base and 14.4 $g.L^{-1}$ glycine (Gibco, Life Technologies Inc., Paisley, Scotland, U.K.) in deionised water. Electrophoresis was carried out at a constant voltage of 200 V with a typical run taking approximately 0.75 h. Staining and destaining of the gels was carried out as per the SDS-PAGE gels.

3.2.6.2 ADH Activity Gels

ADH activity gels were formed by staining native polyacrylamide gels prepared as per the method of Hames and Rickwood (1990). The gels were subjected to electrophoresis on a cooled flat bed LKB 2117 Multiphor II electrophoresis unit (Multiphor, Bromma, Sweden) with a Flowgen Consort E734 power supply (Flowgen, Staffordshire, U.K.) at conditions of pH 8.6, 4°C and 50 mA for approximately 2.75 h using 50 mM glycine-Tris running buffer.

ADH activity was visualised in the gels by coupling NADH production to the reduction of a tetrazolium salt to its corresponding formazan. The activity stain contained 200 mM ethanol, 2.5 mM NAD^+ (Sigma Chemical Co., Dorset, U.K.), 0.03% (w/v) nitro blue tetrazolium chloride and 0.002% (w/v) phanazine methosulphate dissolved in 50 mM Tris-HCl buffer pH 6.8. The gel was incubated in this solution in the dark, with shaking at room temperature for approximately 0.5 to 1 h. Stained ADH activity gels were then washed in deionised water and stored in 7.5% (v/v) acetic acid.

3.2.7 Particle Size Analysis

3.2.7.1 Elzone Method

Particle size analysis above approximately 1.0 μm was carried out using an Elzone model 280 PC particle sizer (Particle Data Ltd., Cheltenham, U.K.) which uses the 'electrical sensing zone' method to determine particle size. The instrument consists of a glass tube with a small orifice located in the tube wall (refer to Figure 3.1 overleaf for a schematic diagram). The tube is immersed in an electrolyte in which the particles to be analysed are suspended. A vacuum pump is used to apply negative pressure across the orifice, causing a flow of electrolyte containing the suspended particles through it and the unbalancing of a mercury column connected to the system. The vacuum source is then isolated and the flow of electrolyte and particles continues through the orifice as the vacuum is slowly released and the mercury column re-balances. The advancing mercury column activates a counter by means of start and stop probes so that a count is carried out while a known volume of electrolyte passes through the orifice.

The instrument can also be operated so that the counter is activated for a given time interval at a constant vacuum, i.e. with a constant flow through the orifice. The electrical resistance across the orifice is measured by immersed electrodes on either side of the tube wall. Any particles passing through the orifice cause a change in the resistance which is converted to a voltage pulse and then amplified. The volume of each particle is proportional to the height of the voltage pulse, while the number of particles passing through the orifice is equal to the number of pulses.

The electric sensing zone method has a lower size limit of particle detection of 0.6 μm. The upper size limit is reached when particles can no longer be kept in suspension (Allen, 1981). For all samples, a 30 μm orifice was used which was calibrated with latex particles of sizes 2.02 μm, 5.00 μm and 9.86 μm (Particle Data Ltd., Cheltenham, U.K.). For whole yeast cells, the electrolyte used was 1% (w/v) sodium chloride in 100 mM potassium dihydrogen phosphate buffer pH 6.5. For homogenate, the electrolyte used was 5% (w/v) sodium chloride in 100 mM potassium dihydrogen phosphate buffer pH 6.5. The measured size range was from 0.93 to 14.55 μm divided into 128 channels.

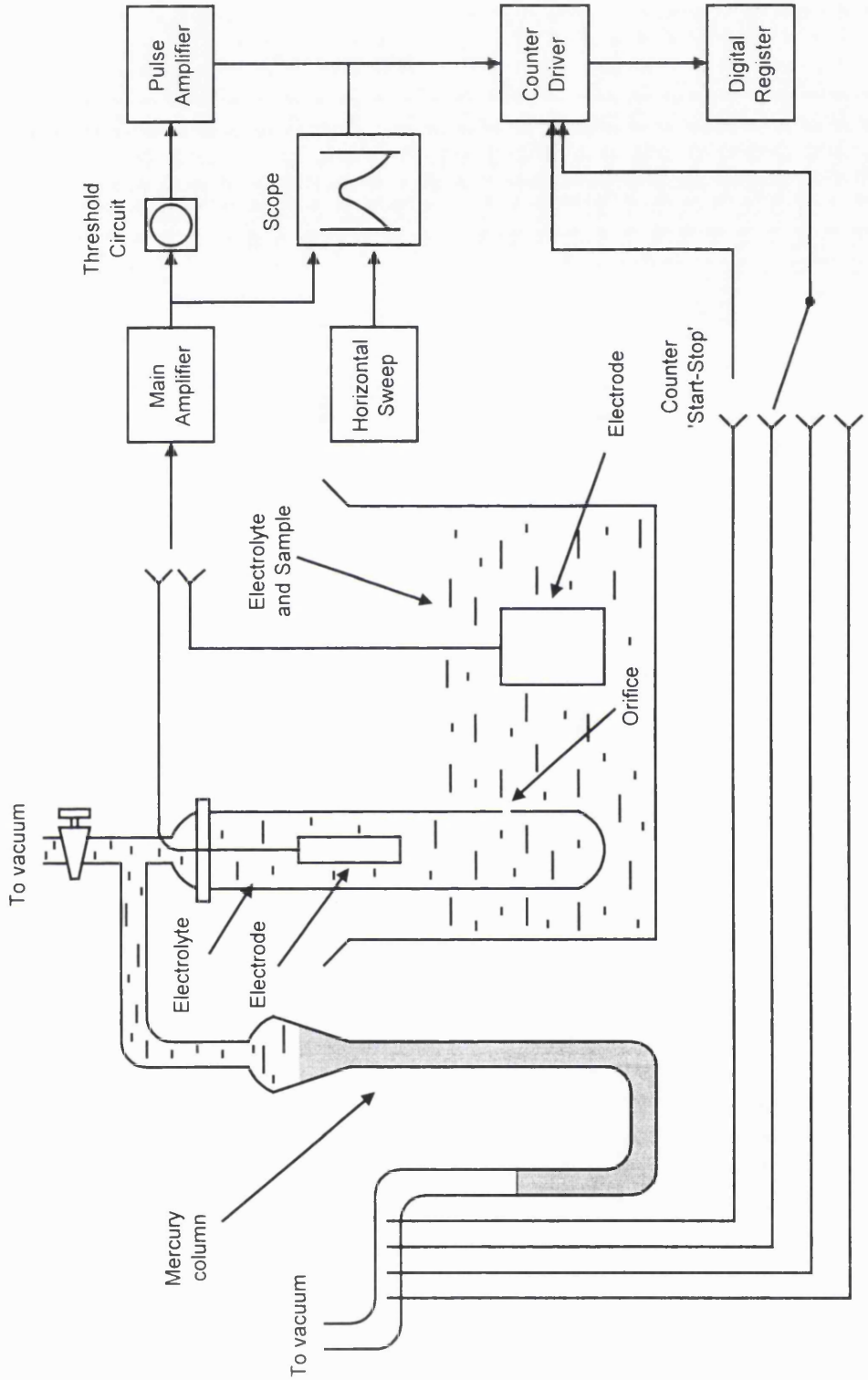

Figure 3.1: Schematic of Elzone 280 PC particle sizer.

All electrolytes were filtered and degassed using 0.2 μm, 47 mm diameter cellulose nitrate filters (Whatman, Maidstone, U.K.) in a vacuum filter apparatus (Millipore, Whatford, U.K.). Adequate dilution (approximately 1 in 2000) was made to eliminate coincidence effects and all particle size distributions were corrected for electrolyte background noise. For each sample three replicate counts were made to ensure consistent results to within ±3.0%.

3.2.7.2 Laser Sizing

Particle size analysis below 1.0 μm was carried out using a Series 4700/ PCS 100 spectrometer laser sizer (Malvern, Worcestershire, U.K.) which uses the photon correlation spectroscopy (PCS) method to determine particle size. In the PCS method, a photon counting detector tracks rapid changes in laser light scattered by a sample containing particulate material. Measurements are taken over given times and fluctuations in intensity are characterised by a digital correlator in order to describe the diffusive movement of the particles. For monosized particles the diffusivity, D_f, is related to particle diameter using Stoke's law and the Einstein equation for Brownian motion (Berne and Percora, 1976) as:

$$D_f = \frac{k_B T}{3\pi\mu d_h}$$

(equation 3.5)

where T is the temperature, k_B is the Boltzmann constant, μ is the solvent viscosity and d_h is the hydrodynamic particle diameter which is slightly larger than the geometric diameter due to solvation and interaction effects. In practice, the diffusion process is quantified by an auto-correlation function, F_{ac}, which arises from the multiplication of the intensity of scattered light by itself, which is known as 'homodyne processing', i.e. successive signals are stored and every 'old signal' is multiplied by the current value of the signal as it is measured. Various methods can then be used to relate F_{ac} to a distribution of intensity over a range of particle sizes.

The main elements of the Series 4700/ PCS 100 spectrometer system are shown in Figure 3.2 on page 90. Monochromatic light emitted by an argon laser is focused onto the sample cell, which is held in a glass vat filled with a liquid. The 'waist of focus', i.e. the point where the beam is narrowest, coincides with the axis of rotation of the photomultiplier.

The beam enters and leaves the vat through flat optical quality windows. An attenuator is mounted on the exit window to reduce back reflection of the laser light. Liquid is placed in the vat to reduce flare at the vat/sample cell interface, and is controlled to a given temperature and filtered using the filter pump to remove dust. The sample is held in a 10 mm circular quart cell. Light scattered by the sample is collected by an optical system and sensed by the photomultiplier, which is sensitive enough to count individual photons. A narrow band filter between the optics and photomultiplier ensures that only light at the wavelength of the laser is detected. The stepper motor allows the scattering angle to be changed from 10° to 150°. Digital signals coming from the photomultiplier are processed by the correlator and then passed to the computer for final analysis and display. A fixed angle of 90° was used during analysis to restrict the laser from seeing the edge of the cuvette. The liquid used in the vat was water and temperature of the vat was set to 20°C.

The intensity distribution is determined by the Series 4700/ PCS 100 spectrometer using both cumulative and multimodal analysis methods:

i) Cumulative method: A polynomial is fitted to the log of the normalised correlation function. The 1st moment is used to derive a mean size (known as the 'Z Average') and the 2nd to give a measure of the width of the distribution (known as the 'polydispersity').

ii) Multimodal Analysis: The overall solution is formed by combining cumulative method solutions for subsets of the overall distribution. The resolution is altered by adjusting the width of the subsets, with the overall number fixed at 24. The solution found is used to generate a 'fit error' by back calculating a correlation function corresponding to the set of size classes in the solution. An iterative process is then carried out in which the width of subsets is reduced until the error no longer improves.

Specifying the refractive index of the particles and sample liquid enabled the intensity distribution to be transformed into a number distribution by dividing the intensity for each size class by a scattering efficiency factor calculated by the instrument. The volume distribution could then be found by assuming the particles were spherical.

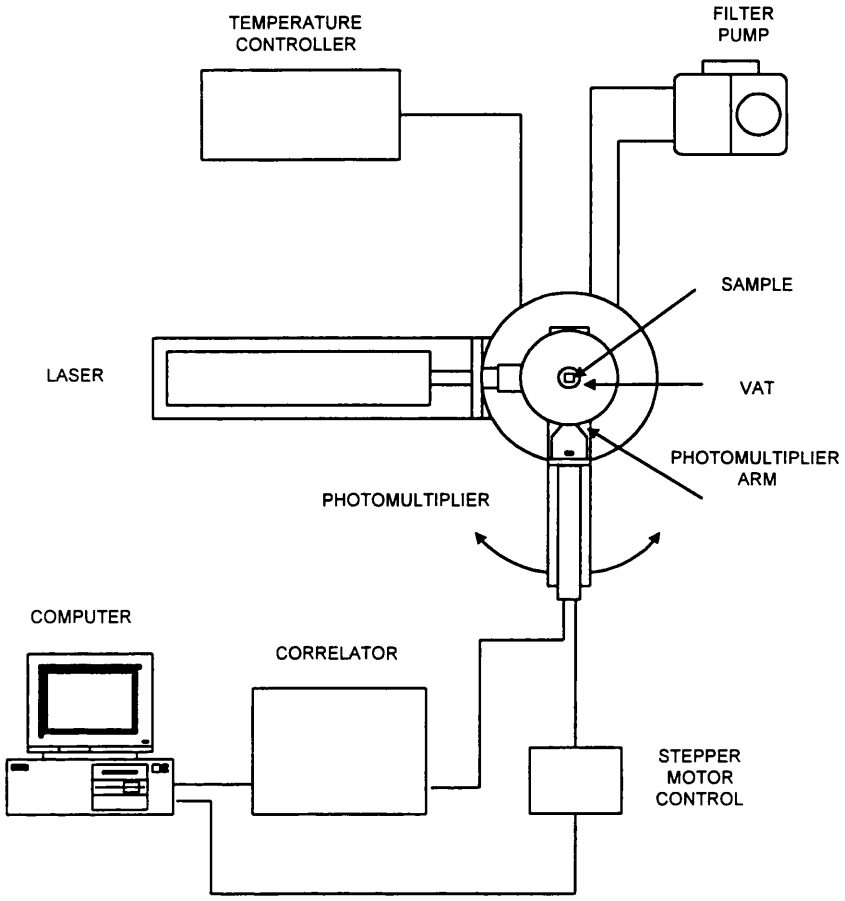

Figure 3.2: Schematic of laser sizer.

Data required by the instrument in order to analyse samples were the sample viscosity, which was measured (Section 3.2.8.4), the refractive index of the sample liquid which was estimated from the literature (Weast, 1978) and the refractive index of the particles which was assumed to be the same as polystyrene latex particles, i.e. a value of 1.59.

Consistency of results was ensured by diluting the sample until the count rate was between 5×10^4 and 100×10^4 counts per second and only accepting the result if the merit, i.e. the percentage of correlatable signal above background, was between 30% and 70%. Samples were analysed in duplicate giving a reproducibility of within ±5% for the 'Z Average' mean size.

3.2.8 Physical Property Determination

3.2.8.1 Liquid Density

The density of sample solutions was measured using PSL specific gravity hydrometers (BDH, Leicestershire, U.K). The hydrometers were used to measure specific gravity in the range of 1000 to 1200 $kg.m^{-3}$ with an accuracy of 5 $kg.m^{-3}$.

3.2.8.2 Particle Density using Percoll gradients

The density of whole cell and cell debris was determined using Percoll (Pharmacia, Hertfordshire, U.K.), a colloidal silica coated with polyvinylpyrrolidone. Centrifugation of Percoll results in the formation of spontaneous density gradients due to the heterogeneity of particle sizes in the medium.

To determine the density of particles in a sample suspension, calibration of Percoll gradients was first carried out using density marker beads (Pharmacia, Hertfordshire, U.K.). The marker beads are coloured derivatives of Sephadex having a specific and reproducible buoyant density in Percoll. A stock Percoll solution was prepared by mixing 49.5 mL of Percoll with 5.5 mL of 1.5 M NaCl at pH 6.5. The stock solution was then mixed with 0.15 M NaCl pH 6.5 in centrifuge tubes with a capacity of 13.5 mL to produce a series of 10 mL standard solutions as shown in Table 3.1.

Tube No.	1	2	3	4	5	6	7	8	9	10
Percoll Stock (mL)	10.0	9.0	8.0	7.0	6.0	5.0	4.0	3.0	2.1	1.0
0.15 M NaCl (mL)	-	1.0	2.0	3.0	4.0	5.0	6.0	7.0	8.0	9.0

Table 3.1: Percoll standard solutions.

10 μL of each type of re-suspended density marker bead was added to the tubes. The tubes were then balanced, capped, mixed by inverting several times, placed in the outer row of a Beckman JA 20.1 angle head rotor (Beckman Instruments, Buckinghamshire, U.K.) and centrifuged at 9,000 rpm (10,400 g) for 0.25 h in a Beckman J2-M1 centrifuge (Beckman Instruments, Buckinghamshire, U.K.). The distance of coloured density marker bead bands which had formed were then measured from the bottom of each tube. The contents of the tubes was then re-mixed by inversion and the centrifugation was repeated at 18,000 rpm (46,500 g) for 0.25 h. The positions of the density marker bead bands were again measured. Calibration curves were then produced for each tube at the two centrifugation conditions by plotting the position of each band against the exact density of the particular marker bead.

To determine the density of particles in a given sample, 50 μL of sample suspension was added to each of the centrifuge tubes containing the standard solutions (Table 3.1). The tubes were then centrifuged at 9,000 rpm for 0.25 h, after which time the position of any visible brown bands which had formed was measured. The process was repeated at 18,000 rpm. By marking the position of bands formed by particles in the sample suspension on the calibration curves, their density was determined. Samples were analysed in duplicate giving a reproducibility of mean density within ±1%.

3.2.8.3 Precipitate Density using Disc Centrifugal Photosedimentation

A disc centrifugal photosedimentometer, model BI-DCP 1000 (Brookhaven Instruments Corporation, New York, U.S.A.) was used to determine the particle density distribution for precipitates. The instrument monitors the rate of particle sedimentation through a known spin fluid at a specified relative centrifugal force. Figure 3.3 on page 94 shows a diagram of the instrument. White light from a tungsten-halogen lamp passes through the disc at a fixed distance from the axis of rotation which corresponds to the height of liquid within the gap when a volume of 5 mL is placed in the disc. As particles pass through the light beam the light intensity is attenuated due to scattering and/or adsorption. The intensity of the transmitted light is measured by a photodiode and recorded as a function of time.

Assuming laminar flow occurs and that particles are spherical, Newton's law can be applied and the terminal radial velocity of particles of diameter d is given by:

$$\frac{dr}{dt} = \frac{(\rho_p - \rho_{sf})d^2}{18\mu}\omega^2 r$$

(equation 3.6)

where r is the radial position with respect to the centre of rotation of the disc, ω is the rotational speed of the disc, ρ_p is the particle density, ρ_{sf} is the spin fluid density and μ is the viscosity of the spin fluid. Integrating equation 3.6 from the initial radius of the injected sample, R_i, at time t = 0, to the radius of the detector, R_d, at time t and rearranging gives the particle density for a given particle diameter as:

$$\rho_p = \frac{18\mu \ln(R_d / R_i)}{\omega^2 d^2 t} + \rho_{sf}$$

(equation 3.7)

For each sample, 15 mL of spin fluid was injected into the spinning rotor and an additional 1 mL of buffer fluid added on top of the spin fluid. The viscosity and density of the buffer fluid were between that of the spin fluid and the suspending fluid in the sample. A density gradient was set up at the outer edge of the spin fluid using the buffered line start method, which involved decelerating the disc for 0.5 s. The purpose of the density gradient was to minimise hydrodynamic shock as the particles sediment outwards through the spin fluid.

For protein precipitates, the spin fluid contained 2.5% sucrose and was adjusted to the final salting-out concentration. The addition of 2.5% sucrose was found to have negligible effect on the precipitate particle size using laser sizing (refer to Section 3.2.7.2 for sizing method). The buffer liquid contained ammonium sulphate at the salting-out concentration, which prevented precipitate dissolution or further precipitation. A small volume, typically 0.2 mL, of the sample (diluted in buffer to less than 1% w/v solids) was injected onto the fluid spinning within the disc rotor. Run times for the samples were up to 0.3 h. Samples were analysed in duplicate giving a reproducibility in sample appearance time of within 1%.

In order to calculate the particle density distribution, the cumulative mass distribution given by the instrument was first matched to the cumulative oversize volume distribution

of the sample (measured using the particle size analysis techniques in Section 3.2.7). Corresponding values of particle diameter, d, and appearance time, t, determined at equivalent cumulative volume/mass values were then substituted into equation 3.7 to give the density for each particle diameter. Accuracy of the method was tested using 2.02 μm polystyrene latex particles with a reported average density of 1005 $kg.m^{-3}$. The experimentally determined average density of 1009.4±0.8 $kg.m^{-3}$ was within 1% of the reported value.

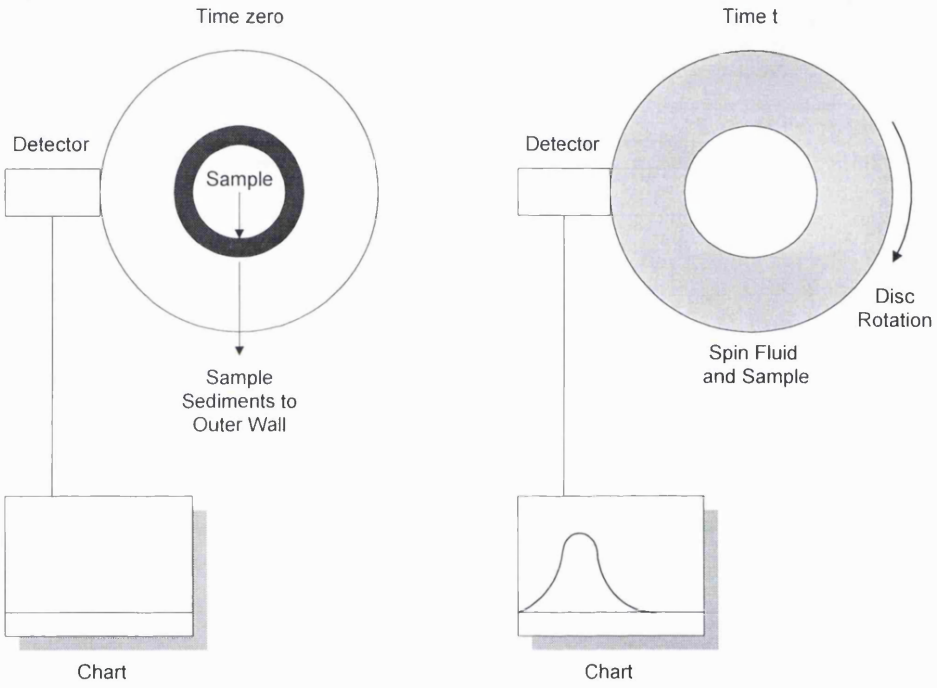

Figure 3.3: Disc centrifuge photosedimentometer operation, from Middelberg and Bogle (1990).

3.2.8.4 Viscosity

Sample viscosity was determined using a Contraves Rheomat 115 rheometer (Contraves AG, Zurich, Switzerland). A coaxial cylinder arrangement was used to measure shear stress at 15 different shear rates. The shear stress-shear rate relationship of the samples examined was linear which indicated Newtonian behaviour, with the viscosity given by the gradient. Measurements were made at room temperature and adjusted to the process temperature in line with the change for water. Samples were analysed in duplicate with a reproducibility of within ±20%.

3.3 Cell Culture and Fermentations

Sterilisation of media components and/or equipment items was carried out using high pressure steam at 121°C for 0.5 h unless otherwise stated.

3.3.1 Yeast Strains

i) Recombinant *Saccharomyces cerevisiae* strain MC1 was kindly donated by E.H. Creaser, Department of Molecular Biology, Research School of Biological Sciences, Australian National University, Canberra, A.C.T., Australia (Creaser *et al.,* 1990).

ii) Recombinant *Escherichia coli* strain WL2 was kindly donated by Eindhoven University of Technology, The Netherlands (Van de Goor-Kucerova, 1992).

iii) The recombinant ADH overexpressing strain, *S. cerevisiae* strain SUB63 + plasmid PMW5-ADH2, and wild type, *S. cerevisiae* strain SUB63, were kindly supplied by K.Sinclair, Department of Biochemistry, University College London, U.K. (Sinclair, 1997).

iv) Natural bakers' yeast, *S. cerevisiae* strain GB4918 produced by Distillers and Company Ltd., West Sussex, U.K., was obtained in packed form from J.W. Pike Ltd., London, U.K.

3.3.2 Culture of *Saccharomyces cerevisiae* Strain MC1

3.3.2.1 Media Formulations

Short term storage of *S. cerevisiae* strain MC1 was carried out on plates and slopes made from sterilised YEPD media, which were stored at 4°C. For longer term storage of up to 3 months, 2 mL of culture broth containing MC1 cells was added to presterilised 7 mL bijoux tubes containing 3 mL of glycerol media. The bijoux tubes were sealed with parafilm and stored at -70°C. The compositions of the culture media used are given in Table 3.2 overleaf.

Component	YEPD media (% w/v)	Gycerol Media (% w/v)
Glucose*	2	4
Mycological Peptone+	2	4
Yeast Extract+	1	2
Agar+	1	-
Glycerol*	-	15

* supplier: Sigma Chemical Co. Ltd., Dorset, U.K.
\+ supplier: Oxoid-Unipath, Hampshire, U.K.

Table 3.2: Culture media for storage of Saccharomyces cerevisiae strain MC1.

Batch, complex media fermentations of *S. cerevisiae* strain MC1 were carried out in 1 L shake flasks (Section 3.3.2.2) and 20 L, 42 L, 450 L and 1500 L fermenters (Section 3.3.2.3). The composition of the complex medium used is given in Table 3.3.

Component	Concentration
Glucose*	30 $g.L^{-1}$
Malt Extract[1+]	17 $g.L^{-1}$
Mycological Peptone[1+]	3 $g.L^{-1}$
Yeast Extract+	10 $g.L^{-1}$
PPG Antifoam[2*]	0.1 $mL.L^{-1}$

1 These components were replaced by 20 $g.L^{-1}$ Malt Broth for 30 L fermentations
2 PPG level used for 30 L fermentations was initially 1 $mL.L^{-1}$ but was reduced to avoid any possible interference with downstream processing operations
* supplier: Sigma Chemical Co. Ltd., Dorset, U.K.
\+ supplier: Oxoid-Unipath, Hampshire, U.K.

Table 3.3: Complex medium for Saccharomyces cerevisiae strain MC1 fermentations.

3.3.2.2 Shake Flask Culture

Shake flask culture of *S. cerevisiae* strain MC1 was carried out in presterilised 1 L flasks containing 200 mL of complex media. The flasks were incubated in a New Brunswick model G25 orbital shaker (New Brunswick Scientific Ltd., Hatfield, U.K.) at 30°C and 200 rpm for up to 24 h. Inoculation was carried out by asceptically placing 1 loopful of MC1 cells from a YEPD plate into a presterilised 20 mL universal bottle containing 5 mL of complex media. This was incubated in the orbital shaker until an optical density at 600 nm of approximately 10 had been achieved, then asceptically transferred to the shake flask. Monitoring of the culture was carried out as described in Section 3.3.5.

3.3.2.3 Fermentations

Fermentations of *S.cerevisiae* strain MC1 were carried out in 20 L (15 L working volume) and 42 L (30 L working volume) LH fermenters (Inceltech Ltd., Berkshire, U.K.), and 450 L (400 L working volume) and 1500 L (1000 L working volume) Chemap fermenters (Alfa-Laval Engineering Ltd, Middlesex, U.K.) for up to 24 h.

In each case, sterilisation of the complex media was carried out in the fermenters using a steam jacket with the temperature at 121°C for 40 minutes. For the 15 L fermentations, inoculum was prepared from two 200 mL shake flask cultures (Section 3.3.2.2) which were asceptically added to a 1 L addition flask for transfer to the fermenter. For the 30 L fermentations, inoculum was prepared from three 200 mL shake flask cultures (Section 3.3.2.2) which were asceptically added to a 2 L addition flask for transfer to the fermenter. For the 400 L fermentations, the inoculum was prepared in the 20 L fermenter, with the 15 L of final fermentation media being asceptically transferred to the 450 L fermenter. For 1000 L fermentations, inoculum was prepared in the 42 L fermenter with the 30 L of final fermentation broth being asceptically transferred to the 1500 L fermenter.

Temperature, pH, agitation rate and air flow were measured and automatically controlled to preset values during each fermentation using TCS instrumentation (refer to Table 3.4 on page 98 for operating conditions). 1M sodium hydroxide and 1M sulphuric acid were automatically added via peristaltic pumps to maintain the pH at the setpoint. Monitoring of each fermentation was carried out as described in Section 3.3.5.

Fermenter	20 L	42 L	450 L	1500 L
Working Volume (L)	15	30	400	1000
Temperature (°C)	30	30	30	30
pH	5.0	5.0	5.0	5.0
Agitation Rate (rpm)	500	700/500[1]/300[2]	250	300
Air Flow ($L.s^{-1}$) (to give ½ VVM)	0.125	0.250	3.333	8.333

[1] agitation rate reduced from 700 rpm to 500 rpm to give similar mixing to the large scale fermentations (refer to Chapter 4.0).

[2] agitation rate reduced from 500 rpm to 300 rpm when antifoam level was reduced from 1.0 $mL.L^{-1}$ to 0.1 $mL.L^{-1}$ in order to prevent foaming (refer to Chapter 4.0).

Table 3.4: MC1 Strain fermenter operating parameters.

3.3.3 Culture of *Eschericia coli* strain WL2

Short term storage of *E. coli* strain WL2 was carried out on plates and slopes made from sterilised nutrient broth media (Table 3.5) to which ampicillin (Sigma Chemical Co. Ltd., Dorset, U.K.) was added to a final concentration of 500 $\mu g.mL^{-1}$ by filter sterilisation through a 0.2 μm disk filter (Whatman, Maidstone, U.K.). The nutrient broth plates and slopes were stored at 4°C. For longer term storage of up to 3 months WL2 strain colonies were harvested from a plate and placed in a presterilised 20 mL universal bottles containing glycerol solution (Table 3.5) and stored at -70°C.

Component	Nutrient Broth media (% w/v)	Glycerol solution (% w/v)
Liquid Broth No. 2[+]	2.5	-
Agar[+]	2	-
Glycerol[*]	-	20

[*] supplier: Sigma Chemical Co. Ltd., Poole U.K.

[+] supplier: Oxoid-Unipath, Hampshire, U.K.

Table 3.5: Culture media for storage of Eschericia coli strain MC1.

Batch, complex media shake flask cultures of *E. coli* strain WL2 were carried out in 1 L presterilised shake flasks containing 200 mL of nutrient broth media (Table 3.5) to which ampicillin (Sigma Chemical Co. Ltd., Dorset, U.K.) was added to a final concentration of 500 $\mu g.mL^{-1}$ by filter sterilisation through a 0.2 μm, 13 mm syringe filter (Whatman, Maidstone, U.K.). The flasks were incubated in a New Brunswick model G25 orbital shaker (New Brunswick Scientific Ltd, Hatfield, U.K.) at 37°C and 220 rpm for up to 24 h. Inoculation of the flasks was carried out by asceptically transferring 2 to 3 loopfuls of WL2 strain cells from a nutrient broth plate to presterilised 20 mL universal bottles to which 5 mL of the nutrient broth media containing ampicillin (Sigma Chemical Co. Ltd., Poole U.K.) had been asceptically added. The inoculum was incubated in the orbital shaker until an optical density at 600 nm of approximately 1 had been achieved, then asceptically transferred to the shake flask.

Monitoring of the culture was carried out as described in Section 3.3.5. The expression of recombinant HLADH was induced by the addition of isopropylthiogalactoside (Sigma Chemical Co. Ltd., Dorset, U.K.) to a final concentration of 1 mM by filter sterilisation through a 0.2 μm, 13 mm syringe filter (Whatman, Maidstone, U.K.) when the optical density of the culture at 600 nm was approximately 1.

3.3.4 Culture of the ADH Overexpressing Strain and Wild Type

Short term storage of the ADH overexpressing strain, *Saccharomyces cerevisiae* strain SUB-63 + plasmid PMW5-ADH2, was carried out on plates and slopes made from sterilised DUC defined media (Table 3.6 overleaf). The glucose, yeast nitrogen base and agar components were presterilised in the shake flasks, with Casamino acids and the uracil being added afterwards by filter sterilisation through a 0.2 μm, 13 mm syringe filter (Whatman, Maidstone, U.K.) to prevent precipitation. For longer term storage of up to 3 months, 2 mL of culture broth containing ADH overexpressing cells was added to presterilised 7 mL bijoux tubes containing 3 mL of 20% (v/v) glycerol.

Shake flask cultures were carried out in 1 L shake flasks containing 200 mL of defined media (Table 3.6). The glucose and yeast nitrogen base components were presterilised in the shake flasks, with Casamino acids and the uracil being added afterwards by filter sterilisation through a 0.2 μm, 13 mm syringe filter (Whatman, Maidstone, U.K.) to

prevent precipitation. The shake flasks were incubated in a New Brunswick model G25 orbital shaker (New Brunswick Scientific Ltd, Hatfield, U.K.) at 30°C and 220 rpm for up to 96 h. Inoculation of the flasks was carried out by asceptically transferring 2 to 3 loopfuls of ADH overexpressing cells from a DUC plate to presterilised 20 mL universal bottles to which 5 mL of shake flask culture media had been asceptically added. The inoculum was incubated in the orbital shaker until an optical density at 600 nm of approximately 5 had been achieved, then asceptically transferred to the shake flask. Monitoring of the culture was carried out as described in Section 3.3.5.

In the case of the wild type, *S. cerevisiae* strain SUB-63, storage and shake flask culture was carried as per the ADH overexpressor except that tryptophan was added at the same time as the uracil by filter sterilisation through a 0.2 μm, 13 mm syringe filter (Whatman, Maidstone, U.K.) to give a final concentration of 0.02 $g.L^{-1}$.

Component	**Storage Media 'DUC' ($g.L^{-1}$)**	**Sterility Check 'DM' ($g.L^{-1}$)**	**Plasmid Check 'DUCT' ($g.L^{-1}$)**	**Shake Flask Culture ($g.L^{-1}$)**
Glucose*	20	20	20	20
Yeast Nitrogen Base#	6.7	6.7	6.7	6.7
Casamino Acids#	5	-	5	5
Uracil*	0.02	-	0.02	0.02
Tryptophan*	-	-	0.02	-
Agar+	20	20	20	-

* supplier: Sigma Chemical Co. Ltd., Dorset, U.K.
\# supplier: Difco Laboratories, Surrey, U.K.
\+ supplier: Oxoid-Unipath, Hampshire, U.K.

Table 3.6: Culture media for the ADH overexpressor.

3.3.5 Monitoring during Cell Culture

Samples were taken from shake flask cultures at regular intervals or fermentations at each hour and the following determined:

3.3.5.1 Cell Optical Density

Cell optical density was determined by measuring the optical density of a sample of broth at 600 nm (Section 3.2.3).

3.3.5.2 Cell Dry Weight

Cell dry weight was determined using the filtered dry weight method (Section 3.2.2.1).

3.3.5.3 ADH Activity and Total Protein Level

The total protein level and ADH activity was determined by assaying a culture sample which was disrupted to release all soluble proteins from within cells. Broth samples were first centrifuged at 9,000 rpm for 0.25 h in a Beckman J2-M1 centrifuge (Beckman Instruments, Buckinghamshire, U.K.), the supernatant discarded and the cell pellet resuspended to the same initial volume with 100 mM potassium dihydrogen phosphate buffer pH 6.5. Disruption was carried out using two discrete passes through a Manton Gaulin LAB-40 high pressure homogeniser (APV Baker, Crawley, U.K.), operated at 1200 barg and cooled to 4°C for 1 h prior to use using glycol cooling around the valve head. For the WL2 strain in some cases, samples were disrupted using a MSE Soniprep 150 sonicator (MSE Ltd., Leicestershire, U.K.) operated at an amplitude of 8 μm for 30 s. Samples were cooled during sonication by immersing in a beaker of ice. Refer to Sections 3.2.1.1 and 3.2.1.2 for a description of the ADH and total protein assays respectively.

3.3.5.4 Ethanol Level

The ethanol level in the broth was determined from the filtrate produced during dry weight determination (Section 3.2.2.1). This ensured that the ethanol assay was not affected by ADH present in cells. Refer to Section 3.2.1.4 for the assay method.

3.3.5.5 Glucose Level

The glucose level in the broth was determined from the filtrate produced during dry weight determination (Section 3.2.2.1). Refer to Section 3.2.1.3 for the assay method.

3.3.5.6 Checks for Contamination

For *Saccharomyces cerevisiae* strain MC1, a check for the presence of wild type yeast or other contaminating organisms was performed up to 4 times during a shake flask culture or fermentation. This was carried out by placing a sample of broth onto CDM defined media plates and CDM defined media plates with added histidine (CDH plates). Table 3.7 overleaf shows the composition of the various parts of CDM media. The CDM plates were made by preparing part A of the CDM media in a 1 L duran bottle, adding 3mL.L^{-1} of part B and 1% (w/v) agar (Oxoid-Unipath, Hampshire, U.K.) and then sterilising. Once cooled, but before the agar had set, 5 mL.L^{-1} of part C and 6 mL.L^{-1} of part D were added by filter sterilising through a 0.2 μm, 13 mm syringe filter (Whatman, Maidstone, U.K.). For the CDH plates, concentrated histidine solution was added with parts C and D by filter sterilisation to give a final histidine concentration of 10 mg.L^{-1}. In both cases the media was then poured to form the plates and allowed to set. Due to the inability of the MC1 strain to produce histidine (Section 1.5.1), characteristic MC1 strain colonies should only form on the plates which contained added histidine. If colonies formed on the plates without histidine, contamination by wild type yeast or another organism was indicated.

For *E. coli* strain WL2, a check for contamination was carried out up to 4 times during culture by placing a sample of broth from the end of the culture onto nutrient broth plates (Section 3.3.3) and checking that the colonies formed were characteristic of the WL2 strain.

Component	Concentration ($g.L^{-1}$)
Part A - Glucose and Salts	
Glucose*	10.0
$MgSO_4.7H_2O$	0.5
KH_2PO_4	4.0
K_2HPO_4	0.5
NaCl	0.1
$CaCl_2.H_2O$	0.1
$(NH_4)_2SO_4$	1.5
Part B - 4 mM Ferrous Sulphate Solution	
Ferrous citrate	2.780
Trisodium citrate.$2H_2O$	1.176
Part C - Trace Element Solution	
$CuSO_4.5H_2O$	0.0400
KI	0.1000
$ZnSO_4.7H_2O$	0.1000
$Na_2MoO_4.2H_2O$	0.1000
$MnSO_4.H_2O$	0.1516
$Na_2B_4O_7.10H_2O$	0.1000
Part D - Vitamin Stock Solution	
Calcium pantothenate*	0.167
Thiamine*	0.167
Inositol*	0.500
Pyridoxal HCl*	0.167
Nicotinic acid*	0.083
Biotin*	0.033

* supplier: Sigma Chemical Co. Ltd., Poole U.K.

Table 3.7: MC1 Strain 'CDM' defined media components.

For the ADH overexpressor and wild type, a check for contaminating organisms was performed up to 4 times during shake flask culture. This was carried out by placing a sample of broth onto agar plates made with DM media (Table 3.5) and checking for the formation of colonies. Since the recombinant strain requires histidine, lysine and uracil for growth and the wild type additionally requires trypyophan (Section 1.5.2), no ADH overexpressor or wild type cells can grow on DM media plates and the presence of colonies indicated contamination with another organism.

3.3.5.7 Plasmid Stability

For *Saccharomyces cerevisiae* strain MC1, plasmid stability was examined by determining the proportion of cells containing the plasmid for protein engineered ADH at up to 4 points during culture. To determine the proportion of cells containing the plasmid, serial dilutions of sample broth from 10^{-1} to 10^{-5} were made under aseptic conditions. Three 10 μL drops of each dilution were placed on a CDH plate and on a CDM plate containing both added histidine and tryptophan (a CDTH plate). To form the CDTH plates, the same procedure was followed as for CDH plate preparation (Section 3.3.5.6) except that concentrated tryptohan solution was also added by filter sterilisation to give a final concentration of 20 $mg.L^{-1}$ at the same time as the histidine. After colonies were visible (approximately 36 to 48 h) the number of colonies for each dilution was counted. The fraction of cells containing the plasmid was then calculated as the number of colonies on the CDH plate at a given dilution divided by the number of colonies on the CDTH plate at the same dilution (Section 1.5.1).

For the ADH overexpressor, plasmid stability was examined by determining the proportion of cells containing the plasmid PMW-ADH2 at up to 4 points during shake flask culture. Serial dilutions of sample broth from 10^{-1} to 10^{-10} were made under aseptic conditions. Three 10 μl drops of each dilution were placed on DUC and DUCT agar plates. After colonies were visible (approximately 36 to 48 h) the number of colonies for each dilution was counted. The fraction of cells containing the plasmid was calculated as the number of colonies on the DUC plate at a given dilution divided by the number of colonies on the DUCT plate at the same dilution.

3.3.5.8 Gas analysis

For fermentations carried out in the 20 L, 42 L, 450 L and 1500 L fermenters the fermenter exit gases were automatically analysed by mass spectrophotometer and fermentation data logged on RT-DAS (Real Time Data Acquisition Systems, Surrey, U.K.). Carbon dioxide evolution rate (CER), oxygen uptake rate (OUR) and respiratory quotient (RQ) values were automatically calculated by RT-DAS.

3.4 Downstream Processing

Downstream processing studies were carried out for the MC1 strain only. Operating conditions were identical to those used by Clarkson (1994) and Siddiqi (1997) to allow comparisons to be made between the processing of natural bakers' yeast and the MC1 strain. Models previously developed at UCL by examining the processing of natural bakers' yeast could then be applied to the MC1 strain (Chapter 2.0).

3.4.1 High Pressure Homogenisation Studies

3.4.1.1 Characterisation using a Scale-down Unit

Characterisation of the high pressure homogenisation of MC1 strain cells was carried out using a Manton Gaulin Micron LAB-40 scaled-down high pressure homogeniser fitted with a SV valve (APV Baker, Crawley, U.K.). The design and dimensions of the SV valve are given by Siddiqi *et al.* (1997), who previously examined the performance of this homogeniser and found that the breakage of packed bakers' yeast was the same as that achieved by the larger pilot-scale LAB-60 and semi-industrial scale K-3 Manton Gaulin high pressure homogenisers operated with CD valves (APV Baker, Crawley, U.K.). A discussion of the use of the scaled-down homogeniser is included in Section 5.4.

MC1 strain cells from 30 L fermentations (Section 3.3.2.3) were harvested in the stationary phase of growth 24 h after inoculation by a 1-P Sharples tubular bowl centrifuge (Alfa-Laval Sharples Ltd., Camberley, U.K.) operated at a flowrate of 30 $L.h^{-1}$ and bowl speed of 40,000 rpm. The centrifugation conditions corresponded to a flowrate to

separation area ratio (Q/Σ) of 3.2×10^{-9} $m.s^{-1}$. The harvested cells were resuspended to 280 or 480 g wet weight per L, i.e. 28% and 45% (w/w) respectively in 100 mM potassium dihydrogen phosphate buffer pH 6.5. This concentration range is typical of what would be produced in a disc stack centrifuge operating as the harvest centrifuge in a large scale process (Clarkson, 1994).

Freshly prepared 40 mL samples of the cell suspension were disrupted at pressures of 200, 340, 400, 500 and 1200 barg and from 1 to 5 and 10 discrete passes in the Manton Gaulin Micron LAB-40 scaled-down homogeniser (APV Baker, Crawley, U.K.). The temperature was maintained at 4°C around the homogeniser valve head using glycol cooling to avoid denaturation of *pe*-ADH. Monitoring of high pressure homogenisation was carried out as described in Section 3.4.1.3.

3.4.1.2 Pilot-Scale Homogenisation

Homogenisation of 280 $g.L^{-1}$ MC1 strain cells was carried out at 500 barg and 1 to 5 passes using the pilot-scale LAB-60 and semi-industrial scale K-3 Manton Gaulin high pressure homogenisers operated with one and two CD valves respectively (APV Baker, Crawley, U.K.) in order to test the scalability of MC1 strain homogenisation models.

Material for LAB-60 homogenisation was produced as in Section 3.4.1.1, while material for K-3 homogenisation was produced in a 450 L fermentation (Section 3.3.2.3) and harvested 24 h after inoculation using a motor driven Pennwalt AS-26 tubular bowl centrifuge at a flowrate of 300 $L.h^{-1}$ and bowl speed of 17,000 rpm. The centrifugation conditions corresponded to a flowrate to sigma factor ratio (Q/Σ) of 2×10^{-9} $m.s^{-1}$. The harvested cells were resuspended to a concentration of 280 g wet weight yeast per L in 100 mM potassium dihydrogen phosphate buffer at pH 6.5. For both LAB-60 and K-3 homogenisation, the temperature was maintained at 4°C using glycol cooling to avoid denaturation of *pe*-ADH. The design and dimensions of the SV and CD valves are given by Siddiqi *et al.* (1997). Monitoring of homogenisation was carried out as described in Section 3.4.1.3.

3.4.1.3 Homogenisation Monitoring

For the homogenisation studies, samples of the starting material and homogenate after each pass were taken. The following analyses were performed:

i) The aqueous fraction and thereby the fraction of solids after each pass at MC1 strain cell concentrations of 28 % and 45 % (w/w) was determined from scaled-down homogeniser samples using the dilution method (Section 3.2.5.2).

ii) The soluble ADH activity was determined. To do this, the sample was centrifuged at 14,000 rpm for 10 minutes in a bench top MSE Micro Centaur lab centrifuge (MSE Ltd., Leicestershire, U.K.) and the supernatant assayed for ADH (Section 3.2.1.1). Correction of the assay results to account for the solid content of the sample was carried out using the solid fraction determined in (i).

iii) The soluble total protein concentration was determined. To do this, the sample was centrifuged at 14,000 rpm for 10 minutes in a MSE Micro Centaur lab centrifuge (MSE Ltd., Leicestershire, U.K.) and the supernatant assayed for protein (Section 3.2.1.2). Correction of the assay results to account for the solid content of the sample was carried out using the solid fraction determined in (i).

iv) The liquid density of the sample was determined (Section 3.2.8.1) and the density of whole cells and/or debris particles in the sample were determined using Percoll gradients (Section 3.2.8.2).

v) The viscosity of the sample was determined (Section 3.2.8.4).

vi) The particle size distribution (PSD) of the sample was determined using the Elzone method (Section 3.2.7.1). The PSD data was stored as ASCII files and imported into EXCEL V3.1 (Microsoft Corp., Redmont, WA, U.S.A.) for analysis (Section 3.5).

vii) Microscopic examination was carried out on samples homogenised at 1200 bar to determine the fraction of viable cells remaining (Section 3.2.4).

3.4.2 Neutral Salt Protein Precipitation Studies

3.4.2.1 Solubility Profiles

Small scale precipitation studies were carried out to compare the solubility profiles of MC1 strain *pe*-ADH and total protein to that of natural bakers' yeast ADH and total protein under various conditions. MC1 strain cells produced in 30 L fermentations and harvested as per Section 3.4.1.1 were used. In some cases the harvested cells were washed by diluting in 5 L of 100 mM potassium dihydrogen phosphate buffer at pH 6.5 and recentrifuging. Polypropylene glycol (PPG) was also added to packed yeast suspensions in some cases at equivalent concentrations to that used in MC1 strain 30 L fermentations (Section 3.3.2.3) to examine the effect of antifoam on subsequent precipitations.

Packed bakers' yeast and fermented MC1 strain cells were resuspended to give concentrations of 280, 93 or 26 g wet weight per L in 100 mM potassium dihydrogen phosphate buffer at pH 6.5 and disrupted using 5 discrete passes through a Manton Gaulin LAB-60 homogeniser (APV Baker, Crawley, U.K.) operated at 500 barg and 4°C. Cell debris was removed using a Sharples 1-P tubular bowl centrifuge (Alfa-Laval Sharples Ltd., Camberley, U.K.) operated at 25,000 rpm and a feed flowrate of 15 $L.h^{-1}$. The centrifuge produced an equivalent settling area (Σ) of 412 m^2 (and a Q/Σ ratio of 1×10^{-8} $m.s^{-1}$) which was the same as that used by Clarkson (1994) and comparable to that used by Mosquiera *et al.* (1981) for bakers' yeast debris removal.

Precipitations were carried out using the clarified homogenate in a 1.4 L baffled vessel (refer to Table 3.7 overleaf for vessel dimensions) at a constant volume of 0.9 L, temperature of 4°C, pH of 6.5 and agitator rate of 520 rpm ($G = 44\ s^{-1}$) for a range of ammonium sulphate concentrations by adding 100% saturated ammonium sulphate solution prepared in 100 mM potassium dihydrogen phosphate buffer at pH 6.5 according to the equations of Di Jeso (1968). The reactor was agitated with a standard 6-blade Rushton turbine and glycol cooled to 4°C using an external jacket. Removal of liquor and addition of 100% saturated ammonium sulphate was achieved using a measuring cylinder and Watson-Marlow 502S peristaltic pump (BDH, Leichestershire, U.K.). The 100% saturated ammonium sulphate was added at a constant rate of 50 $L.h^{-1}$ close to the impeller to give rapid mixing.

Samples were taken for each ammonium sulphate concentration and analysed as described in Section 3.4.2.3. ADH and total protein solubility profiles were constructed by plotting the fractions of ADH and total protein remaining soluble against the corresponding ammonium sulphate concentration expressed as the % saturation.

Dimension (m)	Small Scale (1.4 L)	Medium Scale (4.4 L)	Large Scale (120 L)
Tank Height	0.158	0.220	0.600
Tank Diameter	0.105	0.160	0.505
Impeller Diameter	0.043	0.064	0.148
Baffle Width	0.010	0.015	0.050

Table 3.7: Batch precipitation vessel dimensions

3.4.2.2 Two-cut Precipitation

Two-cut ammonium sulphate precipitations were carried out and examined as part of full process runs for the recovery of *pe*-ADH (Section 3.4.4). The two stage process was used in order to fractionate contaminating proteins and give a degree of purification to the product enzyme. The ammonium sulphate saturation used for the 1st and 2nd cut points were 40% and 60% respectively. These conditions had previously been used by Clarkson (1994) and Alsaffar (1994).

Precipitations were carried out in both a 4.4 L and 120 L baffled reactor (refer to Table 3.7 for dimensions). In both cases a given volume of 100% ammonium sulphate, prepared in 100 mM potassium dihydrogen phosphate buffer at pH 6.5 and determined according to the equations of Di Jeso (1968), was added to give the required ammonium sulphate saturation.

For the 4.4 L reactor, precipitations were carried out at a constant volume of 3.6 L with the reactor agitated using a standard 6-blade Rushton turbine and glycol cooled to 4°C using

an external jacket. Both 40% and 60% protein precipitate suspensions were batch-aged for 0.67 h at impeller speeds of 100, 425 and 735 rpm (G = 5 s^{-1}, 44 s^{-1} and 100 s^{-1} respectively) in order to examine changes in precipitate particle size. For the 120 L reactor a constant volume of 50 L was used with the reactor agitated using a standard 3-blade marine type turbine and glycol cooled to 4°C using an external jacket. Both 40% and 60% protein precipitate suspensions were batch-aged for 0.67 h at an impeller speed of 250 rpm (G = 44 s^{-1}) in order to give a Gt value greater than 10^5.

In both cases the 100% saturated ammonium sulphate solution was added by rapidly pouring in the required volume near the impeller to give good mixing. Samples were taken at 300 s intervals during batch-ageing and were analysed as described in Section 3.4.2.3. The degree of precipitation was determined from the fraction of ADH and total protein remaining soluble after each cut.

3.4.2.3 Precipitation Monitoring

For the precipitation studies, the following analyses were performed:

i) The fraction of solids in the sample was determined using the centrifuge method (Section 3.2.5.1).

ii) The fraction of ADH and protein remaining soluble were determined. To do this, the sample was first centrifuged at 14,000 rpm for 0.5 h in a MSE Micro Centaur lab centrifuge (MSE Ltd., Leicestershire, U.K.). The supernatant was separated from the solid precipitate and assayed to give the aqueous phase ADH activity (Section 3.2.1.1) and total protein concentration (Sections 3.2.1.2). Correction of the assay results to account for the solid content of the sample was based on the solid fraction determined in (i) above.

The solid precipitate was resuspended in 1 mL of 100 mM potassium dihydrogen phosphate buffer pH 6.5 to redissolve precipitated ADH and protein, re-centrifuged as above and assayed to give the precipitate phase ADH activity (Section 3.2.1.1) and total protein concentration (Section 3.2.1.2). The fraction of ADH and total protein remaining soluble for a particular ammonium sulphate saturation (0 to 90%) was then calculated as

the aqueous phase ADH activity or protein concentration divided by the sum of the aqueous and solid phase ADH activities or protein concentrations at that saturation.

iii) The dry weight of the sample was determined using the microtube dry weight method (Section 3.2.2.2). A correction was made to account for the mass of ammonium sulphate present.

iv) For some samples the particle size distribution of the precipitate was determined using laser sizing (Section 3.2.7.2). This method was used instead of Elzone sizing (Section 3.2.7.1) as the MC1 strain precipitate particles were found to be largely below 1 μm in size. Immediately after sample collection, accurate dilution of precipitate particles was carried out using buffer at the appropriate ammonium sulphate saturation to effectively capture the particle size.

v) For some samples the density of precipitate particles was determined using the centrifugal sedimentation method (Section 3.2.8.3)

vi) For some samples the suspension viscosity was determined (Section 3.2.8.4)

3.4.3 Disc Stack Centrifugation Studies

MC1 strain cell harvesting, cell washing, debris removal and precipitate separation by intermittent discharge disc stack centrifugation were examined. In all cases, a Westfalia SAOOH 205 intermittent discharge disc stack centrifuge (Westfalia Separator Ltd., Milton Keynes, U.K.) fed via a type SB14R Monopump (Monopumps Ltd., London, U.K.) was used. Unless otherwise stated, the centrifuge was operated with a full stack of 43 discs and a rotational speed of 10,000 rpm giving a sigma factor (Σ) equal to 1560 m^2 (refer to Section 7.2.2 for a description of the sigma factor). The full scale centrifuge bowl volume and solids holding space were 0.6 L and 0.3 L respectively.

During the experimental trials only full discharges were used with the optimum discharge time for each material determined from optical density measurements at 670 nm (Section 3.2.3). When the ratio of supernatant to average feed optical density equals 1 overflow of the particulate phase into the supernatant stream is indicated due to the filling

of the centrifuge solids holding space. The optimal discharge time was therefore taken when this ratio equalled 0.8. The feed pump was stopped before each discharge to limit the loss of feed material from the bowl.

In order to apply centrifugation models the suspension density (Section 3.2.8.1), the particle density (Sections 3.2.8.2 and 3.2.8.3), the suspension viscosity (Section 3.2.8.4), aqueous fraction (Section 3.2.3.1) and dry weight (Section 3.2.2.2) of each feed material were determined.

3.4.3.1 Cell Harvesting and Washing

For cell harvesting studies, MC1 strain fermentation broth from 30 L fermentations and a 1000 L fermentation was used (Section 3.3.2.3) and processed 24 h after inoculation at flowrates of 100, 200 and 400 $L.h^{-1}$. Washing of the cell concentrate was also carried out by diluting the recovered cells 1:5 with 100 mM potassium dihydrogen phosphate buffer at pH 6.5 and recentrifuging at flowrates of 20 $L.h^{-1}$ and 60 $L.h^{-1}$.

For both stages and at each flowrate, supernatant stream samples were taken at regular intervals during centrifuge operation and were analysed for optical density at 670 nm (Section 3.2.3) and microtube dry weights (Section 3.2.2.2). Steady state samples, i.e. samples collected after 10 bowl volumes had passed through the centrifuge (Clarkson *et al.*, 1993), were analysed for particle size using the Elzone method (Section 3.2.7.1) with recovery efficiencies and grade efficiencies being determined (Section 3.4.3.4). Solids concentrations were also measured for the final discharged solids and supernatant using the microtube dry weight method (Section 3.2.2).

3.4.3.2 Debris Removal

To examine debris removal, disruption of the washed cell slurry was carried out using a Manton Gaulin LAB-60 high pressure homogeniser (APV Baker, Crawley, U.K.) for material prepared in the 42 L fermenter, and a Manton Gaulin K3 high pressure homogeniser (APV Baker, Crawley, U.K.) for material prepared in the 450 L and 1000 L fermenters (refer to Section 3.4.3.1 for the harvest and wash procedure). In both cases 5 discreet passes and an operating pressure of 500 barg was used. To avoid protein

denaturation and enzyme inactivation, the temperature of homogenate was maintained at 4°C by glycol cooling.

Grade efficiency curves were determined for the centrifugation of homogenised cells from 30 L fermentations. Due to the small volume of material available, experiments were carried out by both diluting the homogenate to 1% (w/v) and by scaling down the centrifuge to only 9 active discs (Maybury, 1997). The diluted homogenate was processed at flowrates of 200, 400 and 600 $L.h^{-1}$, while the scaled down centrifuge was operated at 5 and 10 $L.h^{-1}$ so as to maintain the same Q/Σ ratio as the full scale unit operating at flowrates of 25 and 50 $L.h^{-1}$ respectively.

In the case of the scale-down unit, 3 blanking inserts were used and also 1 bottom insert to raise the active discs above the turbulent region at the bottom of the centrifuge bowl (Maybury, 1997). This resulted in an approximately 45% reduction in the bowl volume and solids holding space. Steady state samples, i.e. samples collected after approximately 10 bowl volumes had passed through the centrifuge (Clarkson *et al.*, 1993), were analysed for particle size using the Elzone method (Section 3.2.7.1) and recovery and grade efficiencies determined (Section 3.4.3.4).

Steady state recovery efficiencies for a full scale disc stack at the process concentration were determined at flowrates of 25, 50 and 100 $L.h^{-1}$ using homogenised cells from 450 and 1000 L fermentations and compared to predicted recovery efficiencies based on the smaller scale results.

The effect of high solids loadings on overall recovery efficiency due to solids overflow was examined using homogenised cells from 30 L fermentations processed with the scaled-down disc stack. In both cases, the recovery efficiency, E_t, was determined from Elzone particle size data (Section 3.4.3.4). Solids concentrations of the pooled discharged solids and supernatant were also measured using the microtube dry weight method (Section 3.2.2.2). ADH and protein assays (Sections 3.2.1.1 and 3.2.1.2 respectively) were carried out on the feed material and supernatant to determine the yield of soluble ADH and protein.

3.4.3.3 Precipitate Separation

The separation of precipitate after each cut point was examined as part of full process runs (Section 3.4.4). A feed flowrate of 50 $L.h^{-1}$ was used in the large pilot scale run, while in the small pilot scale run a scaled-down disc stack was used at flowrates of 5 and 10 $L.h^{-1}$ in order to give equivalent processing to a full stack at 25 and 50 $L.h^{-1}$ respectively.

Because the precipitate particle size was below 1 μm and laser sizing was used (Section 3.2.7.2), the precipitate PSD was only described in relative terms and grade efficiency curves could not be determined. The efficiency of precipitate separation was therefore determined from feed material and supernatant optical densities at 670 nm (Section 3.2.3) and also microtube dry weights (Section 3.2.2.2) with correction to account for the mass of any ammonium sulphate present.

3.4.3.4 Recovery and Grade Efficiency Determination

Grade efficiencies (refer to Section 7.2.3 for definition and description) for the processing of a particular material was determined from Elzone particle size data (Section 3.2.7.1) using the approach of Mannweiler (1989).

Results from the Elzone particle sizer were expressed on a cumulative volume basis as a function of particle size logarithmically divided into 128 size channels. To reduce error and give a degree of smoothing to the data, the 128 channels were further reduced to 26 wider size channels. Assuming particles in the feed and supernatant have the same constant density, the recovery efficiency (alternatively known as the mass yield), E_t, was firstly calculated as:

$$E_t = 1 - \frac{v_f}{v_s} \qquad \text{(equation 3.8)}$$

with both v_f, the total volume of solids in the feed, and v_s, the total volume of solids in the supernatant, being determined from the respective volume distribution. Grade efficiencies, T(d), were then obtained from the equation:

$$T(d) = 1 - (1 - E_t) \frac{\Delta F_s(d)}{\Delta F_f(d)}$$

(equation 3.9)

Both $\Delta F_s(d)$, the centrifuge supernatant particle size distribution, and $\Delta F_f(d)$, the centrifuge feed particle size distribution, are expressed as 'percent in range' distributions (i.e. the sum over all size fractions is 100%) and were obtained by calculating the difference between two values in the respective volume distribution for consecutive particle sizes d_1 and $d_2=d_1+\Delta d$, i.e:

$$\Delta F(d_1,d_2) = F(d_1) - F(d_2)$$

(equation 3.10)

Grade efficiencies were obtained in the form of discrete grade efficiency values based on the arithmetic mean particle size $(d_1+d_2)/2$ for each size interval, which were plotted as a function of the dimensionless particle size (d/d_c), where d_c is the critical diameter. Numerical analysis of experimental grade efficiency data was carried out using the ORIGIN software package (Section 3.5).

3.4.4 Full Process Runs

The full process sequence for the recovery of *pe*-ADH from the MC1 strain is shown in Figure 1.2 on page 25. Full process runs were carried out at the small pilot scale of operation, using either tubular bowl or scaled-down disc stack centrifuge stages, and the large pilot scale of operation using full scale disc stack centrifugation stages to enable comparison to model predictions.

MC1 strain cells produced in 30 L fermentations were used for the small pilot scale runs. All centrifugation steps were carried out either using a Sharples 1-P tubular bowl centrifuge (Alfa-Laval Sharples Ltd., Camberley, U.K.) operated at 25,000 rpm and a feed flowrate of 13 $L.h^{-1}$ ($Q/\Sigma = 8.8\times10^{-9}$ $m.s^{-1}$) or a Westfalia SAOOH 205 intermittent discharge disc stack centrifuge (Westfalia Separator Ltd., Milton Keynes, U.K.) operated with a scaled-down disc stack at a flowrate of 10 $L.h^{-1}$ ($Q/\Sigma = 8.5\times10^{-9}$ $m.s^{-1}$). Homogenisation was carried out using a LAB-60 Manton Gaulin homogeniser operated with a CD valve (APV Baker, Crawley, U.K.) as per Section 3.4.1.2. The two

precipitation cuts were carried out in the 4.4 L reactor as per Section 3.4.2.2. Analysis was completed as per the relevant Sections.

Two large pilot-scale runs, designated PPW1 and AW1, were carried out. For run PPW1 MC1 strain cells produced in the 1000 L fermenter were used, while for run AW1, MC1 strain cells produced in the 450 L fermenter were used. In both cases cell harvesting was carried out using an AS26 tubular bowl centrifuge operated at a flowrate of 300 $L.h^{-1}$ and bowl speed of 17,000 rpm ($Q/\Sigma = 2\times10^{-9}$ $m.s^{-1}$). Subsequent centrifugation steps were carried out using a Westfalia SAOOH 205 intermittent discharge disc stack centrifuge (Westfalia Separator Ltd., Milton Keynes, U.K.) operated with a full disc stack at a flowrate of 50 $L.h^{-1}$ ($Q/\Sigma = 8.9\times10^{-9}$ $m.s^{-1}$). High pressure homogenisation was carried out using a K3 Manton Gaulin homogeniser operated with two CV valves (APV Baker, Crawley, U.K.) as per Section 3.4.1.2. The two batch precipitation cuts were carried out in the 120 L reactor as per Section 3.4.2.2. Analysis was completed as per the relevant Sections.

3.5 Data Analysis and Modelling

Analysis of experimental data was carried out using both the EXCEL V5.0 spreadsheet package (Microsoft Corp., Redmont, U.S.A.) and the ORIGIN V3.5 software package (Microcal Software Inc., Massachusetts, U.S.A.).

The EXCEL spreadsheet package enables cells of data to be manipulated. Large amounts of experimental data could therefore be stored, used in calculations and examined using the available graphing options. The ORIGIN package was used for the plotting of result graphs and curve fitting. Within the package, linear and polynomial fits were carried out using the least squares curve fitting method and non-linear fits were carried out using the Levenberg-Marquardt non-linear curve fitting algorithm (Press *et al.*, 1988).

Accuracy of the linear and polynomial fits was determined by the linear regression coefficient r_c, where r_c^2 gives the observed variation of the dependent variable which is accounted for by the relationship with the independent variable (Freund, 1988). For non-linear curve fits, statistical significance was determined from the χ^2 statistic. By defining the number of degrees of freedom as i-1, where i is the number of data points, it was

possible to use the χ^2 probability distribution to ensure a 95% confidence interval for fitted functions (Clark and Cooke, 1982). Only fits with a χ^2 value within that required for the 95% confidence interval, i.e. with a significance greater than 95% were accepted.

The implementation of mathematical models was carried out in both the EXCEL V5.0 spreadsheet package (Microsoft Corp., Redmont, U.S.A.) and the MATLAB V4.1 software package (The Mathworks Inc., Massachusetts, U.S.A). A review of available software packages for use as modelling tools is given in Section 2.4. EXCEL was used for the implementation of steady state unit operation models, while the implementation of dynamic models was carried out using MATLAB. Dynamic equations were solved within MATLAB using an in-built 4th order Runge-Kutta procedure (Forsythe *et al.*, 1977). The modelling of process sequences was achieved by linking both steady state and dynamic unit operation models in a sequential manner within MATLAB.

4.0 COMPARATIVE STUDY OF RECOMBINANT STRAINS AND FERMENTATION CHARACTERISATION

4.1 Introduction

This chapter describes the examination of available recombinant strains in order to select strains suitable for use in the downstream processing studies. The subsequent characterisation of fermentations for the production of the required quantities of recombinant material is also detailed.

The main criteria for selecting recombinant strains for use in the studies were:

- that the scale of fermentations required to produce sufficient quantities of the recombinant cells for downstream processing experiments could be achieved with existing equipment and at reasonable cost.

- that recombinant protein and ADH was produced in a large enough quantity to enable accurate mass balancing during experiments.

- that consistent levels of recombinant protein and ADH were produced during cell culture to ensure reproducible results during subsequent experiments.

Both *Escherichia coli* strain WL2 and *Saccharomyces cerevisiae* strain MC1 were initially available for use in the project, while the ADH overexpressing strain became available during the course of the work. Refer to Section 1.6 for a description of the strains and Section 3.3 for the source of the strains and culture details.

4.2 Shake Flask Comparison of Recombinant Strains

To determine if a recombinant strain was suitable for use in the studies, 200 mL shake flask cultures were carried out and the level of expression of recombinant ADH and total protein examined and compared to that of natural bakers' yeast.

The experimental method for shake flask cultures of *E. coli* strain WL2, *S. cerevisiae* strain MC1 and the ADH overexpressing strain is given in Sections 3.3.2.2, 3.3.3 and 3.3.4 respectively. Results for *E. coli* strain WL2 are shown in Table 4.1, results for *S. cerevisiae* strain MC1 are shown in Table 4.2 and results for the ADH overexpressing strain are shown in Table 4.3 overleaf. In all cases, typical results from the shake flask cultures are shown which were confirmed by repeated experiments. Typical levels of ADH and total protein for bakers' yeast are shown in Table 4.4 overleaf to enable comparison to the recombinant strain results.

Sample	**Total Protein Concentration ($mg.mL^{-1}$)**	***rec*-HLADH Specific Activity ($U.mg^{-1}$)**
Homogenised/Induced[1]	0.0165	0.84
Homogenised/Non-Induced[1]	0.0195	2.16
Sonicated/Induced[1]	0.0115	0.36
Sonicated/Non-Induced[1]	0.0165	0.18
Expected[2]	0.0254	0.0129

[1] sample taken 20 h after inoculation
[2] from Van de Goor-Kucerova (1992)

Table 4.1: Escherichia coli strain WL2 complex media shake flask results.

Sample	**Total Protein Concentration ($mg.mL^{-1}$)**	***pe*-ADH Specific Activity ($U.mg^{-1}$)**
Homogenised[1]	1.90	7.32

[1] sample taken 24 h after inoculation

Table 4.2: Saccharomyces cerevisiae strain MC1 complex media shake flask results.

Strain	Total Protein Concentration ($mg.mL^{-1}$)	ADH Specific Activity ($U.mg^{-1}$)
Wild type[1] (SUB-63 no plasmid)	0.37	6.75
ADH overexpressor[1] (SUB-63 + PMW5-ADH2)	0.37	11.10

[1] maximum levels achieved, samples taken 55 h after inoculation

Table 4.3: ADH overexpressor defined media shake flask results.

Sample	Total Protein Concentration ($mg.mL^{-1}$)	ADH Specific Activity ($U.mg^{-1}$)
Fermented/Complex Media[1]	1.36	1.93
Fermented/Defined Media[1]	1.50	11.67
Packed Bakers' Yeast[2]	-	13

[1] sample taken 24 h after inoculation, data from Deghani (1996)
[2] measured

Table 4.4: Typical levels of ADH and total protein for bakers' yeast.

4.2.1 *Escherichia coli* strain WL2

The results for *E. coli* strain WL2 (Table 4.1) show that the total protein concentration in 200 mL shake flask cultures was between 45% and 77% of the expected value, while the specific activity of recombinant horse liver alcohol dehydrogenase (*rec*-HLADH) was up to 167 times the expected value. The levels of protein and *rec*-HLADH in the sonicated samples were all lower than those in the homogenised samples. This was most likely due to damage to proteins and enzyme denaturation during sonication. A comparison of the values for the induced and non-induced homogenised samples shows that the non-induced sample had higher levels of protein and *rec*-HLADH. This is surprising as it indicates that addition of the IPTG inducer was not required to initiate expression of the *rec*-HLADH.

The measured protein concentrations for *E. coli* strain WL2 were approximately 100 times lower than typical protein concentrations for bakers' yeast fermentations (Table 4.4). *Rec*-HLADH specific activities were generally lower than typical values for ADH from bakers' yeast, the exception being the level in the homogenised/non-induced sample which was 1.12 times the level in a complex media bakers' yeast fermentation.

E. coli strain WL2 was found to be unsuitable for use in the downstream processing studies as it did not meet the required criteria. The low levels of protein and *rec*-HLADH obtained indicate that further work is required to increase the cell density during culture in order to ensure that sufficient material for the downstream processing studies can be produced using available fermentation equipment. The low levels of *rec*-HLADH activity achieved in most cases may also make accurate mass balancing difficult. Because expression of the *rec*-HLADH appeared to occur before addition of the ITPG inducer, the regulation of *rec*-HLADH production would also need to be investigated to ensure a consistent product.

4.2.2 *Saccharomyces cerevisiae* strain MC1

A comparison of the results for *S. cerevisiae* strain MC1 (Table 4.2) and typical values for bakers' yeast (Table 4.4) shows that the total protein concentration in *S. cerevisiae* strain MC1 200 mL shake flask cultures was 1.4 times the value for a complex media bakers' yeast fermentation and 1.27 times the value for a defined media bakers' yeast fermentation. The protein engineered alcohol dehydrogenase (*pe*-ADH) specific activity for *S. cerevisiae* strain MC1 was 3.8 times the value for a complex media bakers' yeast fermentation, 63% of the value for a defined media bakers' yeast fermentation and 56% of the value for packed bakers' yeast. The results obtained for *S. cerevisiae* strain MC1 fulfilled the required criteria for use in the downstream processing studies. The levels of protein and *pe*-ADH were similar to those achieved by bakers' yeast and large scale fermentations would therefore be of a similar scale to bakers' yeast fermentations used to produce material for the work of Clarkson (1994). The strain was therefore selected for use in downstream processing studies.

4.2.3 ADH Overexpressor

A comparison of results for the ADH overexpressor to those of the wild type show approximately 2 fold overexpression of ADH (Table 4.3). This was low compared to the expected overexpression of 6 to 8 times (Section 1.6.2). Plasmid stability during shake flask culture remained high, with 78-106% of cells retaining the plasmid PMW5-ADH2 (refer to Section 3.3.5.7 for method). The level of overexpression achieved was more typical of a standard strain of *S. cerevisiae* containing the plasmid PMW5-ADH2, i.e. a strain without the ubiquitin gene deletion and suggested that there may have been some instability associated with the changes made in order to achieve the large overexpression. The maximum ADH specific activity during shake flask culture of the ADH overexpressor was 6 times that typically achieved by bakers' yeast in complex media fermentations, 5% lower than that achieved in bakers' yeast defined media fermentations and 15% lower than that of packed bakers' yeast. The viability of the ADH overexpressing strain was also highly inconsistent, with cells taken from stocks failing to grow in many cases.

Due to the possible instability of overexpression and inconsistent viability, the ADH overexpressor did not meet the required criteria and was not used in further downstream processing studies.

4.3 MC1 Strain Fermentation Characterisation

A fermentation protocol was determined for *S. cerevisiae* strain MC1 to enable production of sufficient quantities of recombinant cells for downstream processing studies and to ensure consistent levels of biomass, total protein and *pe*-ADH. Refer to Section 3.3.2 for the shake flask culture and fermentation procedures used.

The dry weight of cells, total protein concentration and specific *pe*-ADH activity obtained in shake flask cultures and fermentations carried out at a number of scales and conditions are shown in Table 4.5 overleaf.

.

Complex Media Culture	Dry Weight ($g.L^{-1}$)	Total Protein ($mg.mL^{-1}$)	Specific *pe*-ADH ($U.mg^{-1}$)
200 mL Shake Flask	7.5	1.9	7.32
30 L Fermentations[1]	6.9	1.9	6.59
30 L Fermentations[2]	7.2	2.5	2.20
30 L Fermentations[3]	6.8	2.2	2.79
400 L Fermentation	7.5	1.7	2.78
1000 L Fermentation	6.8	1.5	2.89

[1] Average results for stirrer speed of 700 rpm and PPG antifoam level of 1 $mL.L^{-1}$
[2] Average results for stirrer speed of 500 rpm and PPG antifoam level of 1 $mL.L^{-1}$
[3] Average results for stirrer speed of 300 rpm and PPG antifoam level of 0.1 $mL.L^{-1}$

Table 4.5: Typical results for Saccharomyces cerevisiae strain MC1 complex media shake flask culture and fermentations at various scales.

Typical fermentation trends for dry weight, glucose concentration and ethanol concentration are shown in Figure 4.1 overleaf. Typical trends for dissolved oxygen tension (DOT), oxygen uptake rate (OUR), carbon dioxide evolution rate (CER) and respiratory quotient (RQ) are shown in Figure 4.2. The change in cell number and geometric mean diameter during a 30 L fermentation carried out with a stirrer speed of 500 rpm and the addition of 1 $mL.L^{-1}$ of PPG antifoam is shown in Figure 4.3 on page 125, while plasmid stability results are shown in Figure 4.4.

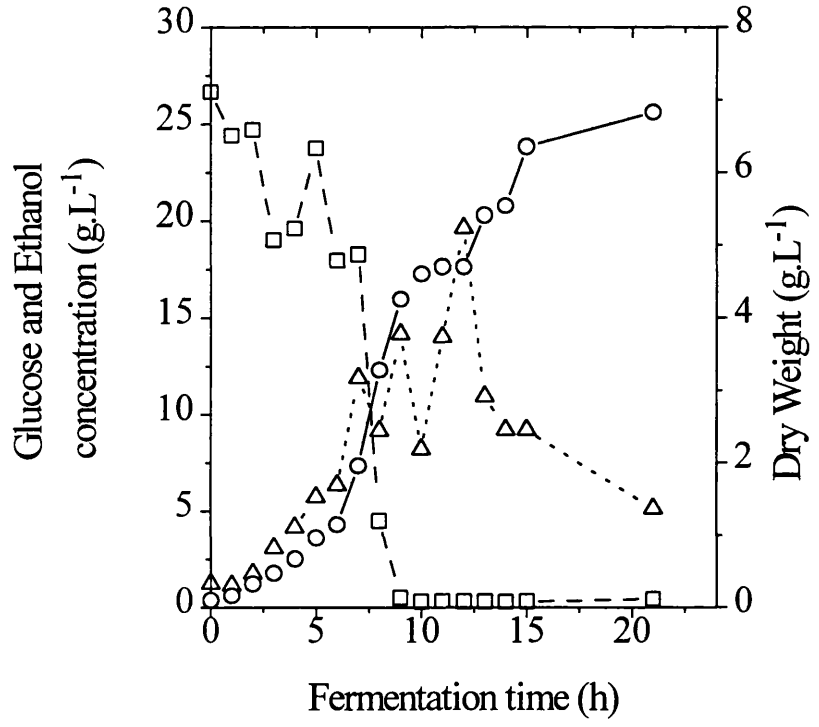

Figure 4.1: Trends in dry weight, glucose concentration and ethanol concentration for a 1000 L fermentation of Saccharomyces cerevisiae strain MC1. Experimental data: (– □ –) glucose, (- - Δ - -) ethanol, (—○—) dry weight.

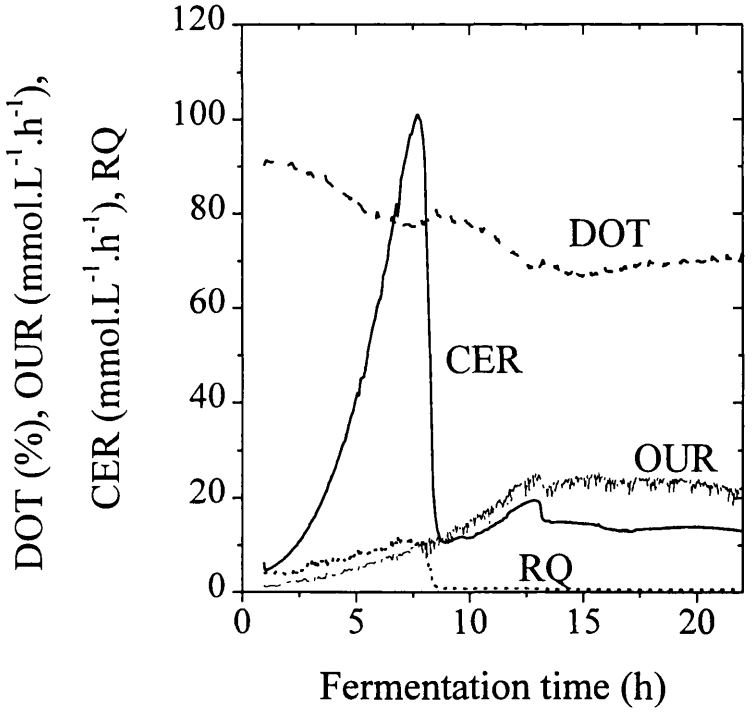

Figure 4.2: Trends in DOT, OUR, CER and RQ for a 1000 L fermentation of Saccharomyces cerevisiae strain MC1. Experimental data: (– – -) DOT, (– - –) OUR, (——) CER, (· · · ·) RQ.

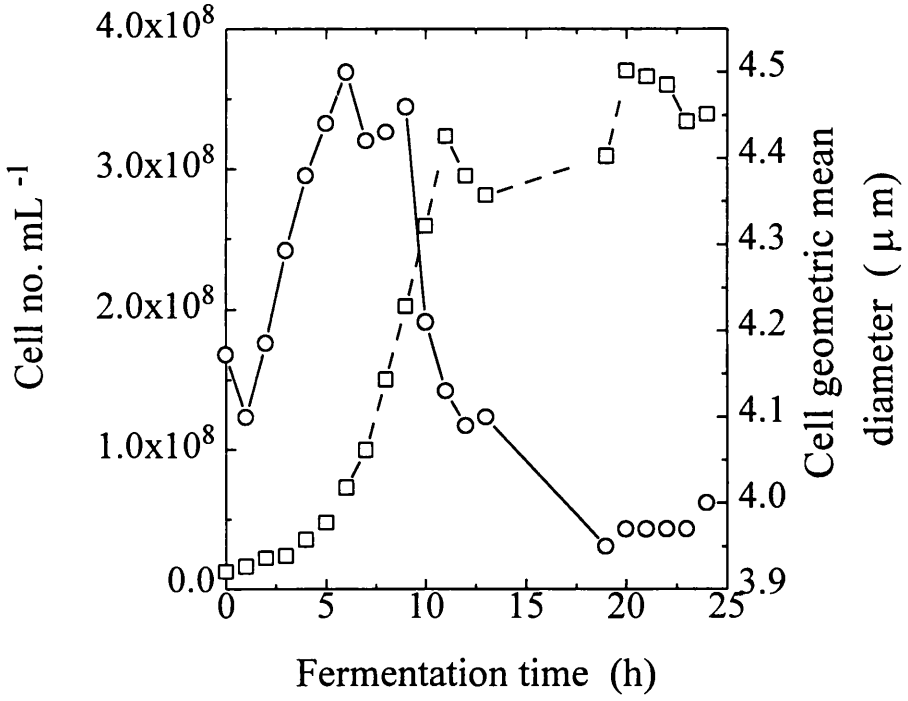

Figure 4.3: Cell number and Geometric mean diameter during a 30 L fermentation of Saccharomyces cerevisiae strain MC1 with a stirrer speed of 500 rpm and 1.0 mL.L^{-1} PPG antifoam. Experimental data: (– □ -) Cell number, (—○—) Cell geometric mean diameter.

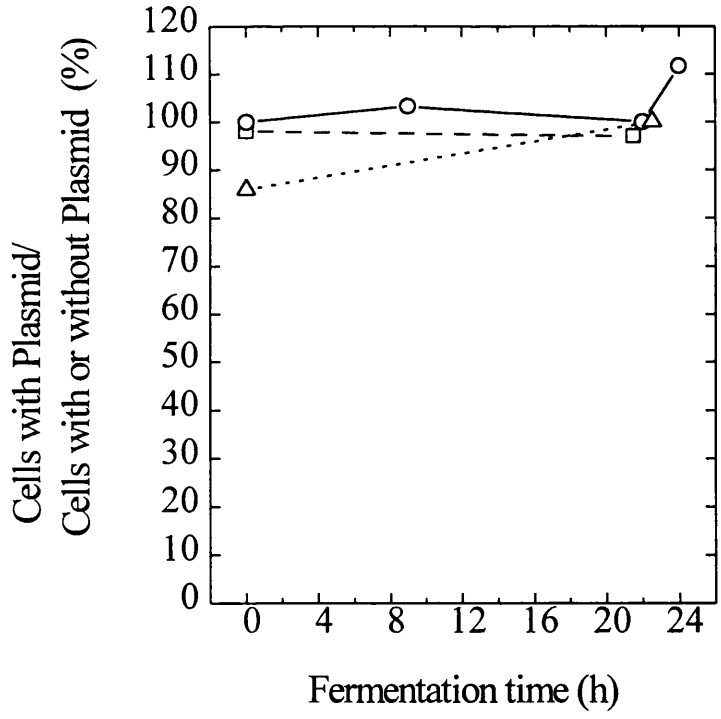

Figure 4.4: Percentage of cells containing the plasmid during Saccharomyces cerevisiae strain MC1 culture. Experimental data: (—○—) 200 mL shake flask, (– □ -) 30 L fermentation, (- - △ - -) 1000 L fermentation.

4.3.1 Typical Fermentation Trends

In a typical *S. cerevisiae* strain MC1 batch, complex media fermentation glucose was utilised first (with ethanol production) and was exhausted after approximately 9 h (Figure 4.1). At this point the CER peaked at approximately 100 $mmol.L^{-1}.h^{-1}$ and the ethanol yield was approximately 0.5 g per initial g glucose (Figure 4.2). After the glucose was used up growth continued at a reduced rate as other carbon sources were utilised. The drop in ethanol level that was observed (Figure 4.1) is thought to be due to evaporation from the fermenter as *S. cerevisiae* strain MC1 lacks YADH-II which is required for ethanol utilisation. Cell harvesting was carried out 24 h after inoculation, when the DOT level was steady at approximately 70% and the OUR was approximately 20 $mmol.L^{-1}.h^{-1}$.

4.3.2 Consistency of Fermentation Results

In order to ensure reproducible results from subsequent downstream processing studies it was essential that the consistency of material produced during fermentations was maintained both at different scales and from one batch to another at the same scale. The demonstration of plasmid stability during culture was also important, since any loss of the plasmid during culture would reduce the level of *pe*-ADH produced. Figure 4.4 shows that the ratio of cells with the plasmid to cells either with or without the plasmid remained close to 100% during culture at all scales of operation and therefore indicates that the plasmid stability was high for the MC1 strain. Although similar dry weights and protein levels were achieved at all scales, results for specific *pe*-ADH production (Table 4.5) showed a 60% reduction in the level achieved in the 1000 and 300 L fermentations compared to that in shake flask culture. The difference was most likely due to the different culture conditions in the shake flask and fermenter. In shake flask culture the pH is uncontrolled, and aeration and mixing occur due to shaking of the flasks. In fermenters the pH level is maintained at a constant value by the addition of acid and base solutions while aeration and mixing are achieved by gas sparging and mechanical agitation. It was possible that low values of dissolved oxygen existed in the fermenter environment, contributing to the observed difference in specific *pe*-ADH production.

Specific *pe*-ADH production in 30 L fermentations operated at a stirrer speed of 700 rpm was 2.3 times the level achieved in 1000 L and 450 L fermentations (Table 3.5). As

previously stated it was important that the 30 L fermentations mimicked the results at the 1000 L and 450 L scale. The stirrer speed used in 30 L fermentations was therefore reduced to 500 rpm so as to give a value for the power input per unit volume closer to that of the 300 L and 1000 L fermentations (Table 4.6). The ratio of power input per unit volume is often used as a scaling factor for fermentations as it directly reflects mass transfer and mixing capabilities (Bailey and Ollis, 1986). For turbulent regimes, the power input is proportional to:

$$P_I \propto N_I^3 D_I^5$$

(equation 4.1)

where P_I is the power input, N_I is the rotational speed of the stirrer and D_I is the diameter of the stirrer. Dividing by V gives the power input per unit volume as:

$$\frac{P_I}{V} \propto \frac{N_I^3 D_I^5}{V}$$

(equation 4.2)

For equivalent impellers, the value of $N_I^3 D_I^5/V$ must therefore be kept constant in order to achieve the same power input per unit volume at different scales. Table 4.6 shows calculated values for $N_I^3 D_I^5/V$ for 30L, 300 L and 1000 L fermentations. All of the fermenters had 3 6-bladed Ruston turbine impellers. Reducing the stirrer speed for 30 L fermentations from 700 to 500 rpm lowered the average specific *pe*-ADH activity by 67% to give a value within 25% of that achieved at the 300 and 1000 L scale (Table 4.5).

Volume (L)	Stirrer diameter (m)	Speed (rpm)	$N_I^3 D_I^5/V$ ($m^2.s^{-3}$)
1000	0.20	300	0.04
300	0.20	250	0.08
30	0.088	700	0.28
30	0.088	500	0.10
30	0.088	300	0.02

Table 4.6: Power input per unit volume for fermentations at various scales.

In order to operate the 42 L fermenter at stirrer speeds of 500 and 700 rpm PPG antifoam was added to the fermentation media at a level of 1 mL PPG per L of broth. During the

course of the studies it was found that carryover of PPG antifoam from the fermentation stage interfered with subsequent ammonium sulphate precipitations (Section 6.3). For some 30 L fermentations the level of antifoam was therefore reduced to 0.1 mL PPG per L, which was the same as that used for 1000 L and 300 L fermentations and limited the maximum stirrer speed to 300 rpm. The reduction in stirrer speed from 500 to 300 rpm resulted in an 80% reduction in the power input per unit volume (Table 4.6), however the specific *pe*-ADH production increased by 27% compared to what was achieved at 500 rpm (Table 4.5). This suggests that the lower specific *pe*-ADH production between 300 and 500 rpm compared to between 500 and 700 rpm may have been due to a degree of oxygen limitation which resulted from the poorer mass transfer and mixing conditions.

The variation in the results from 30 L fermentation batches is shown in Table 4.7. The variation is similar to that observed by Deghani (1996) of ±10% in dry weight and ±65% in specific ADH activity for 5 batch defined media fermentations of *Saccharomyces cerevisiae* strain GB4918. The presence of possibly large deviations in fermentation results meant that the use of individual batches in subsequent downstream processing studies was carefully considered in each case. The impact of such variations on the modelling of high pressure homogenisation, protein precipitation, disc stack centrifugation and the whole process is discussed in Chapters 5.0, 6.0, 7.0 and 8.0 respectively.

Conditions		**Number of batches**	**Maximum deviation from average value (%)**	
Stirrer Speed (rpm)	**Antifoam ($mL.L^{-1}$)**	**(-)**	**Dry Weight**	**Specific *pe*-ADH**
700	1.0	4	±12	±55
500	1.0	4	±17	±30
300	0.1	7	±22	±50

Table 4.7: Variability of 30 L fermentation results (24 h results used in all cases).

4.3.3 Intermediate Storage of MC1 Strain Cells

Intermediate storage of MC1 strain cells prior to use in downstream processing experiments was examined both by freezing at -20°C and by maintaining the cells at 4°C. Freezing of harvested cells was found to result in reductions of specific *pe*-ADH activity of up to 80% and the release of up to 50% of soluble protein and *pe*-ADH on thawing. Overnight storage of harvested MC1 strain cells at 4°C for up to 18 h after harvest was found to have little effect on *pe*-ADH and protein levels. Harvested cells stored at 4°C for 76 h after harvest showed reductions in *pe*-ADH and soluble protein levels of up to 15%, and after 120 h showed reductions in *pe*-ADH and protein levels of up to 40%. For downstream processing studies, cells were therefore used directly at the completion of fermentations or stored at 4°C after harvesting and used as soon as possible to prevent significant reductions in *pe*-ADH and soluble protein levels. The use of frozen cells in downstream processing studies was avoided due to the large reduction in specific *pe*-ADH activity and the breakage of cells on thawing.

4.3.4 Comparison of MC1 strain and Bakers' Yeast

Differences in the properties of *Saccharomyces cerevisiae* strain MC1 and bakers' yeast were examined in order to determine possible impacts on the subsequent downstream processing of the recombinant strain compared to that of bakers' yeast. A comparison of properties of *S. cerevisiae* strain MC1 cells and bakers' yeast cells is shown in Table 4.8. The average cell diameter of *S. cerevisiae* strain MC1 cells was 85% of packed bakers' yeast cells and 71% of fermented bakers' yeast cells (refer to Section 3.2.7.1 for particle size analysis method used). The density of *S. cerevisiae* strain MC1 cells was 2% greater than that of packed and fermented natural bakers' yeast (refer to Section 3.2.8.2 for method of density determination). The smaller size and higher density of MC1 strain cells is likely to have an impact on centrifugation stages in a recovery process for *pe*-ADH (Chapter 7.0)

Gel electrophoresis was carried out to compare the soluble protein spectrum and ADH in *S. cerevisiae* strain MC1 to that of bakers' yeast (refer to Section 3.2.6 for gel electrophoresis methods). A comparison of the protein spectrum is shown in Figure 4.5 on page 131 for denatured conditions using SDS-PAGE and Figure 4.6 for non-denatured

conditions using native-PAGE. The results show that the overall soluble protein spectrum was very similar between *S. cerevisiae* strain MC1 and bakers' yeast under both denatured and non-denatured conditions. This observation suggests that the precipitation behaviour of soluble protein from *S. cerevisiae* strain MC1 will be similar to that from bakers' yeast (refer to Chapter 6.0 for further discussion).

ADH from bakers' yeast and *pe*-ADH from *S. cerevisiae* strain MC1 were compared on activity gels (Figure 4.7 on page 132). A difference in the position of the ADH band was observed and is thought to be due to the different isozymes of ADH produced by each strain (Table 4.8). As described in Section 1.6, *S. cerevisiae* strain MC1 produces a protein engineered version of ADH isozyme I (*pe*-ADH) while packed bakers' yeast predominately contains ADH-II. The differences in ADH due to the protein engineering changes and presence of different ADH isozymes are likely to alter the precipitation behaviour of *pe*-ADH from *S. cerevisiae* strain MC1 compared to that of the ADH from bakers' yeast (Chapter 6.0).

Parameter	**Packed Bakers' Yeast**	**Fermented Bakers' Yeast**	***S. cerevisiae* strain MC1**
Type of ADH produced	mainly ADH II	ADH I/II/III	*pe*-ADH
Average Cell Diameter (μm)	4.7*	5.6+	4.0*
Cell Density (kg/m^3)	1111*	1111+	1130*

* Measured
\+ From Bulmer (personal communication)

Table 4.8: Comparison of properties of Saccharomyces cerevisiae strain MC1 cells and natural bakers' yeast cells.

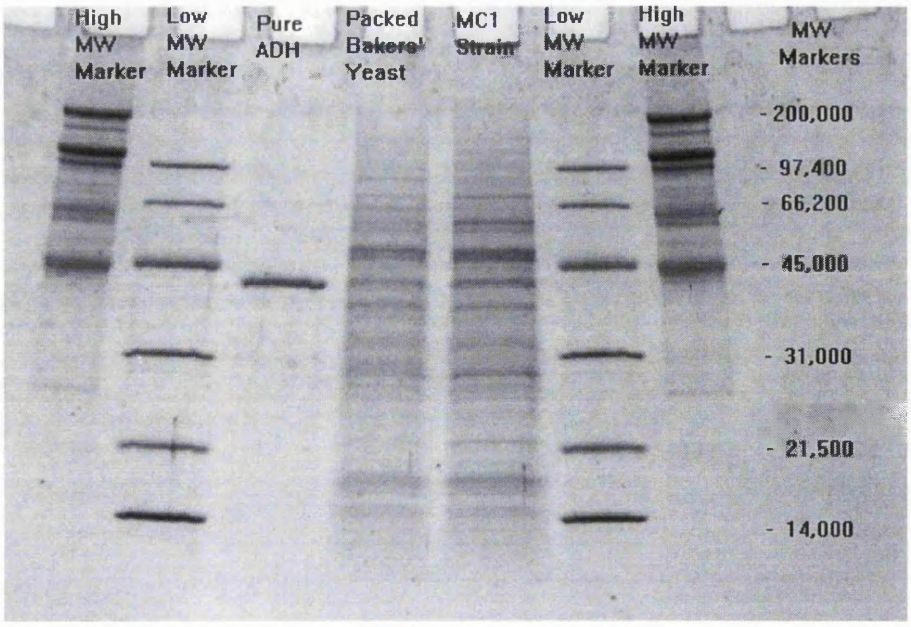

Figure 4.5: SDS-PAGE comparison of protein from Saccharomyces cerevisiae strain MC1, packed bakers' yeast and pure yeast ADH (Sigma Chemical Co., Dorset, U.K.).

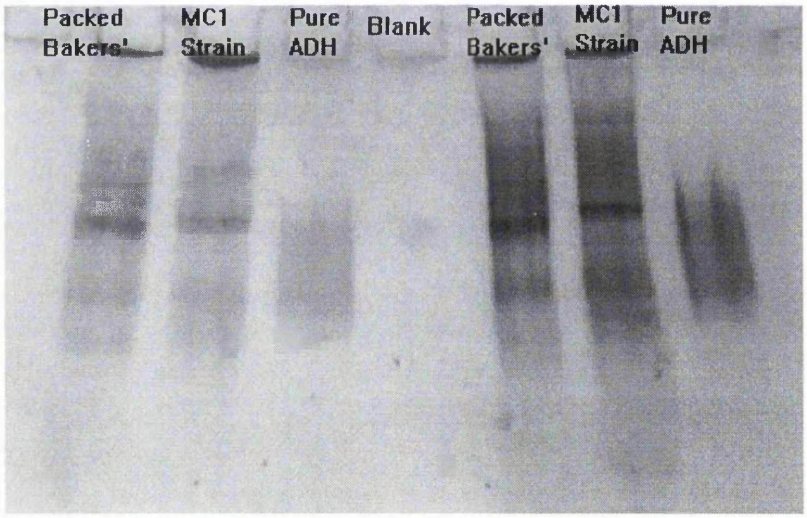

Figure 4.6: Native-PAGE comparison of protein from Saccharomyces cerevisiae strain MC1, packed bakers' yeast and pure yeast ADH (Sigma Chemical Co., Dorset, U.K.).

Figure 4.7: Activity gel comparison of ADH from Saccharomyces cerevisiae strain MC1 and packed bakers' yeast.

4.3 Summary

Available recombinant strains were examined in shake flask culture and the suitability for use in downstream processing studies determined based on a number of criteria. Of the available strains, *E. coli* strain WL2 was found unsuitable as further work was required to boost biomass levels and the action of inducer required further examination to ensure consistent production of recombinant ADH. The ADH overexpressor was also found unsuitable due to possible instability of overexpression and inconsistent viability. *S. cerevisiae* strain MC1 was found suitable for use in the downstream processing studies as similar levels of recombinant protein and ADH were produced compared to bakers' yeast.

Characterisation of *S. cerevisiae* strain MC1 fermentations for the production of the required quantities of recombinant material was detailed. A drop in specific *pe*-ADH production of 60% was observed from the shake flask to 1000 L fermentation. The stirrer speed in 30 L fermentations was reduced from 700 to 500 rpm in order to match the mixing conditions at the 1000 and 300 L scale and gave specific *pe*-ADH activity within 25% of the larger scale fermentations.

To prevent carry-over of antifoam and interference with subsequent precipitations, the antifoam level in some 30 L fermentations was reduced from 1.0 mL PPG per L broth to 0.1 mL per L which limited the maximum stirrer speed to 300 rpm. The specific *pe*-ADH activity in these fermentations remained close to that of the 1000 L and 300 L fermentations. Variability of 30 L fermentation results was within 55% and was similar to that of Deghani (1996). Cells were used as soon as possible after the completion of fermentations, with intermediate storage of harvested cells achieved by maintenance at 4°C rather than the freezing of cells to prevent large reductions in *pe*-ADH and protein levels. A comparison of properties of *S. cerevisiae* strain MC1 cells and packed bakers' yeast cells was also made to identify possible impacts on subsequent downstream processing of the recombinant strain.

5.0 MODELLING OF HIGH PRESSURE HOMOGENISATION

5.1 Introduction

In this chapter the high pressure homogenisation of *Saccharomyces cerevisiae* strain MC1 for the release of protein engineered alcohol dehydrogenase (*pe*-ADH) is examined. Characterisation of the homogenisation stage was carried out by processing small amounts of fermented material from 30 L fermentations using a scaled-down homogeniser (refer to Section 3.4.1.1 for method). The experimental data generated was used to apply existing homogenisation models developed with natural bakers' yeast to the recombinant strain, with model parameters or equations being re-evaluated specifically for the recombinant system where insufficient accuracy was achieved. The scalability of the models was then tested by examining pilot and semi-industrial scale homogenisation (refer to Section 3.4.1.2 for method). This approach enabled highly accurate and experimentally verified models to be developed rapidly for high pressure homogenisation of the recombinant strain.

In Section 5.2 existing models for the high pressure homogenisation of yeast are outlined. Section 5.3 describes the application of existing homogenisation models to the recombinant system, while utilisation of the scaled-down homogeniser is described in Section 5.4. Results of the study are presented and discussed in Section 5.5, with conclusions given in Section 5.6.

5.2 Existing Models for Yeast Homogenisation

Early work by Hetherington *et al.* (1971) developed an empirical relationship between soluble protein release, R, from packed bakers' yeast and the important homogenisation process parameters of operating pressure, P, and batch passes through the homogeniser, N :

$$\log_{10}\left[\frac{R_{max}}{(R_{max} - R)}\right] = KNP^{\alpha}$$

(equation 5.1)

where R_{max} is maximum soluble protein release and K, α are kinetic constants. It should be noted that in determining this relationship, assayed soluble protein concentrations for homogenate samples were corrected to account for the presence of solids using the formula:

$$R = \frac{F\,C_u}{C_y}$$

(equation 5.2)

were F is the aqueous fraction, C_u is the soluble protein assay result and C_y is the yeast concentration on a wet weight basis.

Equation 5.1 was found to be valid for yeast wet weight concentrations between 30% and 60% on a volume basis (v/v) with R_{max} equal to 93 mg protein per g wet weight yeast, α having a value of 2.9 and K, which was found to be a function of temperature, having a value of 3.5×10^{-9} at 5°C and 5.0×10^{-9} at 30°C. Numerous other studies have been carried out with yeasts and other organisms showing that the parameters α and K vary greatly depending on the stage of growth and conditions under which the cells are grown (Harrison, 1991; Keshavarz, 1990; Kula and Schutte, 1987).

Follows *et al.* (1971) showed that the rate of release of enzymes from yeast also depended on their location within the cells. Soluble cytosolic enzymes followed the same or a slightly faster rate of release compared to that of overall soluble protein, while enzymes located outside the cell membrane where released at a faster rate and enzymes within cellular components were released at a slower rate. Milburn and Dunnill (1994) examined the breakage of recombinant *S. cerevisiae* cells in a high pressure homogeniser for the release of virus-like particles (VLPs). Soluble protein release was found to fit equation 5.1, with R_{max} equalling approximately 93 mg protein per g wet weight yeast and α having a value of 2.1 for cells harvested during the exponential growth phase. The VLPs were located in the cytoplasm and showed the same rate of release as soluble protein.

A more theoretical approach for describing cell disruption by homogenisation in which equipment and cell property related parameters are separated has been developed for *Escherichia coli* by Middelberg *et al.* (1992b, 1992c) and extended to packed bakers' yeast and actively growing brewers' yeast by Kleinig and Middelberg (1996). For

multiple passes the following equation is used to give the extent of cells disrupted, D_R, as:

$$D_R = 1 - \int_0^{\infty} (1 - f_D(S))^N f_S(S) dS$$

(equation 5.3)

where S is the effective strength and $f_S(S)$ is the strength distribution of the cells, described by a two parameter normal distribution:

$$f_S(S) = \frac{1}{\sigma 2\pi} \exp\left[\frac{-(S - S_m)^2}{2\sigma^2}\right]$$

(equation 5.4)

where σ is the standard deviation of the strength distribution and S_m is the mean strength of the distribution. Recent work has been carried out by Roberts *et al.* (1994) on the determination of these parameters for brewing yeast cells using micromanipulation techniques. In equation 5.3, $f_D(S)$ describes the stress imposed on the cells by the homogeniser. A three parameter empirical equation was adopted for $f_D(S)$ based on the impact of small cylinders on a plane surface:

$$f_D(S) = \frac{(mP^n)^b}{S^b + (mP^n)^b}$$

(equation 5.5)

where b, m and n are constants. Although it is recognised that the fundamentally based framework of the Middelberg model is an improvement on the highly empirical Hetherington model (equation 5.1), the approach requires knowledge of the way that yeast cells break in a homogeniser. The precise mechanisms of yeast cell breakage during high pressure homogenisation are, however, difficult to determine (Section 1.2.3.1). Keshavarz-Moore *et al.* (1990), who studied disruption over a narrow range of operating conditions, attributed 80% of the disruption of yeast cells in a homogeniser to impingement and 20% due to the valve unit geometry. More recently Shamlou *et al.* (1995) concluded for a wider range of conditions of operation that the effects of elongational stresses prior to impingement best correlated the breakage of packed bakers' yeast.

The above models give the extent of release of products during homogenisation but do not describe the particle size distribution (PSD) of the resultant cell debris. This information is required for full integration of the unit operation with process stages for debris removal such as centrifugation or filtration (Keshavarz, 1990). Choosing operating conditions for the homogeniser then involves a trade off between the extent of product release and subsequent efficiency of the debris removal stage to prevent excessive solid loadings on up-stream operations such as chromatography (Hearle *et al.*, 1993; Zhou *et al.*, 1997).

Siddiqi *et al.* (1995, 1996) have developed an empirical model describing the change in debris PSD characteristics under various homogeniser processing conditions for packed bakers' yeast and fermented bakers' yeast at different stages of growth. Whole cell and resultant debris PSDs are described using the Boltzman function:

$$B(d_{N,P}) = 1 - \frac{1}{\left(1+\exp\frac{(d-d_{50})}{w}\right)}$$

(equation 5.6)

where d_{50} is the average Boltzman diameter and w describes the spread of the distribution. The change in d_{50} is then given by:

$$\log_e\left(\frac{d_{50N=0}}{d_{50N=0}-d_{50}}\right) = \log_e\left(\frac{1}{d^*_{50}}\right) = kN^{-0.4}(P - P_t)$$

(equation 5.7)

where $d_{50N=0}$ is the d_{50} value before homogenisation, P_t is the threshold pressure, k is a constant and d^*_{50} is a normalised form of the d_{50}. The change in w is given by:

$$w^* = -2.3d^*_{50} \qquad d^*_{50} < 0.33$$

(equation 5.8)

$$w^* = 5.5d^*_{50} - 2.4 \qquad d^*_{50} \geq 0.33$$

(equation 5.9)

where w* is a normalised form of w given by:

$$w^* = \frac{(w_{N=0} - w)}{w_{N=0}}$$

(equation 5.10)

Equation 5.8 represents conditions under which cell rupture occurs with little micronisation, while equation 5.9 describes the condition under which cell debris micronisation dominates.

For packed bakers' yeast P_t equals 115 barg and k has a value of 670 $pass^{-0.4}barg^{-1}$. In the case of fermented yeast the value of k was found to be strongly dependent on the culture conditions and ranged from 670 to 2200 $pass^{-0.4}barg^{-1}$ over a 30 hour batch fermentation (Siddiqi *et al.*, 1995).

5.3 Application of Existing Homogenisation Models to the MC1 Strain

Of the models outlined in Section 5.2, equation 5.1 was used as the basis for describing the release of soluble protein and *pe*-ADH during high pressure homogenisation of *S. cerevisiae* strain MC1 since assumptions about the cell strength distribution and mechanism of yeast breakage would not be required. Equations 5.6 to 5.10 were used as the basis for describing debris PSDs to enable integration of homogenisation with subsequent debris removal stages. A k value of 1100 $pass^{-0.4}barg^{-1}$ was used in equation 5.7 as this corresponded to the fermentation time of 24 h used for the recombinant yeast strain (Siddiqi *et al.*, 1995).

Due to the empirical nature of these models it was not possible to directly predict the homogenisation characteristics of the recombinant strain based on system properties alone. Instead, experimental data was required to test the applicability of the models and to re-evaluate model parameters or equations where insufficient accuracy was achieved. Variability in properties of feed material to the homogenisation stage was incorporated into the models by identifying specific values of $R_{max,}$ d_{50} and w for cells from each fermentation batch used in the study. This enabled data generated in each experiment to be normalised and compared to that of other experiments.

In assessing model results, a level of accuracy of ±30% was regarded as sufficient for feasibility studies (Clarkson, 1994), while further accuracy of the order ±10% and less was required for detailed design calculations and for the determination of optimal process operating conditions.

5.4 Utilisation of a Scaled-Down Homogeniser

In this study a Manton Gaulin LAB-40 high pressure homogeniser fitted with a SV valve (APV Baker, Crawley, U.K.) was used to obtain experimental data for the disruption of recombinant strain cells. A sample size of approximately 40 mL was required for operation of the homogeniser. Siddiqi *et al.* (1997) have examined the performance of this homogeniser and found that breakage of packed bakers' yeast was the same as that achieved by the larger pilot-scale LAB-60 and semi-industrial scale K-3 Manton Gaulin homogenisers operated with one and two CD valves respectively (APV Baker, Crawley, U.K.). The equivalent performance was thought to be due to similar velocities being achieved in the homogeniser valve gap and was consistent with elongational stresses acting as the mechanism for disruption. The LAB-40 homogeniser therefore acts as a scaled-down homogeniser, the results from which can be confidently applied to the larger scale units (Siddiqi *et al.*, 1997).

In comparison to the scale-down homogeniser, the pilot-scale LAB-60 homogeniser requires a minimum feed volume of 2 L, while the semi-industrial scale K-3 homogeniser requires more than 30 L of feed material. The amount of recombinant feed material at the typical process concentration of 280 $g.L^{-1}$ (Clarkson, 1994) obtained from 42 L, 450 L and 1500 L fermenters was approximately 2.25 L, 22.5 L and 75 L respectively. Use of the scaled-down homogeniser therefore enabled a large number of experiments to be performed from a single 30 L fermentation batch, facilitating rapid application of existing homogenisation models to the recombinant system.

5.5 Results and Discussion

5.5.1 Homogenisation Characterisation with a Scale-Down Unit

5.4.1.1 Aqueous Fraction and Maximum Release

The aqueous fractions of homogenised recombinant yeast samples were found to be similar to those obtained by Hetherington *et al.* (1971) for packed bakers' yeast (Figure 5.1 overleaf).

Full breakage of recombinant cells was found to occur after 2 passes at 1200 barg, since the release of soluble protein was approximately the same after further passes (Figure 5.2 overleaf). The fraction of non-viable cells was determined to be greater than 0.99 by staining and microscopic counting under these conditions, confirming that full breakage had indeed occurred. This gave an R_{max} value of 70±10 mg protein per g wet weight yeast. This is low but of the right order of magnitude compared to other values of R_{max} for yeast in the literature (Milburn and Dunnill, 1994) which range from 80 to 120 mg protein per g wet weight yeast and indicates that the cells contained slightly less releasable protein than other yeast strains. The use of glycol cooling around the homogeniser valve head and high speed centrifugation of samples prior to assay should reduce the possibility of a low R_{max} value resulting from protein denaturation or assay interference due to the presence of micronised cell debris and other cellular components respectively. The maximum release of *pe*-ADH was found to be 150±28 U per g wet weight of yeast. This corresponds to a specific activity of approximately 2.1 U per mg protein.

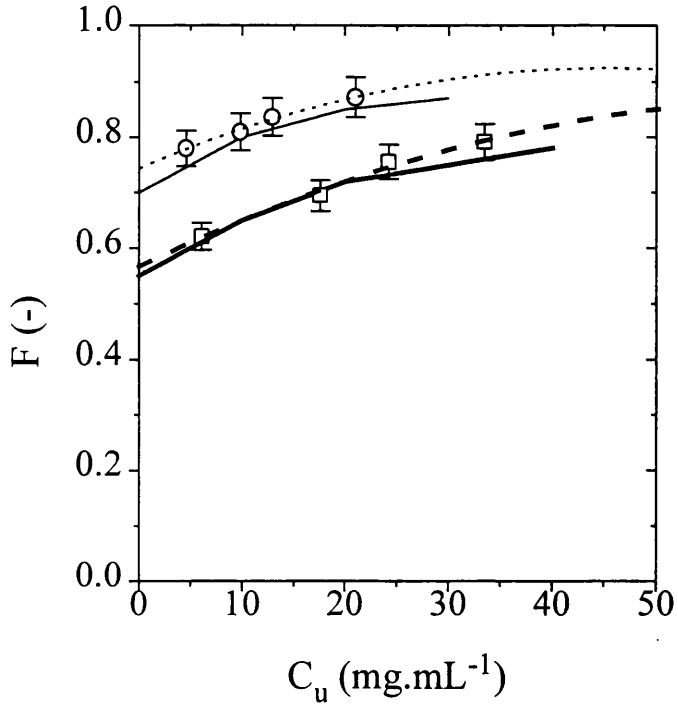

Figure 5.1: Aqueous fraction plotted against soluble protein assay result. ○ 280 g.L^{-1} MC1 strain experimental data, (- - - -) 280 g.L^{-1} MC1 strain fitted curve, (——) 300 g.L^{-1} packed bakers' yeast curve, □ 450 g.L^{-1} MC1 strain experimental data, (- - -) 450 g.L^{-1} MC1 strain fitted curve, (——) 450 g.L^{-1} packed bakers' yeast curve.

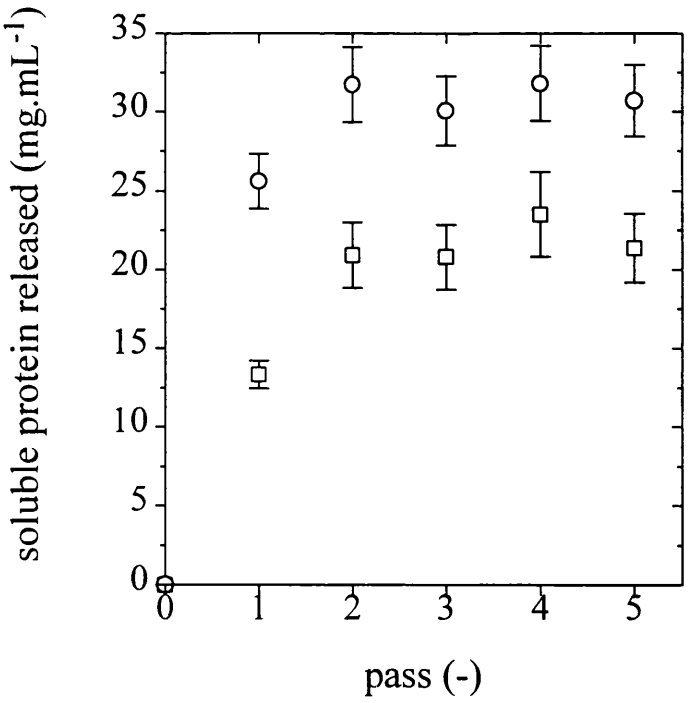

Figure 5.2: MC1 strain soluble protein release at 1200 barg plotted against the number of passes. Experimental data: □ 280 g.L^{-1}, ○ 450 g.L^{-1}.

5.5.1.2 Soluble Protein and *pe*-ADH Release

As expected for a soluble cytosolic enzyme, the release of the *pe*-ADH product was found to match that of the overall soluble protein to within 10% (Figure 5.3 overleaf). The release of soluble protein and *pe*-ADH were found to be unaffected by recombinant yeast concentration within the range 280 to 450 $g.L^{-1}$ wet weight (Figure 5.4 on page 144).

Soluble protein release results are shown as a semi-log plot of $\log_{10}[R_{max}/(R_{max} -R)]$ vs the number of batch passes to normalise the release results from different yeast concentrations and highlight the linear nature of the data. Normalised log soluble protein results for pressures of 200, 340, 400 and 500 barg and 1 to 5 discrete passes are presented in Figure 5.5 on page 144.

The use of packed bakers' yeast parameters obtained by Hetherington *et al.* (1971) in equation 5.1 overestimated the fractional release of recombinant soluble protein (R/R_{max}) by 21.6% on average (Figure 5.5). Although the accuracy achieved is sufficient for feasibility studies, further accuracy of the order ±10% and less is required for detailed design calculations and for the determination of optimum operation conditions. Specific α and K values were therefore determined for the recombinant strain to increase the accuracy of model results to within ±10%.

To evaluate the pressure exponent α for the recombinant strain, linear regression was carried out on a log-log plot of $\log_{10}[(R_{max}-R)/R_{max}]/N$ vs operating pressure P. The value of α was found to be 3.24, as compared to a value of 2.9 for packed bakers' yeast (Hetherington *et al.*, 1971). The fit had an r_c value of 0.98 showing that 97% of variation had been accounted for. The optimum value of the constant K was determined as the value which minimised the overall standard error between calculated and experimentally based values of $\log_{10}[(R_{max}-R)/R_{max}]$. The value of K was found to be 3.4×10^{-10} at the minimum overall standard error of 16.8%. This is an order of magnitude lower than the value of 3.5×10^{-9} for packed bakers' yeast (Hetherington *et al.*, 1971). The variation of K with temperature was not determined as the homogenisation experiments were only carried out at 4°C. Results of the model using the evaluated recombinant strain parameters

decreased the average overestimate of fractional soluble protein release (R/R_{max}) to 3.0% (Figure 5.5).

It is not possible to draw conclusions about the nature of *S. cerevisiae* strain MC1 cells by simply comparing the values of model parameters determined for the recombinant strain to those of other yeasts because of the empirical nature of the model. However, a comparison of fractional soluble protein release results (R/R_{max}) given by the model to fractional release results calculated under the same conditions but using parameters determined for packed bakers' yeast (Hetherington *et al.*, 1971) showed that the results were on average 18.6% lower for the recombinant strain. This does indicate that the recombinant cells were more difficult to break than packed bakers' yeast cells.

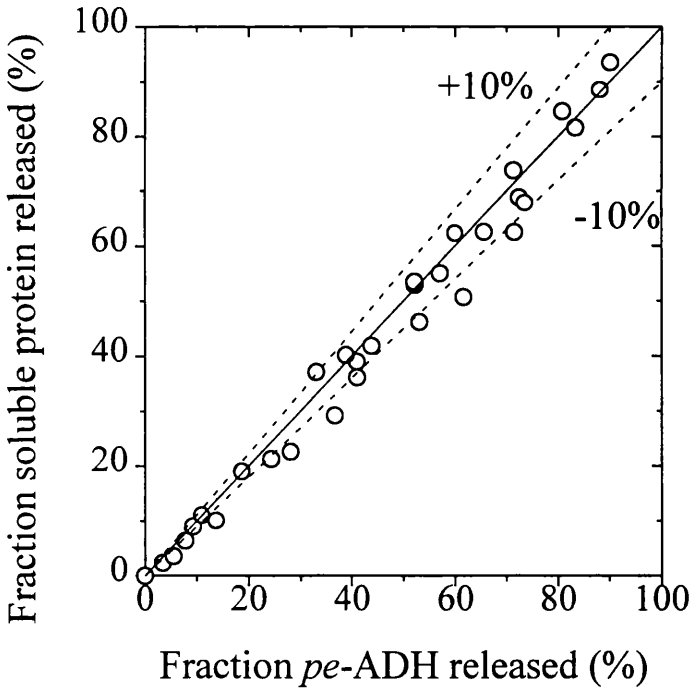

Figure 5.3: MC1 strain percentage of soluble protein released plotted against percentage of pe-ADH released. o *Experimental data, (——) 0% error, (- - - -) +10% and -10% error.*

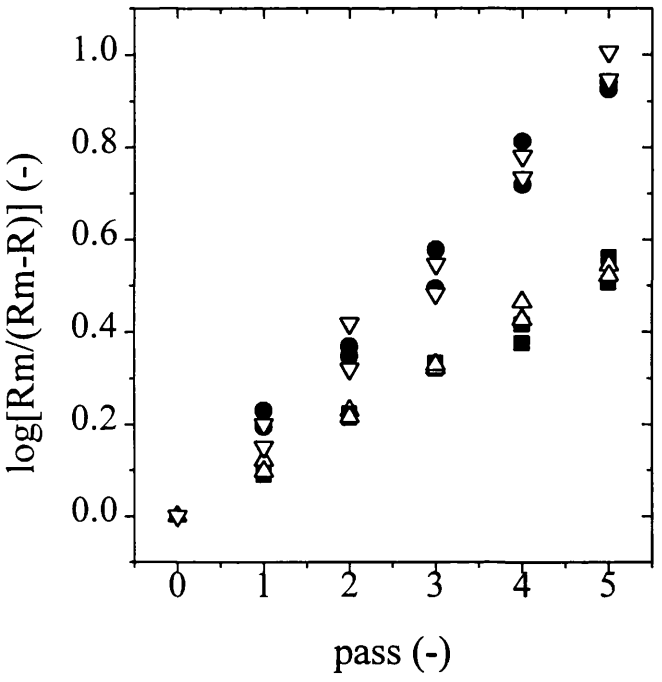

Figure 5.4: MC1 strain normalised log soluble protein release at 280 g.L^{-1} and 450 g.L^{-1} plotted against the number of passes. Experimental data: ■ 280 g.L^{-1} and 400 barg, ● 280 g.L^{-1} and 500 barg, △ 450 g.L^{-1} and 400 barg, ▽ 450 g.L^{-1} and 500 barg.

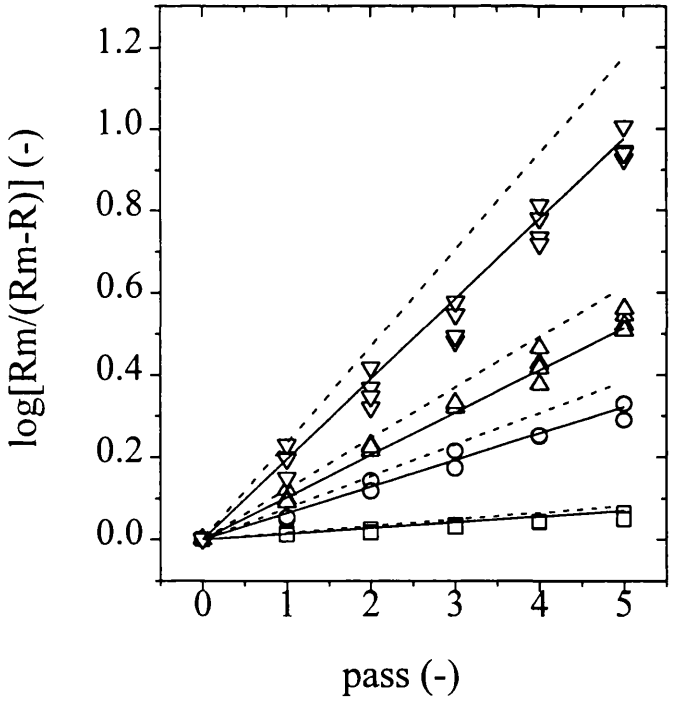

Figure 5.5: MC1 strain normalised log soluble protein release plotted against he number of passes MC1 strain 280 g.L^{-1} and 450 g.L^{-1} experimental data: □ 200 barg, ○ 340 barg, △ 400 barg, ▽ 500 barg. Model results: (——) MC1 strain parameters, (- - - -) bakers' yeast parameters.

5.5.1.3 Debris PSD Modelling

To check the validity of using bakers' yeast model parameters to describe the change in recombinant debris PSD, experimental PSDs were first expressed in the form of cumulative (undersize) volume distributions. Boltzman equations (equation 5.6) were fitted to the experimental PSD's enabling values of d_{50} and w to be determined and compared to values predicted by the PSD model (equations 5.7 to 5.10) using batch fermented bakers' yeast model parameters (Siddiqi *et al.*, 1995). It should be noted that the *S. cerevisiae* MC1 strain whole cell PSD contained two distinct peaks, i.e was bi-modal (Figure 5.6 on page 147). A single peak is typically seen for packed bakers' yeast (Siddiqi *et al.*, 1996) although bi-modal distributions were observed by Siddiqi *et al.* (1995) for some batch fermented samples of bakers' yeast. Microscopic examination and counting of the *S. cerevisiae* strain MC1 whole cells indicated that the larger peak was mostly composed of budded cells, while the smaller peak contained single cells.

The experimental and model d_{50} values calculated with fermented bakers' yeast parameters showed a maximum error of 3.7% (Figure 5.7 on page 147). Siddiqi *et al* (1995) had previously concluded that the homogenisation of cells with a bi-modal PSD would be difficult to describe with only one k value, since the cell age and therefore wall strength in the two peaks are expected to be different. However, in this case a single k value was sufficient to accurately describe the change in d_{50} in the range of conditions examined without any alteration to the model parameters. This suggests that the wall strength of the budded and single cells making up the two distinct peaks was similar. It is possible that the budded and single cells are of similar age or alternatively the presence of budding scars on both the single and budded cells may result in similar wall strengths, although Shamlou *et al.* (1995) concluded that cell age was a more important factor in determining wall strength compared to the presence of budding scars.

Calculation of w values was carried out with equation 9a since d^*_{50} values for the recombinant yeast were all below the critical d^*_{50} value of 0.33 determined for natural yeast strains (Siddiqi *et al.*, 1995). This gave values of w that were much higher than those determined experimentally with errors of up to 76% (Figure 5.8 on page 148). No distinct critical value of d^*_{50} could be identified for the recombinant strain from the experimental data. Rather than using the existing model equations describing w^*

(equations 5.8 and 5.9), a 2nd order polynomial was therefore used to relate experimentally determined d_{50} values to the values of w:

$$w = -1.8641 + 1.3205\, d_{50} - 0.1906\, (d_{50})^2$$

(equation 5.11)

This gave an r_c value of 0.88 which showed that 77% of the observed variation in ω was accounted for. Equation 5.11 was used in preference to a 2nd order polynomial relating d^*_{50} and w^* or a constant value of w, which accounted for 59% and 12% of the variation respectively. The error between experimental w values and values calculated using equation 5.11 was a maximum of 4%. Examination of the recombinant debris PSDs (Figure 5.6) indicated that only a small proportion of the total volume was below 1 μm after 5 passes at 500 barg. Because of this, the fact that the measuring technique had a lower limit of particle detection of approximately 1 μm would not itself cause a reduced variation in w due to the generation of undetectable debris particles below 1 μm. The inability of the existing model (equation 5.9) to predict the change in w was therefore thought to be due to the bi-modal nature of the initial whole cell PSD since separation and breakage of budded cells in the larger peak in the distribution would produce debris in the range of the smaller peak. Since this has the effect of reducing the observed variation in w (Figure 5.8) care must be taken when making statements about the extent of rupture and micronisation. However, the lack of any small debris below 1.5 μm (Figure 5.6) appears to indicate that rupture rather than micronisation was the dominant mode of disruption.

By replacing the existing description of w (equations 5.8 and 5.9) with equation 5.11, the model results show much better agreement with the experimental data (Figure 5.8). Debris PSDs were then re-constructed from the Boltzman parameters produced by the model to give simulated recombinant debris PSDs which matched those obtained experimentally (Figure 5.9 on page 148).

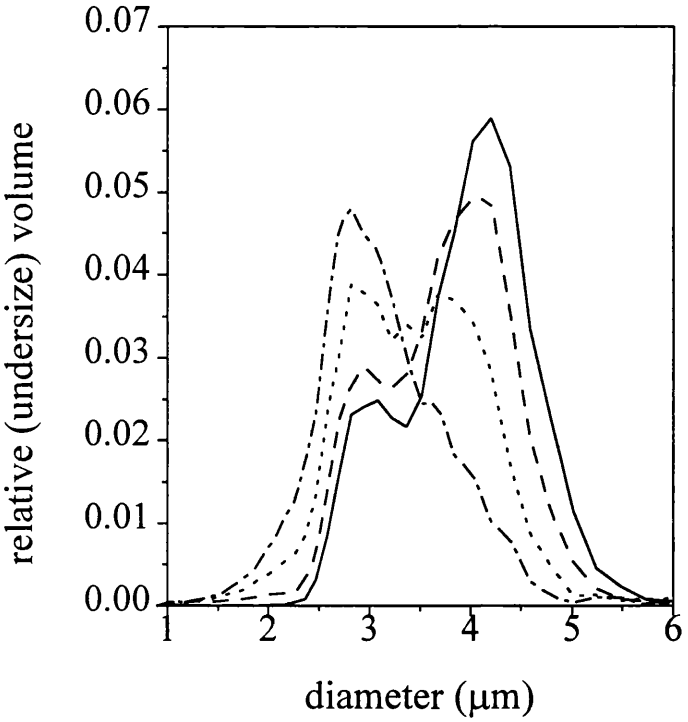

Figure 5.6: MC1 strain homogenisation at 280 g.L^{-1} and 500 barg relative (undersize) volume PSD. (——) whole cells, (– – ·) 1 pass, (· · · ·) 3 passes , (– · –) 5 passes.

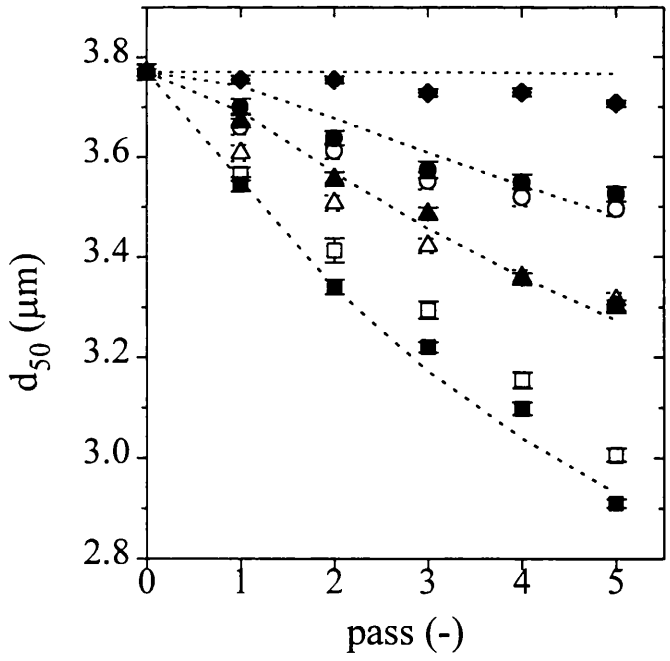

Figure 5.7: MC1 strain debris Boltzman average diameter plotted against the number of homogenisation passes. Experimental data: ◆ 280 g.L^{-1} and 200 barg, ● 280 g.L^{-1} and 340 barg, ▲ 280 g.L^{-1} and 400 barg, ■ 280 g.L^{-1} and 500 barg, ○ 450 g.L^{-1} and 340 barg, △ 450 g.L^{-1} and 400 barg, □ 450 g.L^{-1} and 500 barg. Model results: (· · · · ·) using bakers' yeast parameters.

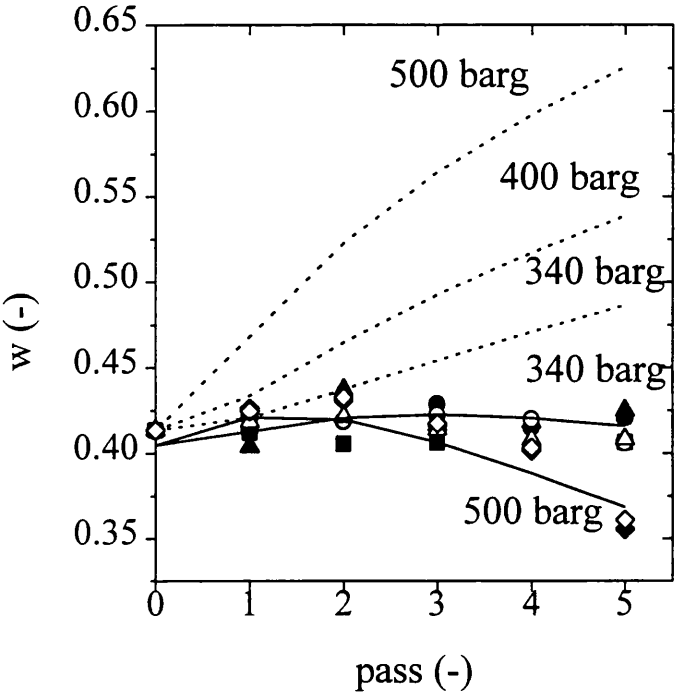

Figure 5.8: MC1 strain debris Boltzman constant w plotted against the number of homogenisation passes. Experimental data: ■ 280 g.L^{-1} and 200 barg, ▲ 280 g.L^{-1} and 340 barg, ● 280 g.L^{-1} and 400 barg, ◆ 280 g.L^{-1} and 500 barg, △ 450 g.L^{-1} and 340 barg, ○ 450 g.L^{-1} and 400 barg, ◇ 450 g.L^{-1} and 500 barg. Model results: (- - - -) using bakers' yeast equations, (——) using MC1 strain equation.

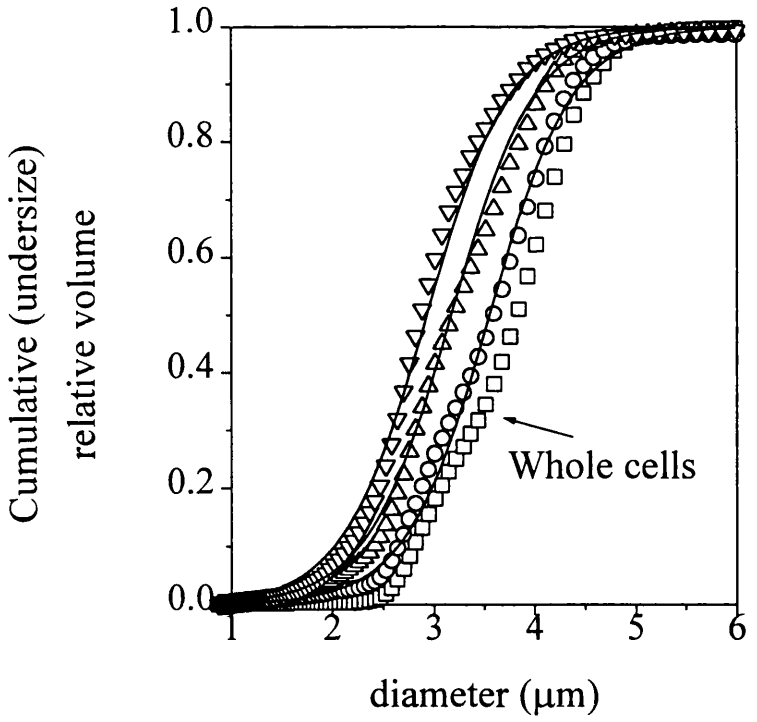

Figure 5.9: MC1 strain homogenisation cumulative (undersize) relative volume PSD at 280 g.L^{-1} and 500 barg. Experimental data: □ whole cells, ○ 1 pass, △ 3 passes, ▽ 5 passes, Model Results: (——) MC1 strain parameters and equation 5.11.

5.5.1.4 Changes in Homogenate Physical Properties

In order to integrate the homogenisation stage with subsequent debris removal operations it is important that changes in homogenate physical properties are quantified. In the case of debris removal by disc stack centrifugation, both the homogenate viscosity and suspension-particle density difference have an effect on the efficiency of separation and must be specified in models for the unit operation (Clarkson, 1994).

Mosquiera *et al.* (1981) observed an increase in viscosity after homogenisation of packed yeast, with the release of glycans during homogenisation thought to be a contributing factor. This change in viscosity has been modelled by Siddiqi (1997) using historical data for packed bakers yeast to give the following equation:

$$\mu = \mu_{max} - \exp(\ln(\mu_{max} - \mu_{init}) - (k_v . C_{rsp}))$$

(equation 5.12)

where μ is the homogenate viscosity, k_v is a constant and equals 0.0029, C_{rsp} is the concentration of released soluble protein, μ_{max} is the maximum possible viscosity and equals 0.03 Pa.s, and μ_{init} is the initial viscosity and is assumed to be linearly proportional to the yeast concentration.

Equation 5.12 was applied to MC1 strain homogenisation at 500 barg, with measured values for μ_{init} being used and the results compared to experimentally determined viscosities after various passes through the scale-down LAB-40 homogeniser (refer to Figure 5.10 overleaf for experimental and model results and to Section 3.2.8.4 for the method of viscosity determination). The model was able to describe the measured increases in homogenate viscosity with a maximum error of 17%, which was within the ±20% experimental error of the viscosity measurements. In applying this model between 280 $g.L^{-1}$ and 450 $g.L^{-1}$ wet weight yeast it was assumed that μ_{init} is linearly proportional to yeast concentration, which is recognised as being a simplistic approach:

$$\mu_{init} = -0.00242 + 0.00017 \times C_y$$

(equation 5.13)

where C_y is the yeast concentration in %(w/v).

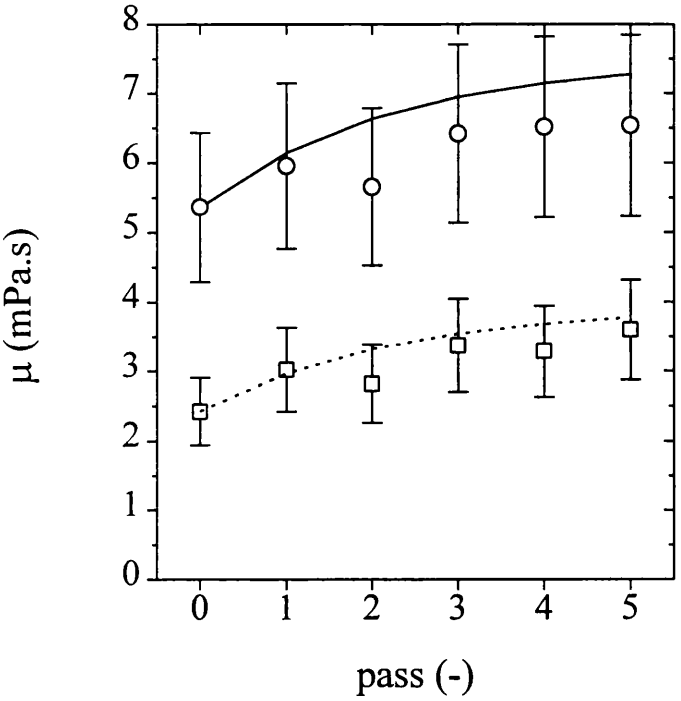

Figure 5.10: MC1 strain homogenate viscosity at 500 barg plotted against the number of batch passes. Experimental data: □ 280 g.L^{-1}, ○ 450 g.L^{-1}. Model results: (- - - - -) 280 g.L^{-1}, (——) 450 g.L^{-1}.

The densities of homogenate particles and the suspending liquid were experimentally determined for MC1 strain homogenisation at 280 g.L^{-1} and 500 barg after various passes using the scale-down LAB-40 homogeniser (refer to Table 5.1 overleaf for experimental results and to Section 3.2.8.2 for the method of density determination). The observed decrease in particle density and corresponding increase in liquid density indicates that high density material is released from the cells during homogenisation. This material is likely to include glycogen, lipid granules and enzymes from the cytoplasm as well as yeast organelles such as ribosomes and mitochondria. Nucleic acids fragments from the yeast nucleus and plasmids are also likely to be released from the cells. In applying these results to other homogeniser passes, a linear relationship was used to relate the concentration of released soluble protein C_{rsp} to the density difference $\Delta\rho$ in kg.m^{-3}:

$$\Delta\rho = 0.250 - 0.00138 \times C_{rsp}$$

(equation 5.14)

The regression coefficient, r_c, for equation 5.14 was -0.99, indicating that 98% of the variation was accounted for. The results of Mosquiera *et al.* (1981) show that the

density difference between disrupted packed bakers' yeast suspensions and their supernatants is approximately constant for original volumetric yeast concentrations between 30% and 40% (v/v). The liquid-particle density difference was therefore assumed to be constant for MC1 strain concentrations between 280 $g.L^{-1}$ and 450 $g.L^{-1}$, i.e. approximately 30% to 47% (v/v).

Homogeniser Pass	Liquid Density ($kg.m^{-3}$)	Particle Density ($kg.m^{-3}$)	Density Difference ($kg.m^{-3}$)
0	1.005	1.130	0.125
3	1.015	1.122	0.107
5	1.020	1.120	0.100

Table 5.1: Experimentally determined liquid and particle densities for homogenisation of 280 $g.L^{-1}$ MC1 strain yeast after various homogeniser passes at 500 barg.

A comparison of recombinant and packed bakers' yeast homogenate physical properties after 5 passes at 500 barg showed an increased density difference, from 0.050 $kg.m^{-3}$ (Mosquira *et al.*, 1981) to 0.100 $kg.m^{-3}$, and a decreased viscosity, from 0.0042 Pa.s (Siddiqi, 1997) to 0.0037 Pa.s, for the recombinant system. It is thought that the observed differences in physical properties were due to a lower degree of disintegration of the cell structure for the MC1 strain compared to that of bakers' yeast. This is consistent with previous observations that cells of the recombinant strain were harder to break than bakers' yeast cells (Section 5.4.1.2) and that there was little micronisation of recombinant cells (Section 5.4.1.3).

5.5.2 Scalability of Homogenisation Models

The homogenisation of MC1 strain yeast at 280 $g.L^{-1}$ and 500 barg was examined at the pilot scale using a LAB-60 homogeniser and the semi-industrial scale using a K-3 homogeniser. Refer to Section 3.4.1.2 for the experimental method and a description of the homogenisers.

Soluble protein release results at each scale of operation, plotted as $\log_{10}(R_{max}/(R_{max}-R))$ for various homogeniser passes, are shown and compared to scale-down and model results in Figure 5.11. Cumulative (undersize) volume PSD's after 5 passes at each scale are shown and compared to scale-down and model results in Figure 5.12 on the following page. In both cases the homogenisation results were similar at all scales of operation and were well described by the models. The maximum deviation of experimental fractional protein release (R/R_{max}) from the model at any scale was approximately 10%, while the d_{50} for experimental homogenate PSDs was within 3% of the model PSD in all cases. The results indicate that models based on the scale-down LAB-40 unit also apply to the larger scale homogenisation of the MC1 strain using LAB-60 and K-3 units.

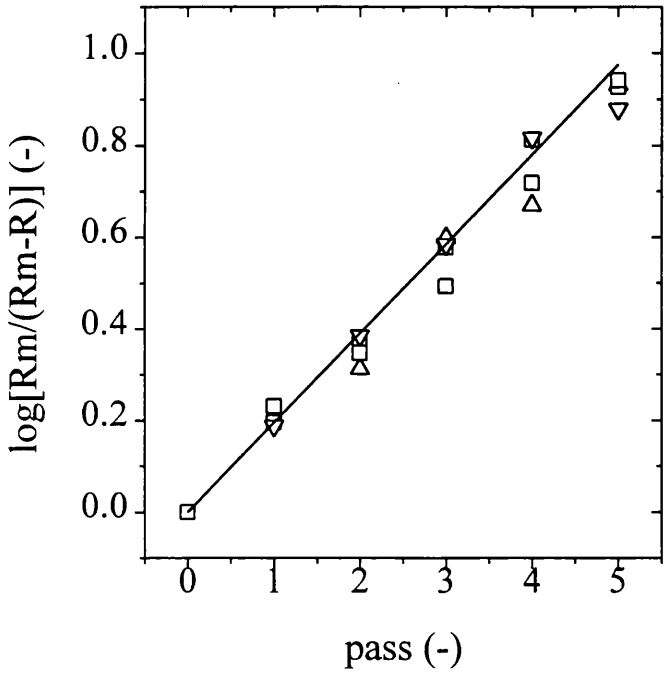

Figure 5.11: MC1 strain normalised log soluble protein release at 280 g.L^{-1} and 500 barg for various scales of operation. Experimental data: □ *scale-down LAB-40 unit,* ▽ *pilot-scale LAB-60 unit,* △ *semi-industrial K-3 unit. (——) model results.*

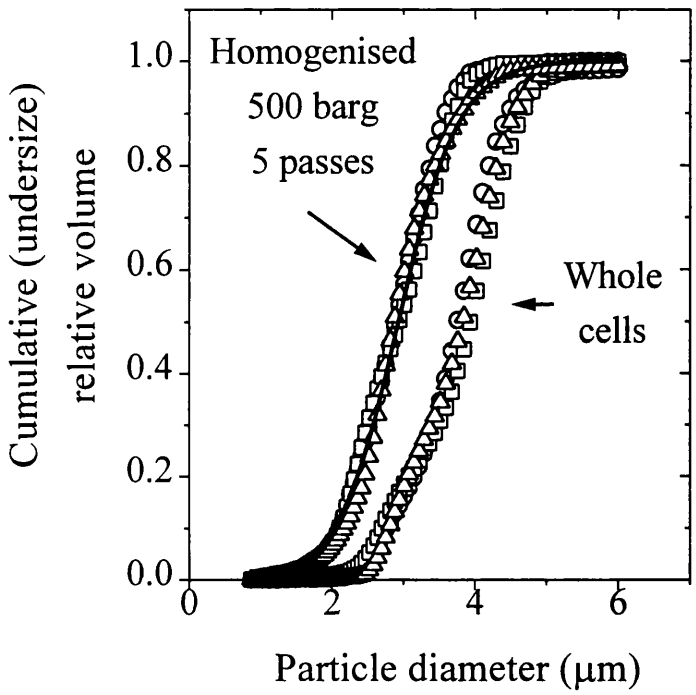

Figure 5.12: MC1 strain cumulative (undersize) volume PSDs after 5 homogenisation passes at 280 g.L^{-1} and 500 barg for various scales of operation. Experimental data: Δ *scale-down LAB-40 unit,* □ *pilot-scale LAB-60 unit,* o *semi-industrial K-3 unit. Model results: (——).*

5.6 Conclusions

Use of a scale-down homogeniser enabled homogenate aqueous fractions, the condition under which full breakage occurs and the R_{max} value for a recombinant yeast strain to be determined from small amounts of sample material. The recombinant yeast aqueous fractions were found to be similar to that of bakers' yeast, while the R_{max} value was low in comparison to that of other yeasts but of the right order of magnitude. Release of the product enzyme, *pe*-ADH, was also shown to occur at approximately the same rate as soluble protein release and the yeast cell concentration was shown to have little effect on release in the range 280 g.L^{-1} to 450 g.L^{-1} wet weight.

The scale-down experimental data was used to apply existing high pressure homogenisation models developed using natural yeast to the recombinant process. Where insufficient model accuracy was achieved specific model equations or parameters were re-evaluated for the recombinant strain.

Use of packed bakers' yeast parameters in the empirical Hetherington equation (equation 5.1) gave a description of the release of soluble protein and *pe*-ADH that could be used for feasibility studies (±30%) but was not accurate enough for detailed design calculations (±10%). Evaluation of specific recombinant strain parameters improved the accuracy of the model to within ±10%. The modelling results also showed that *S. cerevisiae* strain MC1 was harder to break compared to packed bakers' yeast.

To enable full integration of homogenisation with subsequent unit operations, equations describing changes in debris PSD were also considered. Accurate values for the mean diameter of the recombinant debris PSD were obtained when batch fermented bakers' yeast parameters were used. However, the relation describing the width of the PSD was replaced with a 2nd order polynomial specifically relating the Boltzman constants d_{50} and w for the recombinant strain in order to obtain realistic values. Changes in homogenate viscosity, particle density and liquid density were also examined experimentally using the scale-down unit and modelled to enable the affect of physical property changes on subsequent debris removal operations to be incorporated into any whole process model. Differences in physical properties for the recombinant system compared to packed bakers' yeast were consistent with less disintegration of the recombinant cell structure on homogenisation.

The MC1 strain homogenisation models based on the scale-down data accurately described soluble protein release and changes in particle size for a larger pilot scale and semi-industrial scale homogeniser, confirming the scalability of model results.

Application of such models will enable design calculations, unit integration with other process stages and identification of optimum operating conditions to be carried out for the high pressure homogenisation of recombinant yeast early in the process development cycle with a high degree of confidence.

6.0 MODELLING OF PROTEIN PRECIPITATION

6.1 Introduction

In this chapter the concentration and fractionation of protein engineered alcohol dehydrogenase (*pe*-ADH) from *Saccharomyces cerevisiae* strain MC1 clarified homogenate using batch ammonium sulphate precipitation is examined. Characterisation of total protein and ADH solubility profiles for protein engineered and packed bakers' yeast systems was carried out in a small scale precipitation vessel (refer to Section 3.4.2.1 for method). This enabled the solubility behaviour of total protein and ADH from the two systems to be compared. An existing precipitation solubility model was applied to describe the fractional solubility profiles for the typical process concentration of 280 g wet weight yeast per L. The updated models were used to calculate optimum cut points and maximum purification at various yields for a two-cut fractionation procedure, with results for the protein engineered and packed bakers' yeast systems being compared.

A two-cut fractionation procedure, with batch ageing of each cut to increase precipitate strength, was experimentally examined at the medium and large pilot scale (refer to Section 3.4.2.2 for method). Changes in precipitate particle size distribution (PSD) were determined at the medium pilot scale for each cut over the batch ageing time and modelled using a population balance approach. Precipitate physical properties which have an impact on precipitate separation stages were also determined. The fractional solubility of total protein and ADH at the large pilot scale was examined and the results used to test the scalability of solubility models derived from small scale data.

In Section 6.2 existing models for protein solubility behaviour in neutral salts and the description of changes in precipitate particle size are outlined, while the selection and application of precipitation models used in the study are described in Section 6.3. Results of the study are presented and discussed in Section 6.4, with conclusions given in Section 6.5. The intermediate removal and recovery of the precipitate during fractional precipitation is not addressed directly in this chapter, but is included in Chapter 7.0.

6.2 Existing Models for Protein Precipitation

The modelling of protein precipitation involves a description of both the changes in target enzyme and total protein solubility on addition of the precipitant and the changes in particle size distribution (PSD) of the precipitate during batch ageing. Accurate prediction of the precipitant PSD is particularly important since the performance of subsequent centrifugation separation stages will be highly dependent on the size of precipitate particles (Clarkson, 1994). Because saturated ammonium sulphate has been used as the precipitant in this study and other types of precipitation (e.g. polyethyleneglycol) may be governed by different mechanisms, only models for protein solubility behaviour in aqueous salt solutions are considered in the following section.

6.2.1 Protein Solubility Behaviour in Aqueous Salt Solutions

There have been a number of different approaches used to describe the solubility behaviour of proteins in aqueous salt solutions. An extensive review is given by Rothstein (1994) and a summary of current approaches by Foster (1994). The approaches range from fully empirical models to highly theoretical descriptions and are outlined below.

6.2.1.1 Empirical Models

Cohn (1925) developed an empirical log-linear relationship to describe the salting-out of proteins at high salt concentrations:

$$\log S = \beta - K_S m \qquad \text{(equation 6.1)}$$

where S is the protein solubility, i.e. the concentration of soluble protein, m is the molar salt concentration and β, K_S are constants. For a given protein, the value of β depends on pH and temperature and is a minimum at the isoelectric point (Rothstein, 1994; Foster, 1994). While the value of K_S depends on both protein and salt properties (Rothstein, 1994; Foster, 1994). Foster *et al.* (1976) found that the constants β and K_S vary with the mode and rate of salt addition, and Iyer and Przybycien (1994) also found that both parameters vary with mixing conditions.

Although the Cohn equation (equation 6.1) can describe the salting-out behaviour of proteins, it does not apply to salting-in and the transient regions of solubility behaviour which are of more relevance to process control and design (Clarkson *et al.*, 1996b). Richardson (1987) used a polynomial expression to describe solubility behaviour as part of an optimisation routine for fractional precipitation (Section 6.2.2). While Niktari *et al.* (1989, 1990) employed an isotherm equation to describe fully the fractional solubility profile of bakers' yeast alcohol dehydrogenase (ADH) and total protein in ammonium sulphate for control applications:

$$F = \frac{1}{1 + \left(\frac{C}{a}\right)^n}$$

(equation 6.2)

where F is fractional solubility, i.e. the fraction of enzyme or protein soluble, C is the ammonium sulphate saturation and a, n are constants. Clarkson *et al.* (1996b) used equation 6.2 in developing a model for the two-stage fractional precipitation of ADH from bakers' yeast homogenate.

Care must be taken when comparing solubility profiles described by the Cohn equation (equation 6.1) and by equation 6.2. For example Foster (1972) observed that when ammonium sulphate was added to bakers' yeast homogenate the concentration of total protein remaining soluble was independent of the initial protein concentration in the salting-out region. The Cohn profiles obtained for this system for different initial protein concentrations will be the same, however profiles obtained using equation 6.2, which describes fractional solubility, will be shifted to the left as the initial protein concentration increases.

6.2.1.2 Theoretical Models

A number of theoretical models have been developed to describe the solubility of proteins in aqueous salt solutions which are based on thermodynamic considerations, incorporating aspects such as electrostatic and/or hydrophobic interactions, the preferential interaction of solvent and salt with protein molecules, and colloidal surface

interactions. In these theories the precipitation of protein is considered to be an equilibrium phase separation.

An early theoretical description of the solubility behaviour of proteins in aqueous salt solutions was based on the electrostatic theory of Debye and Huckel (1923). The protein molecule is assumed to be a simple ion surrounded by an ionic atmosphere containing an excess of counter charged ions. According to the theory, ionic interaction causes a decrease in electrostatic free energy and thereby chemical activity of the protein in solution resulting in an increase in solubility. The Debye-Huckle theory, however, only gives a realistic description of protein solubility in the salting-in region.

The related theory of Kirkwood (1943) treats the protein molecule as a dipole and is the only electrostatic theory able to predict an extensive salting-out effect. The protein dipoles produce cavities of low dielectric constant in the solvent which induce changes in polarisation. Salting-out occurs when repulsive forces between ions and like charges in the cavities increase until it is energetically unfavourable for the protein to remain in solution. A major limitation of the theory is that it does not account for the large differences in protein solubility behaviour observed with different salts (Richardson, 1987; Alsaffar, 1994). Rajagh *et al.* (1965) also claim that the salting-out term is small compared to the salting-in term and the theory would therefore predict an increase in protein solubility at high salt concentrations. From these criticisms it becomes apparent that protein solubility behaviour can not be described by electrostatic considerations alone.

The importance of hydrophobic interactions in the solubility behaviour of proteins was recognised by Kauzmann (1959). Following on from this observation, the Cavity theory developed by Sinanoglu and Abdulnar (1965) sought to explain the stability of proteins in aqueous environments. In this approach the free energy change between a protein molecule in the gas phase as compared to its free energy in solution was considered. The stability was derived from the free energy required to form a cavity in the solvent to accommodate the solute. The higher the surface tension of the solvent, the greater the energy required to 'stretch' the solvent in order to form the cavity, and hence the greater the structural stability.

Melander and Horvath (1977) extended the Cavity theory to describe the solubility of proteins in salt solutions. Most inorganic salts are known to increase the surface tension of water and thereby affect hydrophobic interactions between protein molecules. Protein solubility was now seen to be a balance between a salting-in process due to electrostatic effects and a salting-out process due to hydrophobic effects:

$$\ln\left(\frac{S}{S_0}\right) = \frac{1}{RT}\left[\frac{Am^{1/2}}{1+Bm^{1/2}} + D\delta m\right] - \frac{1}{RT}\left[N_A\Phi + 4.8N_A{}^{1/3}(k_{ST}-1)V_m{}^{2/3}\right]\sigma_D m$$

(equation 6.3)

where S_0 is the protein solubility at zero salt concentration, R is the gas constant, T is the absolute temperature, A is a constant proportional to the net charge on the protein at low ionic strength, B and D are constants, δ is the dipole moment of the protein, N_A is Avogadro's number, Φ is the surface area of the dehydrated protein on precipitation, k_{ST} is the surface tension correction factor, V_m is the molar volume of the solvent and σ_D is the molal surface tension increment of the salt (a constant which represents the change in surface tension which occurs when the salt is added to water).

The first term on the right hand side of equation 6.3 accounts for electrostatic effects and was derived from a combination of the Debye-Huckel and Kirkwood theories. The second term accounts for hydrophobic effects and was derived from the Cavity theory of Sinanoglu and Abdulnar. In the salting-out region the Debye-Huckel term approaches a constant, β, and equation 6.3 can be reduced to:

$$\ln\left(\frac{S}{S_0}\right) = \beta + \Lambda m - \Omega\sigma_D m$$

(equation 6.4)

In Melander and Horvath's (1977) interpretation, $\Omega\sigma_D$ is the slope of the intrinsic salting out line whose magnitude is determined by the hydrophobic contact area, Ω, between the precipitating protein molecules and the molal surface tension increment of the salt, σ_D, while Λ is the slope of the salting in line which expresses the effect of the salt on the electrostatic free energy of the protein and is linear at sufficiently high salt

concentration. Relating equation 6.4 back to the Cohn equation (equation 6.1) gives the following expression for K_S:

$$K_S = \Omega\sigma_D - \Lambda$$

(equation 6.5)

A relationship between surface hydrophobicity and the Cohn constant K_S has been confirmed by Salahuddin *et al.* (1983) who correlated the increasing surface hydrophobicity of seven natural proteins with increases in K_S.

Melander and Horvath (1977) have also correlated the molal surface tension increment of a salt with its position in the lyotropic series (Section 1.2.3.2). This property was therefore suggested as a measure of salting-out effectiveness which could be used to explain the relative protein solubility behaviour observed with different salts. The theory, however, is unable to account for the solubility behaviour observed with $MgCl_2$ and $CaCl_2$ which have a similar molal surface tension increment to sulphate salts but do not decrease protein solubility by the same degree (Richardson, 1987; Alsaffar, 1994).

An alternate theoretical approach to describe the solubility behaviour of proteins in aqueous salt solutions has been given by Arakawa and Timasheff (1984) in which preferential interactions are considered. For a protein in an aqueous salt solution, the salt ions may associate with it preferentially or the protein may be preferentially hydrated. The term 'preferential interaction' can be thought of as both a measure of the excess of salt or water in the immediate vicinity of the protein compared to their concentrations in the bulk fluid, and, thermodynamically, as a reflection of the change in chemical potential of the protein by the addition of the salt or water. The degree of preferential salt association/hydration can be experimentally determined by densimetric techniques and may be envisaged as the grams of salt/water found in a dialysis bag per gram of protein compared to that found outside.

Using this approach, Arakawa and Timasheff (1982) found that protein was preferentially hydrated in concentrated solutions of a number of sodium salts. This observation is somewhat at odds with the previous theories of protein solubility behaviour in which salting-out occurs due to the destruction of structural water surrounding hydrophobic areas of the protein and a decrease in protein hydration could therefore be expected. Arakawa and Timasheff (1982) were able to correlate the

preferential hydration of proteins by most salts to their molal surface tension increments. In the case of divalent cation salts, however, no correlation was found and it was shown that the binding of the divalent cations overcomes salt exclusions due to the surface tension increase and leads to a decrease in preferential hydration (Arakawa and Timesheff, 1984). It was further shown that the order of the preferential interaction of both anions and cation salts followed the lyotrophic series and therefore preferential interaction may be used as a measure of salting-out effectiveness (Arakawa and Timesheff, 1984).

A further theoretical approach is based on the concepts of colloidal science (Rothstein, 1994). Much of this work has its basis in the DLVO (Deryagin-Landau and Verwey-Overbreek) theory which describes surface interactions between colloidal particles. Mahadevan and Hall (1990) used this type of approach to develop a model for protein precipitation with non-ionic polymers. The precipitation was treated as an equilibrium phase separation using techniques of statistical mechanics. Models of protein and polymer interactions were used to calculate an effective protein-protein interaction potential (known as a potential of mean force). Perturbation theory was then used to calculate chemical potentials and pressure for each phase and a thermodynamic stability analysis employed to predict phase transformation and thus generate a phase diagram. Vlachy *et al.* (1993) extended this approach to describe protein precipitation using electrolytes by considering repulsive electrostatic interactions, attractive van der Waals interactions and osmotic attraction.

This work has been developed further by Kuehner and co-workers (1996) to give a description of the solubility behaviour of proteins in aqueous salt solutions. The salting-out of protein is considered to be a liquid-liquid phase separation based on the observation of Shih *et al.* (1992) that salted-out protein precipitates are a dense liquid phase rather than a pure solid. A random-phase approximation (RPA) is used in order to calculate chemical potentials and pressures in each phase. The RPA approach involves defining a system of hard spheres as a reference condition while remaining spherically-symmetric interactions provide perturbations. An interaction potential takes into account electrostatic, dispersion, osmotic and specific interactions. Repulsive electrostatic interactions are described by the Debye-Huckel theory, attractive dispersion forces are represented using DVLO theory, description of strong short-range osmotic

attraction due to depletion of ions between protein molecules is based on the work of Asakura and Oosawa (1958) and specific interactions, such as hydrophobic effects or self-association, are incorporated using an attractive square-well potential. A consideration of thermodynamic equilibrium conditions enables a description of the partitioning of protein between the phases to be obtained and protein partitioning coefficients calculated. Results for the extent of precipitation obtained were shown to be a strong function of parameters used in the square-well potential describing specific interactions. Using this approach, Kuehner *et al.* (1996) were able to show qualitative agreement between model results and experimental data for the precipitation of hen-egg white lysozyme and α-chymotrypsin using ammonium sulphate.

6.2.1.3 Mixing Considerations

The theoretical descriptions for protein solubility previously described consider precipitation to be an equilibrium phase separation. However, the work of Foster *et al.* (1976) showed that different protein solubility profiles were obtained with different contacting schemes, which led them to conclude that precipitation is a pseudo-equilibrium process. This is thought to result in over-precipitation when local concentrations of salt are higher than the bulk concentration. For an equilibrium process, the over-precipitated protein will re-dissolve once the local concentration is reduced to that of the bulk. However, for a pseudo-equilibrium process the precipitate is 'locked-in' and will not re-dissolve, possibly due to irreversible internal bonding or greatly reduced surface free energy giving the precipitate kinetic stability (Richardson, 1987). The 'freezing' of the size distribution of salted-out casein precipitate by dilution with buffer containing ammonium sulphate at the precipitation concentration (Hoare, 1982b) provides some evidence for the existence of irreversible precipitates.

The existence of over-precipitation will depend on mixing conditions, since if mixing is of the same order or slower than precipitation the protein will experience local salt concentrations higher than that of the bulk (Foster *et al.*, 1976). Based on estimates of the precipitation and mixing rate, Richardson (1987) concluded that application of a simple model for irreversible over-precipitation could explain the solubility behaviour of bakers' yeast proteins during ammonium sulphate precipitation, although the need for detailed experimental data to substantiate such a model was recognised.

Iyer and Przybycien (1994) have developed a model for the fed-batch ammonium sulphate precipitation of catalase which considers the impact of mixing conditions on over-precipitation. The extent of mixing in a vessel can be characterised by both macromixing and micromixing. Macromixing is the dissipation of bulk fluid elements, while micromixing is mixing due to molecular diffusion and gives an indication of the extent of molecular homogeneity. This was represented by considering the precipitation reactor volume to be made up of completely segregated zones and a molecular dissipation zone. The breakup of segregated zones into smaller eddies was assumed to occur as a first-order dissipation process. The eddies are assumed to reach their limiting size once they are reduced to the Kolmogoroff scale, λ, and are then known as points. The Kolmogoroff scale is given by:

$$\lambda = \left(\frac{\nu^3}{e}\right)^{\frac{1}{4}}$$

(equation 6.6)

where e is the power dissipation per unit volume and ν is the kinematic viscosity. The zone in which eddies are reduced to the Kolmogoroff scale is called the molecular dissipation zone, and the precipitation of protein is assumed to occur here. Micromixing in this zone is driven by the concentration gradients between a given point and the surrounding points.

The points in the molecular dissipation zone can be classified depending on their starting conditions as either those formed from the protein solution or those formed from the dissipation of added salt solution. When the protein concentration at a given point exceeds its solubility, as given by the Cohn equation (equation 6.1) precipitation occurs, with the precipitation reaction consisting of protein dehydration, aggregation of dehydrated protein and salt ion hydration. To form the model, mass balance equations are described for each point and integrated using numerical methods to give the overall mass of protein precipitated. The model results obtained showed good qualitative agreement with experimental results for 1 L batch and semi-batch precipitations.

Iyer and Przybycien (1994) concluded that the existence of a kinetically irreversible precipitation depends on the relative rates of desolvation, aggregation and mixing,

which in turn depend on the particular protein and salt, as well as vessel geometry, scale and operating conditions. Suggested scale-up parameters for precipitation were the protein concentration and the dimensionless salt feed rate, $F_S/(V.k_{md})$, where F_S is the precipitant feed rate, V is the reactor volume and k_{md} is the micromixing rate.

6.2.2 Description and Optimisation of Fractional Precipitation

The aim of fractional precipitation is to selectively isolate a target protein from a mixture of other contaminants. In the case of the recovery of ADH from a yeast extract, this can be achieved using a two stage ammonium sulphate precipitation (Richardson, 1987; Alsaffar, 1994; Clarkson, 1994). The aim of the first stage is to leave ADH in solution and precipitate other less soluble contaminating proteins, which are removed. The aim of the second is to leave any remaining contaminating proteins in solution and precipitate the ADH, which is recovered. A degree of purification is therefore achieved over the two stages as well as a reduction in process volume (Section 1.2.3.2).

A number of approaches have been proposed for the description and optimisation of fractional precipitation procedures. Scopes (1982) provided an empirical technique for establishing the optimum concentration of ammonium sulphate, known as a cut point, at each stage of a fractionation process. However, this approach was prone to errors unless a large number of precipitation trials were carried out at gradually decreasing cut points (Richardson, 1987). A graphical approach, known as the specific property solubility test, was described by Falconer and Taylor (1946) and applied to the final stages in the purification of liver esterase. In this approach the total protein concentration is plotted against a specific protein property, such as enzyme activity. The resultant graph can track changes in total protein concentration and specific protein property induced by the addition of precipitant. However, the method relies on discontinuities in the graphical description to identify the onset of precipitation of individual proteins. These may be obscured by overlapping solubilities of background proteins, making the procedure difficult to apply to crude cell homogenates (Richardson *et al.,* 1990).

Dixon and Webb (1961) proposed a representation of protein fractionation known as the derivative solubility line method in which solubility curve gradients for each protein are plotted against the precipitant concentration. The advantages of this method are that

solubility curve gradients for individual proteins can be determined from the Cohn equation (equation 6.1), the amount of protein precipitated between cut points is readily determined and the precipitation of two proteins can be considered on the one plot. The method is, however, somewhat inefficient as the solubility curve gradients must be reintegrated in order to calculate the amounts of protein precipitated and the fractionation is only described with respect to individual protein contaminants rather than against total background protein (Richardson *et al.*, 1990).

Richardson *et al.* (1990) have developed the concept of the 'fractionation diagram' in order to describe both the fractionation of a target protein from a single contaminating protein and from total background protein. In this approach the fraction of target protein remaining soluble is plotted against the fraction of specific protein contaminant or total background protein remaining soluble at the same precipitant concentration. A typical resultant graph for the fractionation of a target enzyme against total background protein is shown in Figure 6.1.

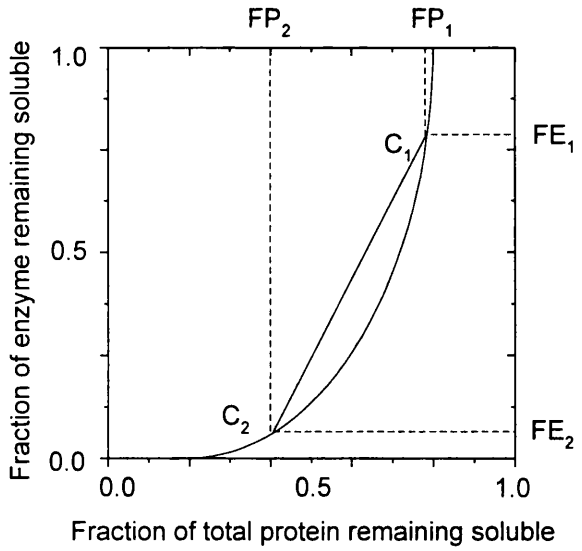

Figure 6.1: Typical enzyme-total protein fractionation diagram.

For a two-cut fractionation, an operating tie-line can be drawn on the fractionation diagram between the two cut points which defines the purification factor, PF, achieved for a given yield, Y:

$$PF = \frac{FE_1 - FE_2}{FP_1 - FP_2}$$

(equation 6.7)

and:

$$Y = FE_1 - FE_2$$

(equation 6.8)

where FE_1, FE_2 are enzyme fractional solubilities and FP_1, FP_2 are total background protein fractional solubilities at cut points C_1, C_2 as shown in Figure 6.2. It becomes evident that the gradient of the operating tie-line must be maximised in order to optimise the purification for a specific yield. Richardson *et al.* (1990) also describe modifications to equations 6.7 and 6.8 in order to take into account occlusion of soluble product in the precipitate phase and difficulty in recovering precipitate particles in subsequent separations. An incremental search algorithm has also been developed by Richardson (1987) to calculate the optimum cut points and the maximum purification factor at given yields for a two-cut fractionation process using high order polynomials to describe fractional protein solubility. The logic behind the incremental search routine is shown in Table 6.1.

Line No.	Action
1.	Calculate coefficients for polynomials to fit enzyme and total protein solubility profiles as a function of precipitant saturation, $FE=f_E(C)$, $FP=f_P(C)$
2.	Increment initial precipitant saturation from C=0 until FE=1 to give $C_0=C$
3.	Set initial fractional precipitate yield, Y=1
4.	Set current maximum purification to zero, $PF_{max}=0$, and start optimisation at $C_1=C_0$
5.	Calculate 1st cut enzyme fractional solubility, i.e. $FE_1=f_E(C_1)$
6.	If $FE_1-Y<0$ go to line 13 else go to line 7
7.	Calculate 2nd cut precipitant concentration, C_2, corresponding to $FE_2=FE_1-Y$
8.	Calculate $FP_1=f_P(C_1)$, $FP_2=f_P(C_2)$
9.	Calculate purification factor PF using equation 6.7
10.	If $PF>PF_{max}$ then set $PF_{max}=PF$
11.	Increment C_1 by 0.01, i.e. $C_1=C_1+0.01$
12.	go to line 5
13.	Ouput optimum conditions for current yield Y, i.e. PF_{max}, C_1,C_2, FE_1,FE_2,FP_1,FP_2
14.	Decrement fractional yield by 0.1, i.e. Y=Y-0.1
15.	go to line 4 unless $Y<0.01$ then end optimisation

Table 6.1: Two cut fractional precipitation optimisation routine of Richardson (1987).

6.2.3 Protein Precipitate Particle Size Distribution

Processes involved in determining the particle size distribution (PSD) of a protein precipitate are nucleation (the formation of primary precipitate particles), perikinetic growth (diffusion-controlled growth of primary particles), orthokinetic growth (shear-controlled aggregation), and shear-controlled breakage. Available models for these processes are described below, along with the description of the resultant PSD of the protein precipitate using population balance approaches.

6.2.3.1 Modelling of Nucleation and Perikinetic growth

The formation of primary precipitate particles, known as nucleation, involves the removal or reduction of hydrostatic or electrostatic barriers in order to facilitate molecular association of protein. The size of primary particles will continue to increase by diffusion-controlled association and aggregation, a process known as perikinetic growth, until a limiting size is reached where shear-controlled collisions become important. The theory of Smoluchowski (1917) describes the rate of decrease of particle number concentration, N, due to diffusion-controlled collisions for a monosized dispersion as a second order process:

$$-\frac{dN}{dt} = K_A N^2$$

(equation 6.9)

where the rate constant K_A is determined by the diffusivity, D_f, and the diameter, d:

$$K_A = 8\pi D_f d$$

(equation 6.10)

Smoluchowski's theory can also be related to the change in molecular weight of primary particles with time, giving a linear relationship (Parker and Dalgleish, 1977). Corrections to Smoluchowski's theory are required to allow for interparticle attractive and repulsive forces, as well as the hydrodynamic removal of free water between particles and particle non-sphericity (Bell *et al.*, 1983). Fuchs (1964) has proposed a modification to equation 6.9 to take into account the presence of an electrical barrier that decreases the rate of association:

$$-\frac{dN}{dt} = \frac{K_A}{W} N^2$$

(equation 6.11)

where W is the stability ratio:

$$W = d\int \frac{\exp\left(\phi(h) / k_B T\right)}{(h+d)^2} dh$$

(equation 6.12)

In equation 6.12, h is the particle separation distance, k_B is Boltzmann's constant and $\phi(h)$ is the potential energy of interaction between two particles. However, Bell *et al.* (1983) have noted that the stability ratio cannot be evaluated readily and the theory does not account for the presence of a hydration barrier around the protein molecules. Protein association may also not be the limiting step in the formation of primary particles, especially if the removal of hydration barriers or electric charges are slow processes.

Nelson and Glatz (1985) considered two models for describing primary particle formation in protein precipitation. The first model assumes that formation of primary particles depends on conditions inside fluid eddies at the Kolmogoroff scale, which is likely to occur if the nucleation rate is much faster than that of micromixing. In this case the rate of nucleation will be a function of both the degree of protein supersaturation and the mixing conditions. The second model is based on the work of Nielson (1964) and assumes homogeneous diffusion-controlled nucleation, with the nucleation rate expressed as a power law function of protein supersaturation and independent of mixing conditions. This situation is likely to occur when the nucleation rate is slower than that of micromixing, with primary particle formation independent of convective fluid motion. Experimental results for the nucleation rate of primary particles during isoelectric soy protein precipitation showed a power law relationship with supersaturation and therefore agreed with the homogeneous diffusion-controlled model of nucleation. The primary particle size was also affected by precipitant and reactor configuration, but this was attributed to concentration rather than mixing effects.

The growth of salted-out casein precipitate under hindered gravity settling conditions likely to favour perikinetic growth was modelled by Hoare (1982b) using a discretised form of equation 6.9. Reasonable agreement with model predictions was seen for the

first period of ageing where minimum settling occurred, with larger deviations observed at longer ageing times being attributed to changes in particle concentration and suspension rheology.

6.2.3.2 Modelling of Orthokinetic Growth

When the primary precipitate particles reach a certain limiting size, shear induced collisions will lead to particle aggregation. This process is known as orthokinetic growth. Smoluchowski (1917) gives the rate of decrease in particle number concentration, N, for a suspension of uniformly sized spherical particles due to collisions in a uniform shear field as:

$$-\frac{dN}{dt} = \frac{2}{3}\alpha G d^3 N^2$$

(equation 6.13)

where d is the particle diameter, G is the shear rate and α is the collision effectiveness factor, i.e. the number of collisions which result in permanent aggregates. Assuming a constant volume fraction of particles, φ_v:

$$\varphi_v = \frac{\pi d^3 N}{6}$$

(equation 6.14)

equation 6.13 becomes:

$$-\frac{dN}{dt} = \frac{4}{\pi}\alpha \varphi_v GN$$

(equation 6.15)

Equation 6.15 can be integrated to give:

$$\frac{N_t}{N_0} = \exp\left(\frac{-4\alpha \varphi_v Gt}{\pi}\right)$$

(equation 6.16)

In practice, deviations to Smoluchowski's description of orthokinetic aggregation are observed due to a number of shortcomings in the theory (Bell *et al.*, 1983). For example, the effectiveness of collision also becomes a function of shear rate and particle size since two particles on a direct collision course will tend to follow the fluid stream

lines around each other, reducing the chance of collision. For most laminar systems there is also a variation in shear rate with position in the shear field, and for turbulent systems the shear field is non-uniform and variable at any point in time. A more rigorous treatment of particle collision in homogeneous turbulent flow fields has been carried out by Saffman and Turner (1956), while Camp and Stein (1943) have proposed that the shear rate in equation 6.13 can be estimated on the basis of the power dissipation per unit volume, e, and the kinematic viscosity, ν:

$$G = \left(\frac{e}{\nu}\right)^{\frac{1}{2}}$$

(equation 6.17)

Virkar *et al.* (1982) modelled the orthokinetic growth of isoelectric soya protein precipitate using Smoluchowski's theory. Model results showed agreement with experimental values over a short period, but thereafter a large deviation was observed. Hoare (1982b) modelled the growth of salted-out casein under conditions likely to favour orthokinetic aggregation using a discretised form of equation 6.13 and assuming an average rate of shear. A large deviation between experimental increases in particle size and that predicted by the model was observed, which was thought to be due to the dominant role of shear-induced breakage.

6.2.3.3 Modelling of Shear-Induced Breakage

The effect of shear forces on precipitate particles may lead to their breakage and thereby have an influence on the final size of a precipitate. Mechanisms for the breakage of protein aggregates have been proposed by Glasgow and Luecke (1980) as bulgy deformation due to pressure differences on opposite sides of the aggregate, primary particle erosion due to hydrodynamic shear, erosion of particles larger than primary particles due to hydrodynamic shear, and fragmentation due to particle-particle collisions. Twineham *et al.* (1984) found evidence for the collisional breakage in a study of the isoelectric precipitation of soy protein. However, most descriptions of precipitate breakage have assumed that collisional events are negligible compared to hydrodynamic shear-initiated events (Brown and Glatz, 1987). In a review on the modelling of precipitation, Glatz and Fisher (1986) concluded that further research was required for an adequate description of aggregate breakage. Recent work by Shamlou *et*

al. (1994, 1996) has shown that the initial frequency of soya protein precipitate breakage in turbulently agitated bioreactors is a function of the energy dissipation rate in the vessel.

Available models for turbulent aggregate breakage have been evaluated by Brown and Glatz (1987). The models included maximum stable aggregate, displacement, statistical and number concentration models. The simplest description of aggregate stability is the maximum stable aggregate model and is obtained by equating the size-independent hydrodynamic forces to the size-dependent strength of the aggregate to identify the largest particle size, d_{max}, able to avoid disruption. Particular relationships have been proposed that are applicable to particle sizes above and below the Kolmogoroff scale which take the general form:

$$d_{max} \propto G^{-n}$$

(equation 6.18)

where G is the average shear rate and n is a constant, the value of which is dependent on the mechanism of breakup. The maximum stable aggregate model lacks any consideration of breakage kinetics or information on the breakage of particles below the maximum size. Experimental results for isoelectric soya protein precipitates did not match those predicted by this model (Brown and Glatz, 1987). The maximum stable aggregate model also has some relevance to the batch ageing of precipitate in stirred tanks in order to increase precipitate strength and improve subsequent recovery (Section 1.2.3.2). The Camp number, Gt, has been used as an ageing parameter, with the work of Hoare (1982b) indicating that a maximum stable size for salted-out casein protein precipitate is achieved for $Gt=10^5$.

The displacement model was developed by Twineham *et al.* (1984) to describe the aggregation and breakage of isoelectric soya protein precipitate. An empirical function was used to describe the rate of change in particle diameter as a displacement from a final aggregate diameter, the rate constant dependent on the collisional rate. Brown and Glatz (1987) found that the displacement model gave good fits to experimental data but had no theoretical basis. The statistical model examined by Brown and Glatz (1987) was based on studies into the breakup of large populations of droplets and described the breakage process in the form of statistical distributions of droplet sizes. A comparison

of model and experimental results showed that two power law functions were required to cover the entire distribution, with a higher exponent for larger sizes.

The number concentration model was presented by Glasgow and Luecke (1980) and provides a mechanistic description of the rate of change in aggregate number concentration, N, at a particular size as a result of breakage. The equations are of the general form:

$$\frac{d\mathrm{N}}{d\mathrm{t}} = f(\mathrm{N}^{\mathrm{a}})$$

(equation 6.19)

A first order dependence is seen for breakage by hydrodynamic shear (a=1) and a second order dependence for breakage by collisional forces (a=2). Brown and Glatz (1987) found that number concentration models gave the best agreement with experimental data for isoelectric soya protein precipitates in nearly all cases.

6.2.3.4 The Population Balance Model

The population balance describes the change in the particle size distribution (PSD) of a system with respect to time. The approach has been widely used to describe the kinetics of particulate processes such as precipitation, flocculation (e.g. Chen *et al.*, 1990) and crystallisation (e.g. Wachi and Jones, 1992). A detailed description of the population balance is given by Randolph and Larson (1971) and Ramkrishna (1985).

A general continuous population balance based on size, for a constant volume well-mixed vessel is (Randolf and Larson, 1971):

$$\frac{\partial n}{\partial \mathrm{t}} + \frac{\partial(\mathrm{G_R} n)}{\partial \mathrm{d}} + \mathrm{D_R} - \mathrm{B_R} = -\sum_{\mathrm{s}} \frac{n_{\mathrm{s}} \mathrm{Q_s}}{\mathrm{V}}$$

(equation 6.20)

where n is the population number density function, B_R is the birth rate, D_R is the death rate, G_R is the growth rate, Q_s is the flowrate of streams into and out of the vessel and V is the vessel volume. For a batch process the term on the right hand side of equation 6.19 becomes zero. The number density function at a size d, n(d), is defined as the ratio of particles in a differential neighbourhood around d and the size of the neighbourhood,

i.e. $n(\mathrm{d}) = dN/d\mathrm{d}$. Equation 6.20 therefore relates the rate of change of particle number in the differential size range d to dd, to the rates of growth into and out of that range and the rates of birth and death in the size range.

The main challenge in applying the population balance to protein precipitation processes is in specifying expressions for particle growth, birth and death. Grabenbauer and Glatz (1981), Petentate and Glatz (1983) and Glatz *et al.* (1986) have used the population balance approach to describe the isoelectric precipitation of soya protein in a continuous stirred tank reactor (CSTR) at steady state. Since there are no particles in the feed and the vessel is well mixed so that the outlet distribution is identical to that in the vessel, equation 6.19 becomes:

$$\frac{d(\mathrm{G_R}n)}{d\,\mathrm{d}} + \frac{n}{\tau} + \mathrm{D_R} - \mathrm{B_R} = 0$$

(equation 6.21)

where τ is the mean residence time.

Grabenbauer and Glatz (1981) considered orthokinetic aggregation to be the rate controlling step in particle growth. The growth rate was assumed to be constant and independent of particle size. Particle death and birth were assumed to occur due to aggregate breakage and modelled as a first order process with respect to particle number, with the rate constant treated as a power law function of size. Particle breakage was assumed to result in two daughter particles, each with half the original protein content. The kinetic parameters were determined using iterative least squares fitting on a linearised form of the population balance and the model was solved using a Runge-Kutta procedure.

Petentate and Glatz (1983) also assumed orthokinetic aggregation to be the rate determining step in particle growth, with both a linear and power law dependence of growth function on particle size being used. The four mechanisms of breakage described in Section 6.2.3.3 were considered and it was assumed that the death rate was a first order process with respect to particle number that occurred as a result of breakage due to hydrodynamic forces. Both a linear and a power law death rate dependence on size were considered. The birth rate was assumed negligible due to thorough breakage, i.e. the formation of debris of negligible size. Combinations of linear and power law

growth functions with either linear, power law or no breakage functions were used in the population balance, which was solved explicitly. Particle sizes above 1 to 2 μm were successfully modelled, with the results indicating that collisions between large particles were ineffective in producing aggregation and that the assumption of thorough breakage was justified. Glatz *et al.* (1986) used a linear growth rate dependence on size. The first order death and birth rates, with power law dependence on size, were used to describe particle breakage such that the total particle volume was conserved. Values of some model parameters were determined using a non-linear least squares fitting routine and the population balance solved using a fourth order Runge-Kutta procedure. Model results matched experimental data and confirmed the observations of Petentate and Glatz (1983).

Rohani and Chen (1993) used equation 6.21 to describe the isoelectric precipitation of canola protein in a CSTR at steady state. A size independent growth rate was used and negligible breakage assumed due to the low concentration of protein. The birth and death rates were therefore based solely on orthokinetic aggregation. Correlations for the nucleation rate, particle growth rate and other model parameters were determined using experimental data from a consideration of moment transforms. Fisher and Glatz (1988) applied equation 6.21 to the polyelectrolyte precipitation of egg-white protein in a CSTR at steady state. The growth rate was determined using both perikinetic growth and orthokinetic aggregation terms, with an enhancement in growth rate due to polymer extension also incorporated. A first order death rate resulting from breakage by hydrodynamic forces and a second order rate resulting from breakage by collisions were considered separately. In both cases the death term was also a power law function of the particle size and a particle birth term was added which ensured that the total particle volume was conserved. The second order breakage rate was found to give a closer agreement with the experimental data and the inclusion of the polymer enhancement term further improved the agreement at low shear.

Przybycien and Bailey (1989) used a population balance approach to describe the kinetics of the salt-induced precipitation of α-chymotrypsin. The precipitation process was assumed to consist of a simultaneous salt-mediated dimerisation step and a conformational change to an altered dimer that is the primary aggregable species. No precipitate breakage was assumed. The rate equations in the population balance were

described using Smoluchowski's theory of perikinetic (Section 6.2.3.1) and orthokinetic aggregation (Section 6.2.3.2). The precipitation process was monitored using stopped flow turbidity and the results used to determine model parameters using a non-linear least squares algorithm. The model results closely matched experimental data, apart from at low temperatures where the turbidity profiles were no longer sigmoidal.

6.2.3.5 The Discretised Population Balance

Analytical solutions for the population balance can be difficult to compute if complex expressions are used for growth, birth and death terms. Discretisation of the population balance is one approach that can ease the calculations involved (Hounslow *et al.*, 1988). The discretised population balance results from a transformation of the continuous population balance model (equation 6.20) into a set of ordinary differential equations. The discretised equations are usually given in terms of the number of particles, N_i, in a finite size range and are of the form:

$$\frac{dN_i}{dt} = f(N_1, N_2, \ldots N_n) \qquad i = 1,2,\ldots n$$

(equation 6.22)

For n size ranges there will therefore be n equations. Both linear and geometric progressions in particle volume have been used for the discretisation of the size domain (Clarkson *et al.*, 1996a). For the linear progression particle volumes are used such that $V_i+V_j=V_{i+j}$, while for the geometric progression the ratio V_{i+1}/V_j is held constant. The most commonly used geometric ratio progression is 2, which gives a $d_{i+1}/d_i=3\sqrt{2}$ discretisation over the size range (Clarkson *et al.*, 1996a).

Hounslow *et al.* (1988) have presented a $3\sqrt{2}$ geometric discretisation of the population balance for batch aggregation which was applied to describe the *in vitro* growth and aggregation of kidney stones. Aggregation was derived from a four binary interaction mechanism in which particle volume is conserved as shown in Table 6.2 overleaf.

Mechanisms	Birth or death in interval *i*	Collision between particles in intervals
1	Birth	*i*-1 and 1→ *i*-2
2	Birth	*i*-1 and *i*-1
3	Death	*i* and 1→ *i*-1
4	Death	*i* and *i*→∞

Table 6.2: Aggregation mechanism.

This leads to the following equation for particle aggregation:

$$\left(\frac{dN_i}{dt}\right)_{Agg} = N_{i-1}\sum_{j=1}^{i-2} 2^{j-i+1}\beta_{i-1,j}N_j + \frac{1}{2}\beta_{i-1,i-1}N_{i-1}^2 - N_i\sum_{j=1}^{i-1} 2^{j-i}\beta_{i,j}N_j - N_i\sum_{j=i}^{i=n}\beta_{i,j}N_j$$

(equation 6.23)

where $\beta_{i,j}$ is known as the aggregation kernel. This parameter can take various forms in different flow fields as shown in Table 6.3:

Mechanism	Kernel, $\beta_{i,j}$
Size-independent	β_0
Brownian motion	$\beta_0(d_i+d_j)(d_i^{-1}+d_j^{-1})$
Shear flow	$\beta_0(d_i+d_j)$
Turbulent flow	$\beta_0(d_i+d_j)\lvert d_i^2-d_j^2\rvert$

Table 6.3: Aggregation kernels.

Particle breakage was incorporated into the discretised population balance using the model of Hartel and Randolph (1986) in which the death rate is proportional to the product of the particle number density function and the particle volume:

$$D_R = -K_D d^3 n(d)$$

(equation 6.24)

where K_D is the breakage rate constant. It was assumed that when a large particle breaks it generates two smaller daughter particles of half the original volume. The birth rate is therefore given by:

$$B_R = 2D_R(2d)$$

(equation 6.25)

A discretised breakage model was derived by Hounslow (1988) from equations 6.24 and 6.25 in which each time a particle breaks in interval *i*, two particles are formed in the interval *i*-1. It follows that the rate of change of particle number in the *i*th interval is given by:

$$\left(\frac{dN_i}{dt}\right)_{Break} = \frac{3}{2}K_D K_V (2d_{i+1}^3 N_{i+1} - d_i^3 N_i)$$

(equation 6.26)

where K_V is the particle shape factor. Equations 6.23 and 6.26 are then brought together to give:

$$\left(\frac{dN_i}{dt}\right)_{Batch} = \left(\frac{dN_i}{dt}\right)_{Agg} + \left(\frac{dN_i}{dt}\right)_{Break}$$

(equation 6.27)

Clarkson *et al.* (1996a) used the discretised population balance of Hounslow *et al.* (1988) to model the batch fractional precipitation of the enzyme ADH from yeast homogenate using ammonium sulphate. Only orthokinetic growth and shear-induced breakage were considered, since nucleation occurs in a fraction of a second after addition of the precipitant and the effect of perikinetic growth on the final precipitate size was assumed to be negligible. Particle aggregation and breakage were modelled using equations 6.23 and 6.26 respectively, with a size independent aggregation kernel being used. Model parameters were estimated from experimental data based on a consideration of changes in the first moment transform. The discretised model was solved using the SPEEDUP simulation package, with model results showing good agreement with the experimental data over a range of mixing conditions.

6.3 Application of Existing Precipitation Models to the MC1 Strain

Selected models describing the solubility behaviour of protein in aqueous salt solutions, the fractional precipitation of a target enzyme from contaminating protein, and the changes in precipitate particle size distribution (PSD) were applied to the protein engineered system. A prediction for the change in solubility behaviour of protein engineered ADH compared to the wild type enzyme was also made based on the theoretical description of protein precipitation of Melander and Horvath (1977).

6.3.1 Description of Solubility Profiles and ADH Fractionation

As can be seen from the theoretical descriptions of protein solubility behaviour in Section 6.2.1.2, a number of different theoretical models have been developed. However, the practical application of these theoretical models is difficult since in most cases the models do not apply to multicomponent systems and required model parameters are not generally available in the literature and thus must be experimentally determined. In terms of available empirical equations, the Cohn equation (equation 6.1) only describes salting-out behaviour and therefore has limited application, while the polynomial approach of Richardson (1987) was found to be too sensitive to fluctuations in experimental data to be applied across the full solubility profile. The isotherm expression (equation 6.2) as used by Niktari *et al.* (1989, 1990) and Clarkson *et al.* (1996a), was able to give a more stable description of the full solubility profile of both ADH and total protein from yeast and was therefore used to describe solubility behaviour in this study. The use of an empirical expression to describe protein solubility did have the disadvantage that the extent of possible overprecipitation could not be explicitly determined by the model. A consideration of mixing conditions therefore became important when scaling-up the 1 L precipitation solubility profiles in order to describe large scale precipitation behaviour. These issues are considered in more detail in Section 6.4.1.5.

In terms of the existing methods for describing and optimising protein fractionation given in Section 6.2.2, the fractionation diagram approach of Richardson *et al.* (1990) was recognised as the most robust method and was therefore adopted for use in this

study. The algorithm developed by Richardson (1987) for optimisation of a two-cut fractionation was modified to incorporate the preferred empirical isotherm expression (equation 6.2) rather than the previously used polynomial function and was used to compare optimal cut points and purification factors at given yields for the protein engineered and bakers' yeast systems (refer to Appendix 1 for a MATLAB program listing of the modified optimisation routine).

6.3.3 Modelling Changes in Particle Size Distribution

Of the existing models describing changes in precipitate particle distribution (PSD), the discretised population balance model developed by Clarkson *et al.* (1996a) was found to be the most suited for application to the protein engineered system. This was the only available model which described fractional batch precipitation, with all the other models describing continuous precipitation. The same aggregation and breakage terms were used as that of Clarkson *et al.* (1996a), with values for the aggregation kernel and breakage constant taken at equivalent shear rates. The shear rate was given by the following equation:

$$G = \left(\frac{2\pi N_I T_M}{V\mu} \right)^{\frac{1}{2}}$$

(equation 6.28)

where N_I is the impeller speed , V is the volume, μ is the dynamic viscosity and T_M is the motor torque determined from N_I and the impeller diameter D_I using the equation:

$$T_M = 7.21 \times 10^2 N_I^2 D_I^2$$

(equation 6.29)

The use of the Clarkson model required the assumption that nucleation and perikinetic growth occurred instantaneously and had little effect on the final precipitate PSD. A major challenge in applying the model was in determining the initial particle number, as the laser sizing method used for precipitates (Section 3.2.7.2) only returned percent in range values.

The initial number concentration of precipitate particles, N_i, was therefore calculated from the precipitated total protein concentration C_{ptp} (determined using equation 6.2), the measured precipitate density ρ_p (Section 6.4.1.4) and the diameter of precipitate particles d (Section 6.4.1.3) using the formula:

$$N_i = \frac{6C_{ptp}}{\rho_p \pi d^3}$$

(equation 6.30)

In equation 6.30 it is assumed that the particles are spherical.

6.3.3 Prediction of Solubility Changes for the Protein Engineered System

A prediction for the expected solubility profiles of ADH and total protein from the protein engineered system was made based on known differences to the bakers' yeast system. Native and SDS protein gels (Figures 4.5 and 4.6 respectively) showed little difference in total protein composition for each system, and therefore the solubility behaviour was expected to be the same for total protein from protein engineered and bakers' yeast sources.

A consideration of the change in surface hydrophobicity, Ω, for *pe*-ADH relative to the wild type enzyme enabled the expected shift in Cohn constant K_S, and hence the change in enzyme solubility, to be predicted from equation 6.5. In the case of *pe*-ADH, the protein engineering changes made to the enzyme involved replacing tryptophan at amino acid position 93 with the smaller but more hydrophobic phenylalanine residue (Section 1.6.1). However, Murali and Creaser (1986) concluded that the amino acid change would decrease the hydrophobicity of the active site area, since the replacement occurs inside the active site pocket, which would lead to a decrease in Ω and hence in K_S. An increase in *pe*-ADH solubility was therefore predicted compared to the wild type enzyme since the decrease in K_S causes the Cohn solubility plot described by equation 6.1 to become less steep.

6.4 Results and Discussion

6.4.1 Precipitation Characterisation using a Small Scale System

6.4.1.1 Solubility Behaviour

i) Consistency of solubility results

To ensure consistent solubility results, a mass balance was carried out for each small scale experiment over the range of ammonium sulphate saturations examined. Results for typical mass balances are given in Appendix 2. After the degree of dilution was considered, no consistent decreases in the overall levels of total protein or ADH were observed. This indicated that there was no significant loss of total protein or denaturation of ADH during small scale experiments.

It was also important to ensure that the solid precipitate was well separated from the liquid phase, as poor separation would effect fractional solubility results. Previous work by Hoare (1982a) showed that separation of isoelectric soya protein by either centrifugation at 20,000 g for 1 h or filtration had little effect on the solubility profile obtained. Clarkson (1994) used bench centrifugation at approximately 30,000 g for 0.167 h in determining fractional solubility profiles of ADH and total protein from packed bakers' yeast homogenate in ammonium sulphate and reported some inefficiency in the separation of precipitate particles above 60% ammonium sulphate saturation. In this study, bench centrifugation was carried out using the same centrifugation conditions as Clarkson (1994) but with a spin time of 0.5 h instead of 0.167 h to give better separation of precipitate above 60% ammonium sulphate saturation (Section 3.4.2.3). Due to variations in the feed material to precipitations, data from each precipitation was considered separately rather than averaging results from different experiments carried out under the same processing conditions.

ii) Effect of antifoam on solubility behaviour

The addition of polypropylene glycol (PPG) at the fermentation stage as an antifoam agent was found to have an effect on subsequent precipitations (Figure 6.2 on page 183).

For an antifoam concentration of 1 mL per L of fermentation medium a distortion of the total protein and *pe*-ADH solubility profiles was seen, with increased fractional solubility occurring at high ammonium sulphate saturation. To check that this distortion was indeed caused by the antifoam, polypropylene glycol was added to packed bakers' yeast at an equivalent concentration which was then processed under the same conditions as the fermented yeast. The same level of solubility curve distortion was seen (Figure 6.3 on page 184).

For fermentations, the addition of PPG has been shown to prevent foaming by decreasing the surface tension of the culture medium (Koch *et al.*, 1995). As stated in Section 6.2.1.2, most inorganic salts are known to increase the surface tension of water, thereby affecting hydrophobic interactions between protein molecules. Furthermore, the increasing effectiveness of salts as salting-out agents, shown by their position in the lyotropic series, has been correlated with the resultant increase in surface tension, given by their molal surface tension increment (Melander and Horvath, 1977). The observed increases in fractional solubility can therefore possibly be attributed to a decrease in surface tension due to the presence of the PPG. Koch *et al.* (1995) have shown that above a critical concentration of PPG, a constant decrease in surface tension is produced. A constant distortion of the fractional solubility profile above a critical PPG concentration would therefore be expected. It should be noted that changes in liquid or precipitate density due to the presence of the PPG may also have prevented full separation of the precipitate, thereby giving an increase in fractional solubility.

The solubility curve distortion was removed and full precipitation achieved either by the inclusion of a wash stage after cell harvest, which reduced the level of antifoam carryover, or by lowering the level of antifoam to 0.1 mL per L of fermentation media, which reduced the overall level of antifoam present (Figure 6.2). The major consequence of adding a wash step is an increase in the overall processing time, while lowering the level of antifoam reduced the stirrer speed that could be applied before foaming occurred from 500 to 300 rpm. The reduction in stirrer speed had little effect on the final biomass level, total protein concentration and *pe*-ADH specific activity achieved in fermentations (Table 4.5 on page 123). For the rest of the study an antifoam level of 0.1 mL per L fermentation broth was therefore used rather than including a wash stage to avoid extending the overall processing time.

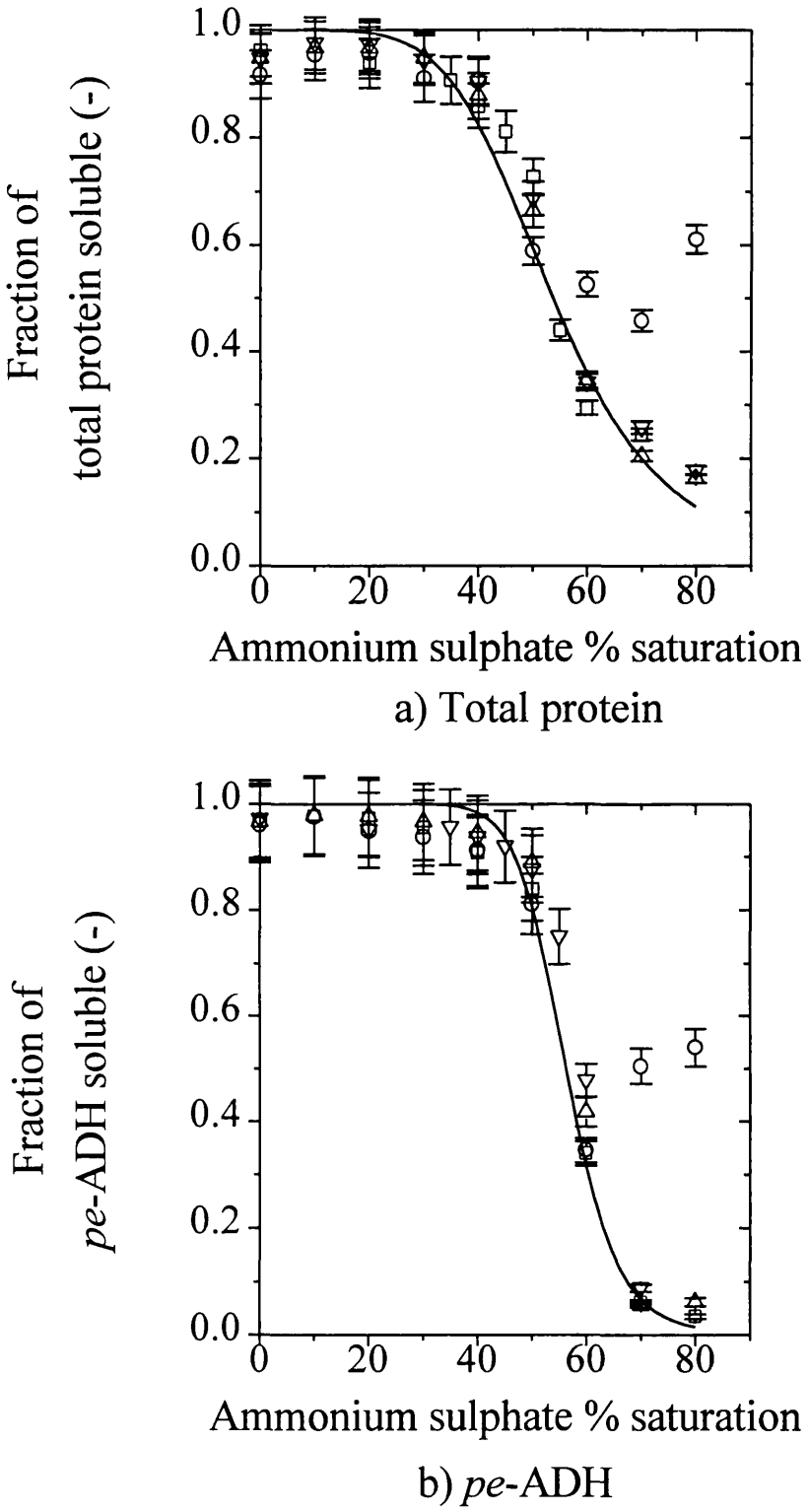

Figure 6.2: Fractional solubility of fermented recombinant yeast a) total protein and b) pe-ADH under various processing conditions. Experimental data: ○ 1.0 mL.L^{-1} added antifoam and no wash, □ 0.1 mL.L^{-1} added antifoam and no wash, △ 1.0 mL.L^{-1} added antifoam and washed, ▽ 0.1 mL.L^{-1} added antifoam and washed. Fitted Curve: (——) 0.1 mL.L^{-1} added antifoam and no wash.

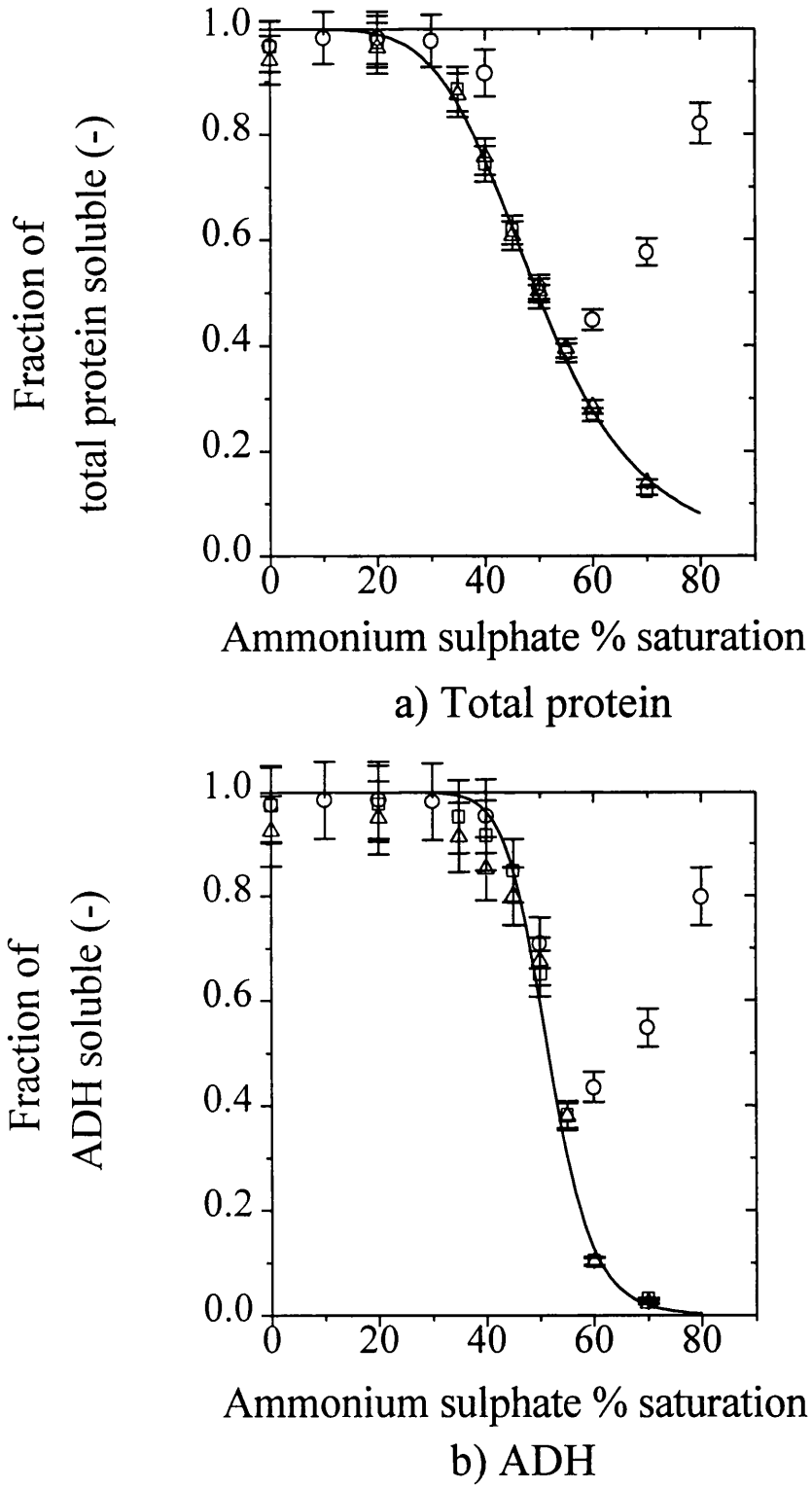

Figure 6.3: Fractional solubility of packed bakers' yeast a) total protein and b) ADH under various processing conditions. Experimental data: Δ no antifoam added, ○ equivalent of 1.0 mL.L^{-1} added antifoam, □ equivalent of 0.1 mL.L^{-1} added antifoam. Fitted Curve: (——) no antifoam and 0.1 mL.L^{-1} added antifoam data.

iii) Comparison of bakers' yeast and protein-engineered solubility profiles

Comparison of fitted ADH and total protein fractional solubility curves for the protein engineered and bakers' yeast systems at 280 g wet weight yeast per L shows that there was an increase in fractional solubility for both *pe*-ADH and total protein (compare fitted curves in Figures 6.2 and 6.3). However, the levels of ADH and total protein were 288.5 $U.mL^{-1}$ and 29.3 $mg.mL^{-1}$ respectively in the bakers' yeast homogenate compared to 27.8 $U.mL^{-1}$ and 10.0 $mg.mL^{-1}$ in homogenate from the protein engineered system. The lower levels of soluble protein and product enzyme obtained from the recombinant yeast were noted in Chapter 5.0 on the modelling of high pressure homogenisation. Precipitation of bakers' yeast and recombinant yeast homogenate suspensions diluted to a level of 93 and 26 g wet weight yeast per L was therefore carried out to enable comparison of solubility profiles over a range of protein and ADH concentrations (Figure 6.4 on page 187). The results are expressed in solubility terms, rather than fractional solubility, so that the initial total protein concentration or ADH activity is shown for each profile.

In the case of total protein from bakers' yeast, the solubility profiles (Figure 6.4a) showed a shift to higher concentrations with increasing initial protein concentration which agreed with the observations of Richardson (1987). Comparison with the total protein profiles from the protein engineered system showed that similar solubility profiles were obtained for both systems at equivalent total protein concentrations (Figure 6.4a). This result was somewhat expected, since SDS-PAGE and native-PAGE protein gels showed similar overall protein spectrums for the bakers' yeast and protein engineered systems (Section 4.3.4). The difference in total protein concentration at 280 g wet weight per L for the protein engineered and bakers' yeast systems was therefore identified as the major factor in the shifting of total protein solubility and fractional solubility behaviour.

In the case of bakers' yeast ADH, the solubility profiles were similar to those obtained by Richardson (1987), with profiles for different initial ADH activities converging to a value of approximately 30 $U.mL^{-1}$ at an ammonium sulphate saturation between 60 and 65% (Figure 6.4b). In order to compare the solubility of *pe*-ADH and bakers' yeast

ADH, Cohn parameters were determined for the ADH solubility profiles and examined to see if they matched that predicted, i.e. constant β and a decreased K_S from the bakers' yeast to protein engineered enzyme (Section 6.3.3). The fitted Cohn parameters are shown in Figures 6.5 and 6.6 on page 188. The results were somewhat inconclusive due to the large standard deviations in some of the fitted Cohn parameters. The values of K_S for *pe*-ADH did appear to decrease at equivalent ADH activities compared to the bakers' yeast system as expected, but there was also a reduction in the value of β which did not match the prediction.

It is interesting to note that a change in shape of the *pe*-ADH solubility profiles compared to that of bakers' yeast ADH gave the reduction in β values (Figure 6.4b). It is possible that the different profile shapes were due to changes in enzyme specific activity between the two systems, with bakers' yeast ADH at 13 $U.mg^{-1}$ while the *pe*-ADH was at 2.8 $U.mg^{-1}$. However, Richardson (1987) found that varying the specific activity of bakers' yeast ADH in the range 13 and 92 $U.mg^{-1}$ caused no consistent shifts in solubility behaviour, although an increased initial ADH purity did give a lower purification factor. Another possible cause of the change in shape of the solubility profile was the presence of different ADH isozymes in the protein engineered and bakers' yeast systems. The protein engineered enzyme is a form of YADH-I, while bakers' yeast is more likely to contain YADH-II (Section 1.6.1).

The inability to identify the exact causes of the observed shifts in ADH solubility and fractional solubility profiles highlights the difficulty in predicting the solubility behaviour of complex protein mixtures, with direct experimentation still being the best way of characterising a precipitation process. The advantage of using small scale systems to achieve this is that process information is then available as early as possible for design purposes.

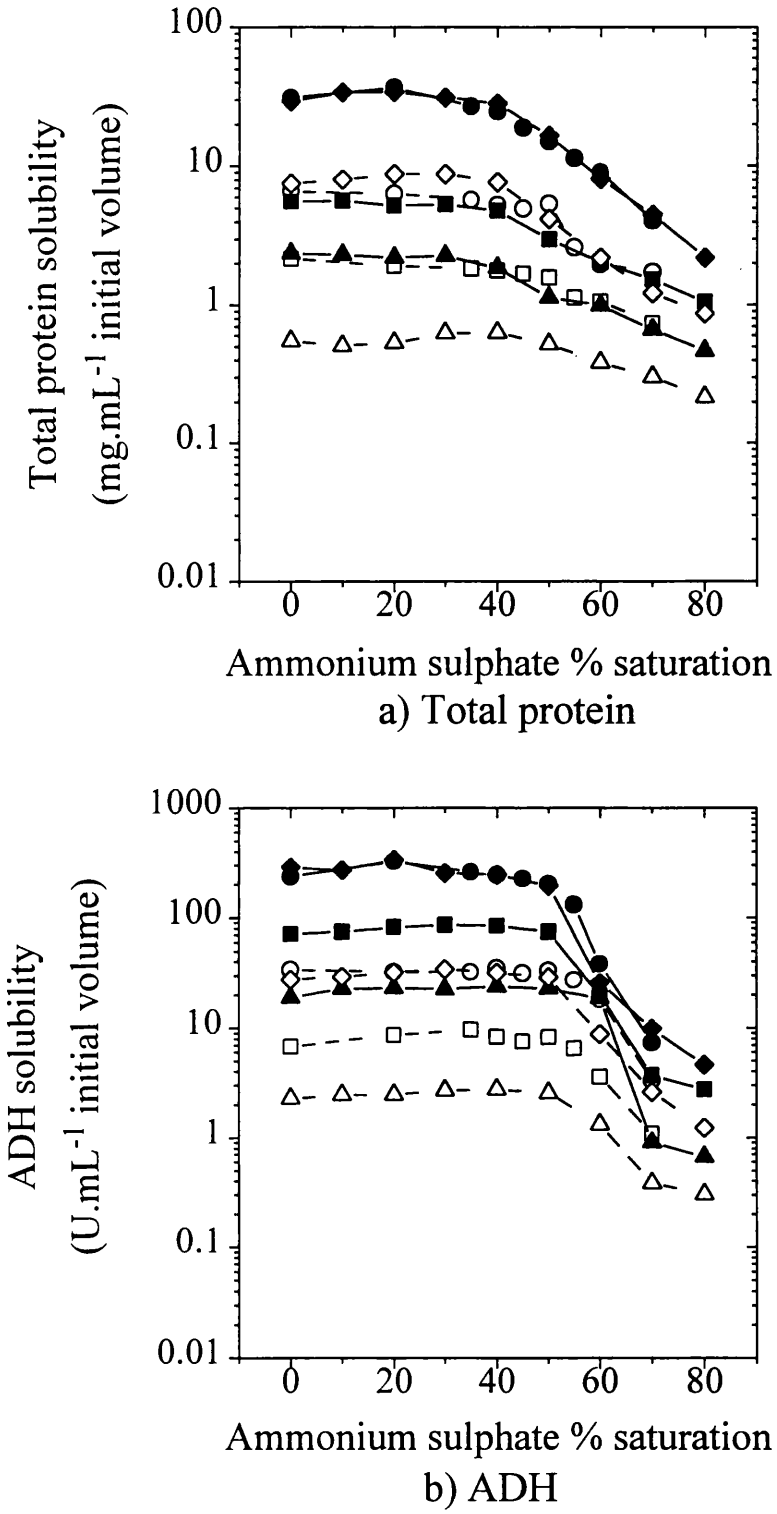

Figure 6.4: Solubility profiles for a) total protein and b) ADH for various initial yeast concentrations. Experimental data: ● ◆ 280 g/L, ■ 93 g/L, ▲ 26 g/L. Closed symbols are packed bakers' yeast, open symbols are fermented recombinant yeast. Data points joined by lines for clarity: (——) packed bakers' yeast, (– – –) recombinant yeast.

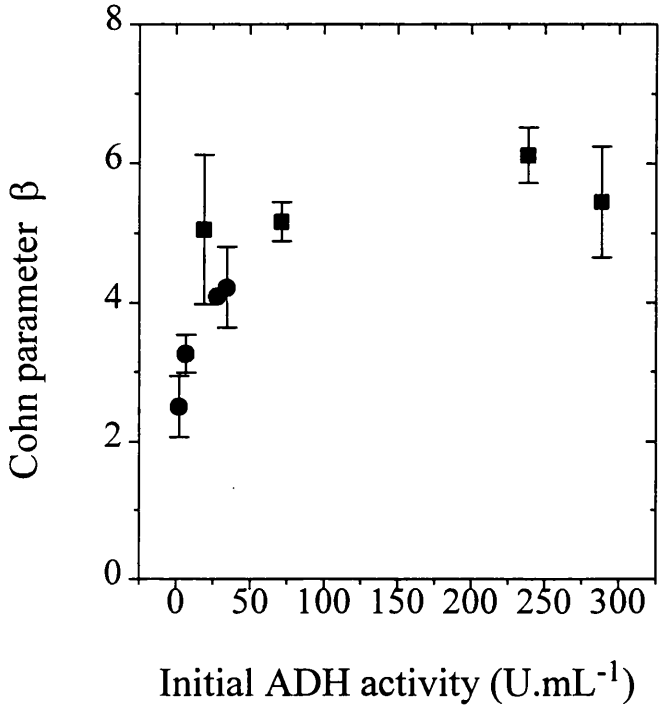

Figure 6.5: Fitted Cohn parameter β plotted against initial ADH activity. Experimental data: ■ packed bakers' yeast, ● fermented recombinant yeast.

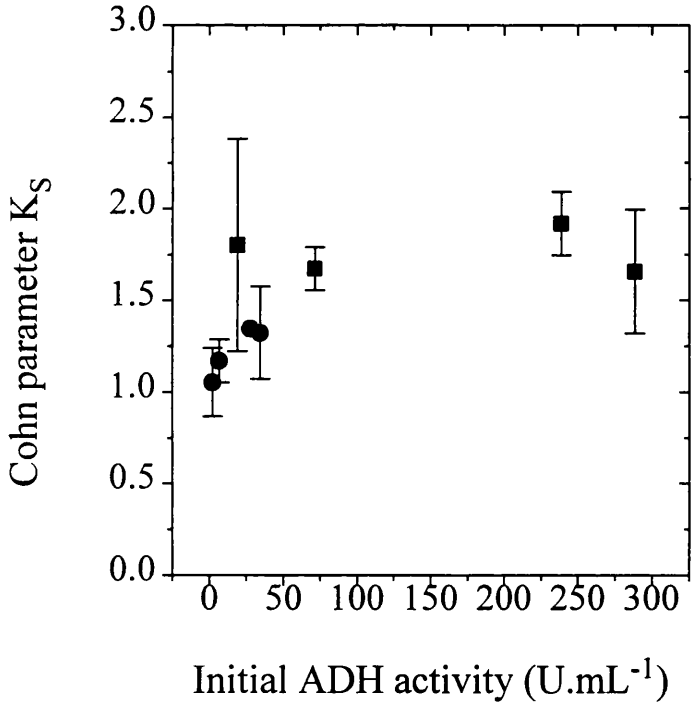

Figure 6.6: Fitted Cohn parameter K_S plotted against initial ADH activity. Experimental data: ■ packed bakers' yeast, ● fermented recombinant yeast

6.4.1.2 Fractional Precipitation

The fitted fractional solubility curves shown in Figures 6.2 and 6.3 were used in a modified version of the incremental search algorithm developed by Richardson (1987) in order to calculate the optimum cut points and the maximum purification factor at given yields for a two-cut fractionation process (refer to Section 6.3.1 and Appendix 1 for a MATLAB program listing). This enabled a comparison to be made between the protein engineered and bakers' yeast process at the typical yeast concentration of 280 g wet weight per L. In applying the incremental search algorithm it was assumed that there was complete separation of precipitate after each cut and the results therefore indicate the ideal case. The calculated optimum cut point and maximum purification factor results are shown in Figures 6.7 and 6.8 overleaf. Comparison of the calculated results for fermented recombinant yeast and packed bakers' yeast show that to achieve the same yield as that of natural ADH the optimum cut points for both stages in the protein engineered process must be increased by approximately 5% saturation (Figure 6.7). An increased level of ammonium sulphate at each stage would result in a more viscous precipitate slurry which will be more difficult to separate by centrifugation (Clarkson, 1994).

A reduction in maximum purification factor of product enzyme of up to 20% was also calculated for the protein engineered system (Figure 6.8 on page 191). The cost-effectiveness of a two-cut precipitation process for the protein engineered system is therefore expected to decrease compared to that of bakers' yeast. A process alternative that may be more economic could be to use only a single cut in which a high yield is achieved with reduced purification. For example a single cut point of 75% would achieve 95% yield and a purification factor of 1.2, while to achieve the same yield with a two stage process cut points of 43% and 75% are required and a purification factor of 1.6 is achieved. Changing to a single cut would remove two stages from the process and thereby shorten the time to process each fermentation batch. The cost-effectiveness of the single cut process could be determined by comparing the cost benefit in additional production to the extra costs incurred in making up for the 60% decrease in purification factor. Use of the results from the small scale experiments coupled to modelling techniques could therefore enable the most economic processing route to be identified for the production of *pe*-ADH.

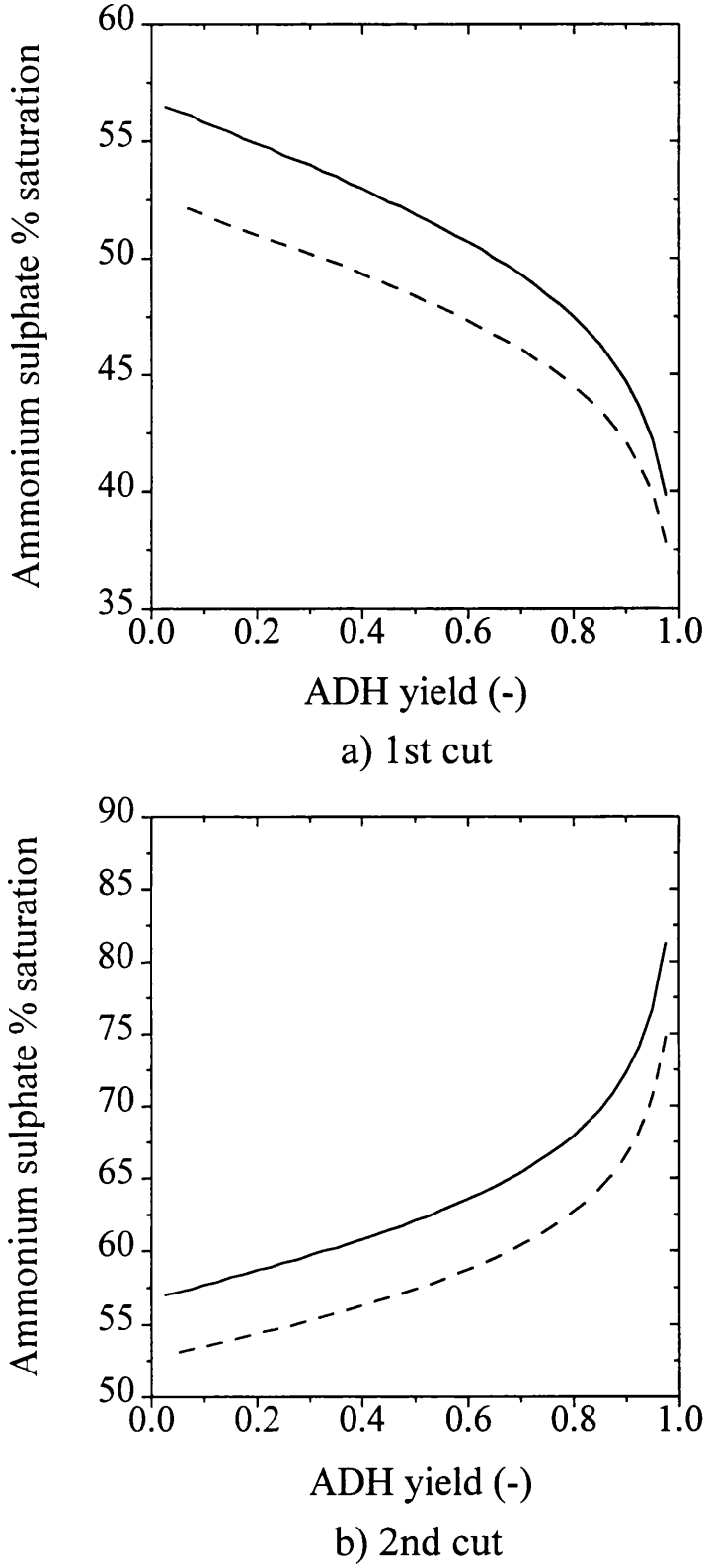

Figure 6.7: Optimum a) 1st Cut and b) 2nd Cut points at various ADH yields for a two-cut fractional precipitation. Calculated results for a yeast process concentration of 280 g.L^{-1}: (———) protein engineered process, (– – –) bakers yeast process.

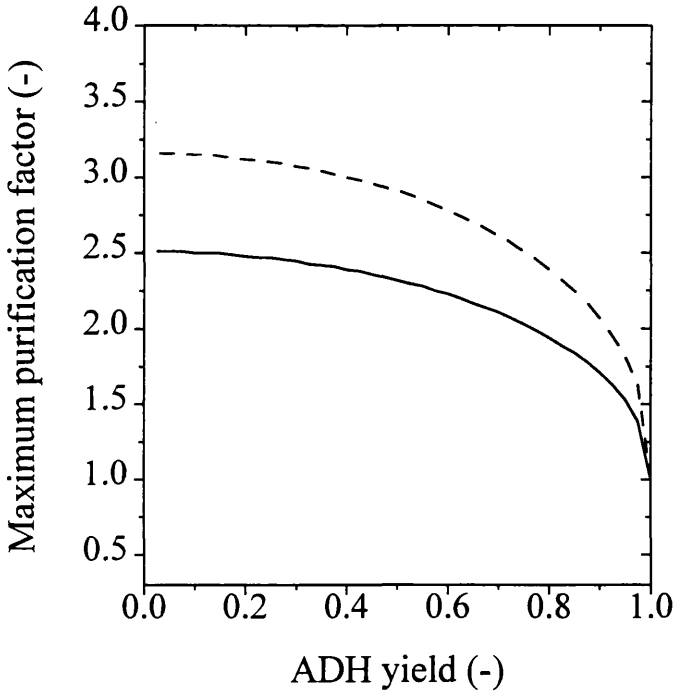

Figure 6.8: Maximum purification factor at various ADH yields for a two-cut fractional precipitation. Calculated results for a yeast process concentration of 280 g.L^{-1}: (——) protein engineered process, (– – –) bakers yeast process.

6.4.2 Modelling of the Precipitate Particle Size Distribution

The population balance model describing changes in precipitate particle size distribution (PSD) of Clarkson *et al.* (1996a) was implemented in the MATLAB programming environment (refer to Appendix 3 for a listing of the MATLAB program). Testing of the model showed that results for the growth and breakage of a log-normal precipitate PSD only agreed with those of Clarkson *et al.* (1996a) when an initial particle number of $1x10^{12}$ was used, indicating that the units for the aggregation kernel had been incorrectly reported as $\mu L.h^{-1}$ instead of $L.h^{-1}$.

Laser sizing results for the protein engineered clarified homogenate showed that two peaks were present (refer to initial PSD in Figure 6.9 on page 193). The larger peak, at approximately 0.80 μm, was thought to consist of unseparated small cell debris fragments. The smaller peak, at approximately 0.25 μm, only appeared after the debris removal stage and was also observed in packed bakers' yeast clarified homogenate. This material was therefore most likely to be small cellular components, such as lipid granules, ribosomes and mitochondria, rather than inclusion bodies from the recombinant cells.

In order to estimate the particle number for the protein engineered system on addition of the precipitate, a primary particle diameter of 0.25 μm was assumed for the 40% cut. This was based on the laser sizing of spun supernatants, which showed samples taken at the point of precipitant addition only contained material from the small peak. This indicated that the material from the larger peak was most probably less dense cellular debris. A primary precipitate particle diameter of 0.85 μm was assumed for the 60% cut, based on the mean size of the precipitate PSD on addition of precipitant (Figure 6.10 on page 194). Use of these primary particle sizes in equation 6.30 gave the initial particle number as $1x10^8$ and $1x10^7$ per μL for the 40% and 60% cuts respectively.

Values of the aggregation kernel and breakage constant for precipitate particles were taken from Clarkson *et al.* (1996a) at equivalent shear rates. At 100 s^{-1}, 44 s^{-1} and 5 s^{-1}, this gave aggregation kernels of 2.0, 0.75 and $0.5x10^{-7}$ $\mu L.h^{-1}$ and breakage rate constants of 0.6, 0.25 and 0.05 $\mu m^{-3}.h^{-1}$ respectively. The measured precipitate PSD distribution on addition of precipitant, the estimated particle number, and bakers' yeast protein precipitate model constants at equivalent shear rate were used in the population balance model for the protein engineered system, which was solved over 0.67 h using a 4th order Runge-Kutta method. The geometric mean diameter and standard deviation of peaks in the model results were calculated using the equations of Irani and Callis (1963) as per the work of Clarkson (1994).

Mean diameter and standard deviations calculated from the model results are shown and compared to experimental data from the 4.4 L vessel at shear rates of 100 s^{-1} and 5 s^{-1} in Figures 6.9 and 6.10. In all cases reasonable agreement was seen between model and experimental values. The model was able to show increases in precipitate mean particle diameter at the higher shear rate for both 40% and 60% precipitates due to an increase in the aggregation rate. The larger increases in mean diameter observed for 60% precipitate compared to that of 40% precipitate at equivalent shear rates was also shown by the model. This was due to the larger particle volumes of the 60% material, leading to bigger aggregate particles and thereby a larger increase in mean particle diameter. The results show that the dependence of the aggregation kernel and breakage constant on shear rate determined for bakers' yeast protein precipitates by Clarkson *et al.* (1996a) also applied to the protein engineered system.

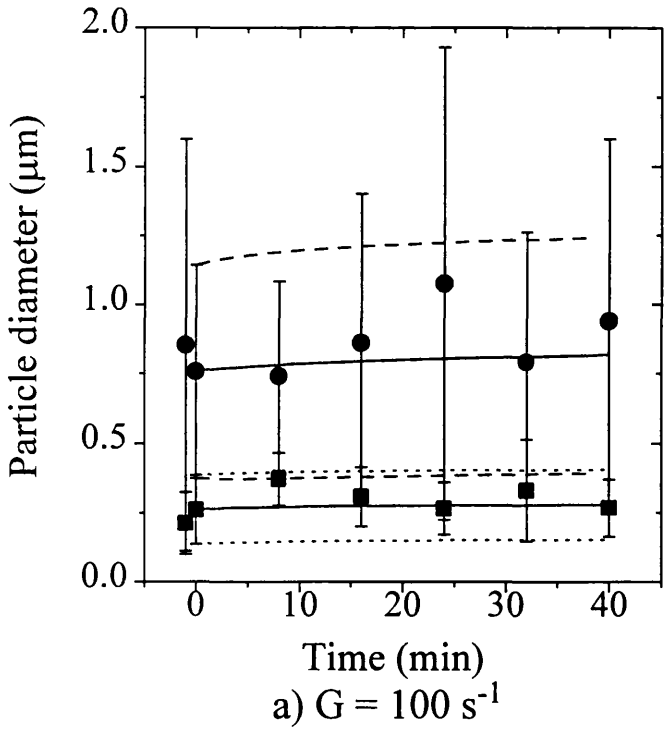

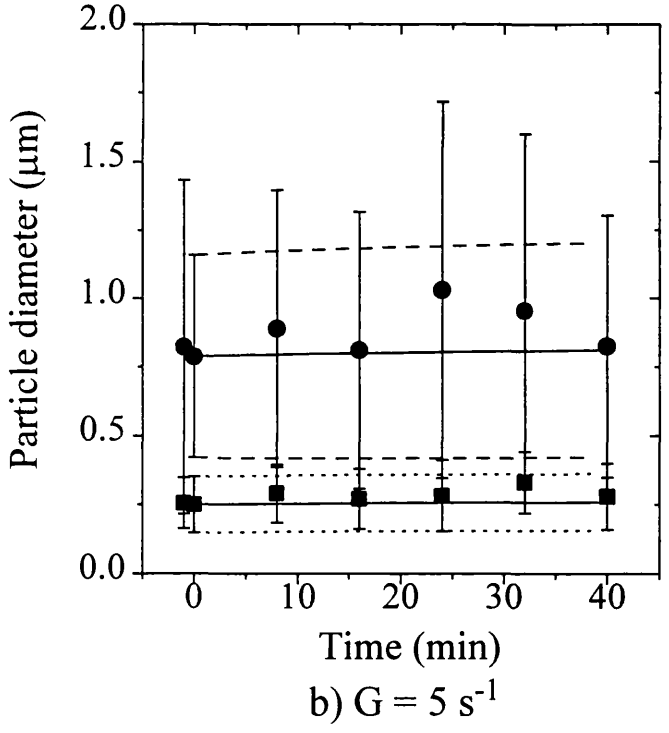

Figure 6.9: 40% cut point precipitate particle diameter plotted against time for batch ageing at a shear rate of a) 100 s^{-1} and b) 5s^{-1}. Experimental data: ● mean size in large peak, ■ mean size in small peak. Bars indicate spread of data in each peak. Model results: (——) large peak mean size, (– – –) spread of data in large peak, (——) small peak mean size, (· · · · ·) spread of data in small peak.

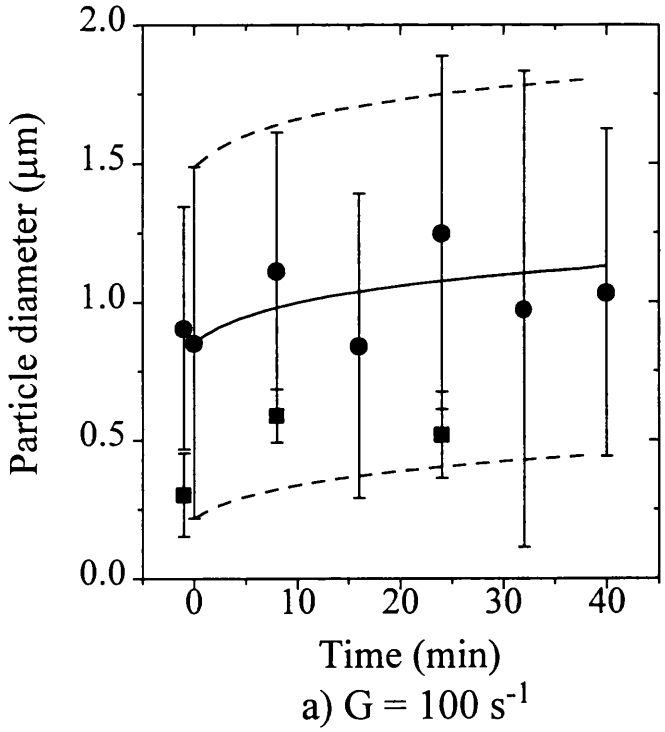

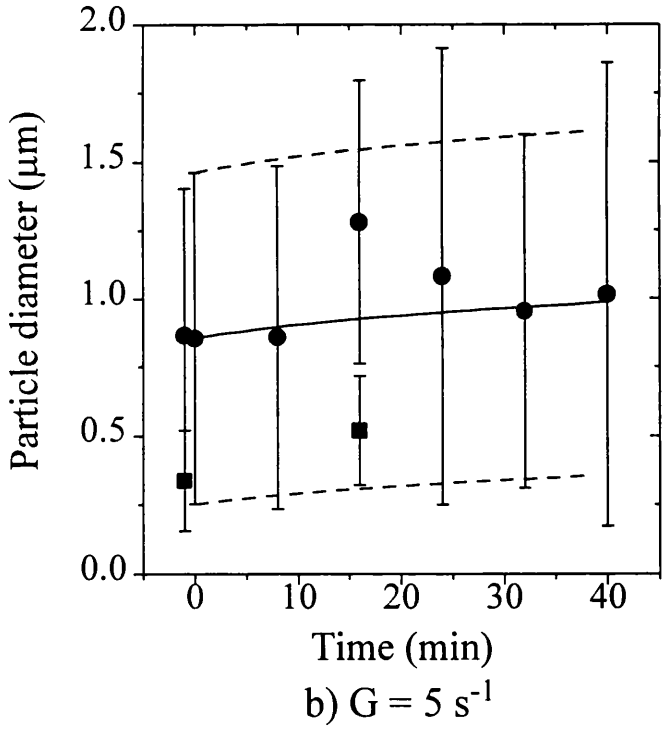

Figure 6.10: 60% cut point precipitate particle diameter plotted against batch ageing time a shear rate of a) 100 s^{-1} and b) 5s^{-1}. Experimental data: ● mean size in large peak, ■ mean size in small peak. Bars indicate spread of data in each peak. Model results: (——) mean diameter, (– – –) spread of data.

6.4.3 Precipitate Physical Properties

In order to integrate precipitation stages with precipitate removal and recovery steps it is essential that changes in relevant physical properties are characterised. For precipitate removal and recovery by disc stack centrifugation, the viscosity of the resulting precipitation liquor and the density difference between solid precipitate and liquid phases must be specified in order to model the unit operation (Clarkson, 1994).

The densities of solvated proteins have been given by Bell *et al.* (1983) as ranging from 1280 to 1366 $kg.m^{-3}$, while maximum crystalline protein densities are of the order 1350 to 1400 $kg.m^{-3}$. The presence of interstitial liquid in aggregated precipitates results in typical hydrodynamic densities of 1050 to 1250 $kg.m^{-3}$, with isoelectric point precipitates of the globular proteins ovalbumin and bovine serum mercaptalbumin having values of 1292 and 1282 (Bell *et al.*, 1983). For isoelectric soya protein precipitate and salted-out casein precipitate, the aggregate density, ρ_a, has been related to aggregate size, d, using an equation of the form (Bell *et al.*, 1982):

$$\rho_a = \rho_{sf} + kd^{-c}$$

(equation 6.31)

where ρ_{sf} is spin fluid density and k, c are constants. For a floc described by the successive random addition of particles c equals 0.676 (Lagranker and Gemmell, 1968). For isoelectric protein precipitate and salted-out casein, c equalled 0.408 and 0.441 respectively, indicating a tighter packing of the precipitate aggregate. Clarkson *et al.* (1996a) has found that for 40% and 60% salted-out protein from bakers' yeast homogenate, c equals 0.635 and 0.839 respectively, although the passage of particles through a water buffer layer during analysis may have had some effect on the density of the precipitate particles.

Experimental results for the density-size relationship of protein engineered 40% and 60% precipitate batch aged at $44s^{-1}$ for 40 min are shown in Figure 6.11 on the next page. In the case of the 40% precipitate, the large peak in the PSD gave density results that were very close to the spin fluid density. Since the large peak was thought to mostly contain debris material, it was ignored and the small peak was solely used in

determining the precipitate density-size relationship (Section 3.2.8.3). For both the 40% and 60% precipitates, the experimental data could be fitted to equation 6.31:

$$\text{40\% precipitate:} \qquad \rho_a = 1130 + 43d^{-0.314} \qquad \text{(equation 6.32)}$$

$$\text{60\% precipitate:} \qquad \rho_a = 1180 + 30d^{-0.614} \qquad \text{(equation 6.33)}$$

The value of c for the 60% precipitate fits that for successive random addition of particles to an aggregate, while the very low value of c for the 40% precipitate indicates a more tightly packed material. It is possible that the presence of dense cellular components in the 40% precipitate material may have contributed to the low value of c in this case.

Experimental values for the density of the precipitation liquor at 40% and 60% were 1120±5 and 1170±5 kg.m^{-3} respectively, while the corresponding viscosity values were 0.0021 and 0.0025 Pa.s respectively. In both cases, the results were similar to those of Richardson (1987) for the ammonium sulphate precipitation of protein from clarified bakers' yeast homogenate.

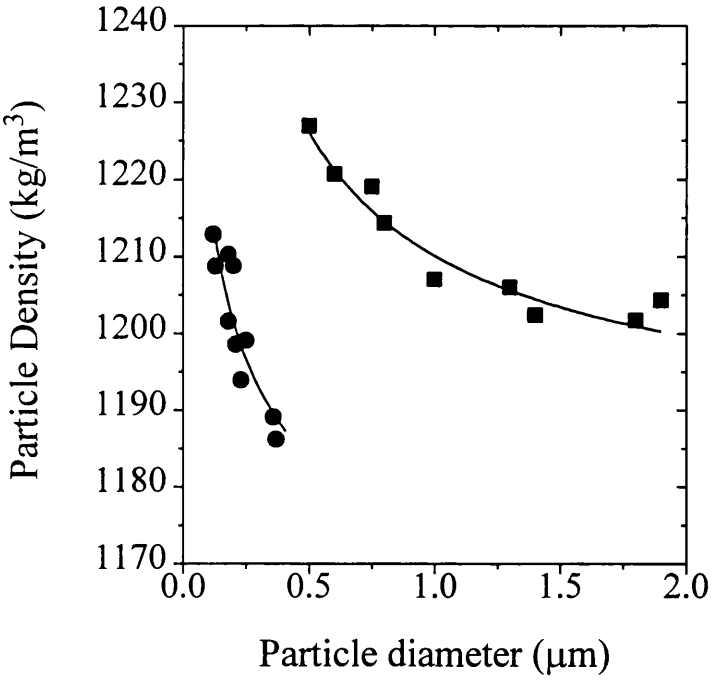

Figure 6.11: Protein engineered system precipitate particle density plotted against particle diameter. Experimental data: ● *40% cut,* ■ *60% cut. Fitted curves: (——)*

6.4.4 Scale-Up of the Solubility Models

Protein engineered ADH and total protein fractional solubilities were determined for a large pilot-scale precipitation at 40% and 60% cut points in order to test the scalability of solubility models derived from small scale data (Figure 6.12 on page 199). Assay results indicated that there was no loss of protein or denaturation of ADH during large scale batch ageing at G = 44 s^{-1} for 0.67 h. Good agreement was seen between experimental and predicted fractional solubilities of protein engineered ADH and total protein for both the 40% and 60% cut points. Some deviation between the large scale fractional solubility at the 60% cut point and that predicted could have been expected since there was no intermediate removal of precipitate at the small scale, but this was carried out during the large scale fractionation. This would have the effect of reducing the overall protein concentration and could potentially lead to a shift of the solubility profile. However, the results indicate that any shifts of this type were not significant.

Foster (1972) concluded that the solubility behaviour of protein in batch precipitations was independent of reactor volume for geometrically similar systems. Clarkson (1994) observed similar profiles for the batch ammonium sulphate precipitation of bakers' yeast protein from clarified yeast homogenate in three geometrically similar vessels of increasing size. However, although the small and medium scale vessels used in this study were geometrically similar, the large pilot-scale vessel used was not geometrically similar to the two smaller vessels. An indication of the mixing conditions in the vessels was gained by calculating the Reynolds number, $Re = \rho N_I D_I^2/\mu$, where ρ is the suspension density, μ is the density, N_I is the impeller speed and D_I is the impeller diameter, with values above 10^4 indicating fully turbulent conditions (Richardson, 1987). For the small scale vessel, the Reynolds number was 8.6×10^3 and 7.5×10^3 for the 40% and 60% saturation cuts respectively, while for the large pilot-scale vessel the Reynolds number was 4.9×10^4 and 4.3×10^4. This indicates that fully turbulent conditions were only present in the large pilot-scale vessel and the possibility of differing degrees of over-precipitation in the small and large scale vessels must therefore be considered.

Based on a model of protein precipitation incorporating the effects of over-precipitation, Iyer and Przybycien (1994) gave the most important scaling factors for matching

precipitation at different scales as the initial protein concentration and the dimensionless precipitant addition rate, $F_S/(V.k_{md})$ (Section 6.2.1.3). For the large scale precipitation, the protein concentration in the clarified homogenate was 16.7 $mg.mL^{-1}$ and was similar to a typical value of 10 $mg.mL^{-1}$ for the small scale system. Pohorecki and Baldyga (1983) have shown that the micromixing rate, k_{md}, in a stirred tank is proportional to the power dissipation per unit volume, e, and the Schmidt number, $Sc = \nu/D_f$, where ν is the kinematic viscosity and D_f the diffusivity. Since the shear rate was maintained at both scales (at $G = 44s^{-1}$) and physical properties were similar in both vessels, the values of e and Sc, and thereby the micromixing rate, were approximately the same in the large and small scale vessels. In order to match the small scale dimensionless addition rate, it was therefore only necessary to scale the precipitant feed rate for the large pilot-scale vessel. The required feed-rate was calculated to be approximately 0.8 $L.s^{-1}$. During large-scale downstream processing, the ammonium sulphate precipitant was added to the precipitation vessel by pouring the required volume rapidly into the centre of the vessel at a typical rate of 30 L in 40 s, i.e. approximately 0.75 $L.s^{-1}$. The required value for matching of the dimensionless addition rate was therefore comparable to the actual precipitant feed rate for the large pilot-scale vessel.

The scalability of solubility models can thereby be attributed to maintaining the scale factors proposed by Iyer and Przybycien (1994) of initial protein concentration and the dimensionless precipitant addition rate. It is recognised that the scalability of the precipitation results might also be due to mixing conditions having little affect on protein solubility and the absence of any over-precipitation. However, this is less likely considering the observations of Foster (1972), Richardson (1987) and Iyer and Przybycien (1994) that different mixing conditions give changes in protein solubility behaviour.

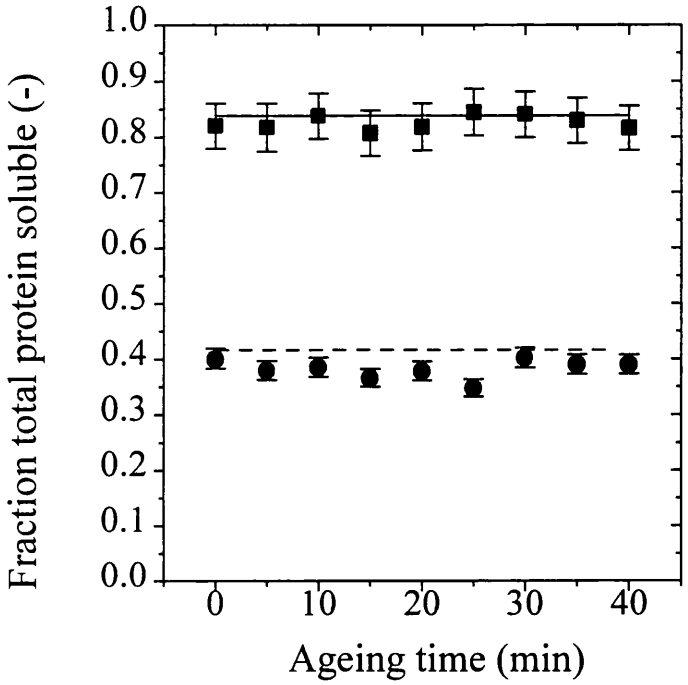

a) Total protein fractional solubility

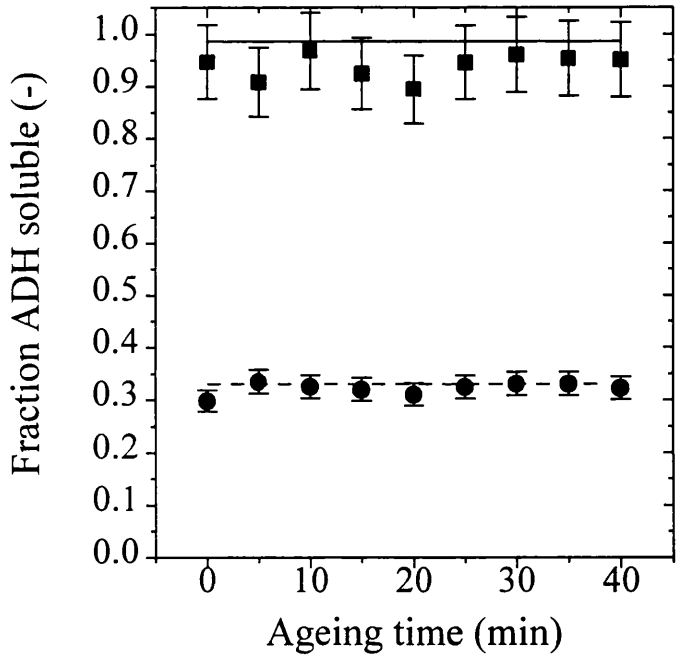

b) ADH fractional solubility

Figure 6.12: Large scale protein engineered system fractional solubility of a) total protein and b) ADH for each cut point over the batch ageing period. Experimental data from the large pilot scale: ■ 40% cut, ● 60% cut. Model prediction based on small scale results: (——) 40% cut, (– – –) 60% cut.

6.5 Conclusions

The solubility behaviour of protein engineered ADH and total protein during ammonium sulphate precipitation was characterised using a small scale system. The addition of high levels of polypropylene glycol antifoam at the fermentation stage was found to distort enzyme product and total protein solubility profiles in subsequent precipitations, possibly due to a reduction in surface tension. The distortion was removed by reducing the concentration of antifoam used or by the inclusion of a wash stage after cell harvest. The results highlight the importance of identifying interactions between the fermentation stage and downstream operations in order to ensure product recovery.

The fractional solubility of both the protein engineered ADH and total protein was found to increase compared to that of bakers' yeast ADH and total protein processed at an equivalent yeast concentration. A low protein concentration in the protein engineered homogenate compared to that for bakers' yeast was identified as the major factor in the shifting of total protein solubility behaviour. The observed changes in ADH solubility profiles did not match those predicted from changes in hydrophobicity between natural and protein engineered ADH. Differences in ADH specific activity or isozymes present in the two systems may have contributed to the observed shifts in ADH solubility. The results highlight the complex precipitation behaviour of protein mixtures.

Results for a two-cut fractional precipitation procedure calculated using solubility models derived from the small scale data showed a 5% saturation increase in the optimal ammonium sulphate saturation for each cut point and a 20% reduction in the maximum purification factor for the protein engineered process compared to that for bakers' yeast ADH at a given yield. The cost-effectiveness of a two cut precipitation for concentration and fractionation of the protein engineered ADH is therefore expected to decrease compared to that for natural bakers' yeast ADH.

The use of a population balance model to describe changes in precipitate particle size distribution for 40% and 60% cut points at various shear rates gave good agreement

with experimental results from the medium scale, and indicated that aggregation and breakage constants derived for bakers' yeast protein precipitate also applied to the protein engineered system. Solubility models derived from the small scale data were found to predict the large pilot scale fractional solubility of protein engineered ADH and total protein at 40% and 60% cut points. The scalability of models was attributed to maintaining the scale factors of protein concentration and dimensionless precipitant addition rate from the small to the large scale. Analysis of physical properties which affect precipitate separation by centrifugation for precipitated material from 40% and 60% cut points gave similar results to that of bakers' yeast homogenate.

The results show that the use of computer modelling techniques in conjunction with data from well defined experimental systems enabled the impact of protein engineering on a fractional precipitation process to be determined.

7.0 MODELLING OF DISC STACK CENTRIFUGATION

7.1 Introduction

A number of disc stack centrifugation stages were present in the downstream process for the recovery of protein engineered alcohol dehydrogenase (*pe*-ADH) from fermented recombinant yeast cells. These included recombinant cell recovery from the fermentation broth, cell washing to reduce the carry-over of contaminants from the fermentation stage, the removal of cell debris after homogenisation and the separation of protein precipitate aggregates (refer to Section 1.2.2 for a description of the typical enzyme recovery process). This chapter explores the modelling of these disc stack centrifugation stages, based on the commonly used Sigma theory. A grade efficiency approach was applied to describe steady state particle separation, while a time-step mass balance model was developed to give a more accurate simulation of the overall separation.

Characterisation experiments were performed for whole cells and cell debris to show that the particles were shear-insensitive and to determine a suitable grade efficiency function (refer to Section 3.4.3 for method). In the case of cell debris, techniques were employed to reduce the volumes of sample material required for these experiments. Predictions for steady state and overall recovery performance were then made based on measured feed properties, with verification carried out at the full pilot-scale. In the case of shear sensitive precipitate separation, particle recovery was predicted using a model which described changes in mean diameter over the centrifuge feed-zone, thereby enabling a shear-insensitive grade efficiency function to be applied. Experiments were performed at the large and small pilot-scale to test the model predictions and determine the success of small-scale operations in mimicking the separation achieved with a full pilot scale disc stack centrifuge (refer to Section 3.4.3 for method).

In Section 7.2 Sigma theory and the grade efficiency approach to centrifuge modelling are described, along with methods of accounting for hindered settling and particle breakage in the centrifuge feed-zone. The application of these models to the recombinant process is then outlined in Section 7.3, with a description of the time-step

mass balance model also being given. The utilisation of a scaled-down disc stack is also described in Section 7.4. Results of the study are presented and discussed in Section 7.5, with conclusions given in Section 7.6.

7.2 Existing Models for Disc Stack Centrifugation

A number of different approaches have been developed to describe particle separation in a disc stack centrifuge (Ambler, 1952; Sullivan and Eriksson, 1961; Gupta, 1981). In this study the commonly applied Sigma theory or settling area method, which is based on Stoke's law, has been used in conjunction with the grade efficiency concept and these are described below.

7.2.1 Theory of Centrifugal Sedimentation

The description of particle sedimentation in a centrifugal field is generally based on Stokes' law, which assumes small, inert spheres, laminar flow conditions and dilute particulate dispersions. Although these conditions are rarely met in practice, Stokes' law still provides a surprisingly useful model of the process of centrifugal sedimentation.

For a particle in a centrifugal field, the change in velocity vector, or centrifugal acceleration, is given by $\omega^2 r$ and the centrifugal force is $m\omega^2 r$, where ω is the rotational speed, m the particle mass and r is the radial position with respect to the center of rotation. For a particle in a fluid, the centrifugal force is opposed by the particle buoyancy, due to the mass of fluid displaced, and a frictional drag force, which is proportional to the radial velocity. Application of Newton's law of motion, i.e. that mass times acceleration is equal to the sum of the forces (which assumes laminar flow), and use of the assumption that the particles are spherical gives the Stoke's law relationship for the centrifugal sedimentation velocity v_z:

$$v_z = \frac{(\rho_p - \rho_f) d^2 \omega^2 r}{18\mu}$$

(equation 7.1)

where ρ_p is the particle density, ρ_f is the suspension density, d is the particle diameter and μ is the suspension viscosity. A similar analysis for a particle settling under gravity gives the Stoke's law relationship for the gravitational sedimentation velocity v_g as:

$$v_g = \frac{(\rho_a - \rho_f)d^2 g}{18\mu}$$

(equation 7.2)

were g is the gravitational acceleration constant. From equations 7.1 and 7.2 it can be shown that the sedimentation velocity, v_z, of a particle settling in a centrifugal field is related to the gravitational sedimentation velocity, v_g, by:

$$v_z = v_g \frac{\omega^2 r}{g}$$

(equation 7.3)

The ratio v_z/v_g is known as the relative centrifugal force or g-number. This parameter is often used to characterise centrifuges but cannot be used to estimate centrifuge capacity (Axelsson, 1985).

7.2.2 The Sigma Concept

Sigma theory is based on the comparison of the settling area of a centrifuge, calculated on the basis of the centrifuge geometry and rotational speed, to the settling area of a gravity settling tank capable of equivalent separation performance to that of the centrifuge. The derived equivalent settling area is known as the sigma factor, Σ, and has the units m^2. The sigma factor is often used as a scale-up parameter for centrifuges since the ratio Q/Σ will be constant under ideal conditions for two centrifuges with the same separation performance (Ambler, 1952).

In the derivation of the sigma factor for a disc stack centrifuge given below, there are a number of assumptions (Mannweiler, 1989). Assumptions concerning the feed material are:

- Particles are spherical and do not aggregate or deaggregate during passage through the disc stack.

- The particles are evenly distributed in the continuous liquid phase and their concentration is low enough to exclude inter-particle interference, known as hindered settling.

- The settling velocity of the particles in the centrifugal field can be described by Stoke's law, i.e. the Reynolds number is less than 0.4.

Assumptions concerning the liquid flow in the centrifuge are:

- Laminar flow occurs at all points in the disc space.

- The continuous liquid phase divides evenly between all the disc spaces.

- Particle separation is irreversible, i.e. separated particles do not re-enter the liquid phase due to back mixing.

- The velocity profile is symmetrical normal to the disc surface.

- The flow lines of the continuous liquid phase are directed radially and no tangential flow occurs.

Since the total flow, Q, is assumed to divide evenly between all the discs, the flow through the space between adjacent discs is q=Q/z, where z is the number of discs. The flow of liquid is also assumed to be in the radial plane and therefore has the same angular velocity as the disc stack. Under these conditions, the single passage throughput q is related to the meridian fluid velocity, v(h), by:

$$q = \int_0^h 2\pi r\, v(h)\, dh$$

(equation 7.4)

where r represents the radial position in the disc space and h is the gap width.

To describe the separation performance of the centrifuge, the gravitational sedimentation velocity of particles which are "just separated" from the liquid phase is considered. Particles that are "just separated" are those that start at the upper surface of the lower of the two discs defining the disc space at the outer disc radius R_o and reach the lower surface of the upper of the two discs before the liquid leaves the disc space at the inner radius R_i (Figure 7.1).

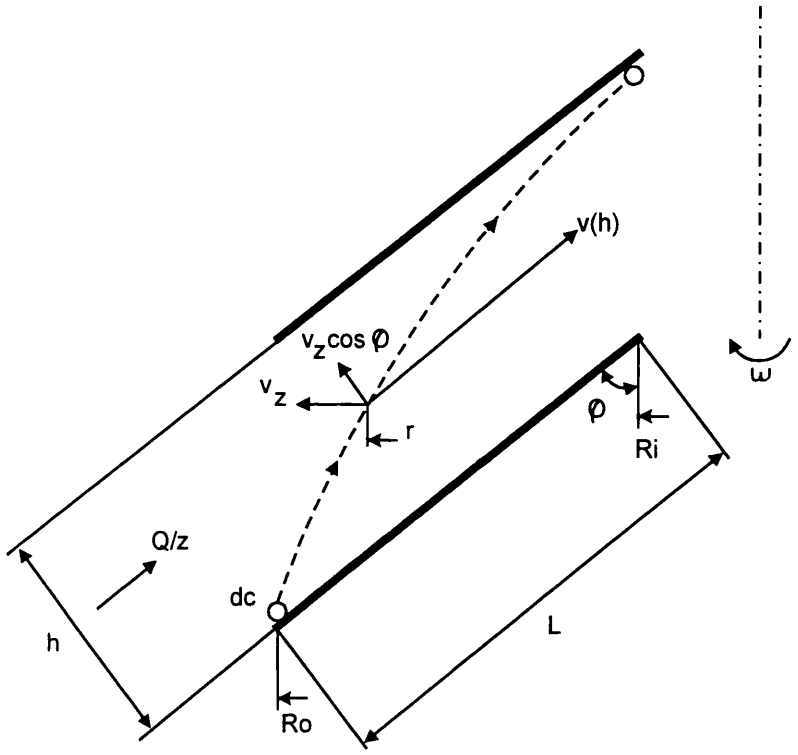

Figure 7.1: Flow through the disc space of a disc stack centrifuge, from Mannweiler (1989).

The flow velocity as a function of the radius of rotation is given by:

$$v(h) = \frac{1}{2\pi r}\frac{dq}{dh}$$

(equation 7.5)

The particle trajectory in the disc space is given by the radial particle settling velocity, v_z:

$$v_z = \frac{dr}{dt} = \frac{dh}{dt\cos\varphi}$$

(equation 7.6)

where φ is the upper disc angle as shown in Figure 7.1. The particle velocity, v_p, parallel to the disc surface is approximately equal to the velocity of the continuous liquid phase, v(h):

$$v_p \approx v(h) = \frac{dL}{dt} = \frac{dr}{dt \sin \varphi}$$

(equation 7.7)

Rearranging equations 7.6 and 7.7 in terms of dt and equating gives the "differential quotient" of the particle trajectory:

$$dr = \frac{v(h)}{v_z} \tan\varphi \, dh$$

(equation 7.8)

Substituting equation 7.5 for v(h) and equation 7.3 for v_z in equation 7.8, rearranging and integrating between R_o and R_i gives:

$$q = v_g \frac{2\pi\omega^2}{3g \tan\varphi}(R_o^3 - R_i^3)$$

(equation 7.9)

Substituting Q/z for q and adding a correction factor, f_L, for the presence of rib spacers gives the equation for a disc-stack centrifuge containing z discs:

$$Q = v_g \frac{2\pi\omega^2 z}{3g \tan\varphi}(R_o^3 - R_i^3) f_L$$

(equation 7.10)

where f_L is given by (Mannweiler, 1989):

$$f_L = 1 - \frac{3 z_L b_L}{4\pi R_o} \frac{1-(R_i/R_o)^2}{1-(R_i/R_o)^3}$$

(equation 7.11)

where z_L is the number of spacer ribs on a single disc and b_L is their width. If point spacers are used rather than rib spacers then f_L=1. In equation 7.10 the first term on the right hand side, v_g, describes the settling characteristics of the particles while the other terms describe the geometric and mechanical features of the disc stack. The equation can therefore be rewritten as:

$$Q = v_g \Sigma$$

(equation 7.12)

where Σ is given by:

$$\Sigma = \frac{2\pi\omega^2 z}{3g\tan\varphi}(R_a^3 - R_i^3)f_L$$

(equation 7.13)

Defining a specific throughput capacity $q_s=Q/\Sigma$ and comparing this to equation 7.12 shows that all particles with a gravitational settling velocity $v_g \geq q_s$ will be removed from the continuous liquid phase:

$$q_s = v_{g,c} = \frac{Q}{\Sigma} = \frac{d_c^2(\rho_a - \rho_f)g}{18\mu}$$

(equation 7.14)

Only particles with a gravitational settling velocity equal to or greater than the critical velocity $v_{g,c}$ will be certain to sediment. The corresponding separation limit or critical particle diameter, d_c, is given by solving equation 7.14 for particle diameter:

$$d_c = \sqrt{\frac{18Q\mu}{(\rho_a - \rho_f)\Sigma g}}$$

(equation 7.15)

Equation 7.15 indicates that only particles with a diameter greater than or equal to d_c are certain to be recovered in the disc-stack. However, d_c is not an absolute cut-off point. Because particles are evenly distributed across the entrance to the disc space, particles with diameter smaller than d_c that start at a position above the upper surface of the lower of the two discs defining the disc space may also be recovered. The probability of recovery for particles with a diameter less than d_c is given by the grade efficiency, which is described in the next section.

7.2.3 The Grade Efficiency Concept

The grade efficiency, T(d), is the fraction of solids of particle size d recovered by the centrifuge. For a single particle the grade efficiency is either 1 or 0, while for two particles of the same size it may be 1, 0.5 or 0. The grade efficiency can be seen as a probability term since, as indicated in Section 7.2.2, different particles of the same size are subject to different positions when entering the disc space. The grade efficiency will increase with the gravitational settling velocity, v_g, until v_g equals the specific throughput capacity ($v_g=v_{g,c}=q_s$). For particles with $v_g>v_{g,c}$, the grade efficiency has a value of 1. For ideal flow and settling conditions within a centrifuge, T(d) can be

described as a function of d/d_c, the normalised particle diameter (Figure 7.2 on page 210):

$$T(d) = \left(\frac{d}{d_c}\right)^2 \qquad \frac{d}{d_c} < 1$$

(equation 7.16a)

$$T(d) = 1 \qquad \frac{d}{d_c} \geq 1$$

(equation 7.16b)

The square relationship in equation 7.16a is due to the form of equations 7.2 and 7.14. In a real centrifuge, however, deviations from this ideal case occur. The main reasons for the deviations are that (Mannweiler, 1989):

- Flow through the disc spacing is not necessarily laminar over the whole gap width and radius.

- Particle sedimentation is not irreversible, i.e. back-mixing of settled solids into the carrier liquid may occur.

- There may be unsymmetrical loading at the entrance to the disc and uneven velocity profiles within the disc spacing.

- At high solids concentrations hindered settling of particles will occur. This is discussed in Section 7.2.4.

The reader is referred to Sokolow (1971), Brunner and Molerus (1979), and Bohman (1974) for descriptions of the hydrodynamics of fluid flow within the disc stack, with a good review of work in this area given by Mannweiler (1989). In order to describe the separation of shear insensitive polyvinylacetate (PVA) particles in a disc stack centrifuge Mannweiler (1989) employed a Rosin-Rammler-Sperling-Bennett (RRSB) distribution (Figure 7.2 overleaf):

$$T(d) = 1 - \exp\left[-k\left(\frac{d}{d_c}\right)^n\right]$$

(equation 7.17)

where k and n are constants and equal 0.865 and 2.08 respectively. Good agreement was observed between model results and experimental data for dilute suspensions. The deviation from ideal theory meant that full particle recovery was not achieved until $d/d_c>2.5$.

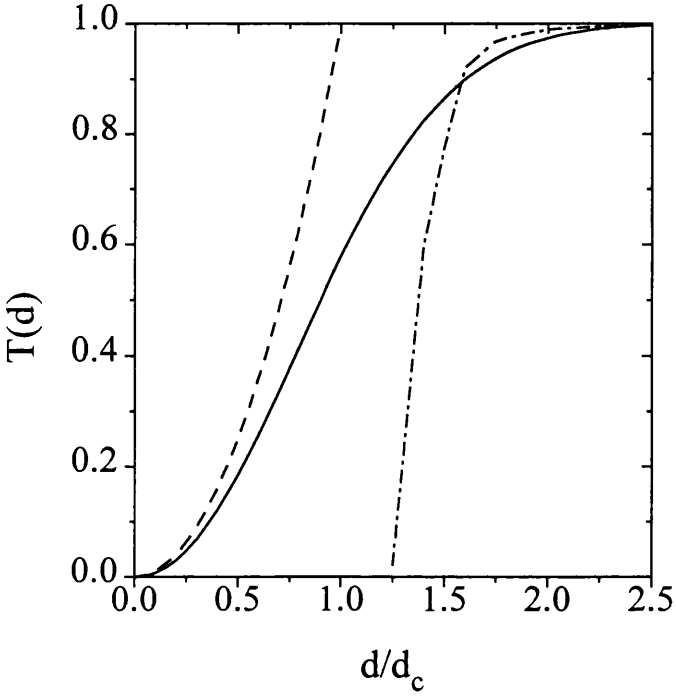

Figure 7.2: Typical grade efficiencies for disc stack centrifugation. (- - - -) Stokes' Law, (——) RRSB fuction, (- · - · -) shear sensitive precipitate data from Mannweiler (1989).

Once the grade efficiency function is defined, the recovery efficiency (alternatively known as the mass yield) of disc stack centrifugation, E_t, can be calculated using the equation:

$$E_t = \frac{\sum_{d_1}^{d_2} T(d) * \Delta M_F(d)}{\sum_{d_1}^{d_2} \Delta M_F(d)}$$

(equation 7.18)

where d_1, d_2 define the particle size range for the material and $\Delta M_F(d)$ is the particle size distribution (PSD) of the feed material on a mass basis.

7.2.4 Accounting for Hindered Settling

A reduction in separation performance in a disc stack centrifuge is seen with concentrated suspensions due to the presence of hindered settling. This occurs at a

solids concentration of more than approximately 2% (v/v) when the mean distance between two particles, L_m, is such that the boundary flow layers overlap (Figure 7.3) and flow of displaced liquid is created in the direction opposite to that of the settling particle (Mannweiler, 1989). This means that particles settle in an upward flowing fluid, resulting in a decrease in settling velocity. The magnitude of this effect will increase as the solids concentration in the suspension increases.

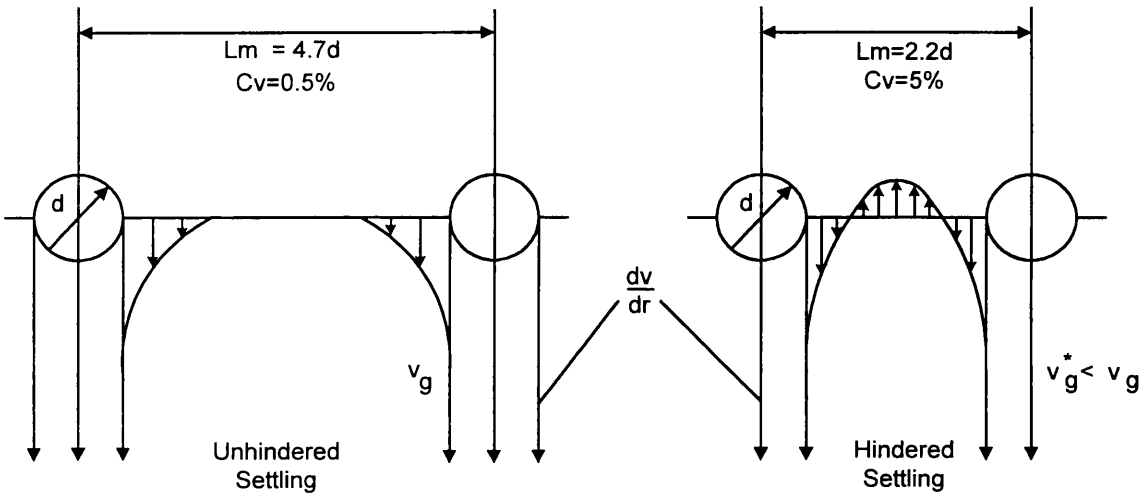

Figure 7.3: Sedimentation of spherical particles, from Mannweiler (1989).

Richardson and Zaki (1954) developed an empirical relationship for the reduced terminal settling velocity of a particle, v_g^*, as a function of volumetric solids concentration, C_v, and a geometric shape factor, σ, which equals 4.6 for spherical particles:

$$v_g^* = v_g(1-C_v)^{\sigma}$$

(equation 7.19)

Equation 7.19 can be used to correct the critical diameter given by equation 7.15 for decreases in separation efficiency due to hindered settling:

$$d_c = \sqrt{\frac{18Q\mu}{(\rho_a-\rho_f)(1-C_v)^{\sigma}\Sigma g}}$$

(equation 7.20)

Using equation 7.20 to calculate d_c makes the grade efficiency curve independent of feed concentration. Clarkson *et al.* (1996b) found that application of the Richardson and Zaki (1954) correction to the critical diameter resulted in a conservative under-

estimate of steady state recovery efficiency for bakers' yeast whole cells and cell debris, which is more desirable than over-prediction for design purposes.

7.2.5 Breakage of Biological Particles

Biological particles such as precipitates are sensitive to shear which can cause them to break into smaller fragments or primary particles and lead to significant losses in centrifugation separation efficiency. Mannweiler (1989) reported that experimental grade efficiencies for soya protein precipitate did not match that of shear insensitive PVA particles given by equation 7.17, but were consistent with the disappearance of larger particles due to breakage and the appearance of smaller particles which were not separated (Figure 7.2). Shear-induced particle breakage has been shown to occur in high-shear regions of centrifuges, such as feed-zones and centripetal pumps (Bell and Brunner, 1983). Mannweiler (1989) concluded that the mechanism of particle breakup in the feed zone of a disc stack centrifuge was a combination of turbulence and collision of particles with the rotating distributor ribs. Research in this area has led to the design of full-hermetic and hydro-hermetic feed zones in which the centrifuge bowl is filled to the center with liquid in order to avoid liquid-air interfaces and to feed particles into the bowl under less severe shear conditions. The work of Mannweiler (1989) showed that breakage of soya protein precipitate was lowest in a full-hermetic feed zone.

The modelling of shear-induced breakage of precipitates was described in Section 6.2.3.3. In the case of disc stack centrifugation, modelling of the separation of shear sensitive material involves determining the sheared particle size distribution (PSD) entering the disc stack so that a shear insensitive grade efficiency relationship can be applied. Mannweiler (1989) used both a directly derived expression for the sheared PSD and an inversion algorithm to back calculate the sheared PSD. The directly derived expression was found to be unsuitable due to its high sensitivity to small errors in the measured supernatant PSD. The inversion algorithm was more successful, but assumed that the sheared PSD could be characterised by a log-normal distribution and that the geometric standard deviation of the sheared PSD was known. Use of the inversion algorithm showed a 44% reduction in the mean size of the soya precipitate due to breakage in the feed zone.

Clarkson *et al.* (1996b) developed a separate 'centrifuge feed-zone' model to determine the sheared PSD and thus give a description of the recovery of salted-out bakers' yeast protein precipitate by disc-stack centrifugation. Log-normal distributions are used for the feed and sheared PSD, with the assumption of constant standard deviation, i.e. $\sigma_m=\sigma_{m(s)}$. The mean size of the feed PSD, d_m, is transformed into the mean size of the sheared PSD, $d_{m(s)}$, using the equation:

$$d_{m(s)} = d_m - \Delta d_m$$

(equation 7.21)

where the change in mean size due to breakage, Δd_m, is a function of flowrate:

$$\Delta d_m = \frac{A_B}{Q}$$

(equation 7.22)

where A_B is the feed-zone breakage rate constant and is directly proportional to the flowrate, Q. This means that Δd_m is actually independent of flowrate, but by forming the relation for A_B in this manner the idea that breakage is both dependent on shear rate (and hence proportional to flowrate) and dependent on exposure time to the shear (and hence inversely proportional to flowrate) is reflected. The sheared PSD is then reconstructed using $d_{m(s)}$ and $\sigma_{m(s)}$ and a shear-insensitive grade efficiency curve applied to calculate the separation efficiency. Model results were within 10% of experimental values determined at the pilot-scale of operation.

7.3 Implementation of Models for Disc Stack Centrifugation

In order to model the disc stack centrifugation of recombinant yeast whole cells, cell debris and precipitate, experimental values of the critical diameter, $d_{c,exp}$, were first calculated for defined centrifugation conditions using experimentally determined physical property values, i.e. of μ, ρ_a, ρ_f and C_v. In all cases the particles were assumed to be spherical. The grade efficiency function for shear-insensitive PVA particles separated using the centrifuge in this study had previously been shown to match equation 7.17 by Rumpus (1997) and Maybury *et al.* (1997). In the case of whole cells and cell debris, centrifugation trials were therefore carried out to give steady state, experimental grade efficiencies and enable comparison to the PVA curve in order to

check that the material was not shear sensitive. Due to the high cost of producing large volumes of recombinant cell debris material, experimental grade efficiencies were determined for debris using feed material diluted to 1% (w/v). To ensure that breakage of cell debris was not dependent on particle concentration, experimental grade efficiencies were also determined using a scaled-down disc stack (Section 7.4) with feed material homogenised at the full process concentration of 28% (w/v) wet weight yeast. Use of these methods reduced the need for recombinant homogenate such that grade efficiencies could be determined from a 30 L fermentation batch.

In the case of precipitate material, experimental grade efficiencies could not be determined as the laser sizing method used only gave the particle size distribution in percentage terms. The precipitate aggregates were assumed to be shear-sensitive and the 'centrifuge feed-zone' model of Clarkson *et al.* (1996b) was used to determine the log-normal mean size of sheared material entering the feed zone. The shear-insensitive grade efficiency function (equation 7.17) could then be applied. Full precipitate breakage to primary particles and no precipitate breakage were also considered.

In all cases, steady state grade efficiencies at the full process concentration were then predicted by using $d_{c,exp}$ in equation 7.17 and the steady state recovery efficiency was calculated using equation 7.18.

One disadvantage of the grade efficiency approach is that changes in solids overflow due to solids discharging and solids breakthrough once the solids holding space is full are not described. This means that an accurate description of solid separation is only obtained under steady state conditions. The overall separation efficiency and the concentration of discharged solids will also depend on the type of discharges employed, the time between discharges, the feed concentration, the size of the solids holding space and the total bowl volume (Zhou *et al.*, 1997). A time-step mass balance model was therefore developed to give a more accurate description of the overall separation. Figure 7.4 overleaf shows an outline of the solids mass balance over each time step. The use of differential equations was avoided in the model due to the presence of a discontinuity as the feed pump was stopped during discharging.

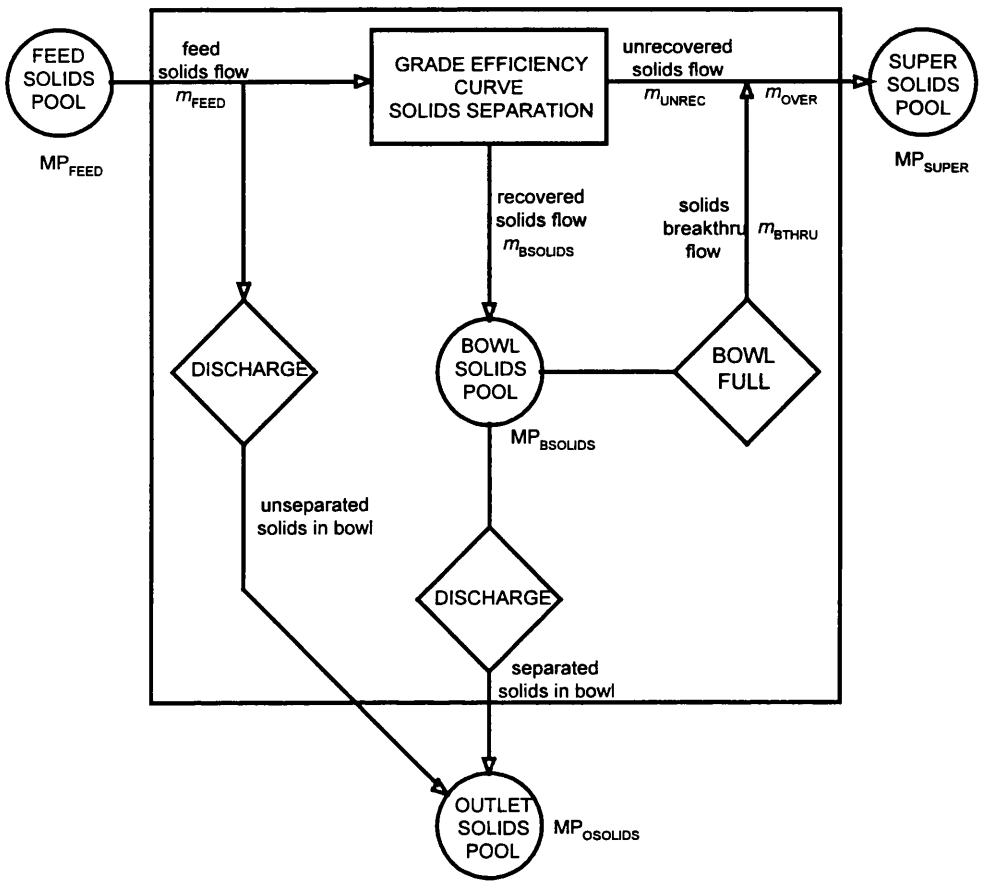

Figure 7.4: Schematic of solid mass balance over the disc stack centrifuge for each time step.

Within the model, the mass of particles recovered in the disc-stack over a small time interval, Δt, and entering the solids holding space, $m_{BSOLIDS}$, was calculated using the predicted, steady state grade efficiency curve, $T(d)_{pred,ss}$ as:

$$m_{BSOLIDS} = \sum_{d_2}^{d_1} T(d)_{pred,ss} * \Delta M_F(d)$$

(equation 7.23)

The mass of unrecovered solids in the supernatant, m_{UNREC}, was then:

$$m_{UNREC} = \sum_{d_2}^{d_1} (1 - T(d)_{pred,ss}) * \Delta M_F(d)$$

(equation 7.24)

The mass of recovered and unrecovered solids over each interval was then added to a bowl solid pool, MP_{BSOLID}, and supernatant solid pool, MP_{SUPER}, respectively. For each time interval, the bowl solid pool was compared to the bowl solids holding volume to determine if the solid holding capacity was exceeded. If this occurred any excess solids overflowed into the supernatant solids pool, with the mass of overflowing solids given by m_{BTHRU}. If a discharge occurred the overall mass of sedimented solids in the bowl solids pool was emptied into an outlet solids pool, $MP_{OSOLIDS}$, and a fraction of unseparated solids in the bowl, set from 0 to 1 depending on the type of discharge, was added to the outlet solids pool.

The recovery efficiency over each time step, $E_{t,ts}$, was then determined from the total mass of solids overflowing into the supernatant pool, m_{OVER} (which equalled $m_{UNREC}+m_{BTHRU}$) and the mass of feed solids entering the centrifuge over the same time interval, m_{FEED}, using:

$$E_{t,ts} = 1 - \frac{m_{OVER}}{m_{FEED}}$$

(equation 7.25)

The overall recovery efficiency of the disc-stack centrifuge, $E_{t,o}$, was then determined at the end of the simulation from the final mass of solids in the supernatant pool, MP_{SUPERf}, and the initial mass of solids in the feed pool, MP_{FEEDi}, using:

$$E_{t,o} = 1 - \frac{MP_{SUPERf}}{MP_{FEEDi}}$$

(equation 7.26)

An overall liquid balance was also calculated to determine the concentration of solids and soluble components in the supernatant and discharged solid streams. This enabled the yield of soluble components to be determined, assuming that no degradation of soluble protein or enzyme inactivation occurred (refer to Appendix 3 for a full MATLAB program listing of the time-step mass balance model).

7.4 Utilisation of a Scaled-Down Disc Stack

Mannweiler (1989) showed that it is possible to scale-down the disc stack area and solids holding space of a centrifuge so that equivalent performance is obtained but less feed material is required. This is achieved by operating the centrifuge with a reduced number of active discs and a lower feed flowrate. Ideally, as long as the ratio of flowrate to separation area (Q/Σ) is held constant the separation performance of the scaled down and full scale centrifuges is equivalent (Ambler, 1952). However, careful consideration of the positioning of the active discs is required as this may alter the flow pattern, and hence the grade efficiency relationship, obtained in the scaled down centrifuge (Mannweiler, 1989). Recent work by Maybury *et al.* (1997) has shown equivalent grade efficiency curves and separation efficiencies for the recovery of PVA particles, bakers' yeast cells and cell debris using a full disc stack and a scaled-down disc stack of only 9 active discs. The scaled-down disc stack was positioned above the turbulent region at the bottom of the bowl where feed streams enter using a bottom insert. The same scale-down system as described by Maybury *et al.* (1997) was used in this study.

7.5 Results and Discussion

7.5.1 Feed Stream Properties and Calculated Critical Diameter

Physical property results for the centrifuge feed streams used in subsequent model calculations are given in Table 7.1 overleaf. A 170% increase in viscosity and a 20% decrease in solid-liquid density difference was observed between the recombinant feed material to the wash and debris removal centrifugation stages, giving a 23% increase in critical diameter. The increase in viscosity was thought to be due to the release of nucleic acids, glycans and other cellular components from the disrupted cells during high pressure homogenisation (Mosqueira *et al.*, 1981), while the decrease in density occurred due to the release of cellular material which were more dense than the remaining cellular debris (Section 5.4.1.4). Recovery efficiencies calculated based on the shear-insensitive grade efficiency function given by equation 7.17 using both bakers' yeast and recombinant properties for various Q/Σ values are shown in Figure 7.5 on

page 219. Only minor differences were observed between results for whole cells, but greater deviation was seen between the results for debris. The main contributing factor in the case of debris was that the solid-liquid density difference for the recombinant process was double that for the packed bakers' yeast process, most likely due to a lower degree of cell disintegration during homogenisation (Chapter 5.0).

Feed Properties	**Harvesting**	**Washing**	**Debris removal**	**1st cut precipitate removal**	**2nd cut precipitate recovery**
Volumetric solid conc. (-)	0.01	0.05	0.2	0.025	0.05
Particle density ($kg.m^{-3}$)	1130	1130	1120	1200^{+}	1210
Suspension density ($kg.m^{-3}$)	1005	1005	1020	1120	1170
Viscosity (mPa.s)	1.1	1.4	3.8	2.1	2.5
$d_{c,exp}$ at 50 $L.h^{-1}$ (μm)	0.39	0.48	1.32	0.69	1.14
Mean particle diameter (μm)	3.8^{b}	3.8^{b}	2.9^{b}	0.27^{g+}	1.01^{g}

Table 7.1: Summary of centrifuge feed material properties and calculated $d_{c,exp}$ values at 50 $L.h^{-1}$ for the recombinant process (^{b} indicates Boltzman d_{50}, ^{g} indicates geometric mean diameter, $^{+}$ indicates data is solely for small peak containing precipitate particles).

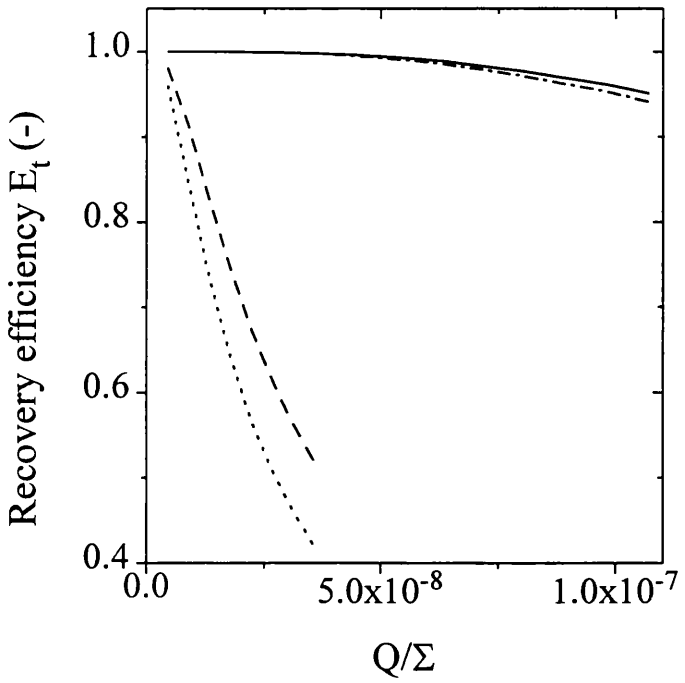

Figure 7.5: Calculated steady state recovery efficiency at various values of Q/Σ from bakers' yeast properties: (– · – · –) cell harvesting, (· · · · ·) debris removal, and from recombinant yeast properties: (——) cell harvesting, (– – –) debris removal.

7.5.2 Separation of Recombinant Whole Cells and Cell Debris

Experimentally determined grade efficiencies for whole cells harvested from the 42 L fermenter using a full disc stack are shown in Figure 7.6 overleaf. Fitting of equation 7.17 to the experimental results gave a curve that was similar to that for shear-insensitive PVA particles, indicating that the recombinant yeast cells were not significantly affected by shear forces in the centrifuge under the processing conditions examined. Some variation in the experimental grade efficiencies was, however, observed with flowrate. This effect was thought to be due to increasing flow disturbances at the higher flowrates giving an increase in the grade efficiency of particles with sizes above the critical diameter. The PVA grade efficiency curve was subsequently used for the calculation of steady state whole cell recovery efficiencies during harvesting and gave values within 1% of experimental values (Table 7.2 overleaf). The calculated values over-predicted cell recovery at flows of 100 $L.h^{-1}$ and 200 $L.h^{-1}$, but under-predicted at 400 $L.h^{-1}$. For design studies, it is more desirable to under-predict recovery since this will lead to an over-capacity in centrifuge specification (Clarkson *et al.*, 1996b).

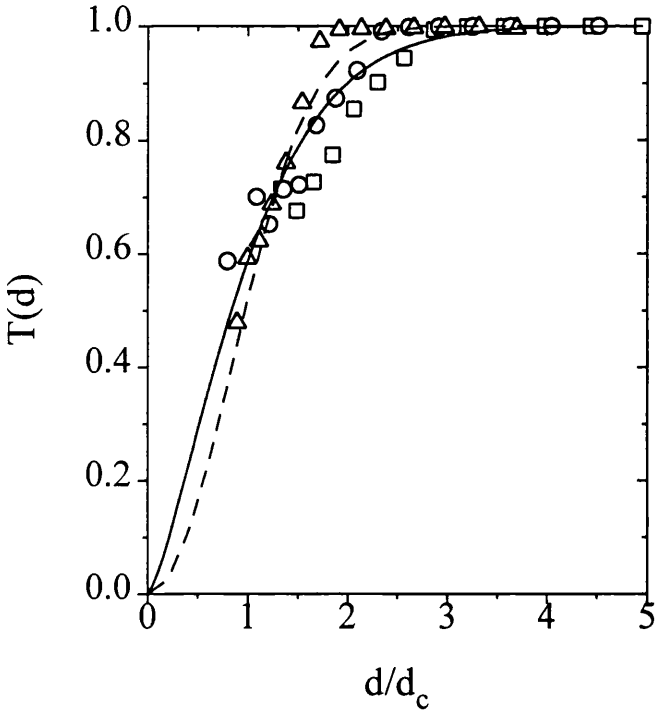

Figure 7.6: Recombinant whole cell grade efficiencies. Experimental data: □ 100 L.h^{-1}, ○ 200 L.h^{-1}, △ 400 L.h^{-1}. Fitted curve: (——), PVA curve: (– – –).

Flow rate (L.h^{-1})	**E_t Experiment**	**E_t Calculated**	**error (%)**
100	0.993	0.999	+0.6
200	0.992	0.998	+0.6
400	0.983	0.975	-0.8

Table 7.2: Experimental and calculated steady state solids recovery for full pilot scale recombinant cell harvesting.

Predictions for the steady state recovery of cells during washing were made by taking into account the affect of changes in solid concentration and viscosity on the critical diameter using the Richardson and Zaki (1954) correlation (Table 7.1). The predicted values closely agreed with the experimental data, being within 0.1% (Table 7.3).

Flow rate ($L.h^{-1}$)	E_t Experiment	E_t Calculated	error (%)
20	0.999	1.000	+0.1
60	0.997	0.997	0

Table 7.3: Experimental and calculated steady state solids recovery for full pilot scale recombinant cell washing.

In the case of the debris removal stage, grade efficiencies were determined from homogenised material originally produced in the 42 L fermenter using both diluted feed material and a scaled-down disc stack. In both cases, fitting of equation 7.17 to the experimental results gave a curve that was similar to that for PVA particles (Figures 7.7 and 7.8 overleaf). This showed that the recombinant debris particles were not significantly affected by shear forces in the centrifuge at low concentrations and that shear damage was insignificant at the full process concentration under the scale-down processing conditions.

The recovery efficiency under steady state conditions for full scale centrifugation of homogenate at the process concentration was predicted using the PVA, dilute and scale-down grade efficiency curves and compared to experimental data for the removal of debris from homogenised material originally produced in the 1500 L fermenter (Table 7.4 on page 223). All of the calculated values were within 7% of the experimental data, with the PVA curve giving the best estimates of within 5% in all cases. The recoveries were under-estimated at flowrates of 25 $L.h^{-1}$ and 50 $L.h^{-1}$ and over-estimated at 100 $L.h^{-1}$.

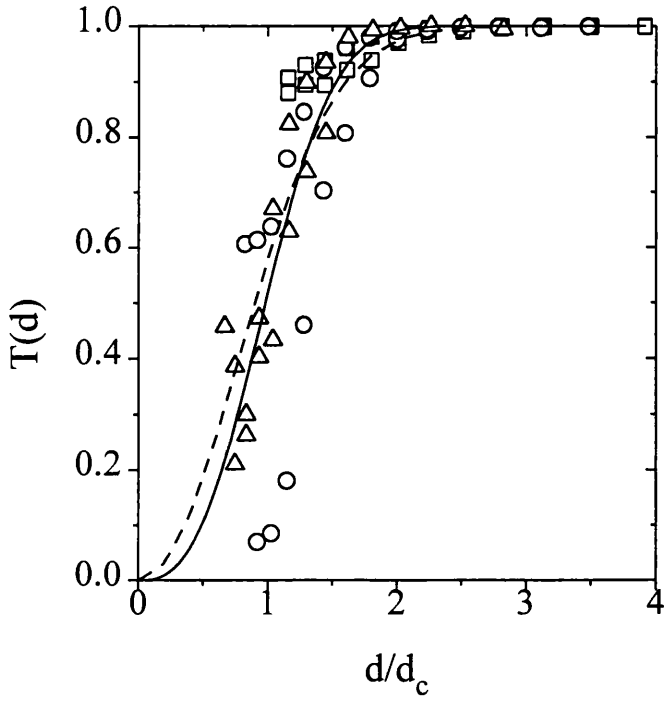

Figure 7.7: 1% (w/v) recombinant debris grade efficiencies. Experimental data: □ 200 L.h^{-1}, ○ 400 L.h^{-1}, △ 600 L.h^{-1}. Fitted curve: (——), PVA curve: (– – –).

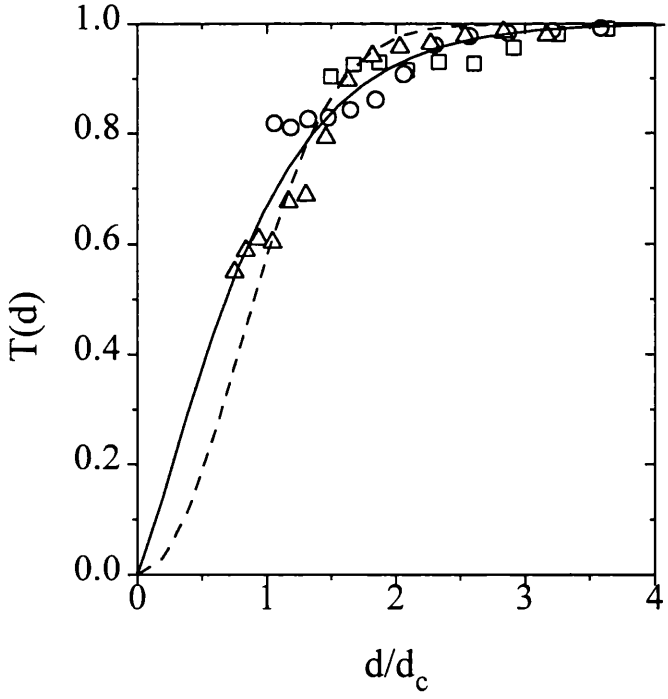

Figure 7.8: Recombinant debris scale-down grade efficiencies. Experimental data: □ 200 L.h^{-1}, ○ 400 L.h^{-1}, △ 600 L.h^{-1}. Fitted curve: (——), PVA curve: (– – –).

Flow rate ($L.h^{-1}$)	E_t Exp.	E_t Calc. (PVA curve)	error (%)	E_t Calc. (Dilute curve)	error (%)	E_t Calc. (S.D. curve)	error (%)
25	0.966	0.957	-0.97	0.963	-0.28	0.954	-1.28
50	0.941	0.903	-4.04	0.922	-1.98	0.903	-4.06
100	0.762	0.780	+2.13	0.812	+6.61	0.813	+6.74

Table 7.4: Experimental and calculated steady state solids recovery for full pilot scale recombinant debris removal at the process concentration.

The time-step mass balance model outlined in Section 7.3 was used to calculate the effect of discharges on the overall recovery efficiency, the concentration of discharged solids and the yield of soluble protein and *pe*-ADH. Table 7.5 on page 225 shows a comparison between experimental and calculated results for each process stage (n.b. no soluble product is present for stages prior to homogenisation). Good agreement was observed between calculated and experimental values, which were within 10% except for the calculated discharged solids concentration for the debris removal stage which was within 30%. The larger error in this case was thought to be due to difficulties in sampling the highly viscous debris concentrate. In the case of soluble bakers' yeast protein and ADH, Clarkson (1994) concluded that no protein degradation or enzyme inactivation occurred over the SAOOH disc stack centrifuge due to temperature increases in the range 278 K to 298 K. No consistent losses of protein and *pe*-ADH were noted over the centrifugation stage in this study, indicating that protein degradation or *pe*-ADH inactivation had also not occurred for the recombinant process.

Prediction of debris recovery during scale-down process runs with and without solids breakthrough occurring was also carried out using the time-step mass balance model (Table 7.6 on page 226) Calculated overall recovery efficiencies were within 2% of the experimental data in all cases, while a 10% error was seen when the grade efficiency model alone was used to predict recovery when solids breakthrough occurred. Recovery efficiencies for each time-step calculated using the mass balance model agreed with

experimentally determined values based on optical density at 670nm in the case of solids breakthrough (Figure 7.9 on page 227). However large deviations were observed for recovery efficiencies over each time step calculated solely on the basis of the steady state grade efficiency during periods of solids breakthrough. This shows that although errors in the overall recovery efficiency calculated using the steady state grade efficiency were not large in the above case, use of the approach is likely to lead to larger errors as the level of solids breakthrough becomes more significant. The scale-down results highlight the sensitivity of the debris removal stage to changes in feed solids concentration, with the presence of solids breakthrough leading to reductions in separation performance. The extra information obtained by applying the time-step mass balance model will therefore be useful for specifying acceptable feed concentration ranges and operating conditions for efficient operation of disc stack centrifuges.

A comparison of calculated recovery efficiencies over each time-step for scale-down centrifugation without discharging using both bakers' yeast debris and recombinant debris properties showed a shorter breakthrough time for the recombinant process (Figure 7.10 on page 227). This was thought to be due to less disintegration of recombinant cells during homogenisation compared to that of bakers' yeast (Chapter 5.0) which resulted in a higher density and volumetric concentration for the recombinant debris.

Process stage	Harvest	Wash	Debris Removal
Discharged solid dry wgt. experiment ($g.L^{-1}$)	96.1	89.0	138.2
Discharged solid dry wgt. calculated ($g.L^{-1}$)	90.2	85.3	174.0
error (%)	-6.14	-4.16	+25.9
yield of *pe*-ADH & soluble protein experiment (-)	-	-	0.80
yield of *pe*-ADH & soluble protein calculated (-)	-	-	0.86
error (%)	-	-	+7.5

Table 7.5: Experimental and calculated discharged solids concentration and soluble product yield for each centrifugation stage. (Harvest: full stack, 60 $L.h^{-1}$, discharges at 3600 s; Wash: full stack, 60 $L.h^{-1}$, discharges at 120 s; Debris Removal: scale-down centrifuge, 9 active discs, flowrate of 10 $L.h^{-1}$, discharges at 3600 s).

Approx. feed solid dry weight	**75 g.L^{-1}**	**100 g.L^{-1}**
Solids overflow?	No	yes
$E_{t,o}$ experiment	0.983	0.868
$E_{t,o}$ calculated (grade efficiency)	0.974	0.956
error (%)	-0.9	+10.1
$E_{t,o}$ calculated (time-step MB model)	0.980	0.888
error (%)	-0.3	-1.3

Table 7.6: Experimental and calculated overall solids recovery for debris removal at process concentration with and without solids breakthrough. (Scale-down centrifuge, 9 active discs, feed volume 2 L, flowrate of 10 L.h^{-1}, discharges at 3600 s).

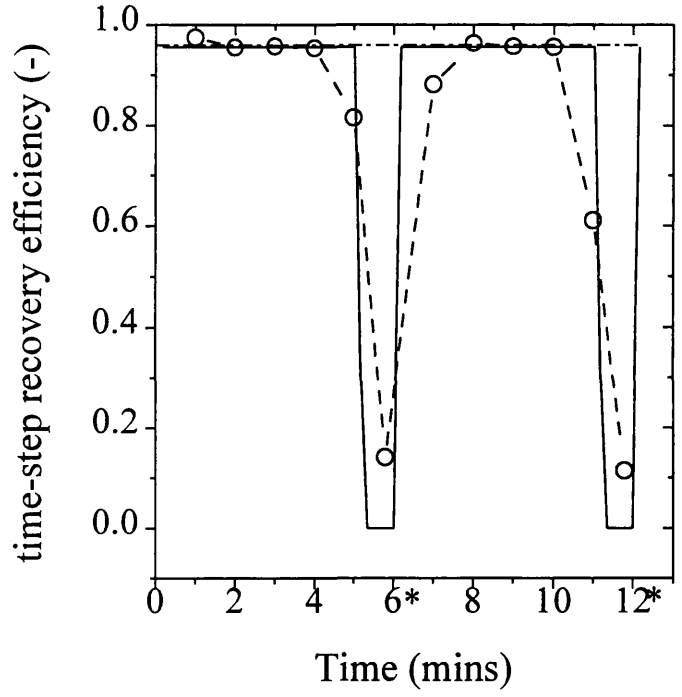

*Figure 7.9: Recovery efficiency plotted against time for scale-down debris removal with solids breakthrough occurring. Conditions: 9 active discs, flowrate 10 L.h^{-1}, feed dry weight 100 g.L^{-1}. Experimental: (– o – -) based on OD670, Calculated: (——) mass balance model,(– · –) steady state grade efficiency. * indicates a discharge.*

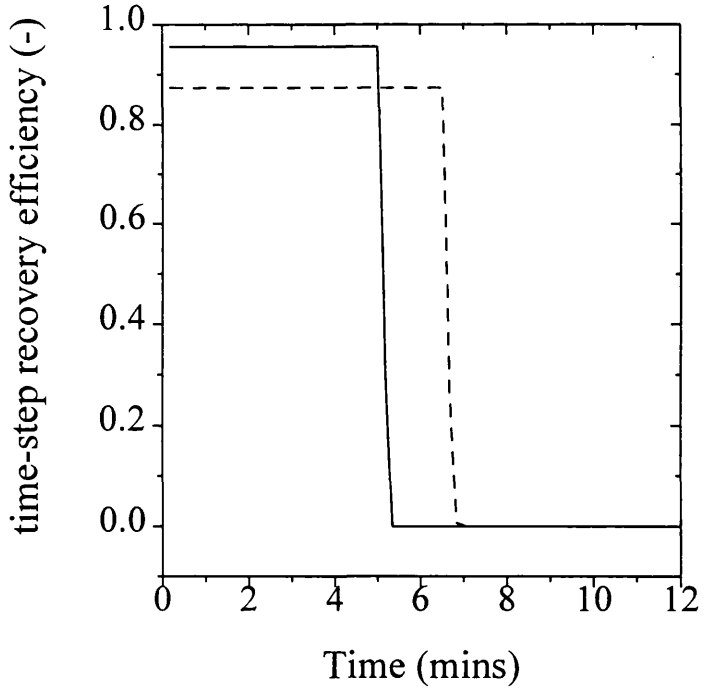

Figure 7.10: Mass balance model recovery efficiencies plotted against time for scale-down debris removal at 10 L.h^{-1}, no discharge and initial 280 g.L^{-1} yeast. (– – –) based on bakers' yeast debris properties, (——) based on recombinant properties.

7.5.3 Separation of Recombinant Protein Precipitate

For both 1st and 2nd cut precipitate feed material, measured physical properties gave calculated values of $d_{c,exp}$ at 50 $L.h^{-1}$ which were greater than the mean diameter (Table 7.1 on page 218). This indicated that recovery of the precipitate particles by disc stack centrifugation would be difficult and results for the large pilot-scale separation of precipitate material at 50 $L.h^{-1}$ do indeed show low overall recovery efficiencies (Table 7.7 on page 230). At equivalent processing conditions, Clarkson (1994) measured pilot-scale recovery efficiencies for salted-out protein precipitate from natural bakers' yeast as 0.1 for 40% material and 0.15 for 60% material, with the low recoveries attributed to aggregate breakage in the feed-zone. Breakage of recombinant precipitate aggregates was also indicated at the large pilot-scale as the measured overall recovery efficiencies were between calculated values which assumed no breakage and full breakage of aggregates to primary particles. However, use of the feed-zone model of Clarkson *et al.* (1996b) with bakers' yeast parameters gave predictions for the overall recovery efficiency that were even lower than the case of full breakage (Table 7.7). This showed that the natural bakers' yeast precipitate breakage parameters did not apply to the recombinant precipitate, possibly due to the smaller size of the aggregates.

Predictions of the overall recovery efficiencies based on the steady state grade efficiency alone were generally lower than experimental values, since unseparated solids contained in liquid exiting the bowl during discharges were not accounted for (Table 7.7). This situation was included in the time-step mass balance model and the predictions obtained were closer to measured values in most cases (Table 7.7).

Experimental recovery efficiencies determined for scale-down centrifugation of the recombinant precipitate were much higher than large pilot-scale results at an equivalent Q/Σ value and suggest particle aggregation must have occurred (Tables 7.7 and Table 7.8 on page 230). It is tempting to conclude that the presence of breakage or aggregation was dependent on flowrate, since this was reduced in the scale-down centrifuge. However this could not be justified since the full range of flowrates was not examined at a single scale. It was also possible that the level of liquid in the feed zone of the scale-down system was different from that at the full scale due to an altering of the pressure balance across the centrifuge, giving different levels of shear in each case.

For both the scale-down and full scale systems, the experimental recovery efficiencies could be matched by shifting the geometric mean size of precipitate to a sheared value, as per equation 7.21. For 40% precipitate at $Q/\Sigma=8.9x10^{-9}$ $m.s^{-1}$ the shift in the smaller peak containing the precipitate was Δd_m= -0.012 μm for the full scale unit, and Δd_m= +0.361 μm for the scale-down unit with a proportional change in the mass fraction of the two peaks. While for 60% precipitate at the same Q/Σ value, Δd_m= -0.238 μm and Δd_m= +0.628 μm for the large and scale-down units respectively. This does indicate that application of equation 7.21 itself is valid, however there was insufficient experimental data to determine the dependence of Δd_m on centrifugation conditions for the recombinant precipitate.

In order to mimic the precipitate recovery achieved in the large pilot-scale disc stack centrifuge, a small pilot-scale tubular bowl centrifuge was operated at the same Q/Σ value of approximately 8.9×10^{-9} $m.s^{-1}$. The Σ value for a tubular bowl centrifuge is given by a different equation compared to that used for the disc stack centrifuge (Ambler, 1952):

$$\Sigma = \frac{\pi\omega^2}{g} 2L_{ib}\left(\frac{3}{4}r_{ib}^2 + \frac{1}{4}r_{il}^2\right)$$

(equation 7.27)

where L_{ib} is the inner bowl length, r_{ib} the inner bowl radius and r_{il} the inner liquid radius. The measured recovery efficiency in the tubular bowl for the 1st and 2nd cut precipitate material was -18% and +37% the value for the disc stack respectively (Tables 7.7 and 7.8). It should be noted that particle separation in a tubular bowl is more efficient compared to a disc stack (Axelsson, 1985) and that the degree of aggregate breakage or aggregation in the tubular bowl feed zone is likely to differ from that of the disc stack centrifuge. Use of the same Q/Σ value for the tubular bowl and disc stack centrifuges was therefore no guarantee of equivalent performance, but instead gave a starting point for the comparison.

	1st cut precipitate		2nd cut precipitate	
Method of Determination	**$E_{t,o}$**	**error(%)**	**$E_{t,o}$**	**error**
Measured	0.077	-	0.217	-
Predicted assuming no aggregate breakage:				
Steady state grade efficiency	0.019	-75.3	0.280	+29.0
Time-step mass balance model	0.079	+0.03	0.321	+47.9
Predicted assuming full aggregate breakage into primary particles:				
Steady state grade efficiency	0.017	-77.9	0.098	-54.8
Time-step mass balance model	0.076	-0.01	0.158	-27.2
Predicted using feed-zone model of Clarkson *et al.* (1996b):				
Steady state grade efficiency	0.001	-98.7	0.017	-92.2
Time-step mass balance model	0.060	-22.1	0.078	-64.3

Table 7.7: Experimental and predicted overall recovery efficiency for large pilot-scale precipitate separation at 50 $L.h^{-1}$ and discharges at 0.167 h ($Q/\Sigma=8.9x10^{-9}$ $m.s^{-1}$).

Operating Conditions	1st cut precipitate $E_{t,o}$	2nd cut precipitate $E_{t,o}$
Scale-down disc stack:		
5 $L.h^{-1}$, 9 active discs	0.451	0.807
10 $L.h^{-1}$, 9 active discs	0.410	0.628
Tubular bowl:		
13 $L.h^{-1}$, 25,000 rpm	0.063	0.297

Table 7.8: Experimental overall recovery efficiency for small pilot-scale precipitate separation (for scale-down disc stack at 10 $L.h^{-1}$ $Q/\Sigma=8.5x10^{-9}$ $m.s^{-1}$, for tubular bowl centrifugation $Q/\Sigma=8.8x10^{-9}$ $m.s^{-1}$).

7.6 Conclusions

The measurement of physical properties for feed streams to disc stack centrifugation stages in the downstream processing of *pe*-ADH enabled critical diameters to be calculated in each case. This showed that the recombinant debris would be more difficult to separate compared to whole cells due to an increase in viscosity and reduction in solid-liquid density difference. The use of bakers' yeast properties was shown to have little effect on calculated solids recovery for whole cells, but caused a larger deviation in the case of cell debris. This highlighted the importance of evaluating properties specifically for the recombinant system in order to ensure optimal disc stack centrifuge operation.

Experimentally determined grade efficiencies showed that the recombinant whole cells and cell debris were shear-insensitive and enabled a grade efficiency function to be defined. The use of diluted feed material and a scaled-down disc stack reduced the fermentation volume required to achieve this for debris separation. Steady state recovery efficiencies calculated for cell harvesting, cell washing and debris removal using the grade efficiency approach agreed with experimental values. Scale-down results showed that in the case of solids breakthrough, however, a more accurate description of the overall separation was obtained using a time-step mass balance model. The results indicate that the time-step mass balance model will be useful for determining process sensitivity and optimum centrifuge operating conditions early in process development with a higher degree of confidence.

For the separation of recombinant precipitate at a flowrate of 50 $L.h^{-1}$, the calculated critical diameter was larger than the average aggregate size indicating a poor separation was likely. This was confirmed experimentally as low recovery efficiencies were measured at the large-pilot scale. Comparison to predicted recovery efficiencies based on full and no aggregate breakage indicated that some breakage of precipitate occurred, although the degree of breakage was less than that based on the larger salted-out bakers' yeast protein precipitate. Higher recovery efficiencies measured for scale-down centrifugation at equivalent separation conditions showed that aggregation had instead occurred in the scaled-down system. The experimental results could be matched by

shifting the mean diameter of the precipitate particle size distribution (PSD) and applying a shear-insensitive grade efficiency function in order to reflect changes in the PSD over the centrifuge feed-zone. However, there was insufficient experimental data to correlate the changes in precipitate PSD with the centrifugation conditions. Tubular bowl centrifugation was found to more closely match the separation achieved in the large scale disc stack centrifuge at 50 $L.h^{-1}$. The results highlighted the challenge in modelling and mimicking precipitate breakage in centrifuge feed-zones and show that further research is required in this area.

8.0 MODELLING OF THE WHOLE PROCESS

8.1 Introduction

In this chapter a whole process model for the recovery of protein engineered alcohol dehydrogenase (*pe*-ADH) from fermented recombinant yeast is implemented using both bakers' yeast and recombinant system equations and parameters. The model results were verified against experimental data from a large pilot-scale run. Based on this work and that of previous chapters, issues such as the need for models to account for process interactions and sensitivity, the generic nature of bioprocess models, the utility of small scale and scale-down systems as an aid to model extension and the use of modelling during process development are discussed. In Section 8.2 existing work on the modelling of downstream process sequences is outlined, while in Section 8.3 the implementation of the model for the *pe*-ADH recovery process is described. Model and experimental results are then presented and discussed in Section 8.4, with conclusions given in Section 8.5.

8.2 Modelling of a Downstream Processing Sequence

The modelling of a bioprocess sequence is typically carried out in a modular fashion, with individual unit models being linked together by process streams to form the whole process model (Clarkson, 1994; Petrides *et al.*, 1989). By linking unit models in this manner mass balances can be calculated throughout the process in order to ensure that all material is accounted for. The use of the modular approach also enables the process to be described in an integrated manner, with interactions between operations being incorporated (Siddiqi *et al.*, 1991; Middelberg, 1995b). A review of previous work on the modelling of downstream process sequences has been given in Section 1.4.5. Once a whole process model has been developed it can then be used to examine process feasibility (Wai *et al.*, 1996), to examine process economics and sensitivity (Petrides *et al.*, 1995), to carry out numerical process optimisation (Samsatli and Shah, 1996) or to specify unit operating conditions using a 'windows of operation' approach (Zhou *et al.*, 1997). The verification of a whole process model against experimental data is also

important in order to ensure that the model is accurate and that all significant process interactions have been included (Clarkson *et al.*, 1994).

8.3 Implementation of a Whole Process Model

In this study a whole process model was implemented for the recovery of *pe*-ADH from a fermented recombinant yeast (refer to Figure 1.2 on page 25 for the process sequence). The process was considered to operate in batch mode, with each process stage being completed before material was passed on to the next operation. A modular approach was adopted to describe the process, with unit operation modules being linked within MATLAB and solved sequentially to give the composition and properties of product streams. This enabled the yield and purity of *pe*-ADH to be calculated over each process stage under specified operating conditions. The linking of unit operation modules was carried out using a set of stream information which included the total stream volume, the concentration of solids, the discretised particle size distribution (PSD) of solids, the concentration of *pe*-ADH and total protein in the soluble and solid phases, and additional attributes of the stream such as physical properties.

For each process stage a volume balance was carried out:

$$\sum_{1}^{i} V_{IN,i} = \sum_{1}^{j} V_{OUT,j}$$

(equation 8.1)

where i is the number of inlet streams, j the number of outlet streams and V is the stream volume. The general mass balance equation over each process stage was:

$$\sum_{1}^{i} (V_{IN,i} C_{IN,i}) + M_{PRODUCED} = \sum_{1}^{j} (V_{OUT,j} C_{OUT,j}) + M_{CONSUMED}$$

(equation 8.2)

where C is the component concentration and M the component mass. Mass balances were carried out for both *pe*-ADH, total protein and solids. Equation 8.2 was also applied to the soluble and solid phases for *pe*-ADH and total protein, with addition of the mass in the soluble and solid phases giving the total mass for each component. Application of equations 8.1 and 8.2 enabled all material within the full process model to be accounted for and highlighted any errors within unit operation modules. The three

general unit modules used in the simulation were high pressure homogenisation, disc stack centrifugation and protein precipitation. These are described below:

8.3.1 High Pressure Homogenisation Module

The modelling of high pressure homogenisation was described in Chapter 5.0. The high pressure homogenisation module had one feed and one product stream. The module consisted of models describing the release of soluble total protein and thereby soluble *pe*-ADH from the disrupted cells (equation 5.1), the changes in homogenate particle size distribution (equations 5.7 and 5.11) and the change in the physical properties of viscosity and density (equations 5.12 and 5.14). Input data required by the module were the homogeniser operating pressure and the number of homogeniser passes. The model also required the maximum releasable soluble protein concentration (R_{max} in mg protein per g wet weight yeast) and the *pe*-ADH specific activity, which were included as an attribute of the feed stream. Other model parameters were fixed within the module and were applicable for inlet yeast concentrations between 280 and 450 g wet weight yeast per L. Physical property attributes included in the output stream were the particle density, suspension density and suspension viscosity.

8.3.2 Protein Precipitation Module

The modelling of protein precipitation was described in Chapter 6.0. The protein precipitation module had a clarified homogenate stream and a saturated ammonium sulphate stream as feed streams, and a single product stream. The module contained an isotherm model (equation 6.2) to describe changes in the soluble fraction of *pe*-ADH and total protein on addition of ammonium sulphate, and a discretised population balance model (equation 6.27) to describe changes in particle size distribution over batch ageing. Equation 6.30 was used to calculate the initial number of precipitant particles. Input data required by the module was the ammonium sulphate saturation, the shear rate and the batch ageing time. Other model parameters and physical property data for 40% and 60% saturation cut points were set within the module. The feed volume of precipitant required to achieve the specified ammonium sulphate saturation was calculated. Physical property attributes included in the output stream were the average particle density, suspension density and suspension viscosity.

8.3.3 Disc Stack Centrifugation Module

The modelling of disc stack centrifugation was described in Chapter 7.0. The disc stack centrifugation module had one feed stream and two product streams; that of supernatant and discharged solids. The module contained the time-step mass balance model to describe the overall separation (Section 7.3), with a feed zone model (equation 7.21) included to account for any particle breakage and a shear insensitive steady state grade efficiency curve (equation 7.17) used to describe particle separation in the disc stack. The feed stream to the module required the physical property attributes of particle density, suspension density and suspension viscosity. Input data required by the module was the centrifuge flowrate and discharge interval. Other centrifuge specifications and model parameters were set within the module. Attributes of whole cells were passed from the feed to product streams.

8.3.4 Describing the Whole Process

The three basic unit modules were arranged, linked and specified to give the whole process model as shown in Figure 8.1 overleaf. A buffer addition step after the debris removal stage (cent2) and a volume reduction step after the third centrifugation stage (cent3) were also included to give approximately 50 L in each precipitation stage. The process model was solved twice; first using bakers' yeast equations and parameters, which assumed that no experimentation had been carried out with the recombinant system, and secondly with the updated recombinant system equations and parameters. The simulation results were compared to experimental results from the large pilot-scale process run PPW1 (refer to Section 3.4.4 for method). The degree of error in results from run PPW1 was reflected by mass balances calculated using the experimental data. This also enabled the presence of significant enzyme denaturation or protein degradation to be discounted. In assessing the success of the simulations a level of agreement with the experimental results of ±30% was considered sufficient for feasibility studies (Clarkson, 1994), while higher accuracy of the order ±10% was required for detailed design work.

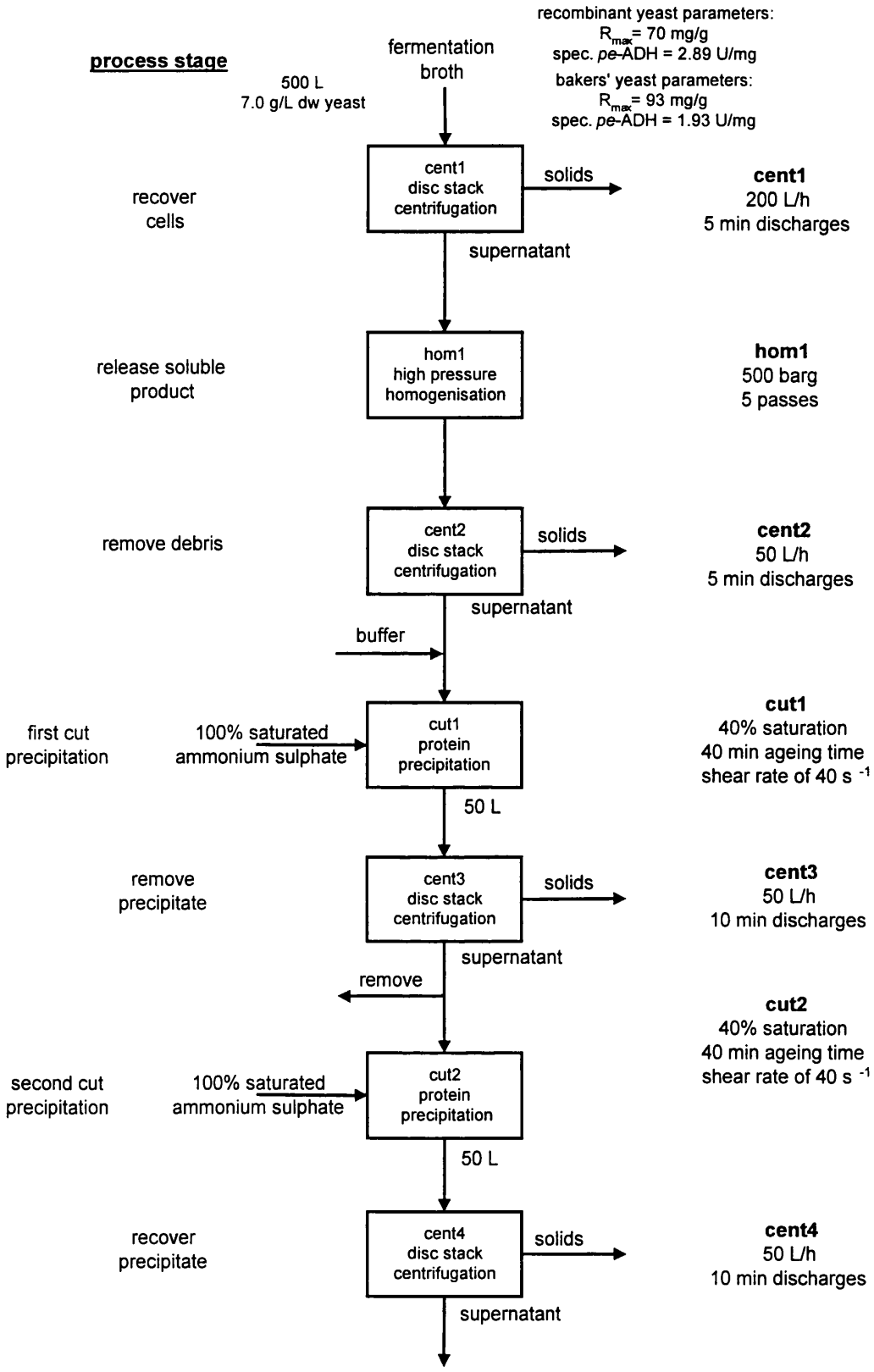

Figure 8.1: Whole process model for the large pilot-scale recovery of pe-ADH from a fermented recombinant yeast.

8.4 Results and Discussion

8.4.1 Comparison of Model and Experimental Results

Experimental ADH and total protein mass balance results for the large pilot-scale run PPW1 are shown in Figure 8.2 overleaf. The mass balances were within 11% in all cases. This level of accuracy is excellent considering that the ADH and protein assays had errors of 5.4% and 3.6% respectively. Other possible sources of error included poor separation of solid and liquid phases prior to assay and inaccuracies in measuring process volumes. Because there was no consistent loss of *pe*-ADH or total protein throughout the process it was concluded that there was no significant denaturation of *pe*-ADH or degradation of protein. For run PPW1 an initial 1000 L fermentation was used, with cell harvesting from the fermentation broth being carried out using a tubular bowl centrifuge (Section 3.4.4). For the subsequent downstream processing half of the recovered cells were then resuspended to give 30 L of 280 g/L wet weight cells. To reflect this, the whole process model had a feed stream of 500 L of fermentation broth to the harvest centrifugation stage (cent1). For the whole process model based on bakers' yeast, a typical ADH specific activity for a complex media bakers' yeast fermentation was used (Table 4.4 on page 120). Mass balances carried out for the whole process model showed small discrepancies in *pe*-ADH and total protein, typically less than 1%, indicating that no significant errors were present in the model.

Experimental and simulated step yields of *pe*-ADH over each process stage are shown in Figure 8.3 on page 240. The values show good agreement until the final precipitate recovery stage (cent4). The latter discrepancy was most likely due to difficulties in modelling the level of precipitate breakage in the disc stack centrifuge feed zone (Section 7.5.3). For the whole process model based on updated recombinant system parameters, simulations were therefore carried out assuming either full breakage of the 2nd cut precipitate into primary particles or no breakage of 2nd cut precipitate.

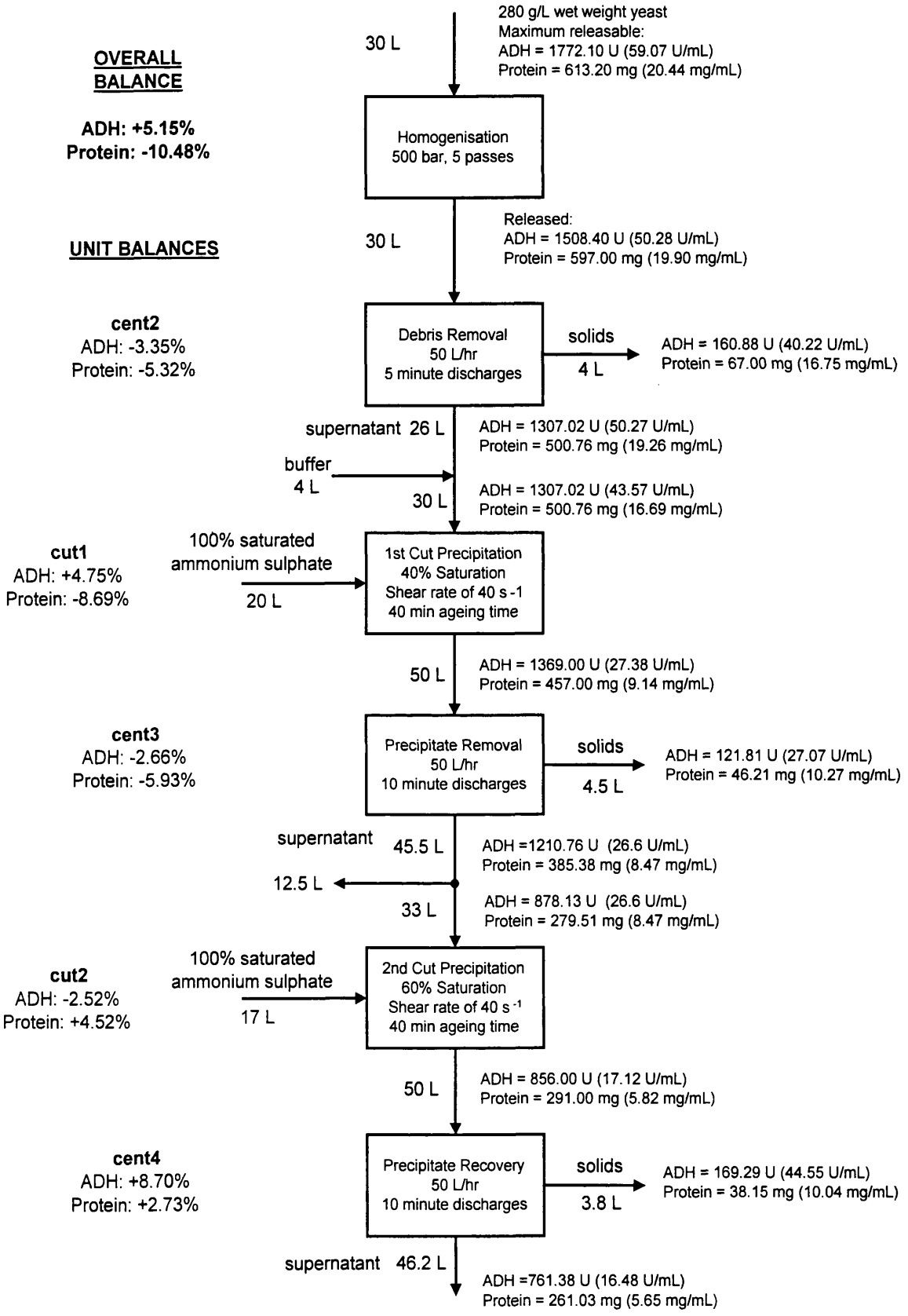

Figure 8.2: Total protein and pe-ADH experimental mass balances for large pilot-scale process run PPW1.

The whole process model based on bakers' yeast equations and parameters predicted a very low recovery of the ADH rich precipitate due to a large reduction in precipitate average diameter over the centrifuge feed zone. This gave a value for the overall *pe*-ADH yield which was 52% lower than the experimental result (Table 8.1 overleaf). The use of an initial ADH specific activity of 1.93 $U.mg^{-1}$ resulted in a difference between experimental and simulated product *pe*-ADH concentration and *pe*-ADH specific activity of -50% and -54% respectively. The discrepancy between experimental and simulated values was outside the target of ±30% required for use of the bakers' yeast process model in feasibility studies.

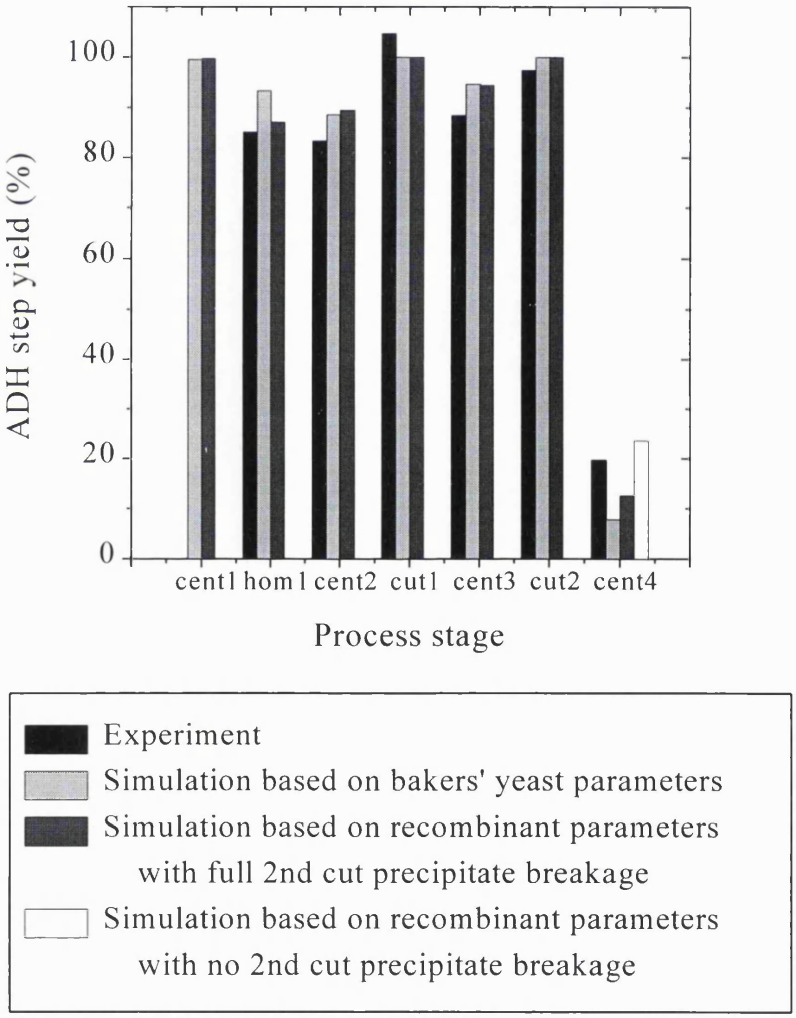

Figure 8.3: Experimental and simulated pe-ADH step yield for the large pilot-scale recovery of pe-ADH from fermented recombinant yeast broth. Note: cell harvest not carried out by disc stack centrifugation for experimental run PPW1.

	Final volume (L)	*pe*-ADH conc. ($U.mL^{-1}$)	Specific *pe*-ADH ($U.mg^{-1}$)	Purification factor (-)	Overall ADH yield* (%)
Experimental results for run PPW1	3.80	44.55	4.44	1.54	12.67
Bakers' yeast model results	2.80	22.18	2.05	1.06	6.10
error (%)	-26	-50	-54	-31	-52
Recombinant model results: full 2nd cut breakage	2.80	28.43	3.15	1.09	9.20
error %	-26	-36	-29	-29	-27
Recombinant model results: no 2nd cut breakage	2.80	53.56	3.26	1.13	16.37
error (%)	-26	+20	-27	-27	+29

* overall yield corrected to take into account processing of material removed prior to 2nd precipitation cut

Table 8.1: Experimental and whole process model results for the large pilot-scale recovery of protein engineered (pe-) ADH from fermented recombinant yeast broth.

Comparison of results from the whole process model based on updated recombinant system equations and parameters to the experimental values showed agreement to within ±30% in all but one instance (Table 8.1). The only prediction outside ±30% was -36% for the product *pe*-ADH concentration assuming full 2nd cut precipitate breakage. The experimental 2nd cut precipitate recovery was between that predicted from the recombinant process model assuming full and no precipitate breakage (Figure 8.3), which showed that an intermediate level of 2nd cut precipitate breakage had occurred. The level of accuracy achieved by the recombinant process model was therefore regarded as sufficient for feasibility studies, but insufficient for use in detailed design work. The major source of error in the recombinant process model came from the inability to predict the extent of precipitate breakage in the disc stack centrifuge feed zone, indicating the need for further experimentation in this area in order to increase the level of accuracy achieved. However, use of the assumption of full 2nd cut precipitate breakage did give an underestimate of process performance which is more desirable for design purposes.

8.4.2 Process Interactions and Sensitivity

In describing a bioprocess sequence the need to account for interactions between unit operations is well documented (Siddiqi *et al.,* 1991; Middelberg, 1995b). In the above whole process model for the recovery of *pe*-ADH a number of interactions have been incorporated, while other interactions were recognised but not specifically included in the model due to a lack of appropriate experimental data. In using such models to examine process sensitivity, it is important that significant interactions are understood otherwise model results will lose accuracy.

A major interaction identified during precipitation experiments was the distortion of *pe*-ADH and total protein solubility characteristics due to polypropyleneglycol (PPG) antifoam carry-over from the fermentation stage (Chapter 6.0). This had the effect of reducing the level of precipitation achieved due to a decrease in surface tension and was only removed by lowering the level of added PPG to 0.1 $mL.L^{-1}$ or the inclusion of a wash stage after cell harvesting. A reduction in the level of PPG at the fermentation stage lowers the maximum stirrer speed that can be used before foaming occurs, while the addition of a wash stage will increase the overall production time. It is important to consider this interaction if optimisation techniques are applied to the recombinant process, especially in the case of process scheduling.

A significant interaction incorporated into the whole process model was that between the high pressure homogenisation stage and subsequent debris removal by disc stack centrifugation. The conditions used during homogenisation impact on the physical properties of the feed to the centrifugation stage and thereby affect the level of debris removal and yield of soluble product achieved. This interaction has been examined by Zhou *et al.* (1997) for the bakers' yeast system using a windows of operation approach. Varying both the homogeniser operating pressure and number of passes was found to alter process performance. At high levels of disruption, high product release is achieved but the generation of fine debris gives poor debris removal.

In Figure 8.4 overleaf, average results from the recombinant process model are used to show the effect of variation in homogeniser feed concentration on the performance of the debris removal stage. As the feed concentration to the homogeniser increases, the

efficiency of debris removal was reduced due to increases in hindered settling and suspension viscosity. At a long discharge interval of 480 s there was also significant breakthrough of solids as the solids holding space filled. Reducing the discharge time, however, also reduced the yield of soluble products. At discharge intervals of 120, 300 and 480 s the yield of soluble *pe*-ADH and total protein was 55%, 90% and 95% respectively, with each value essentially independent of solids loading. Since high pressure homogenisation was independent of recombinant yeast concentration between 280 and 450 $g.L^{-1}$ wet weight (Chapter 5.0), one approach to reducing the sensitivity of the process would be to run the homogeniser at the maximum loading and dilute the product stream to an acceptable solids level prior to carrying out debris removal. This would also lead to cost savings as the homogeniser size would be reduced.

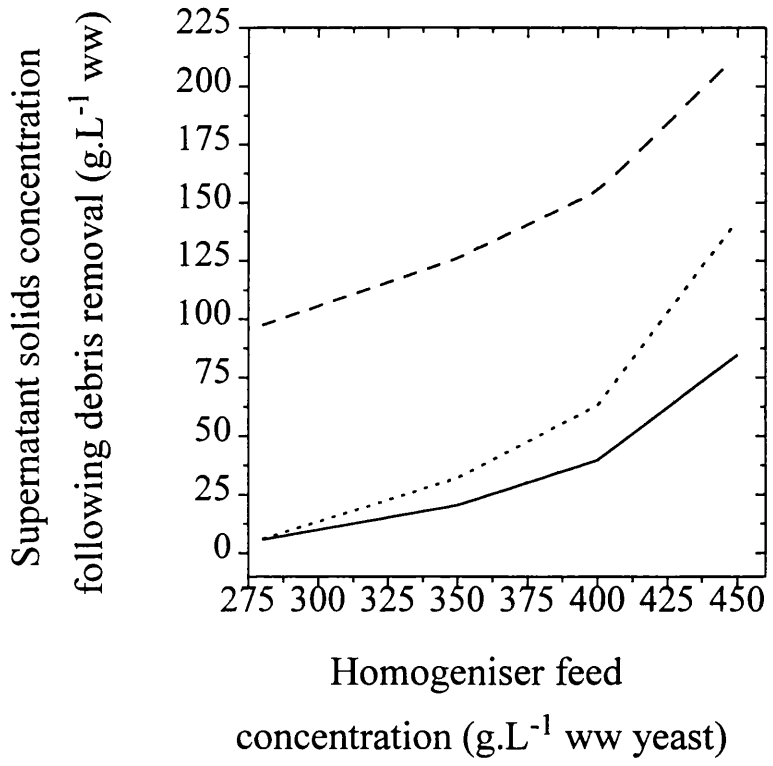

Figure 8.4: Solid concentration in supernatant following debris removal predicted by the recombinant whole process model for a range of homogenisation feed concentrations and for various centrifuge discharge intervals. Conditions used were homogeniser operation at 500 barg, 5 passes and centrifugation feed rate of 50 $L.h^{-1}$. Centrifugation discharge intervals: (——) 120 s, (· · · · ·) 300 s, (– – –) 480 s.

A number of other interactions are not explicitly included within the whole process model, but must be considered when examining process sensitivity. The work of Alsaffar *et al.* (1993) has shown that the degree of solids in the feed to a precipitation stage will effect the position of fractional solubility curves. This interaction was not incorporated in the recombinant process model, as the level of solids entering the first precipitation stage was fixed at a wet weight of approximately 10 $g.L^{-1}$ during characterisation experiments. This interaction must be considered when changing the conditions during debris removal as subsequent precipitation stages will also be altered. This is particularly crucial once process validation and regulatory approval have been completed, as any change in the final protein product will result in the need for re-validation and re-approval.

Since all experimentation with the recombinant system was carried out on cells harvested 24 h after fermenter inoculation, interactions between fermentation conditions and the degree of cell disruption were not incorporated. The time at which cells are harvested effects the degree of fermented bakers' yeast cell breakage during high pressure homogenisation (Siddiqi *et al.*, 1995) and thereby the level of product release. Zhou *et al.* (1997) has shown that a higher product recovery is achieved for fed-batch grown bakers' yeast cells with higher growth rates but that the effect is non-linear.

Another significant interaction occurs between precipitation and subsequent precipitate separation by disc stack centrifugation. In the whole process model physical property data were supplied for precipitation product streams at cut points of 40% and 60% ammonium sulphate saturation. The model would need to be supplied with relevant physical properties for other ammonium sulphate saturations to enable the impact of changes in precipitation cut point on the following centrifugation step to be incorporated. Although the size of precipitate was described for a given batch ageing time within the precipitation module, the strength of the precipitate was not defined. The strength of precipitates is crucial to determining the efficiency of recovery in a centrifuge as particle break-up will lead to poor clarification (Bell *et al.*, 1983). However, the lack of knowledge on the breakage of precipitate within the feed zone of a disc stack centrifuge makes this interaction difficult to describe.

8.4.3 Generic Nature of Bioprocess Models

The results in Section 8.4.1 show that the use of bakers' yeast model equations and parameters gave predictions for the *pe*-ADH recovery process that were not accurate enough for feasibility studies. However, by evaluating model equations and parameters specifically for the recombinant system the level of accuracy was improved by approximately 20% to lie within that required for feasibility studies. An important question is whether the bioprocess models used were therefore generic in nature, or only applied to a specific system. Clarkson (1994) found that models developed using the bakers' yeast system could be successfully applied to describe the isolation of β-galactosidase from *Escherichia coli* with the requirement for only a limited amount of data to re-calculate model parameters and effect an accurate simulation.

In describing the recombinant process in this study, examination of the updated models within each unit module showed that in most cases the underlying structure of the models remained unchanged and only parameter re-evaluation was required to increase accuracy. The applied models can therefore be seen as generic. In the case of high pressure homogenisation, the description of the homogenate cell debris average diameter (equation 5.7) was unchanged although equations describing the change in width of the resultant homogenate cell debris size distribution were modified (equations 5.8 and 5.9 were replaced by equation 5.11), while the Hetherington release model (equation 5.1) only required updated parameters. For protein precipitation the discretised population balance model (equation 6.26) was unchanged, while the isotherm model (equation 6.2) only required parameter re-evaluation. For the modelling of disc stack centrifugation, the grade efficiency approach (equation 7.17) and feed zone breakage model (equation 7.21) still applied, while the structure of the overall centrifuge model was expanded to give a better description of the overall separation (Section 7.3). It should be noted that the majority of the above models are empirical in nature, which explains the need for parameters to be redefined from one system to another. An important consideration is therefore the level of experimentation required to achieve this parameter re-evaluation.

8.4.4 Utility of Small Scale and Scale-Down Systems for Model Extension

In order to extend existing models to give a description of the recombinant process experimentation was required to produce the necessary data. For high pressure homogenisation, characterisation experiments were performed with a scaled-down homogeniser (Chapter 5.0), for protein precipitation a small scale system was used (Chapter 6.0) and for disc stack centrifugation a scaled-down disc stack and diluted feed material were used where feed material was limited (Chapter 7.0). Application of these small scale and scaled-down units proved to be useful in generating the required data without recourse to large scale runs. The scale-up of the models could then be shown to be valid based on the results from limited large scale experimentation. Considering that the cost of a single batch of complex media was lowered from £700 to £20 in reducing the required scale of fermentations from 1000 L to 42 L, considerable cost savings were realised using this approach. There was also a saving in the time required to generate the models as the scope of large scale experimentation was reduced.

The inability of the scale-down centrifuge to describe fully precipitate breakage in the feed-zone does show, however, that some caution is needed when using a scaled-down unit. It must be remembered that scaled-down processes are physical models that attempt to mimic larger scale processes and computer models developed using them will describe the scale-down process, not the full scale process. It is therefore essential that any scaled-down results or scale-up approaches on which models are based are accurate, with frequent verification against experimental results being carried out as the scale of operation increases.

The actual amount of data required to generate models in a specific case largely depends on the intended use of the models. For example a model to be used for numerical optimisation of process conditions will require a high degree of accuracy (within ±10%), must cover the expected operating ranges and incorporate significant interactions. The scope of data required during model generation is therefore likely to be large. On the other hand, models to be used for comparison of alternative processing routes require less accuracy (within ±30%) and may be carried out under fixed conditions. In this case, the minimum data required would be for a single set of conditions. The ability of models to capture the sensitivity of a process will also depend

on the type of model and availability of physical property information. For empirical models large amounts of data will be required to cover ranges of operating conditions, while for theoretical models some extrapolation may be possible. In many cases physical property data required to link unit models and account for process interactions may be lacking and must be determined experimentally. For recombinant systems which are very different to the system on which existing models are based, the use of experimental data during model extension and verification ensures that process models can be applied with a high degree of confidence.

For the recovery of *pe*-ADH, the whole process model was verified under a specified set of conditions and gave at least enough accuracy for feasibility studies. The ability of the whole process model to reflect process sensitivity was directly related to the level of experimental characterisation carried out. In the case of high pressure homogenisation, for example, models and physical property changes were defined for a range of feed concentrations and this enabled the interaction with the debris removal centrifuge to be described (Figure 8.4). As can be seen from Section 8.4.2 on process interactions, further experimentation could be completed to describe precipitate breakage during disc stack centrifugation to increase model accuracy and to also incorporate interactions between fermentation conditions and cell disruption, or precipitation and precipitate separation. Decisions regarding the level of modelling and required experimentation must therefore be made as an integral part of the bioprocess development cycle.

8.4.5 Modelling as part of Process Development

The use of modelling can offer a number of advantages during bioprocess development which include increased speed to market (Cooney *et al.*, 1988), a more optimal process and lower development costs (Evans and Field, 1988). The use of modelling for the encoding of process knowledge and as a focus for, and consistent communication format between, various project teams can also aid in process validation and obtaining regulatory approval (Bhattacharya, 1993), which is especially crucial for recombinant protein products. However, it is important to consider modelling as an integrated activity during all phases of the bioprocess development. The above results show that decisions regarding the accuracy of generated models and thereby the degree of experimental characterisation required are linked to the eventual use of the models. As

the scope and scale of experimentation increase, the costs and time for model extension also increase.

For the whole process model describing the recovery of *pe*-ADH, the level of accuracy achieved (±30%) was only sufficient for the model to be used during the conceptual design and piloting phases of process development. However, the use of small scale and scale-down units would give the advantage of shifting model generation activities and the determination of physical properties to much earlier in the process development cycle by providing a link between bench and pilot-scale operations. The speed and cost effectiveness of modelling activities could therefore be increased.

During conceptual design this type of model could be used to test the feasibility of processing routes using 'what if' studies and to compare process alternatives. Debottlenecking could be achieved to meet production targets, flexible facilities developed for more than one product, process costs estimated and process sensitivity examined. During process piloting and for the production of clinical material, process performance could be predicted and production rates estimated. The model could also show that the process is tightly controlled and that a consistent product is produced, which would aid regulatory approval.

With further experimentation significant process interactions could also be included and optimal operating conditions determined using numerical optimisation or windows of operation approaches. Scheduling of the process could then be examined, with intermediate storage requirements and production schedules specified. The model could also be used for the testing of control schemes and the training of operators well before the final plant was built. Once the process was operational, the incorporation of further data would enable continued updating of the model and use for troubleshooting, debottlenecking and retrofitting. A bioprocess model can therefore be viewed as a way of capturing knowledge on a particular system, with the intended application of the model dictating the required scope of model development activities.

8.5 Conclusions

In this chapter a whole process model for the recovery of *pe*-ADH from fermented recombinant yeast was implemented and verified at the large pilot-scale. The use of bakers' yeast equations and parameters gave results that were not accurate enough for feasibility studies (±30%). The use of equations and parameters specifically updated for the recombinant system, but extensively based on the generic framework established for the natural yeast system, gave results that were accurate enough for process feasibility (±30%) but not accurate enough for detailed design (±10%). The major discrepancy between experimental and model results occurred over the 2nd cut precipitate recovery stage and was due to a poor description of precipitate breakage in the feed zone of the disc stack centrifuge. The assumption of full 2nd cut breakage gave an underestimate of process performance, which is more desirable in design terms.

The results showed that utilisation of small scale and scale-down units enabled the scale of characterisation experiments to be reduced, thereby increasing the speed and cost effectiveness of model extension. The incorporation of unit interactions into a process model was found to be essential in order for process sensitivities to be described. The unit operation models used in the whole process model were also shown to be generic, although some model equations and parameters required re-evaluation from the bakers' yeast to the recombinant system. The level of experimental data required for this model extension was found to depend on the intended use, and thereby the required accuracy, of the model. The need for modelling to be an integrated activity during development of a bioprocess was also highlighted.

9.0 OVERALL CONCLUSIONS

In this thesis, robust and predictive models which describe the downstream processing of a recombinant intracellular enzyme were generated by using verification experiments to extend existing models developed from natural bakers' yeast. The model extension approach was identified as the most suitable method for producing models of the recombinant process as it reduced duplication of modelling effort, and the scope and scale of verification studies could be tailored to match the intended use of the models and the stage of process development respectively.

Specific conclusions for the processing of a protein engineered version of the intracellular enzyme alcohol dehydrogenase (*pe*-ADH) expressed by a recombinant strain of the yeast *Saccharomyces cerevisiae* were:

- existing empirical models for high pressure homogenisation could be applied to the recombinant system after some re-evaluation based on the results from a scale-down unit. The recombinant strain was found to have less releasable soluble total protein, was harder to break and gave different homogenate physical properties after disruption compared to natural bakers' yeast.

- an empirical solubility model could be applied to the recombinant system after parameter re-evaluation based on small-scale results, while an existing precipitate particle size model accurately described the recombinant process. Observed increases in ADH and total protein ammonium sulphate solubility for the recombinant system were mostly attributed to low concentrations in the homogenate. Calculations for a two-cut fractional ammonium sulphate precipitation showed an increase in ammonium sulphate cut-point saturation and a decrease in maximum purification factor for the recombinant process compared to that of natural bakers' yeast. The solubility model was found to be scalable based on maintanance of the scale-up parameters of total protein concentration and dimensionless precipitant feed rate.

- the separation of shear-insensitive recombinant whole cells and cell debris by disc stack centrifugation was accurately predicted using a mass balance model after the evaluation of feed stream physical properties and the determination of grade efficiency characteristics from small sample volumes. Higher recoveries of whole cells and cell debris were achieved for the recombinant system compared to that of natural bakers' yeast. However, existing models describing precipitate breakage in the centrifuge feed zone did not apply to the recombinant system and prediction of recombinant precipitate recovery was therefore made assuming full and no breakage.

- a full process model was implemented by linking individual unit models in a modular fashion. Verification at the pilot-scale showed the process model was accurate enough for determining process feasibility (±30%) but was not accurate enough for detailed design (±10%). The major source of model inaccuracy occurred over the 2nd cut precipitate recovery stage and was due to an inability to describe the extent of precipitate breakage in the disc stack centrifuge feed zone. Use of the assumption of full 2nd cut precipitate breakage gave an underestimate of process performance, which is more desirable in terms of process design and unit specification.

More general conclusions were that:

- the downstream processing of the recombinant, intracellular enzyme under study in this thesis differed from that of the natural enzyme in many respects.

- the utilisation of small scale and scale-down operations reduced the cost and increased the speed of model development.

- the unit operation models considered in this thesis were generic in nature and scaleable.

- experimental verification of models was essential and provided confidence in the scalability and accuracy of models.

- modelling must be an integrated activity during bioprocess development.

10.0 RECOMMENDATIONS FOR FUTURE WORK

Further work is recommended in the following areas:

- the modelling of precipitate breakage in the feed zone of disc stack centrifuges. A better description of precipitate breakage was required in order to improve the accuracy of the process model for the recovery of protein engineered ADH such that it could be used for detailed design work.

- the culture of the ADH overexpressing strain, in order to give consistent growth and ADH production levels. Further model extension could then be carried out for this recombinant system and the benefit of increased titres of ADH assessed.

- model extension to recombinant systems with both a new organism and protein product, in order to test further the generic nature of the models and give increased confidence in model results.

- the building of extensive physical property databases or the determination of physical property prediction methods for biomaterials. Incorporation of such databases or methods into simulation software will reduce the need for experimental determination of physical properties and enable more rapid and cost effective prediction of bioprocess performance and sensitivities. The use of scale-down systems as an aid to generating physical property data should also be investigated further.

- the increased use of models based on fundamental mechanisms as more data is available on downstream process operations. This will allow simulations to be generated more rapidly for new protein products and processes by lessening the need for extensive experimental studies, although verification of models as a routine part of bioprocess development will always be essential.

NOMENCLATURE

Symbols

A	absorbance	-
A	constant in equation 6.3	-
A_B	centrifuge feed-zone breakage rate constant	$m^3.\mu m.s^{-1}$
A_1	change in absorbance due to 1st reaction	-
A_2	change in absorbance due to 1st & 2nd reactions	-
a	constant in equation 6.2 and 6.19	-
B	constant in equation 6.3	-
B_R	birth rate	$\mu m^{-1}.L^{-1}.h^{-1}$
$B(d_{N,P})$	Boltzman distribution	-
b	constant in equation 5.5	-
b_L	width of disc spacer ribs	m
C	component concentration	$g.L^{-1}$
C	precipitant saturation	% (sat)
C_{eth}	ethanol concentration	$g.L^{-1}$
C_{glu}	glucose concentration	$mg.L^{-1}$
C_{pd}	protein concentration of a diluted sample	$mg.mL^{-1}$
C_{ptp}	precipitated total protein concentration	$mg.mL^{-1}$
C_{pu}	protein concentration of an undiluted sample	$mg.mL^{-1}$
C_{rsp}	concentration of released soluble protein	$mg.mL^{-1}$
C_u	protein assay result	$mg.L^{-1}$
C_v	volumetric solids concentration	$m^3.m^{-3}$
C_y	yeast concentration on a wet weight basis	$g.L^{-1}$
C_o	initial cut point in optimisation routine	% (sat)
C_1	1st fractional precipitation cut point	% (sat)
C_2	2nd fractional precipitation cut point	% (sat)
c	constant in equation 6.31	-
D	constant in equation 6.3	-
D_f	diffusivity	$m^2.s^{-1}$
D_I	impeller diameter	m
D_N	dilution factor	-
D_R	degree of disruption	-
D_R	particle death rate	$\mu m^{-1}.L^{-1}.h^{-1}$
d	particle diameter	μm
d_c	critical diameter	μm
$d_{c,exp}$	critical diameter based on experimental properties	μm
d_h	hydrodynamic particle diameter	μm
d_{max}	largest stable particle size	μm
d_m	mean diameter of PSD	μm
$d_{m(s)}$	sheared mean diameter of PSD	μm
d_1	first particle diameter	μm
d_2	second particle diameter	μm

d_{50}	Boltzman average diameter	μm
d^*_{50}	normalised Boltzman average diameter	μm
$d_{50N=0}$	whole cell Boltzman average diameter	μm
E	enzyme activity	$U.mL^{-1}$
E_t	recovery efficiency (or mass yield)	-
$E_{t,o}$	overall recovery efficiency	-
$E_{t,ts}$	time step recovery efficiency	-
e	power dissipation per unit volume	$J.s^{-1}.m^{-3}$
F	aqueous fraction	-
F	fractional solubility	-
F_{ac}	auto-correlation function	-
F_S	salt precipitant feed rate	$L.s^{-1}$
FE_1	fractional enzyme solubility at C_1	-
FE_2	fractional enzyme solubility at C_2	-
FP_1	fractional protein solubility at C_1	-
FP_2	fractional protein solubility at C_2	-
F(d)	particle size distribution (PSD) on volume basis	-
f_L	correction factor for the presence of rib spacers	-
f_D(S)	stress distribution imposed on cells by homogeniser	-
f_S(S)	cell strength distribution	-
f	function	-
G	average shear rate	s^{-1}
G_R	particle growth rate	$\mu m.h^{-1}$
g	gravitational acceleration constant (9.81)	$m.s^{-2}$
h	particle separation distance	m
h	centrifuge disc gap width	m
i	number	-
j	number	-
K	constant in equation 5.1	-
K_A	rate constant	s^{-1}
K_D	breakage rate constant	$\mu m^{-3}.h^{-1}$
K_m	Michaelis-Menten kinetic constant	mM
K_S	salting out constant in equation 6.1	$L.mol^{-1}$
K_V	particle shape factor	-
k	constant in equation 5.7	$pass^{-0.4}.bar^{-1}$
k	constant in equation 6.31 and 7.17	-
k_B	Boltzmann constant (1.380×10^{23})	$J.K^{-1}$
k_{md}	micromixing rate	s^{-1}
k_{ST}	surface tension correction factor	-
k_v	constant in equation 5.12	-
L	centrifuge disc length	m
L_{ib}	inner bowl length	m
l	lightpath	1 cm
M	mass of component	g
$MP_{FEED}i$	initial mass of solids in the feed pool	g

MP_{SUPERf}	final mass of solids in supernatant pool	g
MW_{eth}	molecular weight of ethanol (46.07)	$g.mol^{-1}$
MW_{glu}	molecular weight of glucose (180.16)	$g.mol^{-1}$
m	constant in equation 5.5	-
m	molar salt concentration	$mol.L^{-1}$
$m_{BSOLIDS}$	mass rate of particles entering solids holding space	$g.s^{-1}$
m_{UNREC}	mass rate unrecovered particles in supernatant	$g.s^{-1}$
N	particle number concentration	m^{-3}
N	number of homogenisation batch passes	-
N_A	Avogadro's number (6.02×10^{26})	mol^{-1}
N_I	impeller speed	rpm
N_i	initial particle number concentration	µL-1
N_t	particle number concentration at time t	µL-1
N_0	particle number concentration at time t=0	µL-1
n	constant in equation 5.5, 6.2, 6.18 and 7.17	-
n	population number density function	$\mu m^{-1}.L^{-1}$
P	pressure	bar
P_I	power input	$J.s^{-1}$
P_t	threshold pressure	bar
PF	purification factor	-
PF_{max}	maximum purification factor	-
Q	volumetric flowrate	$m^3.s^{-1}$
q	single passage throughput	$m^3.s^{-1}$
q_s	specific throughput capacity	$m^3.s^{-1}$
R	gas constant (8.31×10^3)	$J.kg^{-1}.mol^{-1}.K^{-1}$
R	soluble protein release	$mg.g^{-1}$
R_d	radius of the detector at time t	m
R_i	initial radius of the injected sample at time t=0	m
R_i	inner disc radius	m
R_o	outer disc radius	m
R_{max}	maximum soluble protein release	$mg.g^{-1}$
Re	Reynolds number	-
r	radial position w.r.t the centre of rotation	m
r_c	linear regression coefficient	-
r_{ib}	inner bowl radius	m
r_{il}	inner liquid radius	m
S	effective strength	-
S	protein solubility	$g.L^{-1}$
Sc	Schmidt number	-
S_m	mean effective strength	-
S_0	protein solubility at zero salt concentration	$g.L^{-1}$
s	stream number	-
T	absolute temperature	K
T_M	motor torque	N.m
T(d)	grade efficiency	-

$T(d)_{pred.ss}$	predicted steady state grade efficiency	-
t	time	s
V	volume	L
V_d	volume of diluent	L
V_{hs}	volume of homogenate suspension	L
V_f	final volume	L
V_m	molar volume	m^3
V_s	sample volume	L
v_g	gravitational sedimentation velocity	$m.s^{-1}$
v_g^*	reduced gravitational sedimentation velocity	$m.s^{-1}$
$v_{g,c}$	critical gravitational sedimentation velocity	$m.s^{-1}$
v_p	particle velocity	$m.s^{-1}$
v_z	centrifugal sedimentation velocity	$m.s^{-1}$
v(h)	meridian fluid velocity	$m.s^{-1}$
v_f	total volume of solids in centrifuge feed	L
v_s	total volume of solids in centrifuge supernatant	L
W	stability ratio	-
w	width of Boltzman distribution	μm
w^*	normalised width of Boltzman distribution	μm
$w_{N=0}$	width of whole cell Boltzman distribution	μm
Y	yield	-
z	number of discs	-
z_L	number of disc spacer ribs	-

Greek Symbols

ΔA	absorbance difference	-
ΔA_{340}	change in absorbance at 340 nm	-
Δd	change in particle size	μm
Δd_m	change in mean particle size due to breakage	μm
$\Delta F(d)$	change in PSD on volume basis	-
$\Delta F_f(d)$	change in feed PSD on volume basis	-
$\Delta F_s(d)$	change in supernatant PSD on volume basis	-
$\Delta M_F(d)$	feed PSD on mass basis	-
Δt	change in time	s
Φ	surface area of dehydrated protein on precipitation	m^2
Λ	slope of the salting in line	-
Σ	sigma factor	m^2
Ω	hydrophobic contact area	-
α	exponent in equation 5.1	-
α	collision effectiveness factor	-
β	constant in equation 6.1 and 6.4	-
$\beta_{i,j}$	aggregation kernal	$\mu L.h^{-1}$
χ	non-linear fitting parameter	-
δ	dipole moment of a protein	e.s.u.
ε_{340}	absorptivity of NAD at 340 nm (6.22)	$cm^2 .\mu mol^{-1}$
$\phi(h)$	potential energy of interaction between 2 particles	J
φ	upper disc angle	rad
φ_v	volume fraction of particles	-
λ	Kolmogoroff scale	m
μ	dynamic viscosity	Pa.s
μ_{init}	initial viscosity	Pa.s
μ_{max}	maximum viscosity	Pa.s
ν	kinematic viscosity	$m^2.s^{-1}$
π	constant (3.14159)	-
ρ_a	aggregate density	$kg.m^{-3}$
ρ_p	particle density	$kg.m^{-3}$
ρ_f	suspension density	$kg.m^{-3}$
ρ_{sf}	spin fluid density	$kg.m^{-3}$
σ	geometric shape factor (4.6 for spheres)	-
σ	standard deviation	-
σ_D	molal surface tension increment	$N.m^{-2}.mol^{-1}$
$\sigma_{m(s)}$	standard deviation of PSD	μm
$\sigma_{m(s)}$	sheared standard deviation of PSD	μm
τ	mean residence time	s
ω	rotational speed	$rad.s^{-1}$

REFERENCES

Ahtchi-Ali B. (1989), Dynamic simulation of fermentors using SPEEDUP, presented at AIChemE Spring National Meeting, Houston, Texas, U.S.A., April 2-6.

Allen T. (1981), Particle size measurement, Chapman and Hall, London, U.K.

Alsaffar L., Newsome P., Titchener-Hooker N.J. (1993), Purification of alcohol dehydrogenase (ADH) from bakers' yeast - process interactions during fractional precipitation, Proc. IChemE Research Event, pp. 132-134.

Alsaffar L. (1994), A process design study of ammonium sulphate fractional protein precipitation, PhD Thesis, University of London, U.K.

Ambler C.M. (1952), The evaluation of centrifuge performance, Chemical Engineering Progress, 48(3) pp. 150-158.

Arakawa T., Timasheff S.N. (1982), Preferential interactions of proteins with salts in concentrated solutions, Biochemistry, 21 pp. 6545-6552.

Arakawa T., Timasheff S.N. (1984), Mechanism of protein salting in and salting out by divalent cation salts: balance between hydration and salt binding, Biochemistry, 23 pp. 5912-5923.

Arnold F.H. (1993), Protein engineering for unusual environments, Current Opinion in Biotechnology, 4 pp. 450-455.

Asakura S., Oosaura F. (1958), Interaction between particles suspended in solutions of macromolecules, Journal of Polymer Science, 33 pp. 183

Asenjo J.A., Herrera L., Byrne B. (1989), Development of an expert system for selection and synthesis of protein purification processes, Journal of Biotechnology, 11 pp. 275-298.

Atkinson T., Scawen M.D. (1987), Hammond P.M., Large scale industrial techniques of enzyme recovery, Chapter 5 in "Biotechnology", Vol. 7a, J.F. Kennedy (ed.), VCH Publishers, Weinheim, Germany.

Axelsson H.A.C. (1985), Centrifugation, Chapter 21 in "Comprehensive biotechnology", Vol. 2, C.L. Cooney and A.E. Humphrey (eds), Pergamon Press, Oxford, U.K.

Bailey J.E., Ollis D.F. (1986), Biochemical engineering fundamentals, Ed. 2, McGraw Hill, New York, U.S.A.

Barford J.P., Phillips P.J., Orlowski J.H. (1992), A new model of uptake of multiple sugars by *S. cerevisiae*, Bioprocess Engng., 7 pp. 297-302.

Bell D.J., Brunner K.H. (1983), A method for the evaluation of floc break-up in centrifuges, Filtration & Separation, (July/August) pp. 274-301.

Bell D.J., Dunnill P. (1982a), Shear disruption of soya protein precipitate particles and the effect of aging in a stirred tank, Biotech. Bioeng., 24 pp. 1271-1285.

Bell D.J., Dunnill P. (1982b), The influence of precipitation reactor configuration on the centrifugal recovery of isoelectric soya protein precipitate, Biotech. Bioeng., 24 pp. 2319-2336.

Bell D.J., Dunnill P. (1984), Mechanisms for the acoustic conditioning of protein precipitates to improve their separation by centrifugation, Biotech. Bioeng., 26 pp. 691-698.

Bell D.J., Heywood-Waddington D., Hoare M. (1982), The density of protein precipitates and its effect on centrifugal sedimentation, Biotech. Bioeng., 24 pp. 127-141.

Bell D.J, Hoare M., Dunnill P. (1983), The formation of protein precipitates and their centrifugal recovery, Advances in Biochemical Engineering/Biotechnology, 26 pp. 1-72.

Belter P.A., Cussler E.L., Hu W.S. (1988), Bioseparations: Downstream processing for biotechnology, John Wiley & Sons, New York, U.S.A.

Benson R.S. (1997), Process modelling - core of tomorrow's "Process Microsoft", Chemical Engineering in Australia, (February) pp. 18-22.

Bergmeyer H.U. (1983), Methods of enzymatic analysis, Vol. 2, Ed. 3, Verlag Chemie, Weiheim, Germany.

Berne B.J., Percora R. (1976), Dynamic light scattering, Wiley Interscience, New York, U.S.A.

Bhattacharya A. (1993), Bioprocess modeling, Abstracts of Papers of the American Chemical Society, 205 pp. 67-BTEC.

Biegler L.T. (1989), Chemical process simulation, Chemical Engineering Progress, (October) pp. 50-61.

Bogle I.D.L., Hounslow M.J., Middleberg A.P.J. (1991), Modelling of inclusion body formation for optimisation of recovery in biochemical processes, presented at PSE 91, 4th International Congress on Process Systems Engineering, Montebello, Canada.

Bogle I.D.L., Middelberg A.P.J., O'Neill B.K. (1993), Modelling for optimisation of biochemical processes involving production and recovery of inclusion bodies, Chem. Biochem. Eng. Q., 7(1) pp. 1-5.

Bohman H. (1974), Hydrodynamics of the liquid in the disc stack of a centrifugal separator, presented at the 1st European Conference on Mixing and Centrifugal Separation, Cranfield, U.K., September.

Bonnerjea J., Oh S., Hoare M., Dunnill P. (1986), Protein purification: the right step at the right time, Bio/Technology, 4 pp. 954-958.

Bradford M.M. (1976), A rapid and sensitive method for the quantitation of microgram quantities of protein utilizing the principle of protein-dye binding, Analytic Biochemistry, 72 pp. 248-254.

Brewer S.J., Haymore B.L., Hopp T.P., Sassenfeld (1991), Engineering proteins to enable their isolation in a biologically active form, Chapter 11 in "Purification and Analysis of Recombinant Proteins", R. Seetharam and S.K. Sharma (eds), Marcel Dekker, New York, U.S.A.

Brock T.D., Madigan M.T. (1988), Biology of microorganisms, Prentice Hall, New Jersey, U.S.A.

Brookman J.S.G. (1974), Mechanism of cell disintegration in a high pressure homogeniser, Biotech. Bioeng., 16 pp. 371-383.

Brown D.L., Glatz C.E. (1987), Aggregate breakage in protein precipitation, Chem. Eng. Sci., 42(7) pp. 1831-1839.

Brunner K., Molerus O. (1979), Theoretical and experimental investigation of separation efficiency of disc centrifuges, Ger. Chem. Eng., 2 pp. 228-233.

Brunner K.H., Hemfort H. (1988), Centrifugal separation in biotechnology processes, pp. 1-50 in "Downstream processes: Equipment and techniques", A.Mizrahi (ed.), Alan R. Liss Inc., New York, U.S.A.

Camp T.R., Stein P.C. (1943), Velocity gradients and internal work in fluid motion, Journal of the Boston Society of Civil Engineers, 30 pp. 219-238.

Chen W., Fisher R.R., Berg J.C. (1990), Simulation of particle size distribution in an aggregation-breakup process, Chem. Eng. Sci., 45(9) pp. 3003-3006.

Chen Y. (1994), Improving the productivity of yeast as a host for synthesis of secreted products, PhD Thesis, University of London, U.K.

Chisti Y., Moo-Young M. (1986), Disruption of microbial cells for intracellular products, Enzyme Microb. Technol., 8 (April) pp. 194-204.

Ciriacy M. (1975), Genetics of alcohol dehydrogenase in *Saccharomyces cerevisiae* I. Isolation and genetic analysis of ADH mutants, Mutation research, 29 pp. 315-326.

Clark G.M., Cooke D. (1982), A basic course in statistics, Edward Arnold Ltd., London, U.K.

Clarkson A.I. (1994), A study of the use of process simulation and pilot-scale verification trials for the design of bioprocesses, PhD Thesis, University of London, U.K., September.

Clarkson A.I., Bogle I.D.L., Titchener-Hooker N.J. (1992), Modelling and simulation of fractional precipitaion - comparison with pilot plant data, Computers Chem. Engng, S16 pp. S441-S447.

Clarkson A.I., Lefevre P., Titchener-Hooker N.J. (1993), A study of process interactions between cell disruption and debris clarification stages in the recovery of yeast intracellular products, Biotech. Prog., 9 pp. 462-467.

Clarkson A.I., Bulmer M., Siddiqi S.F., Titchener-Hooker N.J. (1994), Pilot scale verification of bioprocess models, Computers Chem. Engng, S18 pp. S651-S655.

Clarkson A.I., Bulmer M., Titchener-Hooker N.J. (1996a), Pilot-scale verification of a computer-based simulation for fractional protein precipitation, Bioprocess Engng., 14 pp. 69-80.

Clarkson A.I., Bulmer M., Titchener-Hooker N.J. (1996b), Pilot scale verification of a computer-based simulation for the centrifugal recovery of biological particles, Bioprocess Engng., 14 pp. 81-89.

Cohn E.J. (1925), The physical chemistry of the proteins, Physiol. Rev., 5 pp. 349-437.

Cooney C.L., Petrides D., Barrera M., Evans L. (1988), Computer-aided design of a biochemical process, ACS Symposium Series 362, pp. 39-61.

Creaser E.H., Murali C., Britt K.A. (1990), Protein engineering of alcohol deyhgrogenases: effects of amino acid changes at positions 93 and 48 of yeast ADH1, Protein Engineering, 3(6) pp. 523-526.

Datar R. (1986), Economics of primary separation steps in relation to fermentation and genetic engineering, Process Biochemistry, (February) pp. 19-26.

Datar R., Rosen C.G. (1987), Centrifugal separation in the recovery of intracellular protein from *E. coli*, Chem. Engng. Journal, 34 pp. B49-B56.

Datar R.V., Cartwright T., Rosen C.G. (1993), Process economics of animal cell and bacterial fermentations: A case study analysis of tissue plasminogen activator, Bio/Technology, 11, (March) pp. 349-357.

Debye P., Huckel E. (1923), Physik. Zeitschr., 24 pp. 185

Deghani, M. (1996), Recognition of phase transition in fermentation using on-line monitored variables. PhD Thesis, University of London, U.K.

Di Jeso F. (1968), Ammonium sulphate concentration conversion nomograph for 0°, Journal of Biological Chemistry, 243(8) pp. 2022-2023.

Dixon M., Webb, E.C. (1961), Enzyme fractionation by salting out: A theoretical note, Advances in Protein Chemistry, 16 pp. 197-219.

Engler C.R., Robinson C.W. (1981), Disruption of *Candida utilis* cells in high pressure flow devices, Biotech. Bioeng., 23 pp. 765-780.

Engler C.R. (1985), Disruption of microbial cells, Chapter 20 in "Comprehensive biotechnology", Vol. 2, C.L. Cooney and A.E. Humphrey (eds), Pergamon Press, Oxford, U.K., pp. 305-324.

Erikson R.A. (1984), Disk stack centrifugation in biotechnology, Chemical Eng. Progress, (December) pp. 51-54.

Evans L.B., Field R.P. (1988), Bioprocess simulation: A new tool for process development, Bio/Technology, 6 (February) pp. 200-203.

Falconer J.S., Taylor P.B. (1946), A specific property solubility test for protein purity and its application to the preparation of pure liver esterase, Biochemistry, 40 pp. 835-843.

Farza M., Cheruy A. (1993), A typical bioprocess analysis through CAMBIO - a knowledge-based software for dynamical modelling and simulation of biochemical processes, Computers Chem. Engng, S17 (1993) pp. S165-S170.

Fish N.M., Lilly M.D. (1984), The interactions between fermentation and protein recovery, Bio/Technology, (July) pp. 623-627.

Fisher R.R., Glatz C.E. (1988), Polyelectrolyte precipitation of proteins II. Models and particle size distributions, Biotech. Bioeng., 32 pp.786-796.

Flaschel E., Friehs K. (1993), Improvement of downstream processing of recombinant proteins by means of genetic engineering methods, Biotech. Adv., 11 pp. 31-78.

Follows M., Hetherington P.J., Dunnill P., Lilly M.D. (1971), Release of enzymes from bakers' yeast by disruption in an industrial homogeniser, Biotech. Bioeng., 13 pp. 549-560.

Forsythe G.E., Malcolm M.A., Moler C.B. (1977), Computer methods for mathematical computations, Prentice Hall, London, U.K.

Foster D. (1995), Optimizing recombinant product recovery through improvements in cell-disruption technologies, Current Opinion in Biotechnology, 6 pp. 523-526.

Foster P.R. (1972), A study of protein solubility for the design of a fractionation stage in a continuous enzyme isolation process, PhD Thesis, University of London, U.K., October.

Foster P.R. (1994), Protein precipitation, Chapter 4 in "Engineering processes for bioseparations", L.R. Weatherley (ed.), Butterworth-Heinemann, Oxford, U.K.

Foster P.R. Watt J.G. (1980), The CVSM fractionation process, pp. 17-31 in "Methods of Plasma Protein Fractionation", J.M. Curling (ed.), Academic Press, New York, U.S.A.

Foster P.R., Dunnill P., Lilly M.D. (1976), The kinetics of protein salting out: precipitation of yeast enzymes by ammonium sulfate, Biotech. Bioeng., 18 pp. 545-580.

Fouhy K. (1991), Process simulation gains a new dimension, Chemical Engineering, (October) pp. 47-52.

Fowler P.W., Ball A.J.S., Griffiths D.E. (1972), The control of alcohol dehydrogenase isozyme synthesis in *Saccharomyces cerevisiae*, Canadian Journal of Biochemistry, 50 pp. 35-43.

Freund J.E. (1988), Modern elementary statistics, 7th Ed., Prentice-Hall, London, U.K.

Fuchs N.A. (1964), The mechanics of aerosols, Pergammon Press, Oxford, U.K.

Gallier P.W., Kisala T.P. (1987), Process optimisation by simulation, Chemical Engineering Progress, (August) pp. 60-66.

Giorgio R.J. (1988), Facilities for large-scale protein purification and isolation, BioPharm, (May) pp. 38-46

Glasgow L.A., Luecke R.H. (1980), Mechanisms of deaggregation for clay-polymer flocs in turbulent systems, Industrial and Engineering Chemistry Fundamentals, 19 pp. 148-156.

Glatz C.E., Fisher R.R. (1986), Modelling of precipitation phenomena in protein recovery, ACS Symposium Series 314, pp. 109-120.

Glatz C.E., Hoare M., Landa-Vertiz J. (1986), The formation and growth of protein precipitates in a continuous stirred tank reactor, AIChE Journal, 32(7) pp. 1196-1204.

Goodey A.R., Doel S., Piggott J.R., Watson M.E.E, Carter B.L.A. (1987), Expression and secretion of foreign polypeptides in yeast, Chapter 13 in "Yeast biotechnology", D.R. Berry, I.Russell and G.G. Stewart (eds), Allen & Unwin, London, U.K.

Grabenbauer G.C., Glatz C.E. (1981), Protein precipitation - Analysis of particle size distribution and kinetics, Chem. Eng. Commun., 12 pp. 203-219.

Gritsis D., Titchener-Hooker N.J. (1989), Biochemical process simulation, IChemE Symposium Series 114, pp. 69-77.

Grob R. (1993), Bioprocess simulation: An integrated approach to process development, J. Chem. Technol. Biotechnol., 58(3) pp. 309-310.

Gupta S. (1981), Scale-up procedures for disc-stack centrifuges, Chem. Engng. Journal, 22 pp.43-49.

Haley J.C., Sarma P.V.L.N. (1989), Process simulators on supercomputers, Chemical Engineering Progress, (October) pp. 28-32.

Hamel J.P., Hunter J.B. (1990), Modelling and applications of downstream processing: A survey of innovative strategies, ACS Symposium Series 419, pp. 1-35.

Hames B.D., Rickwood D. (1990), Gel electrophoresis of proteins: A practical approach, Ed. 2, IRL Press, Oxford, U.K.

Harrison S.T.L. (1991), Bacterial cell disruption: A key unit operation in the recovery of intracellular products, Biotech. Adv., 9 pp. 217-240.

Hartel R.W., Randolph A.D. (1986), Mechanisms and kinetic modelling of calcium oxalate crystal aggegates in urinelike liquor Part II: Kinetic modelling, AIChemE Journal, 32(7) pp. 1186-1195.

Healy S.J., Kennedy S.R., Bhattacharya A., Field R.P. (1990), The role of bioprocess simulation in the development and design of a multi-product enzyme production plant., Abstracts of Papers of the American Chemical Society, 200 pp. 165-BIOT.

Hearle D.C., Aguilera-Soriano G., Titchener-Hooker N.J., Wiksell E. (1993), Quantifying the fouling effects of a biological process stream on chromatographic supports, Proc. IChemE Research Event pp. 132-134.

Heinrikson R.L., Tomasselli A.G. (1991), Purification and characterisation of recombinant proteins: Opportunities and challenges, Chapter 1 in "Purification and Analysis of Recombinant Proteins", R. Seetharam and S.K. Sharma (eds), Marcel Dekker, New York, U.S.A.

Hetherington P.J. Follows M., Dunnill P., Lilly M.D. (1971), Release of protein from bakers' yeast (*Saccharomyces cerevisiae*) by disruption in an industrial homogeniser, Trans. IChemE, 49 pp. 142-148.

Higgins J.J, Lewis D.J., Daly W.H., Mosqueira F.G., Dunnill P., Lilly M.D. (1978), Investigation of the unit operations involved in the continuous flow isolation of β-galactosidase, Biotech. Bioeng., 20 pp. 159-182.

Hoare M. (1982a), Protein precipitation and precipitate ageing Part I: Salting-out and ageing of casein precipitates, Trans. IChemE, 60 pp. 79-87.

Hoare M. (1982b), Protein precipitation and precipitate ageing. Part II: Growth of protein precipitates during hindered settling or exposure to shear, Trans. IChemE, 60 pp.157-163.

Hounslow M.J., Ryall R.L., Marshall V.R. (1988), A discretized population balance for nucleation, growth and aggregation, AIChE Journal, 34(11) pp. 1821-1832.

Hounslow M.J. (1988), Solving the population balance, Proc. IChemE 5th International Symposium on Agglomeration, pp. 585-598.

Hsu H.W. (1981), Separations by centrifugal phenomena, Techniques of Chemistry, 16 pp. 767-784.

Hunter D., Johnson E., Short H., Zanetti R. (1989), Accelerating interest in dynamic simulation, Chemical Engineering, (February) pp. 30-33.

Irani R., Callis C.F. (1963), Particle size: Measurment, interpretation and application, John Wiley & Sons, New York, U.S.A.

Iyer H.V., Przybycien T.M. (1994), Protein precipitation: Effects of mixing on protein solubility, AIChE Journal, 40(2) pp. 349-360.

Jackson A.T., DeSilva R.L. (1985), Process flowsheeting for downstream biochemical process analysis and design, Process Biochemistry, (December) pp. 185-189.

Jin K., Thomas O.R.T., Dunnill P. (1994), Monitoring recombinant inclusion body recovery in an industrial disc stack centrifuge, Biotech. Bioeng., 43 pp. 455-460.

Kane J.F. (1993), Environmental assessment of recombinant DNA fermentations, Journal of Industrial Microbiology, 11 pp. 205-208.

Kauzmann W. (1959), Advances in Protein Chemisty, 14 pp. 1

Keshavarz E. (1990), Studies of cell disruption in high pressure homogenisers, PhD Thesis, University of London, U.K.

Keshavarz-Moore E., Hoare M., Dunnill P. (1990), Disruption of baker's yeast in a high-pressure homogenizer: New evidence on mechanism, Enzyme Microb. Technol., 12 pp. 764-770.

Kirkwood J.G. (1943), The theoretical interpretation of the properties of solutions of dipolar ions, Chapter 12 in "Proteins, amino acids and peptides as ions and dipolar ions", E.J. Cohn and J.T. Edsall (eds), Reinhold Publishing, New York, U.S.A.

Kleinig A.R., Middelberg A.P.J. (1996), The disruption of yeasts by high-pressure homogenisation, pp. 607-609 in "Better living through innovative biochemical engineering", Proc. of APBioChEC '94, W.K. Teo, M.G.S. Yap and S.K.W. Oh (eds.), Third Asia-Pacific Biochemical Engineering Conference, Singapore.

Koch V., Ruffer H-M., Schugerl K., Innertsberger E., Menzel H., Weis J. (1995), Effect of antifoam agents on the medium and microbial cell properties and process performance in small and large reactors, Process Biochemistry, 30(5) pp. 435-446.

Kossik J., Miller G. (1993), Manufacturing - The next frontier for biotechnology, BioPharm, (September) pp. 22-26.

Kuehner D.E., Blanch H.W., Prausnitz J.M. (1996), Salt-induced protein precipitation: Phase equilibria from an equation of state, Fluid Phase Equilibria, 116 pp. 140-147.

Kula M., Schutte H. (1987), Purification of proteins and the disruption of microbial cells, Biotech. Prog., 3(1) pp. 31-42.

Kumar P.K.R, Maschke H.E., Friehs K., Schugerl K. (1991), Strategies for improving plasmid stability in genetically modified bacteria in bioreactors, TIBTECH, 9 (August) pp. 279-284.

Lagranker A.L., Gemmell R.S. (1968), J. Am. Water Works Assoc., 9 pp. 1040

Leser E.W., Asenjo J.A. (1992), Rational design of purification processes for recombinant proteins, Journal of Chromatography, 584 pp. 43-57.

Liddell J.M. (1994), Introduction to downstream processing, Chapter 2 in "Engineering processes for bioseparations", L.R. Weatherley (ed.), Butterworth-Heinemann, Oxford, U.K.

Lu Y., Clarkson A.I., Titchener-Hooker N.J., Pantelides C., Bogle I.D.L. (1994), Simulation as a tool in process design and management for production of intracellular enzymes, Trans IChemE, 72 (Part A) (May) pp. 371-375.

Lubbert A., Simutis R. (1994), Using measurement data in bioprocess modelling and control, TIBTECH, 12 pp. 304-311.

Lutstorf U., Megnet R. (1968), Multiple forms of alcohol dehydrogenase in *Saccharomyces cerevisiae* 1. Physiological control of ADH-2 and properties of ADH 2 and 4, Archives of Biochemistry and Biophysics, 126 pp. 933-944.

Mahadevan H., Hall C.K. (1990), Statistical-mechanical model of protein precipitation by nonionic polymer, AIChE Journal, 36(10) pp. 1517-1528.

Mannweiler K. (1989), The recovery of biological particles in high-speed continuous centrifuges with special reference to feed-zone break-up effects, PhD Thesis, Unversity of London, U.K., October.

Mannweiler K., Titchener-Hooker N.J., Hoare M. (1989), Biochemical engineering improvements in the centrifugal recovery of biological particles, IChemE Symposium Series, pp. 105-117.

Maybury J. (1997), PhD Thesis, Univerity of London, U.K., in preparation.

Maybury, J.P.; Titchener-Hooker, N.J.; Hoare, M.; Dunnill, P. (1997), The performance of a scaled down industrial disc stack centrifuge with a reduced feed material requirement, Bioprocess Engng, accepted for publication.

Melander W., Horvath C. (1977), Salt effects on hydrophobic interactions in precipitation and chromatography of proteins: An interpretation of the lyotropic series, Archives of Biochemistry and Biophysics, 183 pp. 200-215.

Middelberg A.P.J. (1995a), Process-scale disruption of microorganisms, Biotech. Adv., 13 pp. 491-551.

Middelberg A.P.J. (1995b), The importance of accounting for bioprocess interactions, Australasian Biotechnology, 5(2) pp. 99-103.

Middelberg A.P.J., Bogle I.D.L. (1990), Sizing biological samples by photosedimentation techniques, Biotechnol. Progress, 6 pp. 255-261.

Middelberg A.P.J., Bogle I.D.L., Snoswell M. (1989), Simulation of a novel biochemical process, presented at CHEMECA 89, Gold Coast, Queensland, Australia.

Middelberg A.P.J., O'Neill B.K., Bogle I.D.L. (1992a), Modelling bioprocess interactions for optimal design and operating strategies, Trans. IChemE, 70 (Part C) (March) pp. 8-12.

Middelberg A.P.J., O'Neill B.K., Bogle I.D.L. (1992b), A new model for the disruption of *Escherichia coli* by high-pressure homogenisation Part I. Model development and verification, Trans. IChemE, 70 (Part C) (December) pp. 205-212.

Middelberg A.P.J., O'Neill B.K., Bogle I.D.L., Gully N.J., Rogers A.H., Thomas C.J. (1992c), A new model for the disruption of *Escherichia coli* by high-pressure homogenisation Part II. A correlation for the effective cell strength, Trans. IChemE, 70 (Part C) (December) pp. 213-218.

Milburn P.T., Dunnill P. (1994), The release of virus-like particles from recombinant *Saccharomyces cerevisiae*: effect of freezing and thawing on homogenisation and bead milling, Biotech. Bioeng., 44 pp. 736-744.

Miller S.R., Bergmann D. (1993), Biocontainment design considerations for biopharmaceutical facilities, Journal of Industrial Microbiology, 11 pp. 223-234.

Moe H.I., Hertzberg T. (1994), Advanced computer architectures applied in dynamic process simulation: A review, Computers Chem. Engng, S18 pp. S375-S384.

Moser A. (1993), Bioprocess simulation in practice: Joint strategy with modelling and experiments according to the formal macroapproach, Chem. Biochem. Eng. Q., 7(1) pp. 21-26.

Mosqueira F.G., Higgins J.J., Dunnill P., Lilly M.D. (1981), Characteristics of mechanically disrupted bakers' yeast in relation to its separation in industrial centrifuges, Biotech. Bioeng., 13 pp. 335-343.

Murali C., Creaser E.H. (1986), Protein engineering of alcohol dehydrogenase - 1. Effects of two amino acid changes in the active site of yeast ADH-I, Protein Engineering, 1(1) pp. 55-57.

Muratet G., Bourseau P. (1993), Artificial intelligence for process engineering - State of the art, Computers Chem. Engng, S17 pp. S381-S388.

Naess L., Mjaavatten A., Li J.O. (1993), Using dynamic process simulation from conception to normal operation of process plants, Computers Chem. Engng, 17(5/6) pp. 585-600.

Naf G. (1994), Stochastic simulation using gPROMS, Computers Chem. Engng, S18 pp. S743-S747.

Narodoslawsky N. (1991), Bioprocess simulation: A systems theoretical approach to biotechnology, Chem. Biochem. Eng. Q., 5(4) pp. 183-187.

Narodoslawsky N., Friedler F., Kiraly L., Altenburger H.J. (1993), SIMBIOS - A new simulation program for biotechnology with novel design, Chem. Biochem. Eng. Q., 7(1) pp. 27-30.

Nelson C.D., Glatz C.E. (1985), Primary particle formation in protein precipitation, Biotech Bioeng., 27 pp. 1434-1444.

Nemeth T., Varga E.I., Mangos K.M., Bay Jorgensen S. (1992), A tool for development of qualitative and approximate quantitative process models, Computers Chem. Engng, S16 pp. S491-S498.

Nielson A.E. (1964), Kinetics of precipitation, Macmillan, New York, U.S.A.

Niida K., Itoh J., Umeda T., Kobayashi S., Ichikawa A. (1986), Some expert system experiments in process engineering, Chem. Eng. Res. Des., 64 (September) pp. 372-380.

Nikatri M. Richardson P., Ravenhall R., Flanagan M.T., Molloy J., Hoare M. (1989), The modelling and control of fractionation processes for enzyme and protein purification, pp. 2436-2440 in " Proceedings American Control Conference", Vol. 3, Omnipress Inc., Wisconsin, U.S.A.

Niktari M., Chard S., Richardson P., Hoare M. (1990), The monitoring and control of protein purification and recovery process, pp. 622-631 in "Separation for biotechnology", Vol. 2, D.L. Pyle (ed.), Elzevier Applied Science, London, U.K.

Ogez J.R., Hodgdon J.C., Beal M.P., Builder S.E. (1989), Downstream processing of proteins: Recent advances, Biotech. Adv., 7 pp. 489-497.

Oyeleye O.O., Kramer M.A. (1988), Qualitative simulation of chemical process systems: Steady-state analysis, AIChE Journal, 34(9) (September) pp. 1441-1454.

Pantelides C.C. (1988), Speedup - Recent advances in process simulation, Computers Chem. Engng, 12(7) pp. 745-755.

Pantelides C.C., Barton P.I. (1993), Equation-orientated dynamic simulation current status and future perspectives, Computers Chem. Engng, S17 pp. S263-S285.

Parker T.G., Dalgleish D.G. (1977), The use of light-scattering and turbidity measurements to study the kinetics of extensively aggregating proteins: α_s-Casein, Biopolymers, 16 pp. 2533-2547.

Petentate A.M., Glatz C.E. (1983), Isoelectric precipitation of soya protein II. Kinetics of protein aggregate growth and breakage, Biotech. Bioeng., 25 pp. 3059-3078.

Petrides D.P. (1994), BioPro Designer: An advanced computing environment for modelling and design of integrated biochemical processes, Computers Chem. Engng, S18 pp. S621-S625.

Petrides D., Cooney C.L., Evans L.B., Field R.P., Snoswell M. (1989), Bioprocess simulation: An integrated approach to process development, Computers Chem. Engng, 13(4/5) pp. 553-561.

Petrides D., Sapodou E., Calandranis J. (1995), Computer-aided process analysis and economic evaluation for biosynthetic human insulin production - A case study, Biotech. Bioeng., 48 pp. 529-541.

Pohjola V.J., Alha M.K., Ainassaari J. (1994), Methodology of process design, Computers Chem. Engng, S18 pp. S307-S311.

Pohorecki R., Baldyga J. (1983), New model of micromixing in chemical reactors 2. Application to a stirred tank reactor, Ind. Eng. Chem. Fundam., 22 pp. 398-405.

Preisig H.A. (1996), Computer-aided modelling - Two paradigms on control, Computers Chem. Engng, S20 pp. S981-S986.

Press W.H., Flannery B.P., Teukolsky S.A., Vetterling W.T. (1988), Numerical recipes in C: The art of scientific computing, Cambridge University Press, New York, U.S.A.

Przybycien T.M., Bailey J.E. (1989), Aggregate kinetics in salt-induced protein precipitation, AIChE Journal, 35(11) pp. 1779-1790.

Rajagh L.V., Puett D., Ciferri A. (1965), Interaction between proteins and salt solutions. I. Thermodynamic parameters of dilution for gelatin and collagen, Biopolymers, 3 pp. 421-437.

Ramkrishna D. (1985), The status of population balances, Rev. Chem. Eng., 3(1) pp. 49-95.

Randolph A.D., Larson M.A. (1971), Theory of particulate processes: Analysis and techniques of continuous crystallisation, Ed. 1, Academic Press, New York, U.S.A.

Ransohoff T.C., Murphy M.K., Levine H.L. (1990), Automation of biopharmaceutical purification processes, BioPharm, (March) pp. 20-26.

Richardson J.F., Zaki W.N. (1954), Sedimentation and fluidisation: Part I, Trans. IChemE, 32 (1954) pp. 35-53.

Richardson P. (1987), A biochemical engineering study of fractional protein precipitation, PhD Thesis, Univeristy of London, U.K., September.

Richardson P., Hoare M., Dunnill P. (1990), A new biochemical engineering approach to the fractional precipitation of proteins, Biotech. Bioeng., 36 pp. 354-366.

Roberts A.D., Zhang Z., Young T.W., Thomas C.R. (1994), Direct determination of the strength of brewing yeast cells using micromanipulation, Proc. IChemE Research Event, pp. 73-75.

Robertson J.L. (1989), The ideal process simulator, Chemical Engineering Progress, (October) pp. 62-66.

Rohani S., Chen M. (1993), Aggregation and precipitation kinetics of canola protein by isoelectric precipitation, Canadian Journal of Chemical Engineering, 71 pp. 689-698.

Rothstein F. (1994), Differential precipitation of proteins: Science and technology, Chapter 6 in "Protein purification process engineering", R.G. Harrison (ed.), Dekker, New York, U.S.A.

Rumpus J. (1997), PhD Thesis, Univerity College London, U.K., in preparation.

Saffman P.G., Turner J.S. (1956), On the collision of drops in turbulent clouds, Journal of Fluid Mechanics, 1 pp. 16-30.

Salahuddin A., Waseem A., Yahiya Khan M., Abul Qasim & Sibghatullah M. (1983), A possible relation between the salting-out behaviour of proteins and their surface hydrophobicity, Indian Journal of Biochemistry and Biophysics, 20 (June) pp. 127-131.

Samsatli N.J., Shah N. (1996), Optimal integrated design of biochemical processes, Computers Chem Engng., S20 pp. S315-S320.

Sargent R.W.H., Westerberg A.W. (1964), "SPEED-UP" in chemical engineering design, Trans. IChemE, 42 pp. T190-T197.

Scawen M.D., Melling J. (1985), Large-scale extraction and purification of enzymes and other proteins, Chapter 2 in "Handbook of enzyme biotechnology Part A: Principles of industrial enzyme isolation and utilization", 2nd Ed., A. Wiseman (ed.), John Wiley & Sons, New York, U.S.A.

Scopes R.K. (1982), Protein purification: Principles and practice, Ed. 1, Springer-Verlag, New York, U.S.A.

Scopes R.K. (1988), Protein purification: Principles and practice, Ed. 2, Springer-Verlag, New York, U.S.A.

Shamlou P.A., Stavrinides S., Titchener-Hooker N.J., Hoare M. (1994), Growth-independent breakage frequency of protein precipitates in turbulently agitated bioreactors, Chem. Eng. Sci., 49(16) pp. 2647-2656.

Shamlou P.A., Siddiqi S.F., Titchener-Hooker N.J. (1995), A physical model of high-pressure disruption of bakers' yeast cells, Chem. Eng. Sci,. 50(9) pp. 1383-1391.

Shamlou P.A., Stavrinides S., Titchener-Hooker N.J., Hoare M. (1996), Turbulent breakage of protein precipitates in mechanically stirred bioreactors, Bioprocess Engng., 14 pp. 237-243.

Shaw J.F.G. (1992), The integration of process simulation and engineering design, Computers Chem. Engng, S16 pp. S465-S472.

Shih Y.C., Prusnitz J.M., Vlanch H.W. (1992), Some characteristics of protein precipitation by salts, Biotech. Bioeng., 40 pp. 1155-1164.

Siddiqi S.F. (1997), PhD Thesis, University of London, U.K., in preparation.

Siddiqi S.F., Clarkson A.I., Keshavarz-Moore E., Titchener-Hooker N.J. (1991), Modelling of process interactions in biochemical processes, Proc. IChemE Research Event, pp. 155-158.

Siddiqi S.F., Bulmer M., Shamlou P., Titchener-Hooker N.J. (1995), The effects of fermentation conditions on yeast cell debris particle size distribution during high pressure homogenisation, Bioprocess Engng., 14 pp. 1-8.

Siddiqi S.F., Titchener-Hooker N.J., Shamlou P.A. (1996), Simulation of particle size distribution changes occurring during high pressure disruption of bakers' yeast, Biotech. Bioeng., 50 pp. 145-150.

Siddiqi S.F., Titchener-Hooker N.J., Shamlou P.A. (1997), The use of scale down operations for the prediction of protein release and cell debris size distribution, Biotech. Bioeng., 55(4) pp. 642-649.

Siletti C.A. (1988), Computer aided design of protein recovery processes, PhD Thesis, Massachusetts Institute of Technology, U.S.A.

Simon F., Narodoslawsky M., Csermely Z., Altenburger J. (1994), Physical property data management in a bioprocess simulation system, Computers Chem. Engng, S18 pp. S675-S680.

Sinanoglu O., Abdulnar S. (1965), Effect of water and other solvents on the structure of biopolymers, Fed Proc., Fed. Am. Soc. Exp. Biol., 24(3) pp. S12-S23.

Sinclair K. (1997), PhD Thesis, University of London, U.K., in preparation.

Smith G.J., Morton W. (1988), Dynamic simulation using an equation-orientated flowsheeting package, Computers Chem. Engng, 12(5) pp. 469-473.

Smoluchowski M. (1917), Mathematical theory of the kinetics of the coagulation of colloidal solutions, Z. Phys. Chem., 92 pp. 129-168.

Sokolow W.J. (1971), Moderne Industriezentrifugen, VEB Technik Verlag, Berlin, Germany.

Spalding B.J. (1991), Downstream processing: Key to slashing production costs 100 fold, Bio/Technology, 9 pp. 229-233.

Stephanopoulos G. (1990), Artificial intelligence in process engineering - Current state and future trends, Computers Chem. Engng, 14(11) pp. 1259-1270.

Stephanopoulos G., Stephanopoulos G. (1986), Artificial intelligence in the development and design of biochemical processes, Tibtech, (September) pp. 241-249.

Stephanopoulos G., Townsend D.W. (1986), Synthesis in process development, Chem. Eng. Res. Des., 64 (May) pp. 160-174.

Stephanopoulos G., Johnston J., Kriticos T., Lakshmanan, Mavrovouniotis M., Siletti C. (1987), DESIGN-KIT: An object-orientated engineering environment for process engineering, Computers Chem. Engng, 11(6) pp. 655-674.

Stephanopoulos G., Henning G., Leone H. (1990), MODEL.LA. A modeling language for process engineering - I. The formal framework, Computers Chem. Engng, 14(8) pp. 813-846.

Sullivan F.E., Eriksson R.A. (1961), De Laval's "KQ value" spelled out. Design factors with the continuous disk centrifuge as a case in point, Ind. Eng. Chem., 53(6) pp. 434-438.

Titchener-Hooker N.J., Gritsis D., Olbirch R., Gardiner S.A.M., Mannweiler K., Fish N.M., Hoare M. (1991), Integrated process design for producing and recovering proteins from inclusion bodies, Pharmaceutical Technology International, (October) pp. 42-48.

Titchener-Hooker N.J., Hoare M., McIntosh R.V., Foster P.R. (1992), The effect of fluid-jet mixing on protein precipitate growth during low-frequency conditioning, Chem. Eng. Sci., 47(1) pp. 75-86.

Titchener-Hooker N.J., McIntosh R.V. (1993), A study of the effect of low-frequency conditioning on the size distribution properties and centrifugal recovery of human albumin precipitate, Bioprocess Engng, 8 pp. 215-222.

Turner R.E., Baines B.S., Asenjo J.A. (1994), Development of a computer based expert system for the rational design of large scale separation of baculovirus-produced proteins, Proc. IChem Research Event, pp. 70-72.

Twineham M., Hoare M., Bell D.J. (1984), The effects of protein concentration on the break-up of protein precipitate by exposure to shear, Chem. Eng. Sci., 39(3) pp. 509-513.

Van de Goor-Kucerova J. (1992), Cloning, expression and site-directed mutagenesis of the gene encoding horse liver alcohol dehydrogenase in *E.coli*, PhD Thesis, Eindhoven University of Technology, The Netherlands.

Van Oss C.J., Good R.J., Chaudhury M.K. (1989), Solubility of proteins, Journal of Protein Chemistry, 5(6) pp. 385-405.

Virkar P.D., Hoare M., Chan M.Y.Y., Dunnill P. (1982), Kinetics of the acid precipitation of soya protein in a continuous-flow tubular reactor, Biotech. Bioeng., 24 pp. 871-882.

Vlachy V., Blanch H.W., Prausnitz J.M. (1993), Liquid-liquid phase separations in aqueous solutions of globular proteins, AIChE Journal, 39(2) pp. 215-223.

Wachi S., Jones A.G. (1992), Dynamic modelling of particle size distribution and degree of agglomeration during precipitation, Chem. Eng. Sci., 47(12) pp. 3145-3148.

Wai P.P.C., Bogle I.D.L., Bagherpour K., Gani R. (1996), Process synthesis and simulation strategies for integrated biochemical process design, Computers Chem. Engng, S20 pp. S357-S362.

Weast R.C. (1978), CRC handbook of chemistry and physics, Ed. 58, CRC Press, Florida, U.S.A.

Weijers S.R., Van't Riet K. (1992), Enzyme stability in downstream processing Part 1: Enzyme inactivation, stability and stabilization, Biotech. Adv., 10 pp. 237-249.

Werner R.G., Langlouis-Gau H. (1989), Meeting the regulatory requirements for pharmaceutical production of recombinant DNA derived products, Drug Res., 39(1) pp. 108-111.

Wheelwright S.M. (1986), Designing downstream processes for large-scale protein purification, Bio/Technology, 5 pp.789-793.

Wheelwright S.M. (1991), Protein purification: Design and scale up of downstream processing, Hanser, Munich, Germany.

Williamson V.M., Bennetzen J., Young E.T., Nasmyth K., Hall B.D. (1980), Isolation of the structural gene for alcohol dehydrogenase by genetic complementation in yeast, Nature, 283 (January) pp. 214-216.

Wimpenny J.W.T (1967), Breakage of micro-organisms, Process Biotechnology, (July) pp. 41-44.

Wiseman A. (1985), Handbook of enzyme biotechnology, Ed. 2, John Wiley and Sons, New York, U.S.A.

Woodley J.M., Titchener-Hooker N.J. (1996), The use of windows of operation as a bioprocess design tool, Bioprocess Engng., 14 pp. 263-268.

Zhang Z., Chisti Y., Moo-Young M. (1995), Isolation of a recombinant intracellular β-galactosidase by ammonium sulphate fractionation of cell homogenates, Bioseparation, 5 pp. 329-337.

Zhou Y.H., Holwill I.L.J., Titchener-Hooker N.J. (1997), A study of the use of computer simulations for the design of integrated downstream processes, Bioprocess Engng., 16(6) pp. 367-374.

APPENDIX 1

Listing of MATLAB two-cut fractional precipitation optimisation program

```
%
% Two-Cut Fractional Precipitation Optimisation
% by Edward Varga 1994
%
% Set Variables
%
pa=0.5007083;
pn=5.33035;
ea=0.52247;
en=12.884;
Y=0;
YO=[];
PFMAXO=[];
C1O=[];
C2O=[];
E1O=[];
E2O=[];
P1O=[];
P2O=[];
%
% overall loop - step yield
%
for Y=1:-0.01:0
if Y<0.01,break,end
PFMAX=0;
C1B=0;
C2B=0;
E1B=0;
E2B=0;
P1B=0;
P2B=0;
PF=0;
%
% inner loop - step first cut
%
for C1=0:0.01:100
E1=1/(1+(C1/ea)^en);
E2=E1-Y;
if E2<0,break,end
C2=ea*(((1/E2)-1)^(1/en));
P1=1/(1+((C1/pa)^pn));

P2=1/(1+((C2/pa)^pn));
PF=(E1-E2)/(P1-P2);
 if PF>PFMAX
  PFMAX=PF;
```

```
 C1B=C1;
 C2B=C2;
 E1B=E1;
 E2B=E2;
 P1B=P1;
 P2B=P2;
 end
end
%
YO=[1,YO Y];
PFMAXO=[PFMAXO PFMAX];
C1O=[C1O C1B];
C2O=[C2O C2B];
E1O=[E1O E1B];
E2O=[E2O E2B];
P1O=[P1O P1B];
P2O=[P2O P2B];
end
%
figure
plot(YO,PFMAXO)
```

APPENDIX 2

Typical small scale precipitation material balances

A. MC1 strain precipitation

Run Details:
(see Section 3.4.2 for experimental method)
Date: 2-2-1996
MC1 Strain Fermentation Batch: MC1C16
Processing Conditions: 0.1 mL PPG per L fermentation medium, cells washed
Homogenisation Cell Concentration: 280 g/L
Precipitation Run No. 11
ADH Specific Activity: 3.84 U/mg total protein
Initial Precipitation Volume: 0.90 L
Final Precipitation Volume: 0.88 L
Precipitation Temperature: 5-6°C
Precipitation pH: 6.4-6.6
Sampled after 5 minutes

ADH Balance:

% SAT	Soluble U/mL	SD +/- U/mL	Solid U/mL	SD +/- U/mL	Total U/mL	SD +/- U/mL	Undiluted Total	Undiluted Initial	error %
0	34.34	1.85	1.01	0.05	35.35	1.86	35.35	35.35	0.00
20	25.97	1.40	1.34	0.07	27.31	1.40	34.14	35.35	-3.43
35	21.14	1.14	0.97	0.05	22.12	1.14	34.02	35.35	-3.76
40	21.22	1.15	1.42	0.08	22.65	1.15	37.74	35.35	6.76
45	17.42	0.94	1.52	0.08	18.94	0.94	34.43	35.35	-2.61
50	16.88	0.91	2.37	0.13	19.24	0.92	38.49	35.35	8.86
55	12.42	0.67	4.13	0.22	16.54	0.71	36.77	35.35	4.00
60	7.35	0.40	8.05	0.43	15.41	0.59	38.51	35.35	8.94
70	1.00	0.05	10.40	0.56	11.41	0.56	38.02	35.35	7.54

Table A2.1: MC1 strain precipitation ADH balance

Total Protein Balance:

% SAT	Soluble mg/mL	SD +/- mg/mL	Solid mg/mL	SD +/- mg/mL	Total mg/mL	SD +/- mg/mL	Undiluted Total	Undiluted Initial	error %
0	8.85	0.32	0.36	0.01	9.21	0.32	9.21	9.21	0.00
20	8.68	0.17	0.31	0.01	8.99	0.17	8.99	9.21	-2.39
35	4.99	0.18	0.52	0.02	5.51	0.18	8.47	9.21	-7.99
40	4.22	0.15	0.69	0.02	4.91	0.15	8.18	9.21	-11.16
45	3.65	0.13	0.85	0.03	4.50	0.13	8.18	9.21	-11.18
50	3.59	0.13	1.34	0.05	4.93	0.14	9.87	9.21	7.15
55	1.57	0.06	2.00	0.07	3.57	0.09	7.94	9.21	-13.77
60	1.06	0.04	2.53	0.09	3.58	0.10	8.96	9.21	-2.69
70	0.70	0.03	2.15	0.08	2.85	0.08	9.49	9.21	3.12

Table A2.2: MC1 strain precipitation total protein balance

B. Packed bakers' yeast precipitation

Run Details:
(see Section 3.4.2 for experimental method)
Date: 5-12-1995
Processing Conditions: 3 mL PPG added
(equivalent to 0.1 mL PPG per L fermentation medium)
Homogenisation Cell Concentration: 280 g/L
Precipitation Run No. 7
ADH Specific Activity: 15.12 U/mg total protein
Initial Precipitation Volume: 0.90 L
Final Precipitation Volume: 0.95 L
Precipitation Temperature: 4.5-6°C
Precipitation pH: 6.2-6.4
Sampled after 5 minutes

ADH Balance:

% SAT	Soluble U/mL	SD +/- U/mL	Solid U/mL	SD +/- U/mL	Total U/mL	SD +/- U/mL	Undiluted Total	Undiluted Initial	error %
0	398.39	21.51	9.96	0.54	408.35	21.52	408.35	408.35	0.00
20	324.55	17.53	7.42	0.40	331.97	17.53	414.97	408.35	1.62
35	247.86	13.38	12.28	0.66	260.14	13.40	400.22	408.35	-1.99
40	233.68	12.62	21.20	1.14	254.88	12.67	424.80	408.35	4.03
45	183.45	9.91	32.76	1.77	216.21	10.06	393.11	408.35	-3.73
50	135.10	7.30	72.45	3.91	207.55	8.28	415.09	408.35	1.65
55	69.14	3.73	110.99	5.99	180.13	7.06	400.29	408.35	-1.97
60	15.21	0.82	131.62	7.11	146.83	7.15	367.08	408.35	-10.11
70	3.65	0.20	114.03	6.16	117.68	6.16	392.27	408.35	-3.94

Table A2.3: Packed bakers' yeast precipitation ADH balance

Total Protein Balance:

% SAT	Soluble mg/mL	SD +/- mg/mL	Solid mg/mL	SD +/- mg/mL	Total mg/mL	SD +/- mg/mL	Undiluted Total	Undiluted Initial	error %
0	26.11	0.94	0.90	0.03	27.01	0.94	27.01	27.01	0.00
20	19.68	0.71	0.47	0.02	20.15	0.71	25.19	27.01	-6.74
35	12.99	0.47	1.68	0.06	14.67	0.47	22.57	27.01	-16.44
40	11.23	0.40	3.86	0.14	15.09	0.43	25.14	27.01	-6.91
45	8.41	0.30	5.19	0.19	13.60	0.36	24.73	27.01	-8.43
50	6.11	0.22	6.29	0.23	12.40	0.32	24.79	27.01	-8.20
55	4.20	0.15	6.67	0.24	10.87	0.28	24.16	27.01	-10.56
60	3.12	0.11	8.45	0.30	11.57	0.32	28.94	27.01	7.13
70	1.02	0.04	7.18	0.26	8.19	0.26	27.31	27.01	1.10

Table A2.4: Packed bakers' yeast precipitation total protein balance

APPENDIX 3

Listing of MATLAB precipitation population balance model

A. 'Popbal.m'

```
% Precipitation Population Balance Model
% Main Program
% By Ed Varga 1995
%
% 60% Cut
% G=5 1/s
%
% Set up size ranges
%
d=[0.2,0.252,0.317,0.4,0.504,0.635,0.80,1.008, ...
   1.270,1.600,2.016,2.540,3.200,4.032,5.08, ...
      6.400,8.063,10.16,12.800,16.127];
%
% Set no. of particles
%
counts=1e+7;
%
% Initialise arrays
%
xn=zeros(1,20);
x0=zeros(1,20);
%
% Set up initial number based on given no. fractions
%
xf=zeros(1,20);
xf=[0,0,0,0,3.6,11.6,24.9,38.1,15.0,5.3, ...
   1.5,0,0,0,0,0,0,0,0,0];
for i=1:20
xn(1,i)=xf(1,i)/sum(xf);
x0(1,i)=xn(1,i)*counts;
end
%
% Solve for number using Runge-Kutta Method
%
t0=0;
tf=0.7;
[t,x]=ode45('popsol',t0,tf,x0)
%
% Determine number of time steps
%
m=size(t,1)
%
% Determine change in average dia and stnd dev.
%
```

```
dinit=0.8522;
spread0=0.6348;
%
dmc=zeros(m,1);
dm=zeros(m,1);
sig=zeros(m,1);
spread=zeros(m,1);
spread1=zeros(m,1);
spread2=zeros(m,1);
%
for i=1:m
sum1=0;
sum2=0;
sum3=0;
for j=1:20
sum1=sum1+x(i,j)*log(d(j));
sum2=sum2+x(i,j);
end
dmc(i)=exp(sum1/sum2);
dm(i)=dmc(i)-(dmc(1)-dinit);
for j=1:20
sum3=sum3+x(i,j)*(log(d(j))-log(dm(i)))^2;
end
sig(i)=exp((sum3/sum2)^0.5);
spread(i)=spread0*sig(i)/sig(1);
spread1(i)=dm(i)-spread(i);
spread2(i)=dm(i)+spread(i);
end
%
```

B. 'Popsol.m'

```
% Population Balance Model
% Set-up Routine for Differential Equations
% By Edward Varga 1994
%
% 60% Cut
% G=5 1/s
%
function xdot = popsol(t,x)
xdot = zeros(20,1);
nnagg= zeros(20,1);
nbre = zeros(20,1);
beta=0.5e-7;
kd=0.05;
d=[0.2,0.252,0.317,0.4,0.504,0.635,0.80,1.008, ...
   1.270,1.600,2.016,2.540,3.200,4.032,5.08, ...
      6.400,8.063,10.16,12.800,16.127];
%
for i=1:20
```

```
  na=0;
  if i>2
    for j=1:i-2
      na=na+(2^(j-i+1))*beta*x(i-1)*x(j);
    end
  end
  nb=0;
  if i>1
    nb=0.5*beta*x(i-1)*x(i-1);
  end
  nc=0;
  nd=0;
  for j=1:20
   if j<1
     nc=nc+(2.0^(j-i))*beta*x(i)*x(j);
   else
     nd=nd+beta*x(i)*x(j);
   end
  end
  nagg(i)=na+nb-nc-nd;
end
%
for i=1:20
  if i == 20
    nbre(i)=-kd*((d(i))^3)*x(i);
  else
    nbre(i)=kd*(2*((d(i+1))^3)*x(i+1)-(d(i)^3)*x(i));
  end
end
for i=1:20
  xdot(i)=nagg(i)+nbre(i);
end
%
```

APPENDIX 4

Listing of MATLAB time-step disc stack centrifuge mass balance model

```
% Time-step mass balance model
% for disc stack centrifugation
% Version 5 by Ed Varga 29/11/96
%
% ----------------------------------
% INPUT DATA
% ----------------------------------
%
% CONSTANTS
%
% pi and time step, t (seconds)
%
pi=3.14159;
t=20;
%
% FEED PROPERTIES
%
% CADH=ADH Conc (U/mL), CPRO=Protein Conc. (mg/mL)
% u=viscosity (Pa.s), sdens=solid density(g/L)
% dp=density difference (kg/m3), Cv=solid volumetric conc(m3/m3)
% o=shape factor (-)
%
CADH=43.4010;
CPRO=17.0678;
u =0.0062;
sdens=1120;
dp=110;
Cv=0.32;
o =4.6;
%
% OPERATING PARAMETERS
%
% QLperhr=Flowrate(L/hr), Q=Flowrate(m3/s)
% V=Volume of feed(L), dt=discharge time (sec)
% ld=fraction of liquid in bowl that goes into discharge 0=none,1=all
%
QLperhr=50;
Q =QLperhr/(3600*1000);
V=30;
dt=480;
ld=1;
% CENTRIFUGE CHARACTERISTICS
%
% Th=half angle(rad), w=speed (rad/s)
% z=disc no. (-), Ro=outer disc radius (m)
% Ri=inner disc radius (m)
```

```
% fbv=full bowl volume (L)
% tsv=solids holding volume (L)
%
Th=0.66;
w =1027;
z =43;
Ro=0.053;
Ri=0.021;
fbv=0.600;
tsv=0.300;
%
% GRADE EFFICIENCY CURVE PARAMETERS
%
K=0.865;
n=2.08;
%
% FEED MATERIAL PSD
%
% diameter=d (micron), total mass for each size range=Mf (g)
%
gpL=130;
tM=gpL*V;
d=[0.87,0.972,1.086,1.213,1.355,1.514,1.692,1.89, ...
   2.112,2.36,2.637,2.946,3.292,3.678,4.109, ...
   4.591,5.13,5.732,6.404,7.155,7.995,8.933, ...
   9.981,11.15,12.46,13.92];
Mfrac=[0,0,.002579,.00296,.003856,.004407,.006731, ...
   .008801,.017735,.051553,.10508,.132984,.171572,.211352,.166094, ...
   .053617,.01547,.006358,.002052,0,.0,.0,.0, ...
   0,0,0];
Mf=Mfrac.*tM;
%
% ----------------------------------
% INITILISATION
% ----------------------------------
%
% INITILISE ARRAYS AND GRAPHS
%
VLwithS=0.0;
Td=[];
Mff=[];
Mfff=[];
Mbsol=[];
Mbsolt=[0,0,0,0,0,0,0,0,0,0,0,0,0,0,0,0,0,0,0,0,0,0,0,0,0,0,0,0,0];
Msupt=[0,0,0,0,0,0,0,0,0,0,0,0,0,0,0,0,0,0,0,0,0,0,0,0,0,0,0,0,0];
Msolt=[0,0,0,0,0,0,0,0,0,0,0,0,0,0,0,0,0,0,0,0,0,0,0,0,0,0,0,0,0];
Msup=[];
ODt=[];
ODR=[];
close(gcf)
```

```
f=figure;
set(f,'position',[300 250 500 840],'name','Dynamic Disc Stack Centrifuge Simulation')
set(f, 'nextplot','add')
subplot(2,1,1)
plot(d,Mf,'r')
xlabel('diameter (um)')
ylabel('mass (g)')
title('Particle Mass Distribution')
text(8,65,'Feed (Red)')%
text(8,45,'Solid (Yellow)')
text(8,25,'Super (green)')
hold on
subplot(2,1,2)
plot(ODt,ODR)
xlabel('time (secs)')
ylabel('ODsuper/ODfeed')
title('OD ratio')
axis([0 1 0 1])
%
% ----------------------------------
% CALCULATIONS
% ----------------------------------
%
% calculate solid concentration in feed (g/L)
%
fconc=Mf./V;
%
% calculate mass of solids in bowl when bowl is full (g)
%
fbsm=tsv*sdens;
%
% calculate critical diameter (micron)
%
dc=10^6*((27*Q*u*tan(Th))/(dp*pi*w^2*z*(Ro^3-Ri^3)*(1-Cv)^o))^0.5;
%
% calculate total time (s), no. of discharges, time of last discharge (s),
% mass flow of feed solids (g/s)
%
tt=(V/QLperhr)*3600;
nd=round(tt/dt);
tld=nd*dt;
Mff=Mf./tt;
%
% Main time loop
%
comment='centrifuge on'
comment='time in seconds'
for i=t:t:tt
 time=i;
 time
```

```
%
% check if at discharge time, if yes then calculate feed
% particle mass and liquid volume lost with discharge
%
 for j=dt:dt:tld
  if i == j
   adlv=fbv-sum(Mbsolt)/sdens;
   Mdisch=(fconc.*adlv).*ld;
   Msolt=Msolt+Mdisch;
   Lperbowl=(adlv-sum(Mdisch)/sdens)*ld;
   VLwithS=VLwithS+Lperbowl;
  else
   Mdisch=[0,0,0,0,0,0,0,0,0,0,0,0,0,0,0,0,0,0,0,0,0,0,0,0,0,0,0];
  end
  if i == j, break, end
 end
%
% calculate grade efficiencies and separation for each time step
%
 Td=1-exp(-(K*(d./dc)).^n);
 Mfff=(Mff.*t)-Mdisch;
 Mbsol=Td.*Mfff;
 Mrec=Mfff-Mbsol;
 Mbsolt=Mbsolt+Mbsol;
%
% check if bowl is full
% if so work out the overflow of solids into the supernatant
%
 if sum(Mbsolt) >= fbsm
  extram = sum(Mbsolt)-fbsm;
  extrafrac = extram/sum(Mbsolt);
  Movr=Mbsolt.*extrafrac;
  comment='bowl full - overflow of solids'
 else
  Movr=[0,0,0,0,0,0,0,0,0,0,0,0,0,0,0,0,0,0,0,0,0,0,0,0,0,0,0];
 end
%
% supernatant flow and pool calcs
%
 Mbsolt=Mbsolt-Movr;
 Msup =Mrec+Movr;
 Msupt=Msupt+Msup;
 ODt=[ODt i];
 sof=sum(Msup)/sum(Mfff);
 ODR=[ODR sof];
%
% check if at discharge time, if yes then empty bowl
%
 for j=dt:dt:tld
  if i == j
```

```
  Msolt=Msolt+Mbsolt;
  Mbsolt=[0,0,0,0,0,0,0,0,0,0,0,0,0,0,0,0,0,0,0,0,0,0,0,0,0];
  comment='discharge'
  figure(f)
  hold on
  subplot(2,1,1)
  plot(d,Msolt,'y')
 end
  if i == j, break, end
 end
%
% ------------------
% Update Graphs
% ------------------
%
% redraw results graphs at each time step
%
 figure(f)
 hold on
 subplot(2,1,1)
 plot(d,Msupt,'g')
 hold on
 subplot(2,1,2)
 plot(ODt,ODR)
 axis([-1 i 0 1])
%
end
comment='centrifuge off'
comment='simulation results'%
%
%-----------------------------------
% Material Balances
%-----------------------------------
%
comment='*******balance results*******'
comment='errors in %'
%
% Solids
%
Mfeed=sum(Mf)
Msolid=sum(Msolt)
Msuper=sum(Msupt)
errMbal=100*((Msolid+Msuper)-Mfeed)/Mfeed
%
% Total Volume
%
tVsolid=VLwithS+sum(Msolt)/sdens
tVsuper=V-tVsolid
errtVbal=100*(tVsolid+tVsuper-V)/V
gpL
```

```
CSOLID=Msolid/tVsolid
CSUPER=Msuper/tVsuper
%
% ADH
%
FADH=V*CADH;
SADH=CADH*VLwithS;
CSADH=SADH/tVsuper;
PADH=FADH-SADH;
CPADH=PADH/tVsuper
errADHbal=100*(SADH+PADH-FADH)/FADH
%
% Protein
%
FPRO=V*CPRO;
SPRO=CPRO*VLwithS;
CSPRO=SPRO/tVsuper;
PPRO=FPRO-SPRO;
CPPRO=PPRO/tVsuper
errPRObal=100*(SPRO+PPRO-FPRO)/FPRO
%
% --------------------------
% Output Final Results
% --------------------------
%
% redraw results graphs at final time step
%
 figure(f)
 hold on
 subplot(2,1,1)
 plot(d,Msupt,'g')
 hold on
 subplot(2,1,2)
 plot(ODt,ODR)
 axis([-1 i 0 1])
%
% output overall performance and balance results
%
comment='*******Performance Summary*******'
dc
Et=sum(Msolt)/sum(Mf)
ConcFact=CSOLID/gpL
YADH=PADH/FADH
YPRO=PPRO/FPRO
%
end
```